NUREG/CR-4307
HEDL-TME 85-14
Vol. 1

LWR Pressure Vessel Surveillance Dosimetry Improvement Program

1985 Annual Report
October 1984 - September 1985

Prepared by W. N. McElroy, E. P. Lippincott

Hanford Engineering Development Laboratory

Prepared for
U.S. Nuclear Regulatory
Commission

NUREG/CR-4307
HEDL-TME 85-14
Vol. 1

LWR Pressure Vessel Surveillance Dosimetry Improvement Program

1985 Annual Report
October 1984 - September 1985

Manuscript Completed: September 1985
Date Published: January 1986

Prepared by
W. N. McElroy, E. P. Lippincott

Hanford Engineering Development Laboratory
Operated by Westinghouse Hanford Company
P. O. Box 1970
Richland, WA 99352

Prepared for
Division of Engineering Technology
Office of Nuclear Regulatory Research
U.S. Nuclear Regulatory Commission
Washington, D.C. 20555
NRC FIN B5988

PREVIOUS REPORTS IN LWR-PV-SDIP SERIES

NUREG/CR-0038	HEDL-TME 78-4	July 1977 - September 1977
NUREG/CR-0127	HEDL-TME 78-5	October 1977 - December 1977
NUREG/CR-0285	HEDL-TME 78-6	January 1978 - March 1978
NUREG/CR-0050	HEDL-TME 78-7	April 1978 - June 1978
NUREG/CR-0551	HEDL-TME 78-8	July 1978 - September 1978
NUREG/CR-0720	HEDL-TME 79-18	October 1978 - December 1978
NUREG/CR-1240, Vol. 1	HEDL-TME 79-41	January 1979 - March 1979
NUREG/CR-1240, Vol. 2	HEDL-TME 80-1	April 1979 - June 1979
NUREG/CR-1240, Vol. 3	HEDL-TME 80-2	July 1979 - September 1979
NUREG/CR-1240, Vol. 4	HEDL-TME 80-3	October 1979 - December 1979
NUREG/CR-1291	HEDL-SA-1949	October 1978 - December 1979*
NUREG/CR-1241, Vol. 1	HEDL-TME 80-4	January 1980 - March 1980
NUREG/CR-1241, Vol. 2	HEDL-TME 80-5	April 1980 - June 1980
NUREG/CR-1747	HEDL-TME 80-73	October 1979 - December 1980*
NUREG/CR-1241, Vol. 3	HEDL-TME 80-6	October 1980 - December 1980
NUREG/CR-2345, Vol. 1	HEDL-TME 81-33	January 1981 - March 1981
NUREG/CR-2345, Vol. 2	HEDL-TME 81-34	April 1981 - June 1981
NUREG/CP-0029	HEDL-SA-2546	October 1980 - September 1981*
NUREG/CR-2345, Vol. 4	HEDL-TME 81-36	October 1981 - December 1981
NUREG/CR-2805, Vol. 1	HEDL-TME 82-18	January 1982 - March 1982
NUREG/CR-2805, Vol. 2	HEDL-TME 82-19	April 1982 - June 1982
NUREG/CR-2805, Vol. 3	HEDL-TME 82-20	October 1981 - September 1982*
NUREG/CR-2805, Vol. 4	HEDL-TME 82-21	October 1982 - December 1982
NUREG/CR-3391, Vol. 1	HEDL-TME 83-21	January 1983 - March 1983
NUREG/CR-3391, Vol. 2	HEDL-TME 83-22	April 1983 - June 1983
NUREG/CR-3391, Vol. 3	HEDL-TME 83-23	October 1982 - September 1983*
NUREG/CR-3391, Vol. 4	**	October 1983 - December 1983
NUREG/CR-3746, Vol. 1	HEDL-TME 84-20	October 1983 - March 1984
NUREG/CR-3746, Vol. 2	HEDL-TME 84-21	April 1984 - September 1984
NUREG/CR-3746, Vol. 3	HEDL-TME 84-31	October 1983 - September 1984*

*Annual Reports.

**No HEDL-TME number assigned because this progress report contains only an NBS contribution on "Compendium of Benchmark Neutron Fields for Pressure Vessel Surveillance Dosimetry."

FOREWORD

The Light Water Reactor Pressure Vessel Surveillance Dosimetry Improvement Program (LWR-PV-SDIP) has been established by the U.S. Nuclear Regulatory Commission (NRC) to improve, test, verify, and standardize the physics-dosimetry-metallurgy, damage correlation, and associated reactor analysis methods, procedures and data used to predict the integrated effect of neutron exposure to LWR pressure vessels and their support structures. A vigorous research effort attacking the same measurement and analysis problems exists worldwide, and strong cooperative links between the U.S. NRC-supported activities at HEDL, ORNL, NBS, and MEA and those supported by CEN/SCK (Mol, Belgium), EPRI (Palo Alto, USA), KFA (Jülich, Germany), and several United Kigdom laboratories have been extended to a number of other countries and laboratories. These cooperative links are strengthened by the active membership of the scientific staff from many participating countries and laboratories in the ASTM E10 Committee on Nuclear Technology and Applications. Several subcommittees of ASTM E10 are responsible for the preparation of LWR surveillance standards.

The primary objective of this multilaboratory program is to prepare an updated and improved set of physics-dosimetry-metallurgy, damage correlation, and associated reactor analysis ASTM standards for LWR pressure vessel and support structure irradiation surveillance programs. Supporting this objective are a series of analytical and experimental validation and calibration studies in "Standard, Reference, and Controlled Environment Benchmark Fields," research reactor "Test Regions," and operating power reactor "Surveillance Positions."

These studies will establish and certify the precision and accuracy of the measurement and predictive methods recommended in the ASTM Standards and used for the assessment and control of the present and end-of-life (EOL) condition of pressure vessel and support structure steels. Consistent and accurate measurement and data analysis techniques and methods, therefore, will be developed, tested and verified along with guidelines for required neutron field calculations used to correlate changes in material properties with the characteristics of the neutron radiation field. Application of established ASTM standards is expected to permit the reporting of measured materials property changes and neutron exposures to an accuracy and precision within bounds of 10 to 30%, depending on the measured metallurgical variable and neutron environment.

The assessment of the radiation-induced degradation of material properties in a power reactor requires accurate definition of the neutron field from the outer region of the reactor core to the outer boundaries of the pressure vessel. The accuracy of measurements on neutron flux and spectrum is associated with two distinct components of LWR irradiation surveillance procedures 1) proper application of calculational estimates of the neutron exposure at in- and ex-vessel surveillance positions, various locations in the vessel wall and ex-vessel support structures, and 2) understanding the relationship between material property changes in reactor vessels and their support structures, and in metallurgical test specimens irradiated in test reactors and at accelerated neutron flux positions in operating power reactors.

The first component requires verification and calibration experiments in a variety of neutron irradiation test facilities including LWR-PV mockups, power reactor surveillance positions, and related benchmark neutron fields. The benchmarks serve as a permanent reference measurement for neutron flux and fluence detection techniques, which are continually under development and widely applied by laboratories with different levels of capability. The second component requires a serious extrapolation of an observed neutron-induced mechanical property change from research reactor "Test Regions" and operating power reactor "Surveillance Positions" to locations inside the body of the pressure vessel wall and to ex-vessel support structures. The neutron flux at the vessel inner wall is up to one order of magnitude lower than at surveillance specimen positions and up to two orders of magnitude lower than for test reactor positions. At the vessel outer wall, the neutron flux is one order of magnitude or more lower than at the vessel inner wall. Further, the neutron spectra at, within, and leaving the vessel are substantially different.

To meet reactor pressure vessel radiation monitoring requirements, a variety of neutron flux and fluence detectors are employed, most of which are passive. Each detector must be validated for application to the higher flux and harder neutron spectrum of the research reactor "Test Region" and to the lower flux and degraded neutron spectrum at "Surveillance Positions." Required detectors must respond to neutrons of various energies so that multigroup spectra can be determined with accuracy sufficient for adequate damage response estimates. Detectors being used, developed, and tested for the program include radiometric (RM) sensors, helium accumulation fluence monitor (HAFM) sensors, solid state track recorder (SSTR) sensors, and damage monitor (DM) sensors.

The necessity for pressure vessel mockup facilities for physics-dosimetry investigations and for irradiation of metallurgical specimens was recognized early in the formation of the NRC program. Experimental studies associated with high- and low-flux versions of a pressurized water reactor (PWR) pressure vessel mockup are in progress in the US, Belgium, France, and United Kingdom. The US low-flux version is known as the ORNL Poolside Critical Assembly (PCA) and the high-flux version is known as the Oak Ridge Research Reactor (ORR) Poolside Facility (PSF), both located at Oak Ridge, Tennessee. As specialized benchmarks, these facilities provide well-characterized neutron environments where active and passive neutron dosimetry, various types of LWR-PV and support structure neutron field calculations, and temperature-controlled metallurgical specimen exposures are brought together.

The two key low-flux pressure vessel mockups in Europe are known as the Mol-Belgium-VENUS and Winfrith-United Kingdom-NESDIP facilities. The VENUS Facility is being used for PWR core source and azimuthal lead factor studies, while NESDIP is being used for PWR cavity and azimuthal lead factor studies. A third and important low-fluence pressure vessel mockup in Europe is identified with a French PV-simulator at the periphery of the Triton reactor. It served as the irradiation facility for the DOMPAC dosimetry experiment for studying surveillance capsule perturbations and through-PV-wall radial fluence and damage profiles (gradients) for PWRs of the Fessenheim 1 type.

Results of measurement and calculational strategies outlined here will be made available for use by the nuclear industry as ASTM standards. Federal Regulations 10 CFR 50 (Cf83) already requires adherence to several ASTM standards that establish a surveillance program for each power reactor and incorporate metallurgical specimens, physics-dosimetry flux-fluence monitors, and neutron field evaluation. Revised and new standards in preparation will be carefully updated, flexible, and, above all, consistent.

CONTENTS

CONTENTS

FIGURES

FIGURES (Cont'd)

FIGURES (Cont'd)

TABLES

TABLES (Cont'd)

TABLES (Cont'd)

TABLES (Cont'd)

TABLES (Cont'd)

TABLES (Cont'd)

TABLES (Cont'd)

ACRONYMS

ASTM	American Society for Testing and Materials
C/E	Calculated-to-Experimental Ratio
CF	Correction Factor
DM	Damage Monitor
DOMPAC	Triton Reactor Thermal Shield and Pressure Vessel Mockup
dpa	Displacements per Atom
dps	Displacements per Second
E-C	Experimental-Minus-Calculated Ratio
ENDF	Evaluated Nuclear Data File
EOL	End of Life
FIM	Field Ion Microscopy
FRDS	Fission/Radiometric Dosimetry Set
GW	Gradient Wire
HAFM	Helium Accumulation Fluence Monitor
HEDL	Hanford Engineering Development Laboratory
HSST	Heavy Section Steel Technology (Program)
LITR	Low-Intensity Test Reactor (ORNL)
LWR	Light Water Reactor
MPC	Metals Property Council
NDTT	Nil Ductility Transition Temperature
NESDIP	NESTOR Shielding and Dosimetry Improvement Program (UK)
NESTOR	PWR Mockup Reactor (Winfrith, UK)
NRC	Nuclear Regulatory Commission
NRE	Nuclear Research Emulsion
ORNL	Oak Ridge National Laboratory
ORR	Oak Ridge Research Reactor (ORNL)
PCA	Poolside Critical Assembly
PF	Perturbation Factor
PL	Power Level
PSF	Poolside Facility (ORNL)
PTS	Pressurized Thermal Shock
PV	Pressure Vessel

ACRONYMS (Cont'd)

PWR	Pressurized Water Reactor
RM	Radiometric Monitor
RPV	Reactor Pressure Vessel
SANS	Small-Angle Neutron Scattering
SDIP	Surveillance Dosimetry Improvement Program
SDMF	Simulated Dosimetry Measurement Facility
SF	Scale Factor
SPV	Simulated Pressure Vessel
SPVC	Simulated Pressure Vessel Capsule
SSC	Simulated Surveillance Capsule
SSTR	Solid-State Track Recorder
SVBC	Simulated Void Box Capsule
T/F	Thermal-to-Fast Neutron Fluence Ratio
TEM	Transmission Electron Microscopy
TLD	Thermoluminescent Dosimeter
VENUS	Low-Flux Pressure Vessel Mockup (Mol, Belgium)

ACKNOWLEDGMENTS

The following organizations are presently participating in the Light Water Reactor Pressure Vessel Surveillance Dosimetry Improvement Program (LWR-PV-SDIP) and will periodically contribute written reports, experimental data, or calculations.

Atomic Energy Research Establishment (AERE-H), Harwell, UK

Atomic Energy Research Establishment (AERE-W), Winfrith, UK

Babcock & Wilcox Company (B&W), USA

Battelle Memorial Institute (BMI), Columbus Laboratory, USA

Brookhaven National Laboratory (BNL), USA

Carolina Power and Light Company, USA

Centre d'Etude de l'Energie Nucleaire - Studiecentrum Voor Kernenergie (CEN/SCK), Mol, Belgium

Centre d'Etudes Nucleaires de Saclay (CEA, Saclay), Gif-sur-Yvette, France

Combustion Engineering, Inc. (CE), USA

Electric Power Research Institute (EPRI), USA

Engineering Services Associates (ENSA), USA

Florida Power and Light Company, USA

Fracture Control Corporation (FCC), USA

General Electric Vallecitos Nuclear Center (GE-VNC), USA

Hanford Engineering Development Laboratory (HEDL), USA

Institüt für Kernenergetik und Energiesysteme der Universitat Stuttgart (IKE), Stüttgart, Federal Republic of Germany

IRT Corporation (IRT), USA

Italian Atomic Power Authority (ENEL), Italy

Japan Atomic Energy Research Institute (JAERI), Japan

Kernforschungsanlage Jülich Gmbh (KFA), Germany

Kraftwerk Union, Germany

Maine Yankee Atomic Power Company, USA

Materials Engineering Associates (MEA), USA

National Bureau of Standards (NBS), USA

Oak Ridge National Laboratory (ORNL), USA

Radiation Research Associates (RRA), USA

Rockwell International Rocketdyne Division, USA

Rolls-Royce & Associates Limited (RR&A), Derby, UK

Science Applications Incorporated (SAI), USA

Ship Research Institute (SRI), Japan

Southwest Research Institute (SwRI), USA

Swiss Federal Institute for Reactor Research (EIR), Switzerland

University of Arkansas (UA), USA

University of California, Santa Barbara (UCSB), USA

University of Tennessee (UT), USA

University of Tokyo, Japan

University of Missouri, Rolla (UMR), USA

Westinghouse Electric Corporation - Nuclear Technology Division (W-NTD), USA

Westinghouse Electric Corporation - Research and Development Division (W-R&D), USA

Additional acknowledgment is due to B. R. Hayward, R. L. Knecht, W. F. Sheely, and H. H. Yoshikawa of HEDL for their constructive comments and help in the preparation and review of program documentation. Very special acknowledgment is given to Senior Technical Editor N. E. Kenny, who edited this document; to D. C. Smith of the HEDL Irradiation Environment Group; and to the HEDL Technical Publications, Word Processing, Graphics, and Duplicating personnel, who contributed to its preparation. A. Taboada is the NRC program manager for the LWR-PV-SDIP and his help and encouragement are greatfully acknowledged.

SUMMARY

HANFORD ENGINEERING DEVELOPMENT LABORATORY (HEDL)

A list of planned NUREG reports is presented in Table S-1. These reports address individual and combined pressurized water reactor (PWR) and boiling water reactor (BWR) physics-dosimetry-metallurgy issues. These will provide a reference base of information to support the preparation of the new set of LWR ASTM Standards (Figures S-1 and S-2).

Current limitations in trend curve analysis for the prediction of reactor pressure vessel embrittlement are examined. It is concluded that a number of systematic effects can exist because of differences in environmental conditions between test reactors and the actual irradiation conditions that accrue in the pressure vessel of an operating LWR commercial power plant. An irradiation test program is advanced to investigate these systematic effects and to produce the requisite data needed to correct for such systematic biases in trend curve analysis.

Gamma-ray induced displacement rates have been calculated for LWR-PV environments using absolute electron spectra observed in the PCA with the Janus probe. Gamma-ray displacement results are presented for the 1/4-T, 1/2-T, and 3/4-T locations of the 12/13 and 4/12 SSC configurations. In addition, the gamma-ray displacement rate at the simulated surveillance capsule (SSC) location was inferred using thermoluminescent dosimeter (TLD) gamma-ray dosimetry results obtained in the 4/12 SSC configuration at the PCA. Compared with neutron-induced displacement rates, the calculated gamma-ray induced displacement rates are negligible at all locations. The ratio of gamma-ray induced to neutron-induced displacement rates never exceeds roughly 5×10^{-3}.

A working relationship with the Metals Property Council (MPC) has been established whereby the Hanford Engineering Development Laboratory (HEDL) and the Nuclear Regulatory Commission (NRC) provide computational services, reports of results, and consultation; while the MPC and the American Society for Testing and Materials (ASTM) affiliates provide data, computational services, consultation, and advice.

The MPC has made available a data set consisting of chemistry and Charpy test results for 843 Charpy transition curve pairs (one irradiated specimen set and one unirradiated set in each pair). The data have been subjected to an extensive program of computer plotting (including stereo 3-D) to uncover any obvious correlations between Charpy upper-shelf drop and relevant variables, such as chemistry concentrations and fluence. In addition, more than 100 nonlinear least-squares fitting exercises have been performed with the same aim. Results to date indicate that Charpy upper-shelf drop is a function of fluence, copper content, and unirradiated upper-shelf energy. Nickel is a possible second chemistry variable, but the evidence is not conclusive.

A part of the PSF experiment has been analyzed in an attempt to determine measurment accuracies required for a definitive statement ranking fluence (E > 1.0 MeV) or dpa as being a preferred neutron exposure parameter. The analysis concerns required accuracies in mechanical property degradation and exposure parameters. The analysis only concerns the comparison of mechanical property degradation in pairs of test capsules having matched exposure values, i.e., the pair consisting of the D-T and simulated surveillance capsule two (SSC-2) capsules. Definite conclusions regarding the relative merits of fluence (E > 1.0 MeV) and dpa, if based solely on matched pair experiments of the type indicated, would require measurement accuracies that are difficult to obtain.

A physically based model for irradiation-induced hardening in pressure vessel steels was developed to incorporate neutron spectrum variations and damage rate effects. A spectrum damage index was found that gives improved correlations of change in nil ductility transition temperature (ΔNDTT) data with exposure. The new damage index, proportional to Frenkel pair production at 4°K, is based on measurements of change in resistivity caused by irradiation in various neutron spectra and with accelerated charged particles.

A damage rate effect, deduced from the correlation of ASTM A302B Reference plate, implied that thermal emission of point defects from clusters was controlling at both low- and high-temperature irradiations. However, the HSST A533B Reference plate 03 and two forging data sets in the poolside facility (PSF) irradiation did not support any discernable or significant damage rate effect. The two weld data sets showed a damage rate effect dominated by recombination. The rate effect for the welds explains why the high-rate simulated surveillance capsule SSC data showed a lower property change than the simulated pressure vessel (SPV) data.

Analytical procedures for correlating and applying surveillance capsule data have been developed and the relative importance of key environmental variables has been studied. Further, the potential value found by the application of these procedures has been tested and demonstrated using the PSF data base and selected PWR and BWR surveillance capsule physics-dosimetry-metallurgy results. The PWR and BWR plant-specific results, together with those of the Poolside Facility (PSF), support the existence of a material-dependent flux-level effect for pressure vessel and support structure steels. It is concluded that the existing and more generic trend curve model equations have, inadvertently, masked the existence of a very real and important flux-level effect.

The existing trend curves do not account for the observed flux-level effect and there may be other physical processes and/or damage mechanisms that contribute to the damage of pressure vessel steels under certain conditions; e.g., phosphorus in the presence of low copper concentrations, nitrogen impact on copper precipitation, etc. Any agreement between measured data and trend curve predictions, which do not adequately represent the important microstructural damage processes, could be fortuitous. The exception to such fortuitous agreememt could be limited to certain variable ranges where some processes may be of less relative importance.

Additional support for the validity of the conclusions of Sections HEDL-A, -E, and -F related to a flux-level effect comes from information presented by Serpan (Se85) and Hawthorne (Ha85) at the 13th Water Reactor Safety Research Information Meeting held at NBS in October 1985. Serpan states: "Increasing evidence for a dose rate effect has come from MEA this year, in the form of results from experiments that demonstrate greater embrittlement at low fluxes than previously anticipated (Ha85). This evidence has been so pronounced in reactor surveillance data that Revision 2 of Reg. Guide 1.99 on Radiation Damage to Reactor Vessel Materials has dropped the test reactor data and now includes only power reactor data which has the low flux-higher embrittlement characteristic."

It is important to understand that Serpan's statement is only partially correct, since it applies only to selected PV steels. That is, the correctness of the statement is dependent on a number of variables, including material properties, neutron exposure, flux-level, and composition. This is demonstrated by the combined results of Sections HEDL-E and -F where it is found that a PV steel may show a decrease, an increase or no change in the measured Charpy Shift with changes in flux level.

The existence of a flux-level effect has important implications for the U.S. commercial nuclear power industry, since accelerated locations have almost invariably been used in PV surveillance programs. These accelerated PV surveillance capsules have provided lead factors that have been applied to obtain projections of PV embrittlement. In fact, accelerated PV capsules comprise the largest existing data base for trend curve analyses. Consequently, it is clear that a flux-level effect would imply that some correction would be necessary in the application and interpretation of lead factors. Otherwise, the application of lead factors could not always ensure a conservative extrapolation. At the same time, it is apparent that any reduction in embrittlement afforded from low leakage cores, which are now being adopted in some U.S. power plants, must be quantified in terms of a flux-level effect, lest the predicted gain be under-or over-estimated.

OAK RIDGE NATIONAL LABORATORY

A list of planned NRC reports that support documentation for the set of ASTM standards for surveillance of LWR nuclear reactor pressure vessels and their support structures is provided with the status of each section for which ORNL has lead responsibility.

Calculated results of Phase I have been completed by CEN/SCK and ORNL, and Phase II results have been reported by CEN/SCK, ORNL, and WHC and are in good agreement.

In the fifth irradiation series of the Heavy Section Steel Technology (HSST) Program, capsules containing a variety of metallurgical test specimens were irradiated to fluences in the range of 1×10^{19} to 3×10^{19} neutrons/cm^2 ($E > 1.0$ MeV). To correltate radiation embrittlement to damage fluences, accurate determination of the neutron fluence spectra at the critical location of the test specimen is needed. The part of the neutron spectrum responsible for the radiation damage is characterized as "damage exposure parameter." Fluences for energies >1.0 MeV ($F > 1.0$ MeV) are the most widely used parameters; however, current thinking favors dpa in iron as better related to the physical mechanism of radiation damage. Fluences for energies >0.1 MeV ($F > 0.1$ MeV) are also considered since neutrons in the 0.1 to 1.0 MeV range are likely to contribute to the damage. In order not to prejudice future investigations, all three damage parameters $F > 1.0$ MeV, $F > 0.1$ MeV, and dpa are considered.

Neutron source distributions in the ORR core are obtained for three of the four SDMF experiments. In particular 3-D neutron sources are obtained for SDMF 1 (ORR PSF Startup Experiment), SDMF 2 (Westinghouse Perturbation Experiment), and SDMF 3 (B&W Perturbation Experiment). However, neutronics calculations are not available for SDMF 4 (Radiometric and Advanced Sensor Calibration Program). Distributions for SDMF 1 through 3 are reported as two 2-D distributions (one horizontal and one vertical). The 2-D distributions are obtained by integrating the 3-D distributions in the appropriate transverse direction.

ASTM Standards are being prepared to support recommendations for proposed modifications, data bases, and methodologies related to Codes and Regulatory Guides.

An expanded and revised paper on the determination and significance of covariances in neutron spectrum adjustment methods is reported and was submitted to the E10.05.01 Task Group on Uncertainty Analysis and Computational Procedures for further consideration and comment.

TABLE S-1

PROGRAM DOCUMENTATION

NRC Report No.	Vol No.	Lab Report No.	LWR-PV-SDIP Program No.*	Issue Date	Editors
NUREG/CR-1861 (PCA Physics-Dosimetry)		HEDL-TME 80-87	NUREG 1-1	July 1981	WN McElroy
NUREG/CR-3295 (PSF Metallurgy)	Vol 1 Vol 2	MEA-2017, Vol 1 MEA-2017, Vol 2	NUREG 13-1 NUREG 13-2	April 1984 April 1984	JR Hawthorne JR Hawthorne
NUREG/CR-3318** (PCA Physics-Dosimetry)	--	HEDL-TME 85-2	NUREG 1-2	September 1984 (Revised 9/86)	WN McElroy
NUREG/CR-3319** (Power Reactor Physics-Dosimetry)	--	HEDL-TME 85-3	NUREG 4	August 1985	WN McElroy
NUREG/CR-3320 (PSF SSC/SPVC Experiments & Blind Test)	Vol 1** Vol 2** Vol 3** Vol 4**	HEDL-TME 85-4 HEDL-TME 85-5 HEDL-TME 86-XX HEDL-TME 86-XX	NUREG 3 NUREG 2 NUREG 5 NUREG 6-1	January 1986 March 1986 June 1986 August 1986	WN McElroy WN McElroy WN McElroy WN McElroy
(PSF SVBC Experiments)	Vol 5	EPRI/PCC/W-NTD	NUREG 6-4	December 1986	JR Hawthorne TU Marston
NUREG/CR-3320 (PSF SSC/SPVC Experiments & Blind Test)	Vol 6	CEN/SCK XX	NUREG 6-2	September 1986	PH Vanderbroeck JR Hawthorne A. Fabry
NUREG/CR-3321** (SDMF Physics-Dosimetry)	--	HEDL-TME 86-XX	NUREG 7	September 1987	WN McElroy FBK Kam JA Grundl ED McGarry
NUREG/CR-3322** (Test Reactor Physics-Dosimetry)	--	HEDL-TME 87-XX	NUREG 8	September 1987	WN McElroy FBK Kam
NUREG/CR-3323 (VENUS Physics-Dosimetry)	Vol 1 Vol 2	CEN/SCK-XX CEN/SCK-XX	NUREG 9-1 NUREG 9-2	September 1986 September 1987	A. Fabry WN McElroy ED McGarry
NUREG/CR-3324 (NESDIP Physics-Dosimetry)	Vol 1 Vol 2 Vol 3 Vol 4 Vol 5	AEEW-R 1736 AEEW-R XXXX AEEW-R XXXX AEEW-R XXXX AEEW-R XXXX	NUREG 10-1 NUREG 10-2 NUREG 10-3 NUREG 10-4 NUREG 10-5	January 1984 September 1986 September 1987 September 1988 September 1988	J. Butler M. Austin WN McElroy
NUREG/CR-3325 (Gundremmingen Physics-Dosimetry-Metallurgy)		HEDL-TME 87-XX	NUREG 11-1	September 1987	WM McElroy
NUREG/CR-3326** (Test Reactor Metallurgy)		HEDL-TME 88-XX	NUREG 12	September 1988	WN McElroy FBK Kam

*These program numbers are not to be used on final reports.
**Loose-leaf document.

Revised 10/15/85

TABLE S-1 (Cont'd)

NUREG/CR-1861 (Issue Date: July 1981)
PCA Experiments and Blind Test - W. N. McElroy, Editor

This document provides the results of calculations and active and passive physics-dosimetry measurements for the PCA 8/7 and 12/13 configurations X/Y: water gaps (in cm) from the core edge to the thermal shield (X) and from the thermal shield to the vessel wall (Y). The focus of the document is on an international Blind Test of transport theory methods in LWR-PV applications involving eleven laboratories, including reactor vendors.

NUREG/CR-3295
PSF Metallurgy - R. Hawthorne, Editor

Vol. 1 (Issue Date: April 1984)
Notch Ductility and Fracture Toughness Degradation of A302-B & A533-B Reference Plate from PSF Simulated Surveillance and Through-Wall Irradiation Capsules

Beyond scope of title, this document will support analysis of the PSF Blind Test and provide as-built documentation and final PSF A302-B and A533-B reference plate metallurgical results for SSC and SPVC.

Vol. 2 (Issue Date: April 1984)
Postirradiation Notch Ductility and Tensile Strength Determinations for PSF Simulated Surveillance and Through-Wall Specimen Capsules

Beyond scope of title, this document will support analysis of the PSF Blind Test and provide as-built documentation and final PSF (NRC, EPRI, RR&A, CEN/SCK, and KFA) steel metallurgical results generated by MEA for SSC and SPVC.

NUREG/CR-3318 (Issue Date: September 1984, Revised September 1986)
PCA Dosimetry in Support of the PSF Physics-Dosimetry-Metallurgy Experiments (4/12, 4/12 SSC configurations and update of 8/7 and 12/13 configurations) - W. N. McElroy, Editor

Beyond scope of title, this document will support analysis of the PSF Blind Test and updates NUREG/CR-1861, "PCA Experiments and Blind Test," (Mc81).

NUREG/CR-3319 (Issue Date: August 1985)
LWR Power Reactor Surveillance Physics-Dosimetry Data Base Compendium - W. N. McElroy, Editor

In loose-leaf form this document will provide new or reevaluated exposure parameter values [total, thermal, and fast (E > 1.0 MeV) fluences, dpa, etc.] for individual surveillance capsules removed from operating PWR and BWR power plants. As surveillance reports are reevaluated with FERRET-SAND, this document will be revised. The corresponding metallurgical data base is provided in the loose-leaf EPRI NP-2428 (Mc82c).

TABLE S-1 (Cont'd)

NUREG/CR-3220
PSF Physics-Dosimetry-Metallurgy Experiments:

Vol. 1 (Issue Date: January 1986)
PSF Experiments Summary and Blind Test Results - W. N. McElroy, Editor

This document will provide PSF experiment summary information and the results of the comparison of measured and predicted physics-dosimetry-metallurgy results for the PSF experiment. This document will also contain (in an appendix) each participants' final report.

Vol. 2 (Issue Date: March 1986)
PSF Startup Experiment - W. N. McElroy, Editor

Beyond scope of title, this document will support analysis of the PSF Blind Test and provide experimental conditions, as-built documentation, and final PSF physics-dosimetry results for the startup experiment.

Vol. 3 (Issue Date: June 1986)
PSF Physics-Dosimetry Program - W. N. McElroy, Editor

Beyond scope of title, this document will support analysis of the PSF Experiment and Blind Test and provide experimental conditions, as-built documentation, and final PSF physics-dosimetry results for SSC, SPVC and SVBC.

Vol. 4 (Issue Date: August 1986)
PSF Metallurgy Program - W. N. McElroy, Editor

Beyond scope of title, this document will support analysis of the PSF Experiments and Blind Test and provide experimental conditions, as-built documentation, and final metallurgical data on measured property changes in different pressure vessel steels for SSC-1 and -2 positions, and the (SPVC) simulated PV locations at the 0-T (inner surface), 1/4-T, and 1/2-T positions of the 4/12 PWR PV wall mockup. The corresponding SSC-1, SSC-2, and SPVC locations' neutron exposures are $\sim 2 \times 10^{19}$, $\sim 4 \times 10^{19}$, $\sim 4 \times 10^{19}$, $\sim 2 \times 10^{19}$, and $\sim 1 \times 10^{19}$ n/cm^2, respectively, for a ~550°F irradiation temperature. It will also contain and/or reference available damage analysis results for SVBC using the Vol. 5 metallurgical data base.

Vol. 5 (Issue Date: December 1985)
PSF Simulated Void Box Capsule (SVBC) Charpy and Tensile Metallurgical Test Results - J. S. Perrin and T. U. Marston, Editors

Beyond scope of title, this document will provide experimental conditions, as-built documentation, and final Charpy and tensile specimen measured property changes in PV support structure and reference steels for the ex-vessel SVBC simulated cavity (void box) for a neutron exposure on the order of 10^{16} n/cm^2 (E > 1.0 MeV) for ~95°F irradiation temperature. This estimate is based on preliminary ORNL calculations, as yet unsubstantiated by measurements.

Vol. 6 (Issue Date: September 1986)
PSF Simulated Surveillance Capsule (SSC) Results - CEN/SCK/MEA - Ph. Van Asbroech, A. Fabry, and R. Hawthorne, Editors

This document, to be issued by CEN/SCK, will provide CEN/SCK/MEA metallurgical data and results from the Mol, Belgium PV steel irradiated in the SSC position for the ORR-PSF physics-dosimetry-metallurgy experiments.

NUREG/CR-3321 (Issue Date: September 1987)
Service Laboratory Procedure Verification and Surveillance Capsule Perturbations - W. N. McElroy, F. B. K. Kam, J. Grundl, and E. D. McGarry, Editors

This loose-leaf volume will provide results to certify the accuracy of service laboratory procedures to determine exposure parameter and perturbation effects for surveillance capsules removed from PWR and BWR power plants.

NUREG/CR-3322 (Issue Date: September 1987)
LWR Test Reactor Physics-Dosimetry Data Base Compendium - W. N. McElroy, Editor

This loose-leaf volume will reference and/or present results from FERRET-SAND, LSL, and other least-squares-type code analyses of physics-dosimetry for US (BSR, PSF, SUNY-NSTF [Buffalo], Virginia, etc.), UK (DIDO, HERALD, etc.), Belgium (BR-2, etc.), France (Melusine, etc.), Germany (FRJ1, FRJ2, etc.), and other participating countries. It will provide needed and consistent exposure parameter values [total, thermal, and fast (E > 1.0 MeV) fluences, dpa, etc.] and uncertainties for correlating test reactor property change data with those obtained from PWR and BWR power plant surveillance capsules. NUREG/CR-3319 and -3322 will serve as reference physics-dosimetry data bases for correlating and applying power and research reactor-derived steel irradiation effects data. These power reactor metallurgical data are provided in EPRI NP-2428 (Mc82c).

NUREG/CR-3323
VENUS PWR Core Source and Azimuthal Lead Factor Experiments and Calculational Tests:

Vol. 1 (Issue Date: September 1986)
Clean (^{235}U) Core Configuration - A. Fabry, W. N. McElroy, and E. D. McGarry, Editors

Vol. 2 (Issue Date: September 1987)
Burnt (^{235}U and ^{239}Pu) Core Configuration - A. Fabry, W. N. McElroy, and E. D. McGarry, Editors

These two documents, to be prepared by CEN/SCK and other participants, will provide VENUS-derived reference physics-dosimetry data on active, passive, and calculational dosimetry studies involving CEN/SCK, HEDL, NBS, ORNL, and other

TABLE S-1 (Cont'd)

Vol. 2 (Issue Date: September 1987) (Cont'd)

LWR program participants for a clean (^{235}U) and a burnt ($^{235}U + ^{239}Pu$) core configuration.

NUREG/CR-3324
NESDIP PWR Cavity and Azimuthal Lead Factor Experiments and Calculational Tests:

Vol. 1 (Issue Date: January 1984)
PCA Replica Experiments: Part I - Winfrith Measurements and Calculations - J. Butler and M. Austin, Editors

Vol. 2 (Issue Date: September 1986)
PCA Replica Experiments: Part II - Further Analysis Including HEDL Measurements - J. Butler and M. Austin, Editors

These two documents, to be prepared by Winfrith-RR&A and other participants, will provide NESDIP-PCA replica-derived reference physics-dosimetry data on active, passive, and calculational dosimetry studies involving Winfrith, CEN/SCK, HEDL, NBS, and other LWR program participants.

Vol. 3 (Issue Date: September 1987)
NESTOR Dosimetry Improvement Programme: Radial Shield Experiments - J. Butler, M. Austin, and W. N. McElroy, Editors

This document will provide NESDIP cavity-derived reference physics-dosimetry data based a Winfrith startup program and Winfrith and LWR-PV-SDIP participants' calculational results.

Vol. 4 (Issue Date: September 1988)
NESTOR Dosimetry Improvement Programme: Cavity Simulation Experiments - J. Butler, M. Austin, and W. N. McElroy, Editors

This document will provide NESDIP 20- and 70-centimeter cavity-derived reference physics-dosimetry data on active, passive, and calculational dosimetry studies involving Winfrith, RR&A, HEDL, ORNL, NBS, and other LWR program participants. Results of zero-centimeter cavity studies will also be discussed and reported, as appropriate.

Vol. 5 (Issue Date: September 1988)
NESTOR Dosimetry Improvement Programme: Nozzle Simulation Experiment - J. Butler, M. Austin, and W. N. McElroy, Editors

This document will provide NESDIP cavity-nozzle-derived reference physics-dosimetry data on active, passive, and calculational dosimetry studies.

NUREG/CR-3325 (Issue Date: September 1987)
Gundremmingen HEDL, W-NTD, and IKE Physics-Dosimetry-Metallurgy Program Results - W. N. McElroy, Editor

This documents will provide results that support the NRC fracture mechanics analysis of pressure vessel base metal using Charpy, tensile, compact tension, and full-wall thickness metallurgical specimens for Gundremmingen. Results of W-NTD 1-D and IKE 3-D physics calculation will be referenced and appropriate results will be included in this document. HEDL dosimetry specimens will be obtained as a function of distance through the PV wall. Some of these specimens will be analyzed for boron and helium by RI. Previous surveillance capsule and cavity physic-dosimetry-metallurgy results will be correlated with new in-wall vessel results, as appropriate. Appropriate PSF results will be used to help NRC obtain the best possible overall data correlations.

NUREG/CR-3326 (Issue Date: September 1988)
LWR Test Reactor Irradiated Nuclear Pressure Vessel and Support Structure Steel Data Base Compendium - W. N. McElroy and F. B. K. Kam, Editors

This loose-leaf volume will reference and/or present data and results for selected metallurgical experiments performed in the US (BSR, PSF, SUNY-NSTF [Buffalo], Virginia, etc.), UK (DIDO, HERALD, etc.), Belgium (BR-2, etc.), France (Melusine, etc.), Germany (FRJ1, FRJ2, etc.), and other participating countries. It will provide needed and consistent Charpy, upper-shelf energy, tensile, compact tension, compression, hardness, etc. property change values and uncertainties. With NUREG/CR-3322 physics-dosimetry data, NUREG/CR-3326 provides: 1) a more precisely defined and representative research reactor physics-dosimetry-metallurgy data base, 2) a better understanding of the mechanisms causing neutron damage, and 3) tested and verified exposure data and physical damage correlation models, all of which are needed to support the preparation and acceptance of the ASTM E706(IE) Damage Correlation and ASTM E706(IIF) ΔNDTT with fluence standards and future revisions of Reg. Guide 1.99.

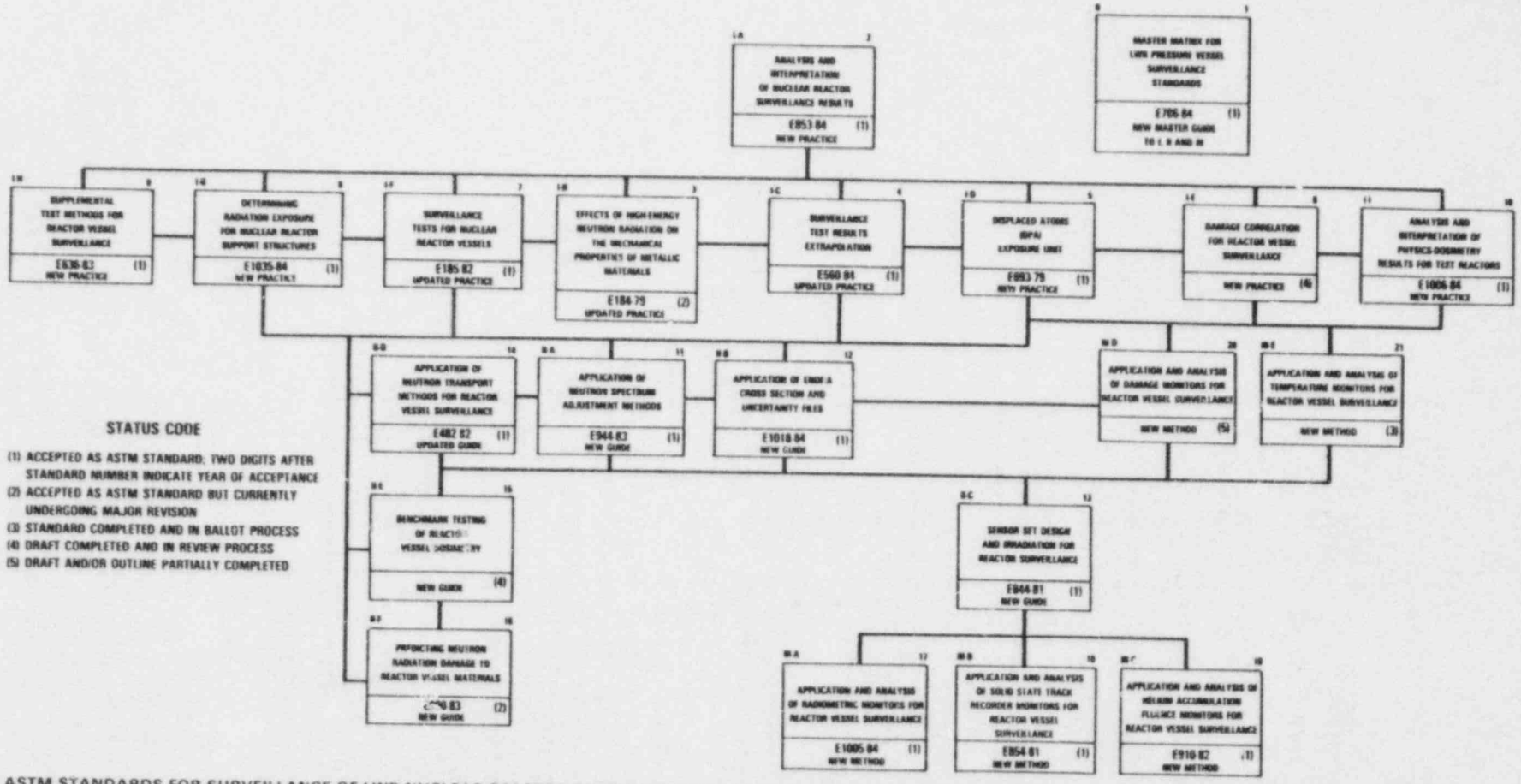

ASTM STANDARDS FOR SURVEILLANCE OF LWR NUCLEAR REACTOR PRESSURE VESSELS AND SUPPORT STRUCTURES

HEDL 8407 057

FIGURE S-1. ASTM Standards for Surveillance of LWR Nuclear Reactor Pressure Vessels and Their Support Structures.

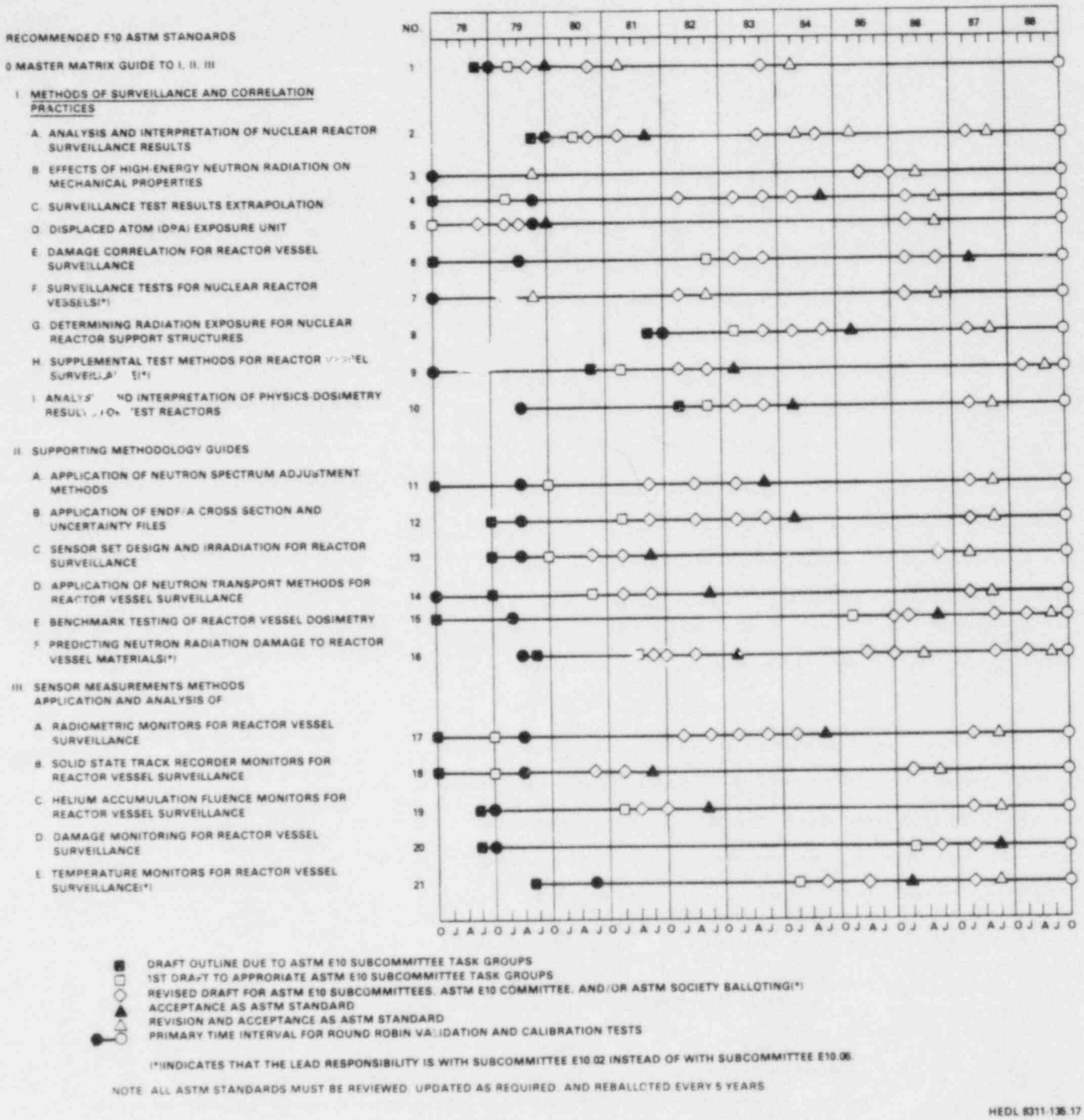

FIGURE S-2. Preparation, Validation, and Calibration Schedule for LWR Nuclear Reactor Pressure Vessels and Their Support Structure Surveillance Standards.

HANFORD ENGINEERING DEVELOPMENT LABORATORY

(HEDL)

A. CURRENT LIMITATIONS OF TREND CURVE ANALYSIS FOR THE PREDICTION OF REACTOR PRESSURE VESSEL EMBRITTLEMENT

Raymond Gold and W. N. McElroy (HEDL)

Objective

The objectives of the present work are to provide insight and understanding into the origins of current limitations in trend curve analyses and to plan irradiation test programs that would produce data to help overcome current deficiencies in trend curve models.

Summary

Current limitations in trend curve analysis for the prediction of reactor pressure vessel embrittlement are examined. It is concluded that a number of systematic effects can exist because of differences in environmental conditions between test reactors and the actual irradiation conditions that accrue in the pressure vessel of an operating light water reactor (LWR) commercial power plant. An irradiation test program is advanced to investigate these systematic effects and to produce the requisite data needed to correct for such systematic biases in trend curve analysis.

Accomplishments and Status

1.0 Introduction

In operating light water reactor (LWR) commercial power plants, neutron radiation induces embrittlement of the pressure vessel (PV) and its support structures. Since the PV and its support structures are nonreplaceable power plant components, embrittlement of these components can limit the effective operating lifetime of the plant. In recognition of this safety issue, the U.S. Nuclear Regulatory Commission (NRC) established the LWR-PV Surveillance Dosimetry Improvement Program (SDIP) in 1977 for improving, maintaining, and standardizing neutron dosimetry, damage correlation, and the associated reactor analysis procedures used for predicting the integrated effect of neutron exposure to LWR-PVs and their support structures. A vigorous research effort attacking the same measurement and analysis problems has gone forward worldwide, and strong cooperative links between the NRC-supported activities at HEDL, ORNL, MEA, and NBS and those supported by CEN/SCK (Mol, Belgium), EPRI (Palo Alto, USA), KFA (Jülich, Germany) and several U.K. laboratories have been established. The major benefit of this program has been and continues to be a significant improvement in the accuracy of the assessment of the remaining safe operating lifetime of LWR-PVs (Mc85).

Neutron-induced PV embrittlement has been recognized as a serious problem for many years, as attested to by surveillance dosimetry programs instituted over the years in U.S. LWR commercial power plants (St83a). While considerable investigation and study have already been conducted over the years on neutron-induced embrittlement of PV steels, the details and subtlelies of this problem apparently still continue to unfold. The complexity of this phenomenon can not be overemphasized. To illustrate this complexity, many scientific disciplines are required to attack this problem. These efforts can be broadly classified into three main disciplines, namely:

- Neutron Metrology or Dosimetry
- Reactor Physics
- Material Science or Metallurgy

To further illustrate the profound nature of this problem, many factors have been identified as basic contributors to radiation-induced PV embrittlement. Some of these factors are summarized in Table HEDL-1. It should be stressed that each of these factors can comprise many variables. For example, factor 1 of Table HEDL-1 concerning composition and microstructure possesses, perhaps, the most variables. Moveover, Table HEDL-1 does not purport to be an exhaustive list of contributory factors since, for example, factors related to the actual physical or metallurgical tests of steel property changes have not been included here.

TABLE HEDL-1

PHYSICS, DOSIMETRY, AND METALLURGY FACTORS
CONTRIBUTING TO PV EMBRITTLEMENT

1) Steel chemical composition and microstructure

2) Steel irradiation temperature

3) Power plant configurations and dimensions - core edge to surveillance to vessel wall to support structure positions

4) Core power distribution

5) Reactor operating history

6) Reactor physics computations

7) Selection of neutron exposure units

8) Dosimetry measurements

9) Neutron spectral effects

10) Neutron dose rate effects

Owing to the complexity of this embrittlement phenomenon, experimental and calculational strategies have been developed in the LWR-PV-SDIP, which are in turn being made available for use by the U.S. nuclear power industry as ASTM Standards. In fact, a primary objective of the multi-laboratory LWR-PV-SDIP is to prepare an updated and improved set of dosimetry, damage correlation, and associated reactor analysis ASTM Standards for LWR-PV irradiation surveillance programs.

While a detailed review of all of these efforts would carry us too far afield, some insight into the full extent of these activities can be gained by examining the ASTM Master Matrix for these standards (As82), which is shown in Figure S-1. Federal Regulation 10CFR50 (Cf83) already calls for adherence to several ASTM Standards in LWR-PV irradiation surveillance. Revised and new standards in preparation under this matrix will be carefully structure to be up-to-date, flexible, and, above all, consistent so that they can provide guidance to the U.S. nuclear power industry in meeting regulatory requirements.

Beyond these needs will be the consideration of what additional criteria will be required for design changes, licensing, regulation, surveillance and research for the safe operation of plants that are operated beyond their present design life; i.e., the definition of the requirements for new and expanded physics-dosimetry-metallurgy information that will be needed to support emerging and new plant life-extension programs (in the range up to, say 50 years or more). One perspective on these activities is forecasted in Figure HEDL-1.

In order to define the effects of neutron radiation damage on LWR pressure-temperature operating limits as well as for fracture toughness assessment of power reactor PV, trend curves for the prediction of PV embrittlement must be used. Appendices A, G, and H of 10CFR50 and U.S. Nuclear Regulatory Commission (NRC) Regulatory Guide 1.99 (Re77), which provide the appropriate procedures to be followed, necessitate plant-specific assessment and projection to end-of-life (EOL) of radiation-induced PV embrittlement. In the absence of verified plant specific trend curves, very general PV embrittlement curves have been developed and used to make the required projections. In such trend curves, the two main measures of radiation damage are the adjusted reference nil-ductility temperature RT_{NDT}(RT_{NDT} initial + ΔRT_{NDT}) and the decrease in upper-shelf energy level determined from Charpy V notch impact tests. Current measures of neutron exposure most commonly used in trend curve analyses are fluence >1 MeV and displacements per atom (dpa). The applicability and conservatism of general trend curve predictions are checked and verified by plant-specific surveillance program data during the operating service life of a given pressure vessel.

The importance of determining and specifying the accuracy of these predictions and projections has increased significantly as a result of new NRC regulations regarding required protection against pressurized thermal shock (PTS) events in PWRs (Di82). The screening criterion proposed by NRC is a "reference temperature" of 270°F for plate materials and axial welds and

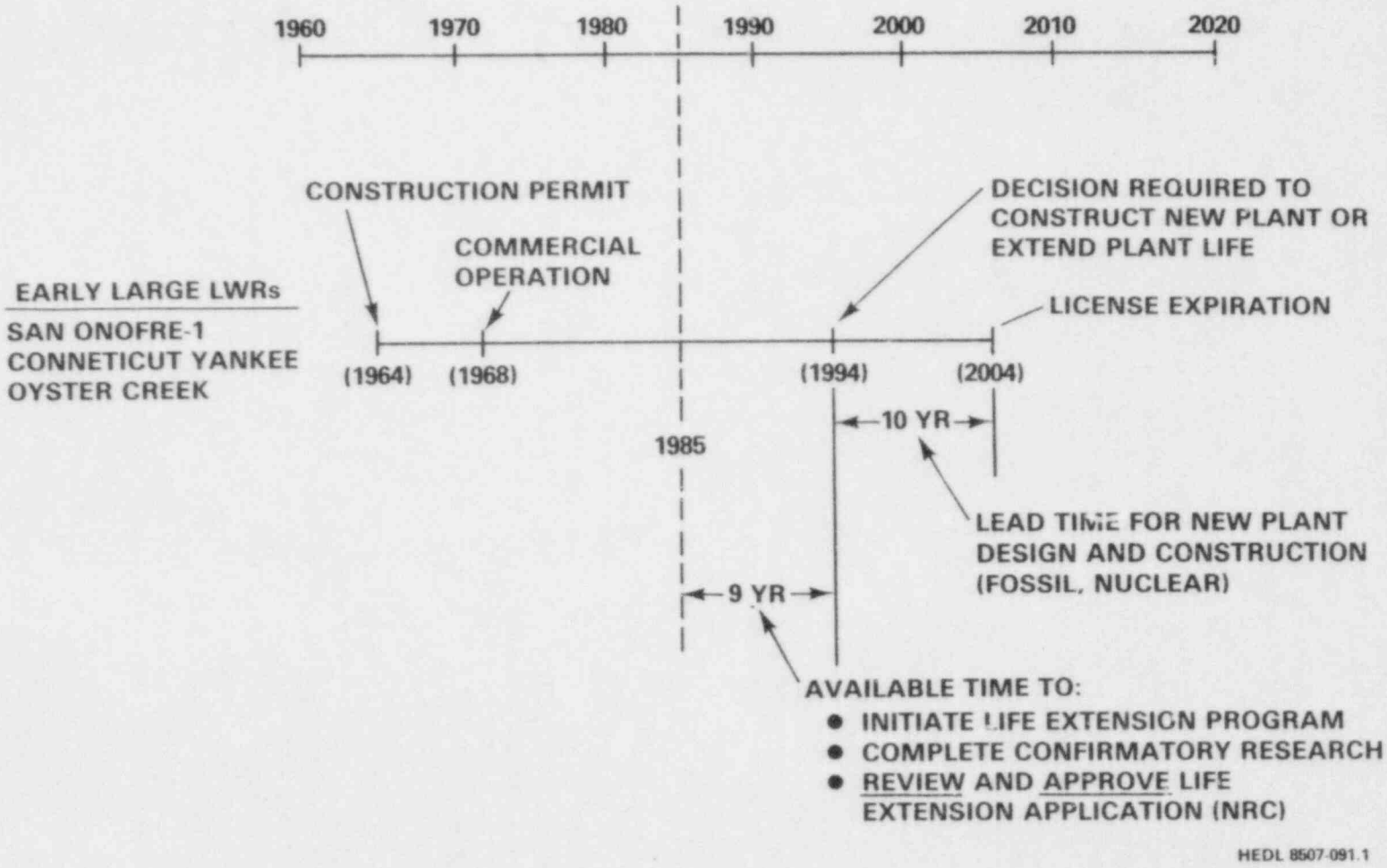

FIGURE HEDL-1. A Scenario for the Early Initiation of LWR Extension Research.

300°F for circumferential welds. Below these temperatures, the risk from PTS events would be considered acceptable. The risk above that level also might prove to be acceptable, but a demonstration would require plant-specific evaluations and, possibly, modifications to existing equipment, systems and procedures.

From this discussion, it is apparent that trend curves play a central role in the assessment of PV embrittlement of operating LWR power plants. Consequently, it is imperative that the limitations of trend curve analyses be clearly delineated. To this end, Section 2.0 considers limitations in both the development as well as the application of trend curves. The current status of trend curve development is examined in Section 3.0, especially from the viewpoint of any deficiencies that may exist for predictions in actual LWR operating power plants. An initial attempt to develop an irradiation test matrix that overcomes some identified deficiencies is described in Section 4.0.

2.0 Limitations of Current Trend Curve Analyses

2.1 Mathematical Formulation

Difficulties that arise in the generation of trend curves surfaced at a special session on PTS and reactor materials which was held at the 1984 annual meeting of the American Nuclear Society (Ma84). One team of experts reported that a definitive correlation existed between copper concentration and ΔRT_{NDT}. In support of their contention, they introduced a physical model in which copper precipitates acted to stabilize damage sites. Still another team of researchers found no statistically significant evidence to support any correlation between copper content and ΔRT_{NDT} in a large weld group under study. Further discussions centered on the effects of nickel with some groups reporting a correlation of nickel content with ΔRT_{NDT} and other groups finding no basis for such a correlation. Still other groups maintained the existence of a cross correlation between copper content, nickel content, and ΔRT_{NDT}.

These differences of view imply the existence of systematic effects that are either not recognized or fully appreciated. The origin of such difficulties can range from the trivial to the profound. For example, it could be as simple as one team working with base metal as opposed to another team that considered weldments. Or it could be more subtle, like both teams using the same material but the history of the material used by each team could be different, e.g., one team might have used more annealed material and the other team used more cold-worked material. Even more subtle systematic effects may be responsible, such as a flux-level effect or a saturation phenomenon, see Sections HEDL-E and F.

An even more profound issue has just started to emerge in trend curve analysis. It concerns the assumption of separability between the chemistry and the exposure dose dependence of ΔRT_{NDT}. Indeed, in the generation of trend curves, it has almost universally been assumed that

$$\Delta RT_{NDT} = F_1(C) \cdot F_2(D), \tag{1}$$

where F_1 is a function of the important chemistry variables, C, and F_2 is a function of the neutron exposure dose variables, D. While this assumption has been adopted, no doubt, because of the convenience and simplicity it introduces in least squares statistical analyses, to our knowledge separability of these two classes of variables has never been rigorously proved. To the contrary, many instances have arisen that indicate that this assumption may not be valid. Recent analyses of the PSF experiment also tend to illustrate this point (Gu85,Mc84h).

Further insight into the physical plausibility of this assumption can be gained from a heuristic extension of Odette's treatment of microvoid density (Pe84). In this treatment, the microvoid density N_{mv} is given by

$$\dot{N}_{mv} = G_{mv} - N_{mv}/\tau_{mv}, \tag{2}$$

where the production term of microvoids G_{mv} is given by

$$G_{mv} = \phi\sigma_{mv}, \tag{3}$$

with ϕ the scalar neutron flux and σ_{mv} the microvoid production cross section. The term N_{mv}/τ_{mv} in Equation (2) represents the thermal annealing rate, where τ_{mv} is the microvoid thermal annealing time.

This equation does not account for the possibility that microvoids could be stabilized by chemical variables such as copper, nickel, and/or helium content in such a way as to prevent or deter annealing. Such a speculation can be investigated by introducing a stabilization term into Equation (2) of the form $+N_{mv}/\tau_S$, where τ_S is the stabilization time. Consequently, a more general description of the microvoid density could be written as

$$\dot{N}_{mv} = G_{mv} - N_{mv}/\tau_{mv} + N_{mv}/\tau_S, \tag{4a}$$

or

$$\dot{N}_{mv} = G_{mv} - \left(\frac{1}{\tau_{mv}} - \frac{1}{\tau_s}\right) N_{mv}. \tag{4b}$$

Here the stabilization time τ_s would obviously depend on the chemical composition and microstructure of the given steel, so that τ_s must generally be assumed to depend on all chemical variables.

Equation (4b) can be written in the form

$$\dot{N}_{mv} = G_{mv} - (1-\alpha)\, N_{mv}/\tau_{mv}, \tag{5a}$$

where

$$\alpha = \tau_{mv}/\tau_s. \tag{5b}$$

Implicit in this description is that $\tau_{mv} \leq \tau_s$; otherwise, another net production term would be added in Equation (4). Consequently, the parameter α satisfies the condition.

$$0 \leq \alpha \leq 1. \tag{6}$$

The solution of Equation (5a) is given by

$$N_{mv} = \frac{\Phi\sigma_{mv}\,\tau_{mv}}{(1-\alpha)} \left\{1-\exp\left[-(1-\alpha)\Phi t/\Phi\tau_{mv}\right]\right\}. \tag{7}$$

Equation (7) provides some very simple physical implications. Since the parameter $\alpha = \tau_{mv}/\tau_s$ generally depends on chemistry variables, this time-dependent representation of the microvoid density obviously does not satisfy any separability criterion. From Equation (7), one finds a saturation value of the microvoid density, N^s_{mv}, which is given by

$$\lim_{t \to \infty} N_{mv} = N_{mv}^{S} = \frac{\phi \sigma_{mv} \tau_{mv}}{(1-\alpha)} \quad . \tag{8}$$

Here the saturated microvoid density, N_{mv}^{S}, depends not only on flux ϕ but chemistry variables as well. In fact, since one would expect τ_S to decrease, or α to increase, with increasing content of trace constituents such as copper, nickel, or helium, then the saturation value would also increase with increasing contents of these trace constituents. The attainment of saturation occurs at a fluence value that also depends on chemical variables through both α and τ_{mv}. In so far as the α-dependence is concerned, increasing trace constituents would shift the onset of saturation to higher fluences.

Equation (7) also implies the existence of a flux-level effect. This can be illustrated in terms of the neutron exposure dose D, which can be defined as

$$D = \int_0^{\infty} \int_0^{t} \phi(E_n, t') dE_n \, dt' \quad , \tag{9}$$

where the neutron flux depends generally on both neutron energy E_n and time t'. Here t is the time duration of the irradiation. For steady-state irradiations of duration t, Equation (9) reduces to

$$D = \phi \cdot t \quad . \tag{10}$$

Consequently for steady-state irradiations, Equation (7) becomes

$$N_{mv} = \frac{\phi \sigma_{mv} \cdot \tau_{mv}}{(1-\alpha)} \left\{ 1 - \exp \left[-(1-\alpha) \, D/\phi \tau_{mv} \right] \right\}. \tag{11}$$

Hence, even for the conceptually simple case of steady-state irradiations, as described by Equation (11), one finds that N_{mv} depends on both D and ϕ. Moreover, since

$$\partial N_{mv}/\partial \phi = (N_{mv} - \sigma_{mv} \cdot D)/\phi \leq 0 \quad , \tag{12}$$

one finds that for the same irradiation dose, D, the microvoid density generated at higher flux levels is lower for this simplified formulation of the problem.

On the basis of even this oversimplified description, it is not surprising to learn that flux-level effects have indeed been observed in the PSF metallurgical test (Gu84d), see Sections HEDL-E and F. While a number of materials were irradiated in the PSF experiment, the most readily observable flux-level effects were discerned for the ASTM A302B Reference plate and the Code R A533B Weld Material. The first indications of a flux-level effect were observed with the British Code R Reference weld material (Da85), a highly radiation sensitive standard material that provided Charpy shift measurements of a few percent accuracy. On the other hand, measurements attained with the other four materials were of considerably less accuracy and a flux-level effect was, therefore, difficult to resolve for these materials. This experience under-scores the need for higher quality data bases in trend curve analyses.

2.2 Variable Effects, Extrapolation, and Lead Factors

The existence of a flux-level effect has important implications for the U.S. commercial nuclear power industry, since accelerated locations have almost invariably been used in PV surveillance programs. These accelerated PV surveillance capsules have provided lead factors that have been applied to obtain projections of PV embrittlement. In fact, accelerated PV capsules comprise the largest existing data base for trend curve analyses. Consequently, it is clear that a flux-level effect would imply that some correction would be necessary in the application and interpretation of lead factors. Otherwise, the application of lead factors could not always ensure a conservative extrapolation. At the same time, it is apparent that any reduction in embrittlement afforded from low leakage cores, which are now being adopted in some U.S. power plants, must be quantified in terms of a flux-level effect, lest the predicted gain be under- or over-estimated.

The flux-level effect discussed here illustrates a general limitation of trend curve analysis that arises through the inadequacy of the data base. Data bases used for trend curve analyses have various origins. Surveillance capsule measurements comprise the largest available data pool and have, therefore, been used most extensively. However, none of these data bases represents the specific conditions of radiation exposure that exists within an actual pressure vessel. As a consequence, trend curves developed by least-squares analyses of these data bases can systematically deviate from the radiation damage that actually accrues in a pressure vessel. This systematic deviation stems from the lack of the data base to truly represent the irradiation conditions that actually arise in the pressure vessel of operating power plants.

The flux-level effect discussed above is just one of a number of systematic effects that can arise because of inadequacy in the data base. Indeed, the neutron spectral dependence of PV embrittlement has been recognized for some time (As82). In recognition of this fact, current trend curve analyses employ, for neutron exposure dose, either the fast neutron fluence, usually above 0.1 MeV or 1.0 MeV, or dpa (As79d). For low-temperature (<230°C)

irradiation of the ASTM A302B Reference plate, Simons has shown in Section HEDL-E that Frenkel pairs per atom (fppa) is a much better spectrum damage index than dpa for the existing ASTM A302B research reactor derived physics-dosimetry-metallurgy data base. At higher temperature (<288°C), however, dpa and fppa appear to be equally good indices. Further, recent analyses reveal that even a correlation with thermal neutron intensity may exist (Mc84h).

This recent conclusion regarding a thermal neutron effect is not a unique interpretation of the data. Indeed, a collection of systematic effects caused by flux level, helium production and gamma-ray heating cannot be ruled out. The intensity of the gamma-ray field found in PV environments is highly correlated with thermal neutron intensity. Consequently, the thermal neutron effect recently reported (Mc84h) may actually arise from a combination of effects, including annealing from gamma-ray heating. In this event, one must recognize that gamma-ray heating at surveillance capsule locations is considerably higher than that which is attained within a pressure vessel. Therefore, the annealing rate from gamma heating at the surveillance capsule location would be considerably higher than the annealing rate from gamma heating within the pressure vessel. Hence, gamma-ray heating could be another factor responsible for introducing a systemic bias in trend curve analyses that use surveillance capsule data bases. In this case, the effect of gamma-ray heating would be nonconservative.

While the systematic effects derived from this model are nonconservative, it must be stressed that other systematic effects can and do exist. Hence, one should not conclude that all systematic effects need be nonconservative. It would be naive indeed to reach such a conclusion based solely on an analysis of the heuristic model considered here. In particular, it is shown in Sections HEDL-E and HEDL-F that the flux-level effect can range from conservative to nonconservative depending on the material under consideration. Infact, the more detailed description developed by Simons (Section HEDL-E) allows a microvoid density that can be 1) lower, 2) higher, or 3) even show no change at higher flux levels, depending on the material properties of the steel under consideration.

From these considerations, it is clear that the present day understanding of the phenomenological processes underlying radiation-induced embrittlement of pressure vessels must be improved. It is also equally clear that use of this improved knowledge in trend curve analyses would be pointless unless differences that exist in environmental conditions between the pressure vessel and the data base are explicitly taken into account. Incorporation of such improvements should provide, in principle, a more rigorous basis for trend curve analyses. Using such advanced trend curve analyses together with plant specific data, bounds for pressure vessel neutron exposure can be realistically set that provide a proper margin of safety without excessive conservatism, which would otherwise penalize the U.S. commercial nuclear power industry.

3.0 Current Status of Trend Curve Analysis

As a part of the LWR-PV-SDIP, statistically based data correlation studies have been made by HEDL and other program participants using existing PWR and BWR physics-dosimetry-metallurgical data in anticipation of the analysis of new fracture toughness and embrittlement data from the BSR-HSST, SUNY-NSTF, ORR-PSF and other experiments. The reader is referred to Refs (Mc84,Mc85a) for additional summary-type information and appropriate references.

In Ref (Si84), Simons presents results of evaluation and reevaluation of exposure units and values for 47 PWR and BWR surveillance capsule reports for W, B&W, CE, and GE power plants. Using a consistent set of auxiliary data and dosimetry-adjusted reactor physics results, the revised fluence values for E > 1 MeV averaged 25% higher than the originally reported values. The range of fluence values (new/old) was from a low of 0.80 to a high of 2.38, see also Ref (Si82a,Mc84). These HEDL-derived FERRET-SAND II exposure parameter values have been used for the HEDL PWR and BWR trend curve studies of this progress report.

In Ref (Ra84), Randall discusses the basis for his Revision 2 of Regulatory Guide 1.99. As stated, the Regulatory Guide is being updated to reflect recent studies of the physical basis for neutron radiation damage and efforts to correlate damage to chemical composition and fluence. Revision 2 contains several significant changes. Welds and base metal are treated separately. Nickel content is added as a variable and phosphorus is removed. The exponent in the fluence factor is reduced, especially at high fluences; and guidance is given for calculating attenuation of damage through the vessel wall.

In Refs (Gu84b) and (Mc84h), the effects of changes in different variables and use of different exposure parameter models for predicting the Charpy shift for the 30-point PSF weld, plate, and forging data base and a 30-point PWR weld data base are discussed in considerable detail.

The main comments and conclusions of Guthrie's study (which is based on the use of PSF and test reactor data) are:

1) In surveying the previously existing data available for the alloys in the PSF experiment, it has become apparent that the fluence exponent is dependent on temperature and flux level. For the A302B alloy, the PWR surveillance data fell consistently below the higher flux level Low-Intensity Test Reactor (LITR) data and showed a lower value for the fluence exponent. The overall scatter of the existing data is such that it is not clear that Charpy tests or K tests can be used to uncover fine details in mechanisms.

2) Because of the possible rate effect (which was predicted by G. R. Odette in his PSF Blind Test submission), the PWR surveillance trend curve laws cannot be expected to work as well in the PSF as might be expected from their stated standard deviations.

3) In applying existing Charpy shift laws to the PSF C_V data, we find that the largest observed shift occurred for the Rolls Royce A533B weld (Code R), which had a high nickel content (1.58%), which is well outside the range of the data base used to develop the HEDL PWR Charpy shift equations (Gu84).

4) There appears to be a rate effect in the PSF Charpy and compression data. The fluence exponent appears to increase with increased flux and appears to decrease with increased copper.

5) The similarity of the spectra at the separate irradiation positions severely limits the possible comments about damage functions.

6) No extra thermal neutron effect, beyond that already represented in the ASTM dpa cross section, was identifiable in the PSF data.

The main comments and conclusions of McElroy's et al. study (which is based on the use of PSF, PWR, and BWR data) are:

1) There is a significant improvement (reduction) in the standard deviation of the fit for weld Charpy shift trend curves that include the effect of low-energy thermal neutrons. For the 30-point weld data set, improvements of the amounts observed could occur at a frequency of no more than approximately 4% by chance.

2) A knowledge of the actual boron content of PV steels and the use of a trend curve that makes use of an exposure parameter dose term, which includes the total production of dpa and helium in iron, could make significant improvements in lowering the standard deviation of the fit for the existing PWR surveillance capsule metallurgical weld data base.

3) Based on the trend curve model that includes the effect of thermal neutrons for both PWR and BWR power plants, up to about 80% of the SS clad/PV steel wall interface and surveillance capsule specimen dose term values could be attributed to helium production in PV steels, depending on the particular surveillance capsule design, Charpy specimen placement, steel boron content, and power plant operating conditions.

4) Existing PWR and BWR surveillance capsule-derived embrittlement trend curves [based on the use of just fast fluence ($E > 1$ MeV) or dpa for the exposure term] cannot be expected to give reliable predictions of the combined fast and thermal neutron contributions to the Charpy shift at the SS clad/PV steel wall interface, 1/4-T, 1/2-T, 3/4-T, or 1-T locations. [It is noted that the PSF experiment provides physics-dosimetry-metallurgy data for predicting the Charpy shift in PV steels at deep in-wall locations, such as the 1/4-T, 1/2-T, and 3/4-T positions, where the thermal-to-fast neutron fluence (T/F) ratios are in the very low range of $\sim$0.14 to $\sim$0.53. However, even for these very low ratios, helium from both boron and steel high energy (n,α) reactions may still contribute 5% to 30% to the exposure parameter dose term value.]

5) None of the Charpy shift trend curve equations studied, Table 1 of Ref (Mc84h), except perhaps the one based on the use of an exposure parameter of fluence E > 0.1 MeV, appear to properly bound all the six PV steel observed PSF damage gradient curves. Based on the French simulated PV-wall DOMPAC Experiment (Mc84,Al83), Alberman concluded that for low temperature (<100°C) irradiations, fast fluence (E > 1 MeV) is too "optimistic" and is not, therefore, a conservative neutron exposure parameter and that, at low temperature, 95% of the measured damage (based on tungsten and graphite DM results) comes from neutrons with energy E > 0.1 MeV. This led him to conclude that the exposure parameter, fluence (E > 0.1 MeV), is perhaps "pessimistic," but has the advantage of being the lower threshold of all (displacement) damage models and thus it takes into account all neutrons that create (displacement) damage.

6) The plant specific weld data sets used in the PWR and BWR data base studies, except for one, do not support a saturation effect at high fluences above $\sim 1 \times 10^{19}$ n/cm² (E > 1 MeV). Consequently, the existing Reg. Guide 1.99 (Re77) upper-bound (truncated) trend curve model shape (or plant specific curves) may have to be used for high fluence embrittlement predictions for PV steel welds, and perhaps forging and plates.

7) Any significant thermal neutron contribution to PV steel embrittlement is, most probably, a result of (n,α) reactions in boron-10 rather than by neutron-induced $Fe(n,\gamma)$ recoil reactions.

8) It appears that the current ASTM E693 (As79d) dpa cross section should not be used to correlate highly thermalized light or heavy water moderated power or test reactor irradiation effects data because it significantly overestimates the low-energy thermal neutron dpa contribution.

9) The PV-wall SS clad/PV steel interface surface T/F ratio for PWR and BWR power plants is expected to be in the range of 2 to 6 on the basis of surveillance capsule measurements, Westinghouse transport calculations, GE measurements, and PSF experiment physics-dosimetry results.

10) Individual Charpy specimens (with natural boron content ranging from ~0.4 up to perhaps 5 wt ppm) in PWR and BWR surveillance capsules will be subject to ξ neutron exposures with T/F ratios in the range of ~0.5 to 5, depending on the surveillance capsule design, its placement, and the reactor operating conditions. The T/F variation for individual Charpy specimens, therefore, could be an important parameter for the correlation of a set of Charpy specimen results and derived ΔRT_{NDT} values.

11) From this study, that of Grant and Earp (Gr84), and others discussed in Ref (Mc84h), a final conclusion is: the PSF experiment and PWR and BWR surveillance program results clearly show that comparison of the effects of radiation damage on yield strength, hardness, RT_{NDT} and USE will be needed to aid in improving and refining our knowledge of trend curves and PV wall damage gradients. Implicit in this are the current observations that the establishment of separate trend curves for welds, forgings, and plates will give increased understanding and accuracy in projections of the present and future metallurgical condition of PV steels.

3.1 Test Matrix Formulation

While it is our intent to develop a preliminary test matrix that addresses neutron-induced embrittlement of LWR-PV, an often overlooked aspect of such efforts is the quality of the measurements. Charpy data are often beset with large fluctuations of statistical or otherwise unknown origin that undermine not only the data base, but any analyses based thereon. Although development of a new set of Charpy data would certainly add to the data base, the quality of such data is deemed more important at this time. Consequently, our recommended first priority is for high quality data. Next in priority would be the type and quantity of measurements. Our priorities are based on the view that the underlying phenomenological processes are more readily resolved and better understood in terms of the quality of the data base rather than the size of that data base. The aforementioned references to the observation of a flux level effect for the PSF experiment provide rather convincing support for this viewpoint. Indeed, we cannot overemphasize the need for high quality data at the present time. Considering this aspect of the problem, it is essential that high-quality Charpy, tensile, hardness, TEM, SANS, and FIM experimental results be obtained and reported, as well as those related to the physics-dosimetry measurements and data analysis.*

In view of the many damage effect variables that exist in neutron-induced embrittlement of LWR-PV steels, selection of the most relevant variables is an extremely difficult process. Nevertheless, such a selection process is mandatory. In fact, since the range of the selected variables actually define the domain of the test matrix, it is clear that the size of the test matrix will grow rapidly as the number of selected damage effect variables is increased. Because of the expensive nature of irradiation tests of this type, one must clearly limit the number of variables to keep overall funding requirements at realistic levels.

In order to start the selection process, Table HEDL-2 displays our choice of the most relevant damage effect variables. Here we have partitioned variables into three main classes, namely material properties, environmental irradiation conditions, and material effects. Even if considerations are restricted to those variables cited in Table HEDL-2, a test matrix comprising all these variables would still be too large to implement.

In order to stay within budgetary constraints and still generate data that bear upon the pressure vessel embrittlement process, one can restrict consideration to submatrices of the larger overall test matrix. In this event, those variables that are not treated within a given submatrix must be held constant. Clearly, values must be prescribed for those variables which are held constant that are representative of the range of values that actually exist in the pressure vessels of operating LWR power plants. Otherwise, the data generated would not be applicable for trend curve analyses of operating LWR power plants.

*TEM - Transmission electron microscopy; SANS - Small-angle neutron scattering; FIM - Field ion microscopy.

From this point of view, U.S. irradiation test programs already exist (Ka82a,Ka82b,Mc85a,Me84,Gr84,Od85) that address distinct submatrices of this overall test matrix. The submatrices addressed in the ongoing irradiation programs deal chiefly with material effects and material properties, i.e., Columns 1 and 3 of Table HEDL-2. These already existing efforts focus primarily on the following phenomena:

- Compositional Effects
  - -- Dependence on impurities and/or alloying elements
  - -- Annealing Recovery
- Irradiation-Anneal-Reirradiation Characteristics
- Dose Rate (i.e., Flux-Level) Effects

As a consequence of these already existing efforts, we have chosen to restrict our considerations here to a submatrix example involving environmental irradiation variables only, i.e., Column 2 of Table HEDL-2. Rather than focusing on material properties and effects, this submatrix will concentrate on the investigations of systematic biases that can arise because of differences in environmental conditions between current data bases and the actual conditions that exist in LWR pressure vessels. For this submatrix to be of realistic proportions, one can consider no more than five or so environmental irradiation variables. Hence, we have limited our considerations to the five environmental irradiation variables shown in Table HEDL-3.

In general, the purpose of such an environmental irradiation submatrix is to define the overall dependence of the Charpy shift on all relevant environmental variables. From this submatrix viewpoint, the functional form of the Charpy shift trend curve can be written as

$$\Delta RT_{NDT} = F(x_i, \ldots x_m; a_i, \ldots a_m), \qquad (13)$$

where $\{x_i\}$ are the relevant environmental variables and $\{a_i\}$ are a set of parameters. Here the set of parameters $\{a_i\}$ represents all remaining variables that are not treated within the environmental irradiation submatrix, such as those enumerated in Columns 1 and 3 of Table HEDL-2.

In order to examine the detailed dependence of ΔRDT_{NDT} on environmental variables, materials of high radiation sensitivity must be chosen for the environmental irradiation test submatrix. The R material of the PSF test is an excellent example of such a material. With materials of this type, an absolute and/or relative accuracy of Charpy shift measurements as good as a few percent can be attained. To quantify the behavior of systematic environmental effects of the order of 10% to 20%, such an improved accuracy level is mandatory. While Table HEDL-3 indicates that only one plate and two weld materials are to be included in the environmental irradiation submatrix, it

TABLE HEDL-2

SELECTED DAMAGE EFFECT VARIABLES

Material Properties	Environmental Irradiation Conditions	Material Effects
• Type of Steel	• Fast Neutron Fluence	• Mechanical Treatment
		• Heat Treatment
• Impurities: Cu, Ni, Mn, Mo, Cr, P, Si, S, C, B, N	• Neutron Flux Level	• Annealing
	• Thermal* Neutron Fluence	Pre-Irradiation
• Microstructure		
	• Thermal-to-Fast Neutron Ratio	During Irradiation
	• Gamma-Ray Fluence	Post-Irradiation
	• Gamma-Ray Flux Level	(Time and Temperature Dependence)
	• Gamma-Ray Heating	
	• Temperature (including any gradients)	% Recovery
	• Irradiation Time	

*Implicit here is the contribution from epithermal as well as thermal neutrons.

TABLE HEDL-3

ENVIRONMENTAL IRRADIATION SUBMATRIX

Material Properties*		Environmental Irradiation Variables*	
• Weld	(2)	• Flux Level	(3)
• Plate	(1)	• Dose Term	(3)
• Forging	(1)**	• Thermal-to-Fast Neutron Fluence	(3)
		• Temperature	(3)
		• Gamma Heating	(3)***

*The number in parentheses following the variable is the recommended number of different values to be used for this given variable in the test submatrix.

**A possible future option, which is not included in the present submatrix.

***This variable is identified here because of the possibility of systematic effects associated with gamma-ray induced temperature gradients.

is essential that the radiation sensitivity of these materials be high enough to furnish Charpy shift and other property measurements of required accuracy levels. A forging is also identified in Table HEDL-3 as an additional option, but it is not included in the present discussion.

As already noted in the general submatrix approach, the important parameters that lie outside the submatrix must be assigned constant values that are representative of LWR-PV commercial power plant irradiations. For our environmental variable submatrix, the remaining parameters have already been identified in Columns 1 and 3 of Table HEDL-2. Examples of representative values for these remaining parameters are given in Table HEDL-4. These values are based on the preliminary analysis of PSF experimental results, the power reactor data base, and recent irradiation test results obtained in the UK (Fi84) (see Section HEDL-F).

In spite of the restrictions that have been adopted, the effort to implement this submatrix can still be quite formidable. Let us assume that only three metallurgical tests are employed, namely Charpy, yield strength, and hardness. Since two welds and one plate material have been selected for this submatrix, one would need 9 test specimens for each of the environmental irradiation conditions specified. Using three values for each of the five parameters recommended in Table HEDL-3 requires a total of $3^5 = 243$ different irradiations. Consequently, one would require a total of roughly 2200 irradiation test specimens.

TABLE HEDL-4

REPRESENTATIVE VALUES OF PARAMETERS
FOR THE ENVIRONMENTAL SUBMATRIX

Parameter / Material Type	Steel*	Composition (wt%)										
		Cu	Ni	Mn	Mo	Cr	P	Si	S	C	B	N
• Weld	A533	0.36	1.0	1.5	0.5	0.1	0.01	0.3	0.01	0.2	**	**
• Weld	A533	0.25	1.0	1.5	0.5	0.1	0.01	0.3	0.01	0.2	**	**
• Plate	A533	0.25	1.0	1.5	0.5	0.1	0.01	0.3	0.01	0.2	**	**
Forging (Option not used for matrix)	A533	0.12	1.0	1.5	0.5	0.1	0.01	0.3	0.01	0.2	**	**
Microstructure	To Be Determined											
Heat Treatment	To Be Determined											
Annealing	To Be Determined											

*Steels have been chosen that should possess large Charpy shifts, such as those attained with the Rolls-Royce Code R weld of the PSF experiment.
**To be determined, but representative of actual PV steels. Also, other minor alloying constituents, such as V, Al, etc., should be maintained as constant as possible and be representative of actual steels.

Actually, more than 2200 specimens would be required because of the nature of the thermal neutron tests. Recent trend curve analyses have demonstrated that improvements can be effected if the dose term is generalized to a linear combination of different spectral fluence components, i.e., thermal, intermediate, fast, dpa, ..., etc. As an example, the dose D can be expressed in the form

$$D = aT + bI + cF, \qquad (14)$$

where T, I, and F are the thermal, intermediate, and fast neutron fluence with a, b, and c appropriate constants.

A simple test of the validity of this representation involves the commutativity of the different components of the dose. Let us first consider a simplified example that is obtained by limiting the partition of the irradiation dose into just two groups, namely thermal and fast neutrons. For this test,

let S represent the available set of metallurgical specimens, which is divided into four subsets; S_1, S_2, S_3, S_4. The size of these subsets is chosen to provide an adequate measurement base. The target dose is fixed in the environmental submatrix given in Table HEDL-3 at one of the three designated values. These values should be chosen based on relevant results from the surveillance capsule data base and/or the PSF experiment. All four subsets should be irradiated to this target dose, using a different sequence of thermal and fast neutron irradiations. The dose commutativity submatrix for these sequential irradiation tests is shown in Table HEDL-5.

This dose commutativity submatrix will examine not only the commutativity assumption, but equally important issues, such as whether or not the thermal neutron component of the dose enters as a defect stabilization mechanism or can help produce trend curve saturation. In addition, the validity of the coefficients used in the linear combination to represent the dose are also tested.

Inclusion of this dose commutativity submatrix increases the total number of irradiation test specimens by 729 from roughly 2200 up to 3000. Moreover, the simplest kind of dose commutativity submatrix has been considered here since it corresponds to the partitioning of the dose into just two energy groups. Extension of this commutativity submatrix by partitioning into more than two groups, as would arise by inclusion of such components as intermediate neutron energy fluence I or dpa, would produce a substantial expansion of this commutativity submatrix. Other directions could also be considered, such as the inclusion of different materials in order to examine dependence on impurities and alloying elements. In this case, information could be obtained on the chemistry dependence of the coefficients that arise in the partitioning process, i.e., a, b, c, ... However, this would also produce a submatrix of significantly expanded proportions.

TABLE HEDL-5

DOSE COMMUTATIVITY SUBMATRIX*

Subset	Thermal Neutron Irradiation	Fast Neutron Irradiation
S_1	First	Second
S_2	Second	First
S_3	First	None
S_4	None	First

*All subsets are subjected to the same target dose.

Our current view is not to pursue either of these latter two options at this time, since some work is already in progress and the analysis of existing data remains to be completed (Mc85a,Me84,C.85,St83,Wi82a,Pa83). The submatrix, without these options, represents an irradiation test program of environmental factors that is more manageable in scope and one that can more readily be implemented. The need and/or justification to pursue these as well as other options will become more apparent when the results of this more modest irradiation program are already in hand and can then be compared with results from already existing programs. Of higher priority at this time is the need to more fully understand environmental effects from

- Flux-level
- Dose
- Thermal neutrons
- Gamma-ray heating and temperature

Each of these effects can produce a systematic deviation in trend curve analysis that is non-conservative. Hence, the immediate goal of the irradiation test program defined by this submatrix is to generate the information needed to correct trend curve analyses for systematic biases introduced by these environmental effects.

4.0 Conclusions

This completes our initial attempt to formulate a test submatrix that treats environmental variables. Implementation of such an irradiation test program would provide the basis for understanding systematic effects from environmental radiation conditions. This knowledge would permit, in time, a realistic evaluation of the limitations of current data bases. As a consequence, significant systematic effects could be included in trend curve analyses that would lead to more accurate assessment and prediction of PV embrittlement in operating U.S. LWR commercial power plants.

Expected Future Accomplishments

Appropriate parts of this work will be extended and incorporated in PSF Experiment physics-dosimetry-metallurgy NUREG reports.

B. DETERMINATION OF GAMMA-RAY DISPLACEMENT RATES

Raymond Gold, J. H. Roberts and D. G. Doran (HEDL)

Objective

The objective of this work is to use absolute electron spectral measurements obtained with Janus probe gamma-ray spectrometry to quantitatively assess the displacement rate produced by the gamma-ray field in LWR-PV environments.

Summary

Gamma-ray induced displacement rates have been calculated for LWR-PV environments using absolute electron spectra observed in the PCA with the Janus probe. Gamma-ray displacement results are presented for the 1/4-T, 1/2-T, and 3/4-T locations of the 12/13 and 4/12 SSC configurations. In addition, the gamma-ray displacement rate at the simulated surveillance capsule (SSC) location was inferred using thermoluminescent dosimeter (TLD) gamma-ray dosimetry results obtained in the 4/12 SSC configuration at the PCA. Compared with neutron-induced displacement rates, the calculated gamma-ray induced displacement rates are negligible at all locations. The ratio of gamma-ray induced to neutron-induced displacement rates never exceeds roughly 5×10^{-3}.

Accomplishments and Status

1.0 Introduction

The need to characterize the gamma-ray component of the mixed radiation field that exists in LWR-PV environments has already been emphasized in the two earlier NUREG reports on the PCA (Mc81,Mc84). In these earlier efforts, displacement phenomena produced directly by the gamma-ray component were not addressed. It was tacitly assumed that gamma-ray displacement effects are negligible relative to neutron displacement effects in LWR-PV environments. This position is not unusual, since current practise is to ignore gamma-ray displacement effects in all reactor environments.

What has been lacking in the past is a quantitative assessment of the basis for this assumption. Indeed, even for a gamma-to-neutron displacement ratio (γ/n) of only 10 percent, gamma-ray displacement effects would have to be accounted for in trend curve analyses that are used to predict PV embrittlement. Otherwise systematic biases could exist that would introduce non-negligible errors in the prediction and extrapolation of PV embrittlement. On the other hand, for a γ/n displacement ratio of one percent or less,

gamma-ray displacement effects can be ignored in current trend curve analyses. Consequently, quantitative assessments of the γ/n displacement ratio that arise in LWR-PV environments are needed.

1.1 Description of Gamma-Ray Induced Displacements

In condensed matter, the gamma-ray component of the mixed radiation field induces an energetic electron spectrum and this electron spectrum is the principal mechanism for gamma-ray produced displacements. Consequently, gamma-ray displacement rates can be determined by measuring the induced electron spectrum. It is this very same electron spectrum that is observed in continuous gamma-ray spectrometry (Go84c).

In continuous gamma-ray spectrometry with Si(Li) detectors, such as utilized in the Janus probe for PCA gamma-ray measurements (Go82b,Go83a,Go84c,Mc84k), the observed electron spectrum is that which is created in silicon. However, in condensed matter of low atomic number (low Z), the electron mass density, i.e., electrons/g, is essentially constant. As a consequence, the gamma-ray field component produces essentially the same electron spectrum in all low Z condensed media. Hence, with appropriate scaling, measurements in silicon will provide the electron spectrum that is induced in a PV (which is principally iron). Interestingly enough, it is for this very same reason that the induced gamma-ray dose rates in iron and silicon are virtually identical, as was demonstrated in earlier Si(Li) gamma-ray dosimetry in the PCA (Ka84a).

With Si(Li) gamma-ray spectrometry probes, one observes a pulse-height spectrum, B(I), which represents the number of electron events produced in the I^{th} pulse-height channel bin. These data are collected with a measured electron energy conversion gain, G, possessing units of MeV/channel, so that electron energy is defined by

$$E(I) = G \quad I - G/2 \quad . \tag{1}$$

Here, E(I) is the mid-bin electron energy of the I^{th} channel.

Let us assume that an electron spectrum is collected during a live time, t. The equilibrium creation rate spectrum in the Si(Li) detection probe, p(E), is then simply

$$p(E) = \frac{B(E)}{G \cdot t} \quad . \tag{2}$$

Here p(E) possesses units of the number of electrons created at energy E per MeV per second. Upon division of p(E) by the mass of the sensitive volume of the detector, m, one obtains the creation rate per gram, $C_m(E)$, given by

$$C_m(E) = \frac{B(E)}{G \cdot t \cdot m} \quad . \tag{3}$$

The creation rate spectrum per electron, $C_e(E)$, can be obtained from Equation (3) by introducing the electron mass density, ρ_m, which is given by

$$\rho_m = \frac{Z \cdot N}{A} \quad , \tag{4}$$

where Z is the atomic number, A is the mass number, and N is Avagadro's number. Using the value of ρ_m for silicon, i.e., $\rho_m = \rho_m(Si)$, one has

$$C_e(E) = \frac{B(E)}{G \cdot t \cdot m \cdot \rho_m(Si)} \quad . \tag{5}$$

For silicon, $\rho_m(Si) = 3.00 \times 10^{23}$ electrons/g. Since $Z/A \sim 0.5$ for low Z condensed matter, one has $\rho_m \simeq N/2 = 3.01 \times 10^{23}$ electrons/g. Consequently, the $C_e(E)$ spectrum is essentially invariant for low Z condensed matter.

To obtain the creation rate spectrum per unit volume, $\Psi(E)$, in a low Z medium of density, d, multiply $C_V(E)$ by the electron volume density, ρ_V, of the medium. The electron volume density in medium, x, is simply

$$\rho_V(X) = d \cdot \rho_m(X) = d \cdot \left(\frac{Z_x N}{A_x} \right) \quad , \tag{6}$$

where d is the density of the medium.

Consequently, the creation rate spectrum per unit volume in the condensed medium, $\Psi(E)$, is given

$$\Psi(E) = \frac{B(E) \cdot d}{G \cdot t \cdot m} \left[\frac{\rho_m(x)}{\rho_m(Si)} \right] \quad . \tag{7}$$

Using units of g/cm³ for d, $\Psi(E)$ possesses units of the number of electrons created at energy E per second per MeV per cm³. For low Z condensed media, where $\rho_m(x) \simeq \rho_m(Si)$, one has approximately

$$\Psi(E) \simeq \frac{B(E) \cdot d}{G \cdot t \cdot m} \quad . \tag{8}$$

Let $\sigma_d(E)$ be the displacement cross section per atom in the condensed medium for electrons of energy E. However, electrons created at some initial energy, E_i, can also produce displacements at lower energy. In fact, these electrons can produce displacements as they slow down in the medium from their initial energy, E_i, to some threshold energy, E_t; i.e., in the energy interval $E_t \leq E \leq E_i$. The total production of displacements by electrons of initial energy, E_i, must, therefore, be obtained by suitable integration over the path of the electron.

To this end, let r(E) represent the energy dependence of the electron range in the medium. Then the variation of the displacement cross section along the path of the electron is simply given by $\sigma_d(r)$, where $r = r(E)$. Further, let $R = r(E_i)$ be the range of electrons of initial energy E_i. The displacement rate, $\Phi(E_i)$, in a volume of the medium dV possessing an atom density, ρ_a, produced by electrons of initial energy, E_i, is, therefore, given by

$$\Phi(E_i) = \int_0^R \Psi(E_i)\sigma_d(r)(dV \cdot \rho_a)dr \tag{9a}$$

or

$$\Phi(E_i) = (dV \cdot \rho_a)\Psi(E_i)\int_0^R \sigma_d(r)dr \quad . \tag{9b}$$

Substituting the energy dependent range, r(E), into Equation (9b) yields

$$\Phi(E_i) = (dV \cdot \rho_a)\Psi(E_i)\int_{E_t}^{E_i} \sigma_d(E)\frac{dE}{(-dE/dr)} \quad , \tag{10}$$

where (-dE/dr) is the rate of energy loss of electrons in the medium as a function electron energy, E.

Equation (9) can be used to obtain a representation of the displacement rate that possesses a particularly simple physical interpretation. The first step is to obtain the displacement rate per atom (dpa) produced by electrons of energy E_i, $\delta_a(E_i)$. From Equation (10), one has

$$\delta_a(E_i) = \frac{\Phi(E_i)}{(dV \cdot \rho_a)} = \Psi(E_i) \int_{E_t}^{E_i} \sigma_d(E) \frac{dE}{(-dE/dr)} \quad . \qquad (11)$$

This expression for the dpa produced by electrons of initial energy, E_i, can be expressed in the form

$$\delta_a(E_i) = \varphi_a(E_i) \cdot n(E_i) \quad , \qquad (12)$$

where:

$$\varphi_a(E_i) = \Psi(E_i)/\rho_a \quad , \qquad (13)$$

and

$$n(E_i) = \rho_a \int_{E_t}^{E_i} \sigma_d(E) \frac{dE}{(-dE/dr)} \quad . \qquad (14)$$

Equations (12) through (14) provide the representation we seek. Here, $\varphi_a(E_i)$ is the number of electrons created with initial energy E_i per second per MeV per atom in the medium and $n(E_i)$ is the number of displacements produced in the medium by electrons of initial energy, E_i.

The total dpa, Δ_a, can be obtained by integrating Equation (12) over E_i. Hence, one can write

$$\Delta_a = \int_0^\infty \varphi_a(E_i) \cdot n(E_i) dE_i \quad . \qquad (15)$$

Using Equations (7) and (13), the electron creation rate spectrum per atom can be expressed in terms of observations as

$$\varphi_a(E_i) = \frac{B(E_i) \cdot d}{G \cdot t \cdot m \cdot \rho_a} \quad \frac{\rho_m(x)}{\rho_m(Si)} \quad . \qquad (16)$$

Using Equations (14) and (16) in Equation (15), one has the more detailed expression for the total dpa of

$$\Delta_a = \frac{d \cdot \rho_m(x)/\rho_m(Si)}{G \cdot t \cdot m} \int_{E_t}^{\infty} B(E_i) \left[\int_{E_t}^{E_i} \sigma_d(E) \frac{dE}{(-dE/dr)} \right] dE_i \quad . \quad (17)$$

A summary of the physical quantities introduced in this description of gamma-ray induced displacements can be found in Table HEDL-6.

1.2 Data Analysis

1.2.1 Computation of $n(E_i)$

The number of displacements per electron of initial energy E_i, $n(E_i)$, has been calculated by numerical integration of Equation (14). The actual displacement cross sections used in these calculations are displayed in Figure HEDL-2. These electron cross sections had been calculated earlier for nickel using two different threshold displacement energies, namely T_d = 24 eV and 40 eV. It is clear from these curves that secondary displacements made a significant contribution. Since electron displacement cross sections vary systematically with Z and A, these nickel cross sections should be an adequate approximation of the displacement cross section for iron. As can be seen in Figure HEDL-2, the two different threshold displacement energies of T_d = 24 eV and 40 eV give rise to electron threshold energies of approximately E_t = 0.45 MeV and 0.70 MeV, respectively.

Two values of T_d were retained in order to determine the sensitivity of the displacement rate to this parameter. In irradiating a crystal with electrons, the probability of a displacement rises gradually to unity over a range of electron energies. The detailed shape of the curve depends on the orientation of the electron beam relative to the crystallographic axes, because the energy required to displace an atom depends on the direction of ejection. (A different range of ejection angles is associated with each electron direction.) The ejection energy of an atom may range from less than 20 eV to over 100 eV.

In calculating the displacement cross section, the probability of a displacement is assumed to rise from zero to unity in a single step at an effective displacement energy T_d. Values of T_d can be inferred from the onset of damage in electron-irradiated polycrystals. Typical values are in the range 25 eV to 40 eV for iron, nickel and chromium.

TABLE HEDL-6

DEFINITION OF PHYSICAL QUANTITIES

Quantity	Symbol	Units
Isotopic Mass Number	A	Grams per mole
Observed Electron Pulse Height Spectrum	B(E)	Events per channel
Mass of Sensitive Volume of Si(Li) Detector	m	Grams
Density of the (Condensed) Medium	d	Grams per cm^3
Live Time or Effective Collection Time Internal	t	Seconds
Electron Energy Conversion Gain	G	Mev per channel
Electron Mass Density	ρ_m	Electrons per gram
Electron Volume Density	ρ_v	Electrons per cm^3
Atom Density	ρ_a	Atoms per cm^3
Electron Energy	E	MeV
Initial Electron Energy	E_i	MeV
Energy Dependent Electron Range	r(E)	cm
Electron Rate of Energy Loss	(-dE/dr)	MeV per cm
Electron Creation Rate Spectrum	p(E)	Electrons/(MeV•s)
per Gram	$C_m(E)$	Electrons/(MeV•s•g)
per Electron	$C_e(E)$	Electrons/(MeV•s•electron)
per cm^3	$\Psi(E)$	Electrons/(MeV•s•cm^3)
per Atom	$\varphi_a(E)$	Electrons/(MeV•s•atom)
Displacement Rate per Atom	$\delta_a(E_i)$	Displacements/(MeV•s•atom)
Total Displacement Rate per Atom	Δ_a	Displacements/(s•atom)
Displacement Cross Section	$\sigma_d(E)$	cm^2
Number Of Displacements Produced by an Electron of Energy E_i	$n(E_i)$	Displacements per electron

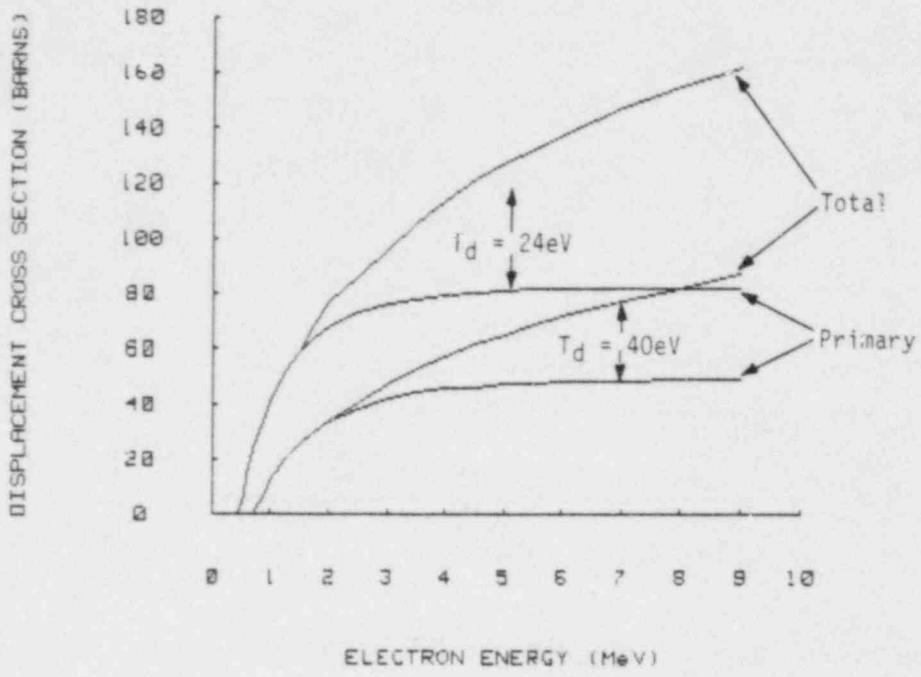

FIGURE HEDL-2. Displacement Cross Sections, σ_d, in Nickel for Threshold Displacement Energies of T_d = 24 eV and 40 eV.

The estimate of the contribution of secondary displacements is necessarily crude at these very low recoil energies, perhaps uncertain by a factor of two.

A recent review (Se82a) was used to numerically evaluate the rate of electron energy loss (-dE/dr) in iron. This evaluation is shown in Figure HEDL-3. Note that the variation of (-dE/dr) is considerably less than that of $\sigma_d(E)$ over the energy region of interest here.

Numerical integration of Equation (14) was carried out using these results. The two different values of $\nu(E_i)$, which are displayed in Figure HEDL-4, corresponding to the two threshold displacement energies of T_d = 24 eV and 40 eV, both increase rapidly with increasing electron energy.

1.2.2 Observed Electron Spectra

The most recent Si(Li) electron spectra measured at the LWR-PVS mockup in the PCA will be used for these gamma-ray displacement calculations. These

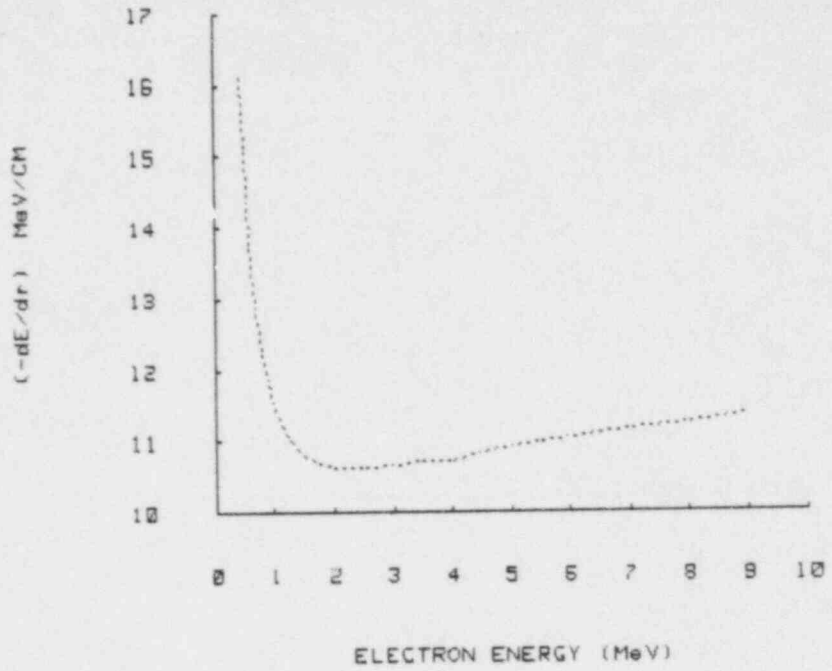

FIGURE HEDL-3. Rate of Energy Loss (-dE/dr) of Electrons in Iron.

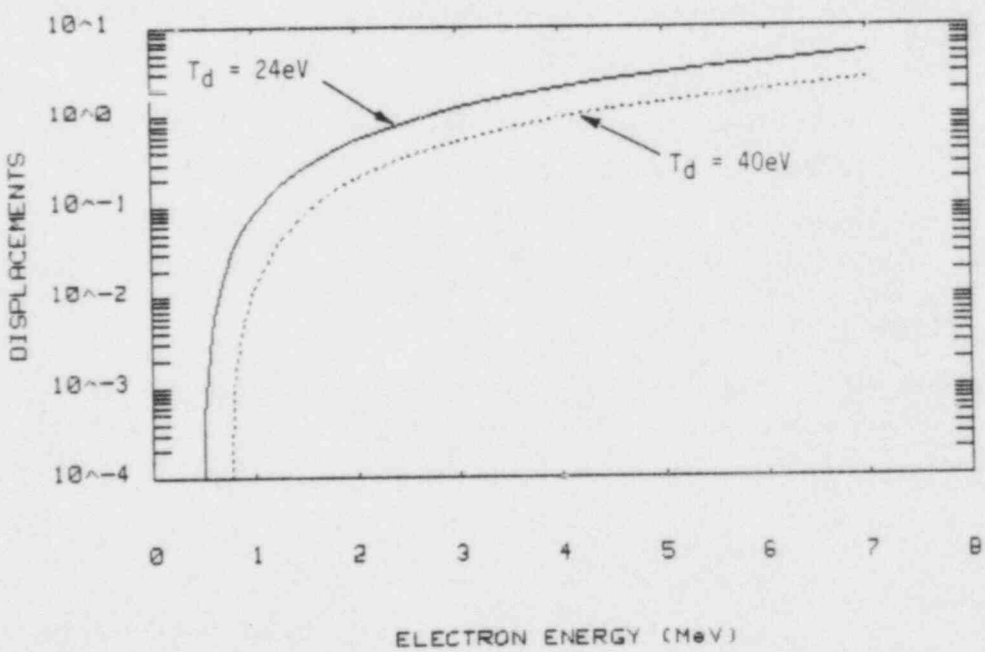

FIGURE HEDL-4. Number of Displacements per Electron as a Function of Initial Electron Energy, $n(E_i)$, for T_d = 24 eV and T_d = 40 eV.

measurements were conducted in the 1/4-T, 1/2-T, and 3/4-T locations of the 12/13 and 4/12 SSC configurations in October 1981. Figures HEDL-5 through HEDL-10 show the electron spectra, B(E), observed in these measurements. To convert these observed spectra to $\varphi_a(E)$, the following values were employed in Equation (16):

$$m = 4.53 \text{ g}$$

$$t = 3600 \text{ s}$$

$$G = 0.03 \text{ MeV}$$

$$d = 7.86 \text{ g/cm}^3$$

$$\rho_a = 8.476 \times 10^{22} \text{ atoms/g}$$

$$\rho_m(Fe)/\rho_m(Si) = 0.934$$

Consequently for these observed spectra, one has the numerical result

$$\varphi_a(E_i) = 1.770 \times 10^{-25} B(E_i) \quad . \tag{18}$$

Equation (18) does not account for two factors that arise in the PCA measurements that are configuration and location dependent. These two factors are the perturbation factor (PF) created by introduction of the Janus probe and the power level (PL) used in the specific PCA irradiation. Table HEDL-7 provides the PF and PL for each of these six PCA spectral measurements. The PF values in Table HEDL-7 were obtained from follow-on experiments at NESDIP, as described in the second NUREG report on the PCA (Go84d).

These two factors can be combined to produce a single scale factor, SF, given by

$$SF = PF \cdot PL \quad , \tag{19}$$

which in turn can be applied to $\varphi_a(E_i)$ to obtain $\varphi_w(E_i)$, the creation rate electron spectrum per atom per watt of PCA power. One has

$$\varphi_w(E_i) = \varphi_a(E_i)/SF \quad . \tag{20}$$

For the purpose of comparison with neutron-induced dpa, the creation rate electron spectrum, $\varphi_n(E_i)$, possessing units of electrons per atom per PCA core neutron is needed. The creation rate spectrum, $\varphi_n(E_i)$, is given by

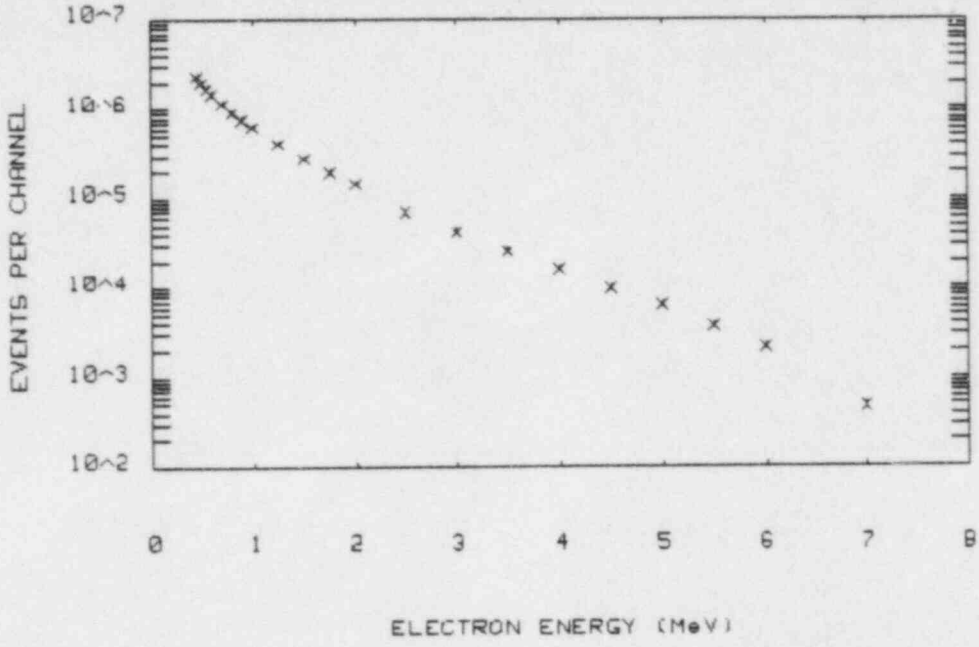

FIGURE HEDL-5. Si(Li) Observed Electron Spectrum at the 1/4-T Location of the 12/13 Configuration.

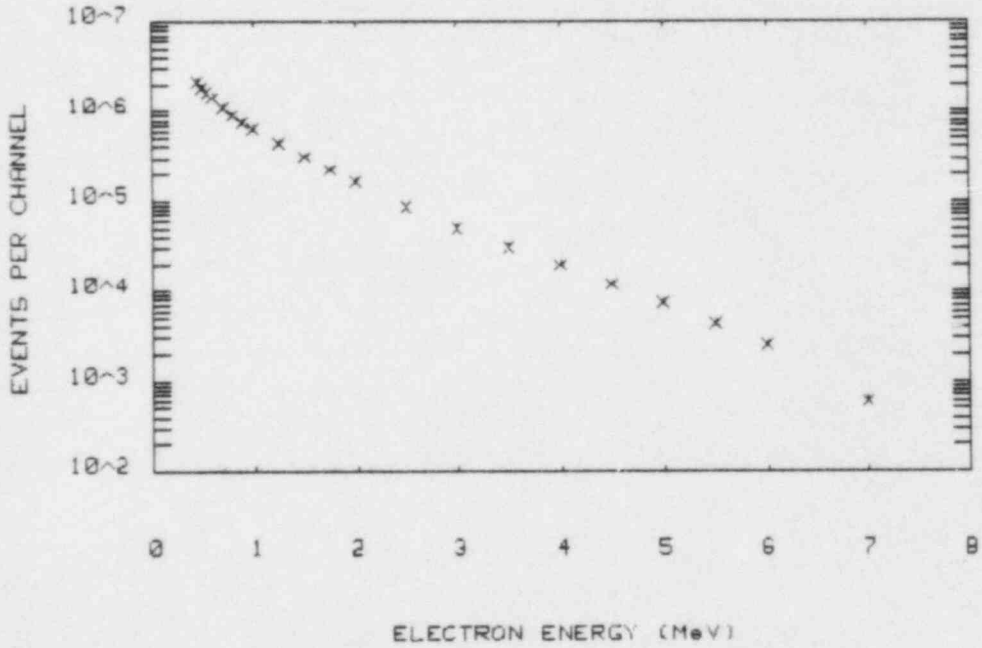

FIGURE HEDL-6. Si(Li) Observed Electron Spectrum at the 1/2-T Location of the 12/13 Configuration.

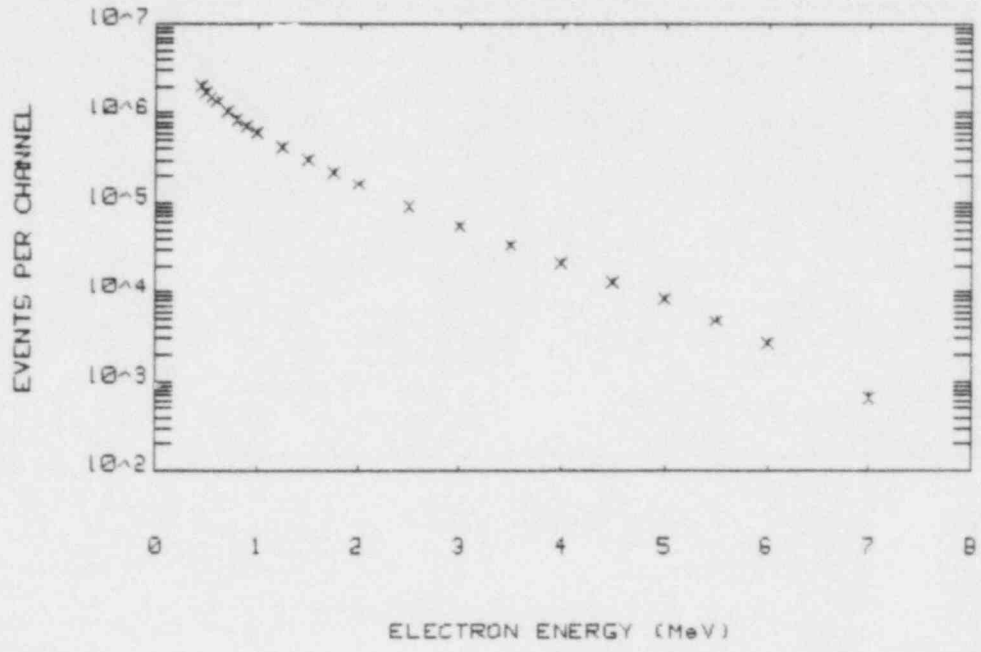

FIGURE HEDL-7. Si(Li) Observed Electron Spectrum at the 3/4-T Location of the 12/13 Configuration.

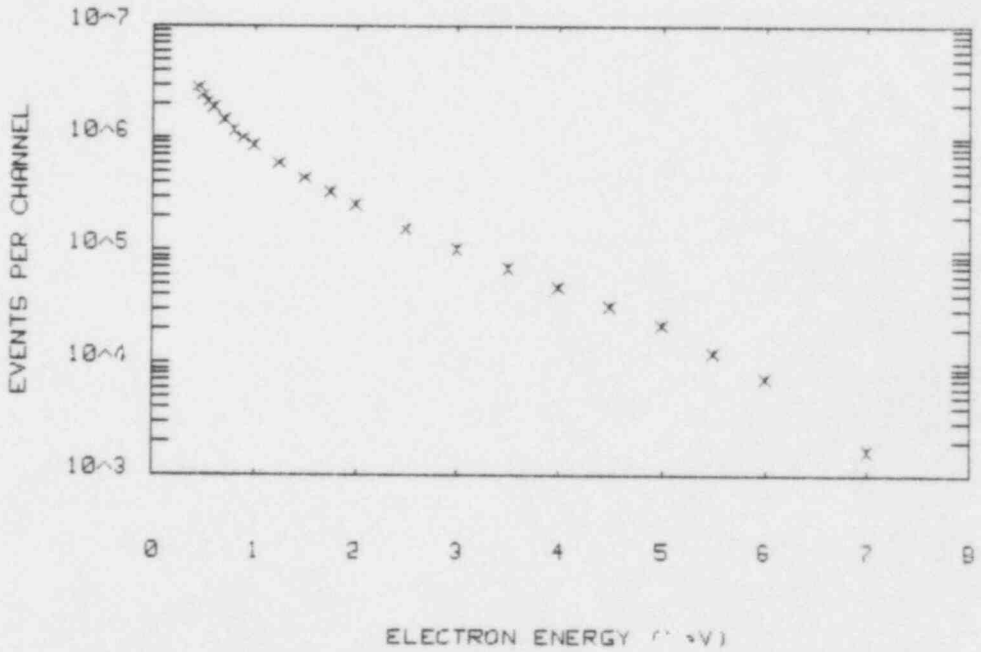

FIGURE HEDL-8. Si(Li) Observed Electron Spectrum at the 1/4-T Location of the 4/12 SSC Configuration.

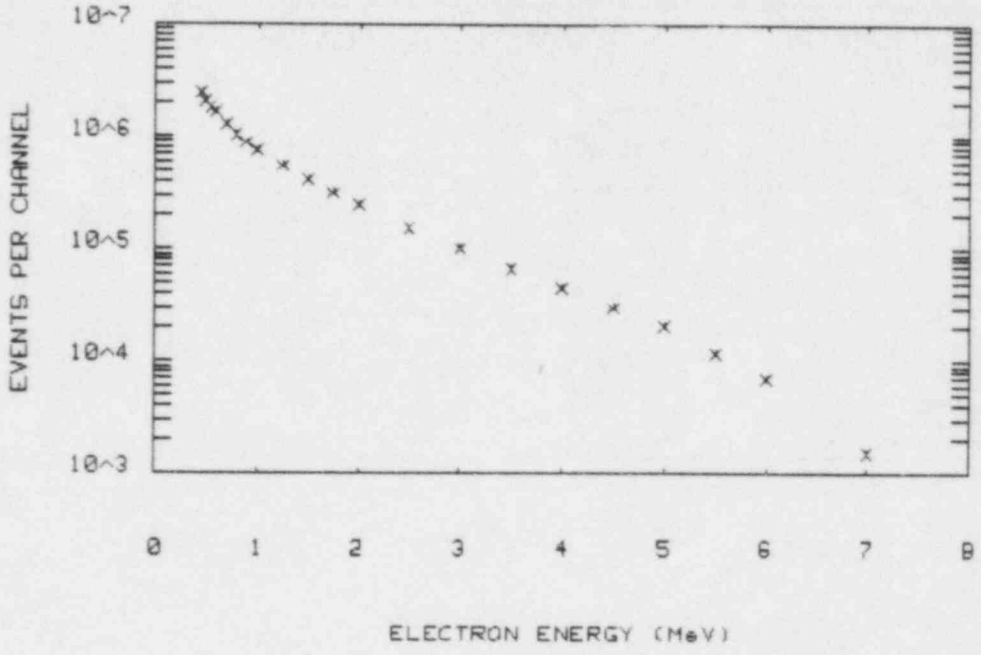

FIGURE HEDL-9. Si(Li) Observed Electron Spectrum at the 1/2-T Location of the 4/12 SSC Configuration.

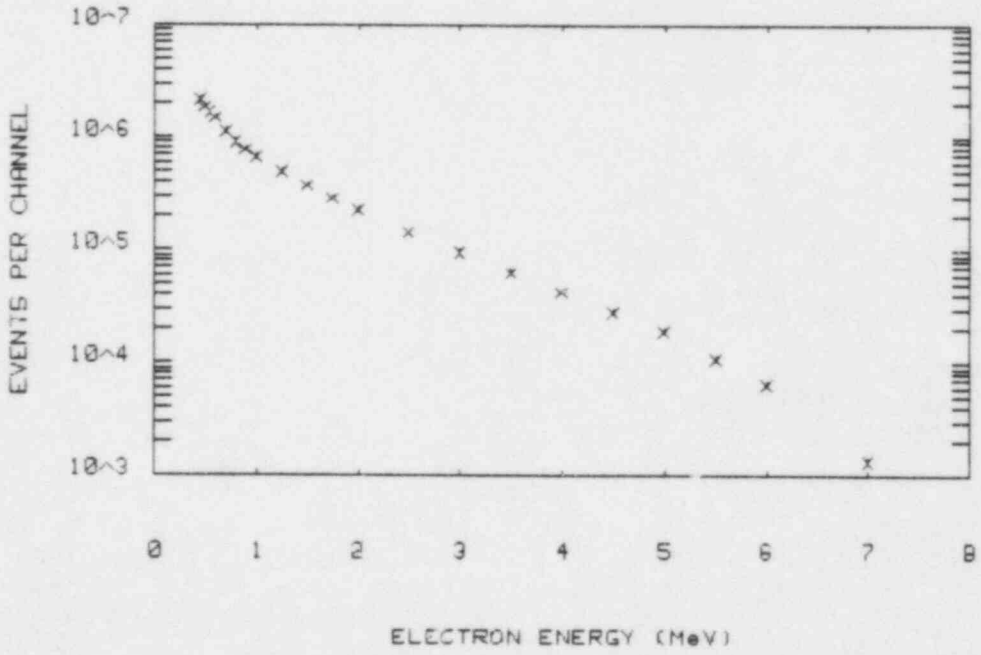

FIGURE HEDL-10. Si(Li) Observed Electron Spectrum at the 3/4-T Location of the 4/12 SSC Configuration.

TABLE HEDL-7

LOCATION-DEPENDENT FACTORS FOR PCA ELECTRON SPECTRA

	Configuration			
	12/13		4/12 SSC	
Location	PL*	PF	PL*	PF
1/4-T	1.19	1.30	1.08	1.16
1/2-T	5.04	1.24	3.93	1.14
3/4-T	20.0	1.18	11.86	1.11

* PCA power level in watts.

$$\varphi_n(E_i) = \varphi_a(E_i)/CF \quad , \tag{21}$$

where CF is the conversion factor from watts to neutrons/second. Numerical evaluation of CF has already been performed in Ref (Fa81a), which provides CF = 7.553×10^{10} n/(s•watt). Combining Equations (18) through (21), one, therefore, has

$$\varphi_n(E_i) = 2.343 \times 10^{-36} B(E_i)/SF \quad . \tag{22}$$

Use of $\varphi_n(E_i)$ in Equation (15), instead of $\varphi_a(E_i)$, will furnish the displacement rate, Δ_a, in units of displacements per atom per PCA core neutron.

1.2.3 Gamma-Ray Displacement Rate Results

The creation rate spectrum, $\varphi_n(E_i)$, has been used in Equation (15) and Δ_a has been determined by numerical integration. Gamma-ray displacement rates have been calculated for the six PCA electron spectra using the two values of $n(E_i)$ computed in Section 1.2.1 for the two different threshold displacement energies, T_d = 24 eV and 40 eV. As a typical example, the integrand of Equation (15) is displayed in Figure HEDL-11 for the 1/4-T location of the 12/13 configuration for T_d = 24 eV. This figure shows that the integrand decreases rapidly with increasing electron energy so that any error that results from the electron spectrum extending only up to 7 MeV is negligible. The behavior displayed in Figure HEDL-11 is typical of all the cases treated here.

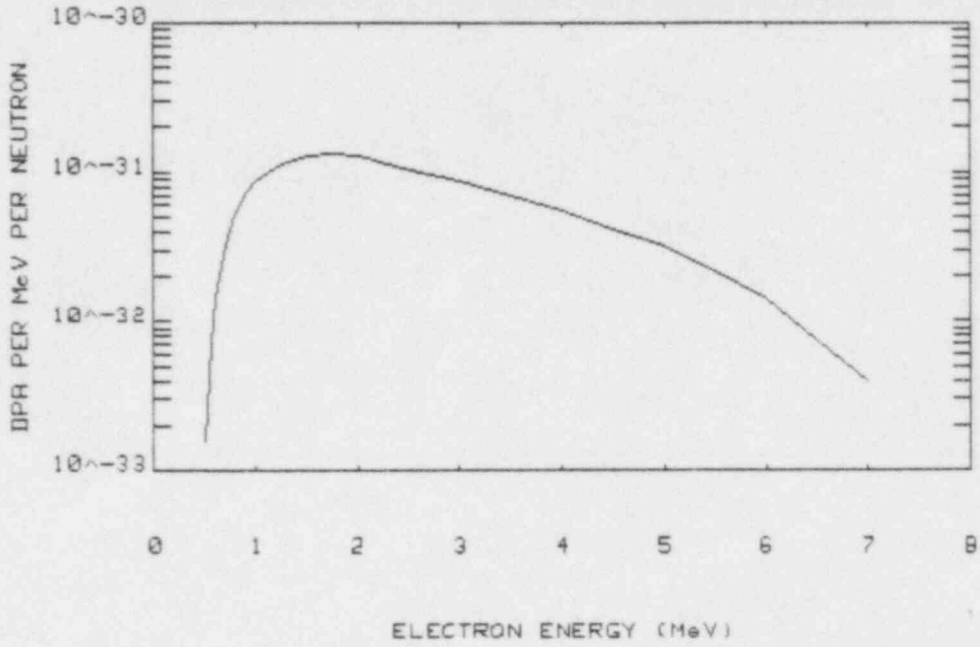

FIGURE HEDL-11. Integrand of Equation (15), $\varphi_n(E_i) \cdot n(E_i)$, as a Function of Initial Electron Energy attained at the 1/4-T Location of the 12/13 Configuration Using T_d = 24 eV.

The resulting gamma-ray displacement rates are summarized in Table HEDL-8. The relative gamma-to-neutron displacement rate ratio (γ/n) can be calculated from these results and the neutron displacement rates already reported for these configurations in the second NUREG report on the PCA (Li84b). The γ/n ratios so obtained are enumerated in Table HEDL-9. For both the 12/13 and 4/12 SSC configurations, the γ/n ratio decreases with increasing distance into the PV. This behavior is in accord with very simple physical considerations, since gamma-rays are attenuated more rapidly than neutrons in the steel medium of the PV.

These γ/n results prove that gamma-ray induced displacements are negligible compared with neutron-induced displacements within the PV. A quantitative result of the γ/n ratio attained at the surveillance capsule location is highly desirable, in view of the crucial use of this location in ongoing surveillance programs of commercial LWRs. Unfortunately, gamma-ray spectrometry was not conducted at the SSC location in the PCA. However, TLD was used at the SSC location of the 4/12 SSC configuration (Fa81b). Hence, it is possible to use observed gamma-ray dose rates as a rough scale factor to generate crude estimates of the gamma-ray displacement rate at the SSC location.

TABLE HEDL-8

GAMMA-RAY DISPLACEMENT RATES* IN THE PCA

	Configuration			
	12/13		4/12 SSC	
Location	T_d = 24 eV	T_d = 40 eV	T_d = 24 eV	T_d = 40 eV
1/4-T	3.90 E-31	1.45 E-31	1.06 E-30	4.15 E-31
1/2-T	1.12 E-31	4.23 E-32	2.83 E-31	1.12 E-31
3/4-T	3.06 E-32	1.17 E-32	8.84 E-32	3.49 E-32

* Units of displacements per atom per core neutron.

TABLE HEDL-9

γ/n RATIOS FOR THE PCA

	Configuration			
	12/13		4/12 SSC	
Location	T_d = 24 eV	T_d = 40 eV	T_d = 24 eV	T_d = 40 eV
1/4-T	5.2 E-3	1.9 E-3	2.6 E-3	1.0 E-3
1/2-T	2.7 E-3	1.0 E-3	1.2 E-3	4.7 E-4
3/4-T	1.4 E-3	5.2 E-4	7.2 E-4	2.8 E-4

Actually, the results of Si(Li) gamma-ray dosimetry and TLD measurements in the 4/12 SSC configuration are in good agreement (Ka84a). Since Si(Li) gamma-ray dosimetry was not conducted at the SSC location, only the TLD observations provide a consistent set of data that can be used for scaling. These TLD data together with the present gamma-ray displacement calculations can be found in Table HEDL-10.

The desired dose scale factor is simply the calculated Δ_a divided by the TLD dose rate. The last column in Table HEDL-10 provides the dose scale factor results. It can be seen from Table HEDL-10 that the dose scale factor is remarkably consistent for all three locations. Indeed, the average dose scale factor shows a deviation of less than 1 percent for both T_d = 24 eV and 40 eV. The gamma-ray displacement estimates generated with these scale factors are given in Table HEDL-11. In terms of these quantitative results, one can also conclude that the gamma-ray induced displacements at the SSC location are negligible relative to neutron induced displacements.

TABLE HEDL-10

DOSE RATE SCALE FACTOR

Location	TLD*	Δ_a**		Δ_a/TLD	
		T_d = 24 eV	T_d = 40 eV	T_d = 24 eV	T_d = 40 eV
1/4-T	255	1.06 E-30	4.15 E-31	4.157 E-33	1.628 E-33
1/2-T	68	2.83 E-31	1.12 E-31	4.162 E-33	1.647 E-33
3/4-T	21.5	8.84 E-32	3.49 E-32	4.112 E-33	1.623 E-33
Avg Dose Scale Factor:		(4.144 ± 0.028)E-33		(1.633 ± 0.013)E-33	

*TLD gamma-ray dose rate in units of mrad/h at a PCA power level of 1 watt (Fa81a).
**Units of displacements per atom per PCA core neutron.

TABLE HEDL-11

GAMMA-RAY DISPLACEMENT ESTIMATES FOR THE SSC LOCATION OF THE 4/12 SSC CONFIGURATION

T_d(eV)	Δ_a	γ/n*
24	1.36 E-29	2.7 E-3
40	5.36 E-30	1.1 E-3

*The neutron displacement rate for the SSC location was obtained from (Th84).

Expected Future Accomplishments

Future gamma-ray displacement data will be generated as measured and/or revised electron spectra become available.

C. CHARPY UPPER-SHELF DROP AS A FUNCTION OF CHEMISTRY AND FLUENCE-I

G. L. Guthrie (HEDL)

Objective

The ultimate objective of the present work is to determine a relationship giving the Charpy upper-shelf drop as a function of chemistry and fluence. The relationship is intended for use as part of future editions of Reg. Guide 1.99 (Re77). A more immediate objective is to assess the need for additional data and to provide interim formulas.

Summary

A working relationship with the Metals Property Council (MPC) has been established whereby the Hanford Engineering Development Laboratory (HEDL) and the Nuclear Regulatory Commission (NRC) provide computational services, reports of results, and consultation while the MPC and the American Society for Testing and Materials (ASTM) affiliates provide data, computational services, consultation, and advice.

The MPC has made available a data set consisting of chemistry and Charpy test results for 843 Charpy transition curve pairs (one irradiated specimen set and one unirradiated set in each pair). The data have been subjected to an extensive program of computer plotting (including stereo 3-D) to uncover any obvious correlations between Charpy upper-shelf drop and relevant variables, such as chemistry concentrations and fluence. In addition, more than 100 nonlinear least-squares fitting exercises have been performed with the same aim.

Results to date indicate that Charpy upper-shelf drop is a function of fluence, copper content, and unirradiated upper-shelf energy. Nickel is a possible second chemistry variable, but the evidence is not conclusive. There is even weaker evidence for a phosphorous effect that may be important in plate material.

Accomplishments and Status

Nonlinear least-squares fitting procedures and computer plotting techniques have been used to uncover functional relationships connecting: 1) irradiation-induced decrease in Charpy upper-shelf energy, 2) Charpy specimen chemistry, and 3) irradiation fluence.

The data base used was supplied by the MPC. It contained 843 records, in which each record consisted of a set of information intended to yield a value for an irradiation-induced shelf drop, together with the needed data on associated items, such as specimen chemistry, heat treatment, fluence, tensile properties, and the irradiation-induced shift in the ductile-to-brittle transition temperature.

The MPC data base was made available by John Koziol, Steve Byrne, and other members of the MPC with the cooperation of A. Schaeffer of the MPC. The MPC involvement was originated and negotiated by P. N. Randall of the NRC, who has also supplied advice on correlations to be investigated in the analysis of the data. Cooperation has also been obtained from B. Levine and D. McCune, who are currently doing an analysis of the irradiation-induced increase of the Charpy transition temperature using the same data base and who have offered useful suggestions on graphical techniques for uncovering correlations and possible errors in the data.

The data base contains information on several items, including weld flux type, heat chemistry, specimen chemistry, and a variety of fluence values (e.g., $E > 1.0$ MeV, $E > 0.1$).

With collaboration from P. N. Randall, a decision was made to concentrate on Cu, P, S, Si, and Ni as the chemistry variables. Actual specimen chemistry analysis results were used where available, and heat analysis values were used to fill in where the specimen values were absent.

The chosen procedure disregarded any data records that were deficient in chemistry information. For the neutron exposure values, displacements per atoms (dpa) would have been preferred as at least an alternate exposure index, but the information was lacking for a large fraction of the records. Consequently, fluence (n/cm^2, $E > 1.0$ MeV) was used for the exposure parameter, adopting the HEDL-revised value where available, or the reported calculated value supplied by the surveillance report analyst when the HEDL quantity was missing.

The 843 records were screened for gaps in information (e.g., missing chemistry values for one of the five chosen elements), and deficient records were omitted in a reduced list. This decreased the usable data set to 466 records.

An attempt was made to make use of knowledge gained in previous correlation studies involving the irradiation-induced increase in the 30 ft·lb Charpy transition temperature. The Charpy upper-shelf drop for each record was plotted as a function of the irradiation-induced increase in the 30 ft·lb Charpy transition temperature. Similar plots were made using percent shelf drop versus irradiation-induced transition shift. The use of percent shelf drop was suggested by previous work by P. N. Randall (Reg. Guide 1.99, Rev 1) (Re77) and Odette et al. (Od85).

The advantage of plotting shelf drop and percent shelf drop versus Charpy shift is that errors in reported chemistry values and in reported exposure values are largely suppressed in their effects on the plot. It could be expected that specimens exhibiting a large Charpy shift in a given irradiation experiment would also exhibit a large shelf drop. The plots can be used, among other purposes, to detect errors in the data compile.

An extreme scatter pattern on both types of plots would mean that the shelf drop data and perhaps the material itself were irascible and unpredictable

in a way that was unlikely to be improved by obtaining better chemistry values or better fluence values. A straightline relationship between shelf drop (or percent drop) and Charpy shift would indicate that the fluence part of the shelf drop funcional relationship could be largely borrowed from the previous work on Charpy trend curves (i.e., the functional form could be expected to be adequate).

Following a suggestion by B. Levine, another feature was added to the plots. As an example, percent drop was plotted versus Charpy shift using one symbol for specimens having higher-than-average sulfur content and a second symbol for lower-than-average sulfur content. The purpose of this is: if changes in sulfur content have little effect on the Charpy shift but have a large effect on the shelf drop, all points of a given chemistry (other than sulfur) and a given fluence will plot at the same level of Charpy shift (similar ordinate values), but will spread in the abscissa values with the higher-than-average sulfur points showing larger abscissa values. Thus, any discernable pattern of the two plotting symbols will indicate a drastic change in the importance of sulfur for the two phenomena.

156 separate plots of the type indicated were made for all five elements and for various subdivisions of the data. The subdivisions were pressurized water reactor (PWR), boiling water reactor (BWR), and test reactor irradiations, plate, forging and weld product forms, and Linde 80® and non-Linde 80 weld fluxes.

A typical plot is shown in Figure HEDL-12 showing percent shelf drop versus Charpy shift for plates in a PWR irradiation, with the data points tagged for being above or below average in phosphorus content. The lack of any discernable bowing of the overall plot (concave or convex) leads to the conclusion that the fluence dependence of the shelf drop is about the same as for the Charpy shift. The lack of any distribution pattern in the X and square symbols shows a lack of any overwhelming difference in the relative importance of phosphorus in the two phenomena. The magnitude of the overall scatter indicates that very satisfying success will be obtained only after a struggle.

Similar graphic guidance was sought from 3-D stereo pair computer plots examined under a stereo viewer, again with a wide variety of choices of variables for the three axes. The overall impression was that percent shelf drop correlated better than shelf drop against any independent variables showing hope, and these latter were almost completely restricted to copper and fluence.

Charpy trend curve formulas generated at HEDL in recent years have, for the most part, been of the form

$$\Delta T = f_1(\text{chem}) \cdot f_2(\text{fluence}) \qquad (1)$$

®Linde 80 is a registered trademark of Union Carbide, New York, NY.

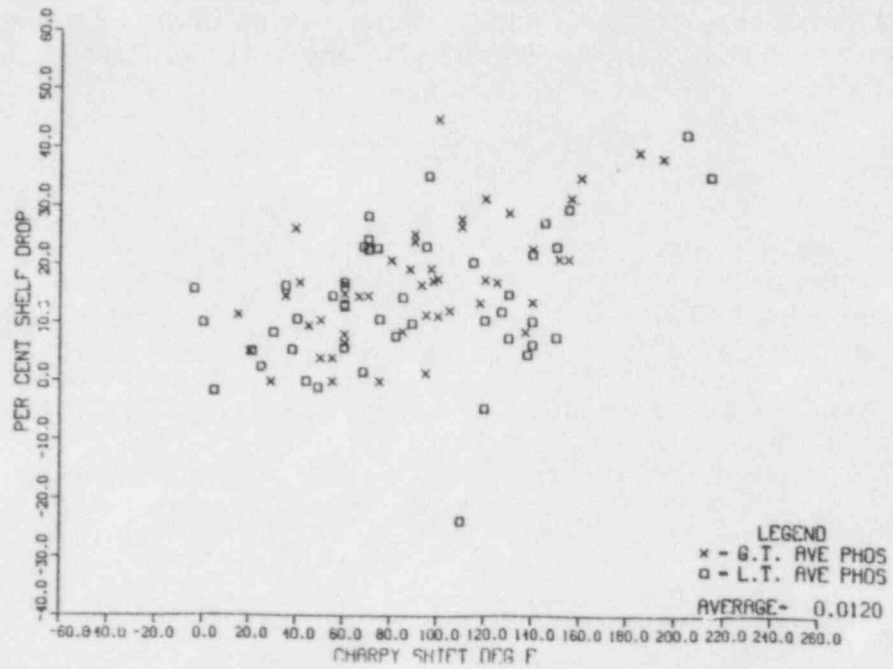

FIGURE HEDL-12. Percent Shelf Drop Versus Charphy Shift for Plates in PWR Irradiation.

where the fluence function has been of the form

$$f_2(\text{fluence}) = \text{fluence}^{(A + B\ \ln\text{fluence})} \qquad (2)$$

The lack of any obvious nonlinear pattern in the plots of percent shelf drop versus Charpy shift suggested that such a fluence functional dependence could be used for percent shelf drop. Then, since copper seemed to be the only obvious important chemical variable,

$$\frac{\text{Shelf Drop}}{\text{Original Shelf}} = (A + B \cdot \text{Copper})\text{fluence}^{C + D\ \ln\text{fluence}} \qquad (3)$$

seemed to be a reasonable start.

To allow some additional flexibility, the form

$$\text{Drop} = (\text{Orig Shelf})^{x(1)} \cdot [x(2) + x(3)\text{Cu}]\ (\phi t)^{x(4) + x(5)\ \ln(\phi t)} \qquad (4)$$

was used. Besides copper as the independent variable, Si, S, Ni, and P were also tried. This approach was applied to several subsets of the data base. Table HEDL-12 shows results for a data set consisting of 143 combined points from irradiations of the welds in PWRs, BWRs, and test reactors. The equation used was

$$USD = UUS^{x(1)} \cdot [x(2) + x(3)El]flu^{x(4) + x(5)\ ln(flu)} \qquad (5)$$

where:

USD = Upper-shelf drop

UUS = Unirradiated upper-shelf energy

El = Element proposed as an important independent variable

flu = Fluence (E > 1.0 MeV) in units of 10^{19} n/cm^2

The column marked ID in Table HEDL-12 identifies the computer run and σ is the standard deviation. The data used for the exercise consisted of all the weld data available from the 466-point reduced set, except for one PWR, one test reactor, and three BWR points that showed a large scatter in other preliminary fitting and plotting exercises. This gave 143 weld data points and 138 degress of freedom.

When the same data set was fitted to the law

$$USD = x(1) \qquad (6)$$

the standard deviation was 15.43 ft•lb, so the success of the formulas above is not spectacular. Eq. (5) only eliminates 52% of the original [Eq. (5)] sum of square of "errors" when compared to a simple average . However, copper is clearly an improvement over Si, S, Ni, or P as a choice for El.

Using the same data set, the formula of Eq. (5) was expanded to add a second element, using

$$USD = UUS^{x(1)} \cdot [x(2) + x(3)Cu + x(4)El]flu^{x(5) + x(6)\ ln(flu)} \qquad (7)$$

The results are shown in Table HEDL-13.

The improvement in the standard deviation going from Eq. (5) to Eq. (7) is not as striking as the improvement using copper in Eq. (5) versus Eq. (6). Nickel gives the best results in Eq. (7), but not by an amount to give great confidence that it represents a real physical phenomenon.

If an F test is used to decide if the improvement from the added nickel term is real, the F value is 13, which is well over the 99% confidence level for a real improvement. Phorphorus as an added term shows an F of 9.38, which

TABLE HEDL-12

NUMERICAL VALUES FOR PARAMETERS IN EQUATION (5)

ID	El	x(1)	x(2)	x(3)	x(4)	x(5)	σ
4.2.13.50	Cu	1.149	0.0133	0.463	0.242	-0.0253	10.876
4.2.14.03	Si	-0.0319	39.7	-34.4	0.149	-0.0715	13.971
4.2.14.04	S	0.386	4.68	-36.39	0.132	-0.110	14.326
4.2.14.05.02	Ni	0.352	3.74	2.31	0.148	-0.131	14.162
4.2.14.05.46	P	0.480	1.98	49.0	0.164	-0.101	14.340

TABLE HEDL-13

NUMERICAL VALUES FOR PARAMETERS IN EQUATION (7)

ID	El	x(1)	x(2)	x(3)	x(4)	x(5)	x(6)	σ
4.2.16.04	Si	1.097	0.0242	0.585	-0.0191	0.240	-0.026	10.91
4.2.16.06	S	1.142	0.0170	0.477	-0.2157	0.242	-0.027	10.90
4.2.16.03	Ni	1.188	-0.008	0.403	0.0312	0.248	-0.039	10.51
4.2.16.05	P	1.272	-0.006	0.252	1.257	0.255	-0.043	10.56

is also over the 99% confidence level for a real improvement. However, this line of reasoning requires great confidence in the nonlinear least-squares result, and also relies on the applicability of linear F function theory. Tentatively, we choose to accept the use of Eq. (7) for welds, with copper and Ni as independent chemical variables using the parameters as determined in computer run 4.2.16.03, i.e.,

$$\text{Upper-Shelf Drop} = \text{UUS}^{1.188} \cdot (-0.008 + 0.403\,\text{Cu} + 0.0312\,\text{Ni})\text{flu}^{0.248 - 0.039\ln(\text{flu})} \quad (8)$$

where fluence is measured in units of 10^{19} n/cm² (E > 1.0 MeV), and the shelf drop is in ft•lb.

We may compare Eq. (8) to the 4.2.13.50 version of Eq. (5), as given by Table HEDL-14. This compares 1) the shelf drop formula [Eq. (5)] with copper as the only independent chemical variable and 2) the shelf drop formula after the nickel term is added [Eq. (8)]. The coefficients are given in Table HEDL-13. We find that the copper coefficients are similar [0.463 for Eq. (5) and 0.403 for Eq. (8)]. The decrease (0.463 to 0.403) going to Eq. (8) is because copper and nickel are correlated in the data so that adding a positive nickel coefficient allows the copper coefficient to be reduced. The constant part of the fluence exponent is about the same in each case, ∿0.24, and agrees roughly with the similar value found for formulas for Charpy transition temperature increases (∿0.28 to 0.30).

The UUS exponents (1.149 and 1.188) are not far from the 1.0 values used by Randall and Odette et al. Some confidence in the UUS exponent may be gained by looking at data fits of the type

$$\text{Shelf drop} = x(1)\,UUS^{x(2)}\,flu^{x(3)} \tag{9}$$

or

$$\text{Shelf drop} = x(1)\,(\Delta T_{CV})^{x(2)}\,UUS^{x(3)} \tag{10}$$

where errors in reported chemistry do not affect the fitting procedure.

Eqs. (9) and (10) have been used for various subdivisions of the weld data, and UUS exponents have generally ranged from 1.28 to 1.6 for data sets where the fit resulted in low standard deviations ($\sigma < 13$). Thus, we suspect that the UUS exponent is indeed >1.0 and may be slightly higher than the values given in Table HEDL-14. The log(flu) coefficients are negative in agreement with the values found in Charpy trend curve formulas and about the same order of magnitude.

Lower standard deviations were found for fitting exercises using smaller subsets of the weld data. The 36 PWR welds with non-Linde 80 weld flux were used to develop the equation

$$USD = UUS^{1.80}(-0.00179 + 0.0306Cu + 0.0042Ni) \cdot flu^{0.176 - 0.052\ \ln(flu)} \tag{11}$$

where again flu is fluence (E > 1.0 MeV) in units of 10^{19} n/cm². For Eq. (11), the standard deviation was 7.8 ft•lb.

TABLE HEDL-14

COMPARISON OF NUMERICAL VALUES OF PARAMETERS IN EQUATIONS (5) AND (8)

Equation No.	UUS x(1)	Constant Term x(2)	Cu x(3)	Ni Coeff	Constant Flu Exp	lnflu Coeff
(5)	1.149	0.0133	0.463	0	0.242	-0.0253
(8)	1.188	-0.008	0.403	0.0312	0.248	-0.039

Figures HEDL-13 and HEDL-14 show shelf drop and percent shelf drop versus Charpy shift for all PWR welds. The stray non-Linde 80 point in the lower right was omitted from the fitting exercise just mentioned. The cause of the deviation of the stray point was found to be clerical.

Casual examination and comparison of the two figures gives the impression that USD/UUS (percent drop) correlates better than USD alone when the correlation is versus Charpy shift. In fact, as is shown in Eq. (11), $USD/USS^{1.51}$ was found to give a better correlation than $USD/USS^{1.0}$ for the best least-squares fit. The Linde 80 welds show such a scatter that little faith can be placed in any significance of parameters developed in a separate Linde 80 fitting procedure.

For the plata data, a fitting exercise of the type already described in Eq. (5) and Eq. (8) was performed using 243 data records from PWR, BWR, and test reactor data. For the fit to Eq. (5), it was found that

$$USD = UUS^{1.89}(0.00093 + 0.007Cu)flu^{0.2875 + 0.024\ \ln(flu)} \qquad (12)$$

gave a better fit than similar equations using P, Si, Ni, or S in place of copper.

The flu term is fluence ($E > 1.0$ MeV) in units of 10^{19} n/cm^2. The standard deviation was 11.57 ft•lb for Eq. (12), compared to 12.36, 12.55, 12.58, and 12.53 ft•lb when the other elements were substituted for copper in the order given above.

When a fit of the type shown in Eq. (8) was performed to pick the next element after copper, phosphorus was the apparent winner with

$$USD = UUS^{1.86}(0.000555 + 0.00792Cu + 0.0542P)flu^{0.3129 + 0.0224\ \ln(flu)} \qquad (13)$$

where the terms are as described previously. The standard deviation was 11.46 ft•lb.

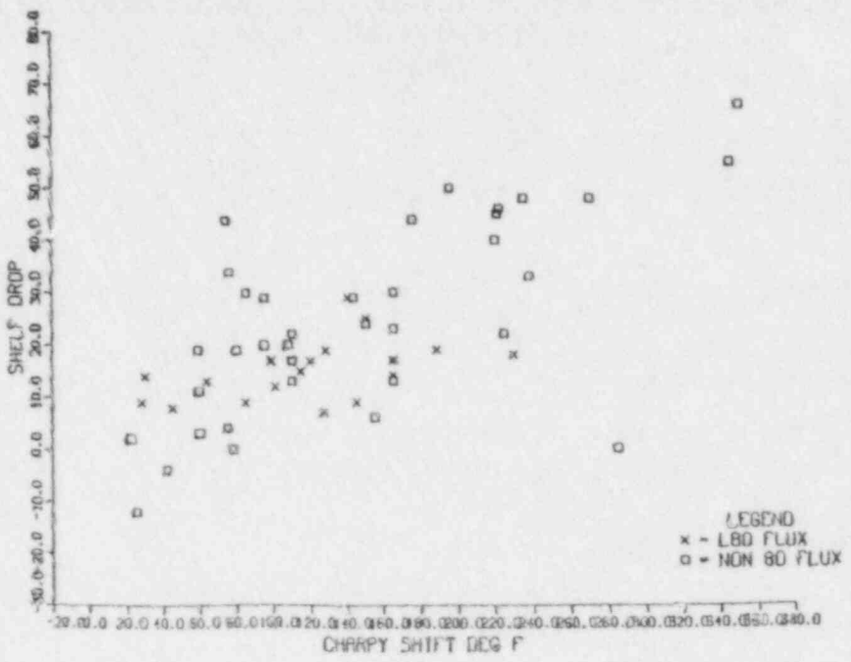

FIGURE HEDL-13. Shelf Drop Versus Charpy Shift for All Welds in PWR Irradiation.

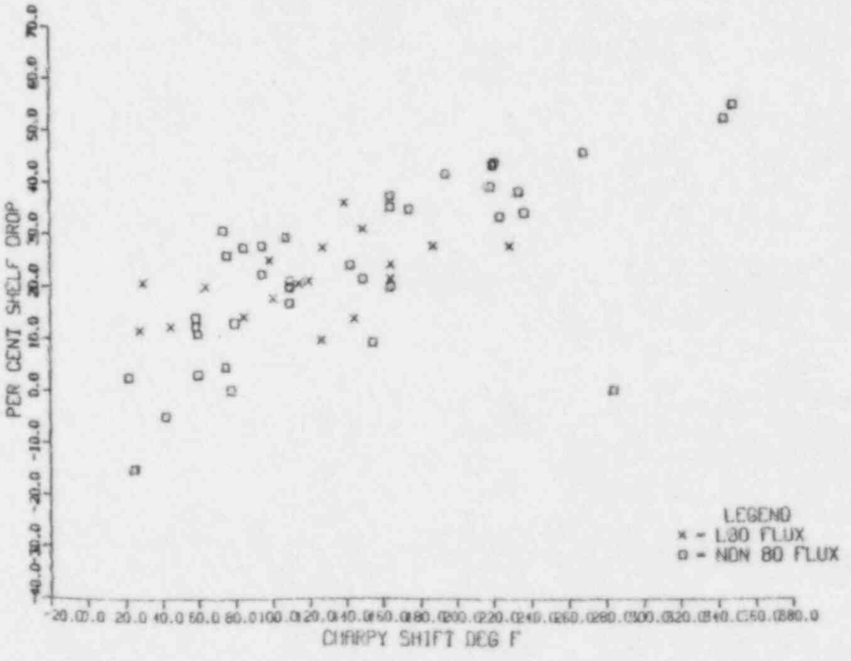

FIGURE HEDL-14. Percent Shelf Drop Versus Charpy Shift for All Welds in PWR Irradiation.

As was found with the welds, various subsets of the data could be used to produce formulas with lower standard deviations. A set of 93 PWR plate data records gave a standard deviation of 9.62 ft•lb in the simple formula

$$USD = 0.00242 \cdot UUS^{1.916} \cdot flu^{0.3092} \quad (14)$$

and 9.58 ft•lb standard deviation for the same data set in the formula

$$USD = UUS^{1.90}(0.000075 + 0.00056Cu)^{0.6827} \cdot flu^{0.273 - 0.021 \ln(flu)} \quad (15)$$

For BWR plates, a standard deviation of 6.67 ft•lb was found for

$$USD = UUS^{1.26}(-0.00033 + 0.0040Cu)^{0.364} flu^{0.587 - 0.266 \ln(flu)} \quad (16)$$

In all the above, flu is fluence ($E > 1.0$ MeV) in units of 10^{19} n/cm^2.

Conclusions

The scatter in the data is more of an impediment than in previous work involving the Charpy shift. Current examinations of the data do not give any reason to abandon fluence functions of the type used in the previous studies of Charpy trend curves.

Copper is the only element that has been reliably identified at this time as a contributor to the irradiation-induced drop in upper shelf for both welds and plates. Nickel is a possible secondary element. There is even weaker evidence for phosphorus, which may possibly be important in plate material.

The drop in upper shelf energy appears to correlate with the unirradiated shelf energy raised to some fixed power "N". The value of N appears to be >1 and <2.

Expected Future Accomplishments

Work on this subject is continuing and will be reported in the next LWR-PV-SDIP progress report.

Acknowledgments

The help of P. N. Randall, John Koziol, Steve Byrne, Tom Magers, Steve Yanichko, A. Schaeffer, B. Levine, and D. McCune are gratefully acknowledged. Thanks are also extended to R. L. Simons for help and comments in regard to the HEDL fluence values, and to Gary Hammons and Doreen Amodio for help in setting up and reading the MPC tape.

D. MEASUREMENT ACCURACIES REQUIRED FOR A DEFINITIVE STATEMENT RANKING DPA AND FLUENCE IN A PSF-TYPE EXPERIMENT

G. L. Guthrie (HEDL)

Objective

The objective of this study is to obtain general guidelines indicating the measurment accuracies required in the Poolside Facility (PSF) experiment to allow the extraction of particular information in the analysis of the experiment. This allows analytical effort on the PSF data to be directed toward goals that are attainable and away from efforts where the data are insufficient to produce conclusions.

The objective of the PSF is to generate information on flux spectral effects, rate effects, chemistry effects, and falloff of pressure vessel embrittlement damage with penetration into the pressure vessel wall. This information is useful as guidance in writing regulations for surveillance programs.

Summary

A part of the PSF experiment has been analyzed in an attempt to determine measurment accuracies required for a definitive statement ranking fluence ($E > 1.0$ MeV) or dpa as being a preferred neutron exposure parameter. The analysis concerns required accuracies in mechanical property degradation and exposure parameters. The analysis only concerns the comparison of mechanical property degradation in pairs of test capsules having matched exposure values, e.g., the pair consisting of the 0-T and SSC-2 capsules. Definite conclusions regarding the relative merits of fluence ($E > 1.0$ MeV) and dpa, if based solely on matched pair experiments of the type indicated, would require measurement accuracies that are difficult to obtain.

Accomplishments and Status

This study investigates the accuracies required in mechanical property degradation measurements and exposure parameters, when matched exposures (SSC-2 vs 0 T or SSC-1 vs 1/4 T) are used to endorse either dpa or fluence ($E > 1.0$ Mev) as being a preferred exposure index for property degradation predictive purposes. We assume that identical alloy mechanical specimens are exposed to approximately the same neutron damage levels in two capsules (A and B) having slightly different ratios of fluence/dpa. We also assume that over some short range of exposure, the property deterioration can be expressed as

$$\text{Damage} = C \cdot (\text{dose})^N \qquad (1)$$

where N is approximately 0.3 and the value of C will depend on: 1) whether dpa or fluence is used as a measure of "dose" and 2) the property and alloy being observed. Then for any matched capsules A and B, for a specific alloy and a specific property, (e.g., Charpy transition temperature)

$$\text{Ratio of predicted damage} = (\text{dpa}_A/\text{dpa}_B)^N \qquad (2)$$

using dpa as the measure of dose. Using fluence (n/cm^2, $E > 1.0$ Mev) we find the predicted ratio is

$$\text{Ratio of predicted damage} = (\text{fluence}_A/\text{fluence}_B)^N \qquad (3)$$

In both Eqs. (1) and (2), the damage ratio refers to the ratio of property change in Capsule A to that in Capsule B for a given property of a particular alloy. For matched experiments similar to the 0 T and SSC-2, we assume that the dpa/dpa or fluence/fluence ratios are close to unity, and the exponent N is approximately 0.3.

For any given single alloy, we can measure the damage ratio for the specimens in the two capsules. If a large series of "identical" experiments is undertaken and a series of calculations is made of the above predicted ratios, we might find results depicted in Figure HEDL-15, assuming random errors in all calculated and measured quantities.

In any given case, we might find that the peaks of the distribution curves for the damage ratios fall in the sequence: 1) dpa, 2) measured, and 3) fluence, as shown, or in any of the other five possible sequences. But whatever the sequence, if we wish to choose dpa rather than fluence as a preferred exposure index, we need to have noticeably better agreement between the dpa-based ratio calculation and the measurement ratio than between the fluence-based ratio calculation and the measurement ratio.

Using a notation where dpa_A is P_A and fluence_A is F_A, while damage measurement in Capsule A is M_A, we have the requirement

$$\left| (P_A/P_B)^N - M_A/M_B \right| \ll \left| (F_A/F_B)^N - M_A/M_B \right| \qquad (4)$$

if we are to endorse dpa rather than fluence.

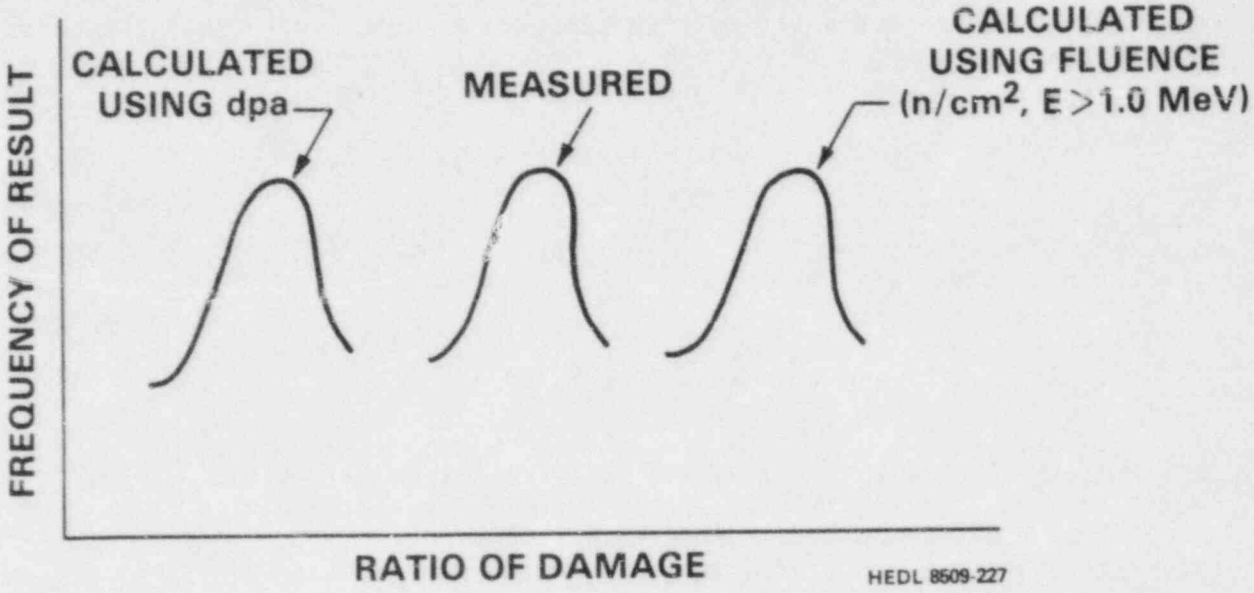

FIGURE HEDL-15. Ratio of Damage in Capsule A to That in Capsule B.

We cannot be sure of the truth of Eq. (4) unless the difference between $(P_A/P_B)^N$ and $(F_A/F_B)^N$ is large compared to the uncertainty in either of these quantities.

Note that

$$\left(\frac{P_A}{P_B}\right)^N = \left(\frac{P_A + P_B - P_B}{P_B}\right)^N = \left(1 + \frac{P_A - P_B}{P_B}\right)^N \tag{5}$$

$$\approx 1 + N\left(\frac{P_A - P_B}{P_B}\right) = 1 - N + N\,\frac{P_A}{P_B} \tag{6}$$

when P_A/P_B is close to unity.

Similarly,

$$\left(\frac{F_A}{F_B}\right)^N \approx 1 + N\left(\frac{F_A - F_B}{F_B}\right) = 1 - N + N\ (F_A/F_B). \tag{7}$$

We define Z to be

$$Z = 1 - N + N\,(P_A/P_B) \tag{8}$$

and derive the expectation value of the error in Z, taking variations in all quantities to obtain

$$\delta Z = -\delta N + \delta N \cdot (P_A/P_B) + N \left(\frac{P_B \cdot \delta P_A - P_A \cdot \delta P_B}{P_B^2} \right) \tag{9}$$

$$\delta Z = \delta N \left((P_A/P_B) - 1 \right) + N \left(\frac{P_B \cdot \delta P_A - P_A \cdot \delta P_B}{P_B^2} \right) \tag{10}$$

Squaring both sides, averaging, dropping uncorrelated product terms, and taking square roots, we obtain

$$\overline{\delta Z} = \sqrt{(\overline{\delta N})^2 \left(\frac{P_A}{P_B} - 1 \right)^2 + N^2 \left[\frac{P_B^2 \, (\overline{\delta P_A})^2 + P_A^2 \, (\overline{\delta P_B})^2}{P_B^4} \right]} \tag{11}$$

In the above, $\overline{\delta Z}$ is the expectation value of the error in Z, and therefore the expectation value of the error in $(P_A/P_B)^N$.

In the above, product terms involving $\delta N \cdot \delta P_A$, $\delta P_A \cdot \delta P_B$, and $\delta P_B \cdot \delta P_A$ have been dropped on the assumption that (e.g.,) δN and δP_A are uncorrelated and will average to zero.

If $\overline{\delta P}_A$ is roughly equal to $\overline{\delta P}_B$ we may factor N out of the square root of Eq. (11) and obtain

$$\overline{\delta Z} = N \sqrt{\left(\frac{\overline{\delta N}}{N} \right)^2 \left(\frac{P_A}{P_B} - 1 \right)^2 + \left(\frac{\overline{\delta P}}{P_B} \right)^2 \left[1 + \left(\frac{P_A}{P_B} \right)^2 \right]} \tag{12}$$

where $\overline{\delta P}$ is the uncertainty in either P_A or P_B. Now, N has generally been found to be between ~0.25 and 0.35, so that we may estimate $N \simeq 0.3$ and $\delta N \sim 0.05$. Also, for the matched experiments SSC-2 vs 0 T or SSC-1 vs 1/4 T, we can estimate that P_A/P_B is between 3/4 and 4/3.

Substituting these numbers in Eq. (12), we find that the first term under the square root can be neglected compared to the second term.

Consequently, we find

$$\overline{\delta Z} \approx \sqrt{2}\, N \, \frac{\overline{\delta P}}{P} \tag{13}$$

or

The expected error in $(P_A/P_B)^N$ is given by

$$\delta \left[\overline{\left(\frac{P_A}{P_B}\right)^N}\right] \approx \sqrt{2}\, N \, \frac{\overline{\delta P}}{P} \tag{14}$$

where P is either P_A or P_B, since the two are nearly equal. Similarly the expected error in $(F_A/F_B)^N$ is given by

$$\delta \left[\overline{\left(\frac{F_A}{F_B}\right)^N}\right] \approx \sqrt{2}\, N \, \frac{\overline{\delta F}}{F} \tag{15}$$

using a similar notation.

We must now make use of the fact that when two quantities x and y have comparable uncertainties, the uncertainty in $(x - y)$ is $\sqrt{2} \cdot \overline{\delta x}$. Consequently

$$\delta\left[\overline{(P_A/P_B)^N - (F_A/F_B)^N}\right] = 2N \cdot \overline{\delta P}/P \tag{16}$$

If we require a better agreement between $(P_A/P_B)^N$ and (M_A/M_B) than between $(F_A/F_B)^N$ and (M_A/M_B), we must be able to distinguish between $(P_A/P_B)^N$ and $(F_A/F_B)^N$. If we require that

$$(P_A/P_B)^N - (F_A/F_B)^N \geq 3\delta\left[\overline{(P_A/P_B)^N - (F_A/F_B)^N}\right] \tag{17}$$

where $\delta[\overline{(P_A/P_B)^N - (F_A/F_B)^N}]$ is the expected value of the error in $[(P_A/P_B)^N - (F_A/F_B)^N]$ then for the comparison of SSC-2 and 0 T we require that

$$\frac{\overline{\delta P}}{P} < \frac{1}{3} \cdot \frac{1}{2} \cdot \frac{1}{0.3} \left| \left(\frac{0.0850}{0.0648}\right)^{0.3} - \left(\frac{5.465}{4.065}\right)^{0.3} \right| \tag{18}$$

In the above, we have assumed N = 0.3 and have used the concensus values of the capsule center dpa and fluence exposure parameters. Eq. (18) was obtained by combining Eqs. (16) and (17). From Eq. (18) we find that

$$\frac{\overline{\delta P}}{P} < 0.00447 \tag{19}$$

or it is necessary to measure the exposure values to better than 0.5% to reach a reliable (3σ) conclusion about the relative merits of dpa and fluence, using a comparison of the 0 T and SSC-2 mechanical properties experiments. When a comparison of the SSC-1 and 1/4-T capsules is used, the required accuracy is less stringent. For this case,

$$\frac{\overline{\delta P}}{P} < \frac{1}{3} \cdot \frac{1}{2} \cdot \frac{1}{0.3} \left| \left(\frac{0.03955}{0.03985}\right)^{0.3} - \left(\frac{2.56}{2.195}\right)^{0.3} \right| \tag{20}$$

or

$$\frac{\overline{\delta P}}{P} < 0.0275 \tag{21}$$

requiring a 2.75% accuracy in the dose measurements to get a reliable (3σ) determination of the superiority of dpa over fluence.

If we also require that the difference in dpa and fluence based predictions should be large compared to the error in the measured properties, then

$$\left| (P_A/P_B)^N - (F_A/F_B)^N \right| \Big/ \left[\delta \left(\overline{M_A/M_B}\right) \right] > 3 \tag{22}$$

where (M_A/M_B) is the ratio of the observed property change in Capsules A and B. The relation

$$\delta\left(\overline{M_A/M_B}\right) = \sqrt{2}\left(\frac{\overline{\delta M}}{M}\right) \tag{23}$$

can be derived by the methods used previously.

Then Eq. (22) becomes

$$\frac{\delta M}{M} < \frac{1}{3} \cdot \frac{1}{2} \left| \left(\frac{P_A}{P_B}\right)^{0.3} - \left(\frac{F_A}{F_B}\right)^{0.3} \right| \qquad (24)$$

Using the concensus values for the SSC-2 and 0-T exposure values, Eq. (24) becomes

$$\overline{\frac{\delta M}{M}} < 0.19\% \qquad (25)$$

whereas

$$\overline{\frac{\delta M}{M}} < 1.17\% \qquad (26)$$

for a comparison of SSC-1 and 1/4-T capsules. The basic information developed above is summarized in Table HEDL-15.

Table HEDL-15 gives a necessary but not sufficient condition for the 1σ measurement accuracy needed to make a 3σ choice that dpa (or fluence) is a better damage correlator than fluence (dpa), using a comparison of results from two matched capsules having similar property damage but different ratios of dpa/fluence, working with a single alloy. More stringent necessary requirements exist when the measured damage ratio (Capsule A/Capsule B) has a value that falls between the damage ratios calculated using dpa and fluence.

Of course, if we use several different alloys, and if we assume that relative merits of the two exposure indices are the same for all of them, then the accuracy requirement are decreased. For six alloys, we should expect the required accuracy to be relaxed by $6^{0.5}$, or the required accuracy for $\overline{\delta M}/M$ becomes 2.72% for the property change in each alloy when working with six independent alloys in capsules SSC-1 and 1/4 T.

In all of the above, no account has been taken of the added complications because of possible rate effects or possible errors in the correlations.

The derivations above give necessary but not sufficient conditions for accuracies required to distinguish between the merits of dpa and fluence. The derived relations are necessary conditions for all the sequences alluded to in Figure HEDL-15 and in the text immediately following the figure.

TABLE HEDL-15

ACCURACY REQUIREMENTS

PARAMETERS MEASURED \ CAPSULES COMPARED	SSC-2 vs 0T	SSC-1 vs 1/4 T
NEUTRON EXPOSURE	0.45%	2.75%
MECHANICAL PROPERTY DEGRADATION	0.19%	1.17%

However, for the sequence actually depicted in Figure HEDL-15, the methods used above can also be used to derive the necessary condition that

$$\left| RM - \frac{RP + RF}{2} \right| >> 3 \sqrt{\left[\delta(\overline{RM})\right]^2 + \frac{1}{2}\left[\delta(\overline{RP})\right]^2} \qquad (27)$$

where we have used the notation

$$RM = M_A/M_B \qquad (28)$$

$$RP = (P_A/P_B)^{0.3} \qquad (29)$$

$$RF = (F_A/F_B)^{0.3} \qquad (30)$$

This relationship Eq. (27) is slightly more restrictive than the relations already derived but depends on the sequence of values for $(F_A/F_B)^N$, $(P_A/P_B)^N$ and $(M_A/M_B)^N$ and therefore might not apply for all alloys. The relations derived in detail in Eqs. (1) through (24) apply as necessary conditions in all cases.

Expected Future Accomplishments

No definite plans for additional work on this topic exists at the present time.

E. DAMAGE RATE AND SPECTRUM EFFECTS IN FERRITIC STEEL ΔNDTT DATA

R. L. Simons (HEDL)

Objective

The objective of the present work is to derive formulas that improve the accuracy of the prediction of the irradiation-induced shift in the Charpy transition temperature for pressure vessel steel. The results are applicable to developing and testing procedures that will be recommended in the ASTM Standard, "Damage Correlation for Reactor Vessel Surveillance." These objectives are closely associated with and support those reported in Sections HEDL-A, -B, -C, -D, and -F.

Summary

A physically based model for irradiation-induced hardening in pressure vessel steels was developed to incorporate neutron spectrum variations and damage rate effects. A spectrum damage index was found that gives improved correlations of change in nil ductility transition temperature (ΔNDTT) data with exposure. The new damage index, proportional to Frenkel pair production at 4°K, is based on measurements of change in resistivity caused by irradiation in various neutron spectra and with accelerated charged particles.

A damage rate effect for a neutron exposure of 0.03 dpa ($\sim$2 x 10^{19} n/cm², E > 1 MeV), deduced from the correlation of the ASTM A302B Reference plate steel, implied that thermal emission of point defects from clusters was controlling at both low- and high-temperature irradiations. However, the HSST A533B Reference plate 03 and two forging data sets in the poolside facility (PSF) irradiation did not support any discernable or significant damage rate effect for an exposure of 0.03 dpa. The two weld data sets showed a damage rate effect dominated by recombination at 0.03 dpa. The rate effect for the welds explains why the high-rate simulated surveillance capsule (SSC) data showed a lower property change than the simulated pressure vessel (SPV) data. These results are applicable for neutron exposure rates in the range of $\sim 10^{-10}$ to 10^{-8} dpa/s.

The results of this physcially based study are consistent with those reported by McElroy et al., Section HEDL-F, for the same PSF data base and a wider range of weld materials with copper content up to 0.36 wt%. The present study is limited to plate, forging, and weld materials with copper content in the 0.05 to 0.24 wt% range.

Accomplishments and Status

1.0 Introduction

To ensure the service integrity of LWR containment vessels researchers have developed trend curves for ΔNDTT as a function of neutron fluence (>1 MeV) or

displacements per atom (dpa) in order to predict the condition of the reactor vessel wall (Gu85,Pe84). The equations are generally developed for a narrow irradiation temperature range and are based primarily on data from existing LWR surveillance programs.

There are three areas of trend curve model development that will be addressed in this report: 1) physically based models that relate the irradiation-induced microstructure to ΔNDTT, 2) spectrum effects beyond $\phi t > 1$ MeV and dpa, and 3) damage rate effects. The data base to be used will be limited to data on low-irradiation temperature (<230°C) ASTM A302B Reference plate steel and to data obtained on the same and five other plate, forging, and weld materials irradiated at high-temperature (288°C) in the PSF irradiation of a SSC and SPV. The low-irradiation temperature of the A302B steel was accomplished in research reactors, including SSC and SPV mockups at the Industrial Research Laboratory (IRL) (Se71,Si80b,Si83). For the ASTM A302B plate material, this provided a unique opportunity to study through wall embrittlement data for both low- (<116°C) and high-temperature (288°C) irradiations.

2.0 Physically Based Model

As a first step, the macroscopic property change (ΔNDTT) should be related to the existing microstructure. Odette (Od83a) has demonstrated empirically that ΔNDTT at 30 ft·lb absorbed energy is directly proportional to the change in 0.2% yield strength ($\Delta\sigma$). The proportionality constant is between 0.5 and 0.7 when ΔNDTT is in °C, and yield strength is expressed as MPa. It has been proposed that the dominant microstructure hardening mechanism is coherent copper clusters that nucleate and grow early in the irradiation. Since copper and nickel are important chemistry elements in correlations with ΔNDTT, other obstacles could be related to nickel or copper/nickel clusters including helium. If coherent precipitates are causing the material to harden, then the hardening model of Russell and Brown (Ru72) would be appropriate. In their work, the change in yield stress was correlated with an Orowan-type equation modified to account for differences in the elastic modulus of the solution matrix and the precipitate. The form of the equation is

$$\Delta NDTT \propto \Delta\sigma = 0.8\sqrt{3}\ \frac{\mu b}{L}\left[1 - \left(\frac{E_{Cu}}{E_{Fe}}\right)^2\right]^{1/2} \qquad (1)$$

where the $\sqrt{3}$ factor converts from shear to tensile stress by the Von Mises Criterion, μ is the shear modulus of iron (temperature dependent), b is the Burger vector (b = 2.48 Å), L is the mean distance between obstacles in the slip plane, and the last term accounts for the difference between the energy of the dislocation in the precipitate and the energy of the dislocation in the iron matrix in terms of the elastic modulus of the two materials.

The value of L is geometrically derived from the microstructure and is equal to $1/\sqrt{Nd}$, where N is the volume density of obstacles and d is their diameter. Expressions for both N and d can be derived from simple rate theory models. In actual fact, N and d should be coupled. However, in order to arrive at a closed form solution it must be assumed that they are independent. That is, nucleation is completed before significant growth of the obstacles occurs.

The ratio E_{Cu}/E_{Fe} proposed by Russell and Brown was precipitate size dependent. The maximum value for the ratio is equal to the ratio of the Cu-to-Fe elastic modulii (0.6). The ratio should also depend on the density of copper atoms and vacancies in the cluster. Russell and Brown rationalized the use of a logarithmic function of diameter to describe the ratio E_{Cu}/E_{Fe}. Their function reduces to the form

$$E_{Cu}/E_{Fe} = 1 - A \ln (d/\ell b) \qquad (2)$$

where A and ℓ are adjustable parameters (ℓ controls the threshold size for obstacle hardening), d is the obstacle diameter, and b is the Burger vector. In Russell and Brown's work, they find A = 0.133 and ℓ = 5 when the precipitate size was in terms of the diameter.

In addition, an empirical factor [arc sin (E_{Cu}/E_{Fe})] was included in Eq. (1). This multiplying factor enhances the impact of the threshold size and may only be a compensation for inadequacies in Eq. (2).

2.1 Obstacle Density

Field ion microscopy observations have shown that copper atoms are associated with the vacancy clusters (Br78). Thus, it is inferred that vacancy clusters produced in the displacement cascade are stabilized by copper atoms or possibly helium atoms and then continue to grow by attracting copper atoms. The net production rate of vacancy clusters depends on the production rate in the cascade less those annihilated by cascade overlap and those lost by thermal annihilation. The rate process is described by

$$\dot{N} = \alpha H - \beta G_o N - \nu N \qquad (3)$$

where α and β are constants, H is the cluster production rate, G_o is the cascade overlap rate (assumed to be proportional to the total defect production) and ν is the thermal annihilation rate. The thermal annihilation can take place by two means: 1) thermal emission of vacancies given by

$$\nu_e = 4\pi r_o D_v C^o \qquad (4)$$

and 2) absorption by diffusing iron interstitials given by

$$\nu_a = 4\pi r_o D_i C_i \qquad (5)$$

where r_o is the cluster radius, D is the diffusion coefficient for either vacancies (v) or interstitials (i), C^0 is the equilibrium vacancy concentration and C_i is the mobile interstitial concentration. Solving Eq. (3) gives the exposure dependence of the obstacle density

$$N = \frac{(\alpha/\beta)(H/G_o)}{1 + \nu/\beta G_o}\left[1 - e^{-\left(1 + \frac{\nu}{\beta G_o}\right)\beta G_o t}\right] \quad . \qquad (6)$$

The product of the diffusion constant and concentration ($D_V C_V$) for a vacancy cluster can take on two forms in microstructural extremes. The first condition is for a well-annealed material with low defect sink density; and consequently, recombination of defects is dominant and

$$D_i C_i \propto D_V C_V \propto \sqrt{D_V F} \quad . \qquad (7)$$

F is the free defect production rate; i.e, F is associated with cluster growth by absorbing free defects. Eq. (7) assumes that the defect density from thermal emission from sinks is much less than the density produced by displacement of atoms.

The second condition occurs when there is a high density of sinks for point defects. This conditions can occur from microstructures produced in the preirradiation thermomechanical conditioning of the steel or as a result of irradiation buildup of microstructure. In this case, the product DC is

$$D_i C_i \propto D_V C_V \propto D_V F \quad . \qquad (8)$$

Consequently, the obstacle site density can have three rate dependences involving the term $\nu/\beta G_o$ in Eq. (6). For the purpose of simplifying the discussion, it is assumed that F and G_o are proportional to one another. If they are not then a spectrum sensitivity in the ratio F/G_o will also exist. When emission of point defects dominates [Eq. (4)], the damage rate term shows a 1/F rate dependence. For absorption of point defects and a recombination dominant microstructure [Eq. (5) and (7)], the denominator shows a $1/\sqrt{F}$ rate dependence. Finally with absorption of point defects and a point defect sink dominant microstructure [Eq. (5) and (8)], there is no rate dependence.

2.2 Obstacle Size

For spherical obstacles, the growth rate is given by

$$\frac{dd}{dt} = \frac{4\Omega}{d}\left(D_v C_v C_c - \frac{\pi d^3}{6} N\right) \tag{9}$$

where the product $D_v C_v$ is the irradiation-enhanced diffusion constant for the defect migrating by a vacancy diffusion mechanism, C_c is the initial concentration of chemical elements in the lattice that contributes to the growth of the precipitate, Ω is the atomic volume, d is the diameter of the obstacle as a function of time, and N is the concentration of clusters. The latter term in parentheses accounts for the depletion of chemical species contributing to the growth of the cluster. Eq. (9) can be integrated to a closed form solution as done by Odette (Od83a). However, the resultant equation can not be solved explicitly for the cluster diameter. In the interim analysis, it will be assumed that depletion of the chemical species is not important. In addition, it is assumed that the product DC is approximately independent of time. In actual fact, DC decreases slowly with time. With these approximations in mind, the integration of Eq. (9) gives

$$d = \sqrt{d_o^2 + 8\,\Omega\, D_v C_v C_c t} \tag{10}$$

Substituting either Eq. (7) or (8) into Eq. (10) for $D_v C_v$ gives the size dependence of the obstacle for two different microstructural conditions. For recombination dominate conditions, the diameter has a $1/\sqrt[4]{F}$ damage rate dependence.

$$d = \sqrt{d_o^2 + 8\,\Omega C_c\left(\sqrt{\frac{D_v}{F}}\right)Ft} \tag{11}$$

However, for a sink-dominate microstructure, there should be no significant damage rate dependence, that is

$$d = \sqrt{d_o^2 + 8\,\Omega C_c D_v F t} \tag{12}$$

Combining the above equations, the general form for precipitate hardening gives the following equation

$$\Delta TT = 0.48\sqrt{3}\,\mu b \sqrt{\frac{C_o(H/G_o)}{1+\frac{C_1}{G_o^{\,n}}}\left\{1-\exp\left[-C_2\left(1+\frac{C_1}{G_o^{\,n}}\right)G_o t\right]\right\}}\sqrt{d_o^{\,2}+\frac{C_3}{F^m}Ft}$$

$$\cdot\left[1-\left(E_{Cu}/E_{Fe}\right)^2\right]^{1/2}\cdot \text{arc sin}\,(E_{Cu}/E_{Fe}) \qquad (13)$$

where from Eq. (2), $E_{Cu}/E_{Fe} = 1 - A \cdot \ln(d/C_4 \cdot b)$ and where the constants C_o, C_1, C_2, and C_3 are determined by fitting the equation to the data. The concentration of chemical species C_c has been incorporated into the constant C_3. Thus, Eq. (13) is applicable only to a single material. The constants n and m may have values of 0, 0.5, or 1.0, which depend on the prevailing microstructure. The ratio E_{Cu}/E_{Fe} accounts for differences in energy of the dislocation in the precipitate and the iron matrix (Equation 2). In Eq. (13) the parameters H, G_o, and F are all spectrum dependent. As stated before, H is associated with vacancy cluster production, G_o is associated with annihilation of clusters by cascade overlap, and F is associated with cluster growth by absorbing free defects.

2.3 Data Tabulation

There were three basic data sets analyzed. The first two sets included research reactor data on ASTM A302 B reference plate F previously used to develop a damage function for low temperature (<240°C) irradiations (Mc69,Se71). This included the physics-dosimetry-metallurgy data base for the low temperature (<116°C) IRL-SSC-SPV tests. The third set is from the PSF-SSC-SPV experiment run at 288°C, which also included ASTM A302B steel from reference plate F (Mc85b). The first two sets had the largest spectral variation that included light water reactor, heavy water reactor, and graphite-moderated reactor spectra. The light water reactor data bases, therefore, included results from three SSC-SPV experiments, see Table HEDL-16.

The neutron spectra used for the low temperature data set was taken from Serpan and Menkes' compilation of neutron spectra (Se74) used in the damage function analysis by McElroy et al. (Mc69) and a reevaluated analysis of the spectra in the SSC-SPV experiment in the Industrial Research Reactor test (IRL-5)(Si82b).

Heinisch and Mann (He84) calculated neutron cross sections for copper that included production of Frenkel pairs (fppa), interstitial clusters (ic), their size (i.e., number of interstitials per cluster) and mobile interstitials (mi), vacancy cluster (vc), their size, and mobile vacancies (mv), and lobe (or subcascade) production. ENDF/B-V nuclear cross section were used in their calculations. These calculations were repeated for this work using iron neutron cross section data based on ENDF/B-V nuclear data. The iron damage cross sections will be reported elsewhere.

The calculated exposure parameters are tabulated in Table HEDL-16. Also included are fluence E > 1 MeV, dpa, irradiation time, irradiation temperature, and ΔNDTT for A302B steel. The PSF parameters are for the spectral set location at the center of the capsule. The actual PSF SSC-SPV data and dpa dose are shown in Table HEDL-17. These values are the consenses evaluation (CE) values from the PSF blind test results (Mc85b).

2.4 Data Analysis and Results

The low-temperature ΔNDTT data were used to determine which set of defect production cross sections discussed in Section 2.3 best fits the defect production parameters H, G_0, and F. The constant C_4 is a obstacle hardening parameter, so it may also be determined from these data. In all analyses, the constant C_2 was driven to a large value which indicated that the site density was saturated; and consequently, C_2 is not important in the correlation. This leaves three constants plus selection of the parameters n and m that control the damage rate effect. After several trial fits to the low-temperature ΔNDTT data on A302 B, the best results were obtained with n = 1 and m = 0. This implies that the thermal annihilation of obstacle sites was controlled by emission of defects and the growth of the obstacles occurred in a sink dominant microstructure.

Table HEDL-18 shows the various combinations of H, G_0, and F that were tried and the respective variance per degree of freedom (σ^2/df). The lowest variance is obtained with the Frenkel pair per atom function (fppa). The function is significantly better than all other combinations tried except the dpa function. The fppa variance was only 15% smaller than the dpa variance. The fppa function is consistent with the damage function unfolded by McElroy et al. (Mc69) using the same data set. Their damage function showed an enhanced low-energy damage component. The low-energy component of the fppa cross section arises because the decreased density of defects in the cascade results in less recombination in the displacement cascade at low primary recoil energies (PKA). The interstitial clusters (ic) and mobile interstitials (mi) show fairly low variance. The interstitials are known to cause loop formation.

TABLE HEDL-16

INTEGRATED DAMAGE EXPOSURE PER ATOM FOR ΔNDTT DETERMINED FROM IRRADIATION EXPERIMENTS

Spectrum	φt > 1 x 10²²	dpa	Frenkel Pairs	Interstitial			Vacancy			Lobes	Time (s)	T_{IRR} (°C)	ΔNDTT (A302B) (°C)
				Clusters	Size (I)	Mobile	Clusters	Size (V)	Mobile				
CVTR 10-L	0.691	1.87-02	1.07-02	5.10-04	5.1	5.65-03	4.52-04	5.5	4.77-03	4.22-05	2.11+07	<240	133.
LITR C-53	1.44	2.17-02	9.91-03	9.17-04	5.3	2.72-03	6.96-04	6.1	1.60-03	8.14-05	4.85+06	<116	119.
LITR C-53	2.01	3.02-02	1.38-02	1.27-03	5.3	3.78-03	9.67-04	6.1	2.22-03	1.13-04	6.74+06	<116	167.
LITR C-49	1.05	1.53-02	6.89-03	6.82-04	5.3	1.49-03	5.12-04	7.0	6.10-04	5.82-05	4.76+06	<116	114.
LITR C-28	1.37	1.86-02	7.93-03	8.52-04	5.3	1.53-03	6.30-04	7.4	5.47-04	7.77-05	1.91+06	<116	122.
LITR C-48	1.94	2.72-02	1.16-02	1.24-03	5.3	2.28-03	9.22-04	7.4	8.04-04	1.19-04	3.91+06	<116	142.
LITR C-55	2.56	3.53-02	1.51-02	1.61-03	5.3	3.02-03	1.20-03	7.4	1.09-03	1.43-04	6.47+06	<93	161.
BGR W-44	0.816	1.50-02	7.13-03	5.95-04	5.2	1.40-03	4.65-04	6.2	1.40-03	4.65-05	2.50+07	<138	114.
IRL3 4-5/8"	0.232	3.15-03	1.34-03	1.46-04	5.4	2.46-04	1.07-04	7.5	8.27-05	1.37-05	2.44+06	<116	58.
IRL3 5-5/8"	0.175	2.36-03	1.00-03	1.09-04	5.3	1.85-04	8.07-05	7.7	5.94-05	9.99-06	2.44+06	<116	44.
IRL3 6-5/8"	0.126	1.74-03	7.38-04	8.00-05	5.3	1.39-04	5.92-05	7.7	4.49-05	7.11-06	2.44+06	<116	28.
IRL3 7-5/8"	0.0861	1.25-03	5.34-04	5.72-05	5.3	1.04-04	4.25-05	7.7	3.42-05	4.90-06	2.44+06	<116	28.
IRL3 8-5/8"	0.0632	9.39-04	4.04-04	4.27-05	5.3	8.11-05	3.18-05	7.6	2.74-05	3.55-06	2.44+06	<116	19.
LITR C-43	3.21	4.43-02	1.89-02	2.03-03	5.3	3.64-03	1.51-03	7.5	1.26-03	1.85-04	4.36+06	<116	172.
HWCTR Gray Rod	0.616	1.21-02	6.11-03	4.36-04	5.3	2.38-03	3.46-04	5.7	1.83-03	3.83-05	1.72+06	<240	106.
IRL5-1	0.748	1.04-02	4.47-03	4.73-04	5.4	9.02-04	3.51-04	7.0	3.63-04	4.35-05	1.54+07	<116	92
IRL5-2	0.331	4.65-03	1.98-03	2.14-04	5.3	3.71-04	1.58-04	7.6	1.23-04	1.95-05	1.54+07	<116	69
IRL5-3	0.199	2.99-03	1.28-03	1.37-04	5.3	2.43-04	1.02-04	7.8	7.66-05	1.19-05	1.54+07	<116	44
IRL5-4	0.119	2.00-03	8.73-04	8.86-05	5.3	1.94-04	7.90-05	7.6	6.25-05	8.98-06	1.54+07	<116	28
IRL5-5	0.0478	9.87-04	4.31-04	4.37-05	5.2	9.77-05	3.31-05	7.4	3.45-05	3.32-06	1.54+07	<116	11
IRL5-6	0.0200	4.94-04	2.19-04	2.15-05	5.2	5.23-05	1.64-05	7.4	1.92-05	1.49-06	1.54+07	<116	0
IRL5-7	0.0178	4.45-04	1.97-04	1.94-05	5.2	4.71-05	1.48-05	7.4	1.73-05	1.34-06	1.54+07	<116	0
PSF SSC-1	2.64	4.39-02	1.75-02	1.87-03	5.3	3.46-03	1.39-03	7.7	1.12-03	1.54-04	3.84+06	288	*
PSF SSC-2	5.65	8.82-02	3.79-02	4.01-03	5.3	7.56-03	2.99-03	7.7	2.48-03	3.30-04	8.42+06	288	*
PSF 0-T	4.25	6.80-02	2.[illegible]-02	3.08-03	5.3	6.09-03	2.30-03	7.5	2.17-03	2.53-04	5.10+07	288	*
PSF 0-T	2.28	4.16-02	1.80-02	1.88-03	5.3	4.74-03	1.41-03	7.7	1.23-03	1.44-04	5.10+07	288	*
PSF H-T	1.09	2.39-02	1.04-02	1.07-03	5.3	2.25-3	8.06-04	7.7	7.42-04	7.52-05	5.10+07	288	*

*See Table HEDL-17.

TABLE HEDL-17

INTEGRATED DAMAGE EXPOSURES FOR ΔNDTT DATA FROM THE PSF EXPERIMENT

Material	Location	ΔNDTT* (°C)	dpa	$\phi t > 1$ MeV (10^{19} n/cm^2)	Time (s)
A302B(F23)	SSC-1	81	0.0400	2.72	3.342+06
	SSC-2	93	0.0844	5.73	8.420+06
	0-T	78	0.0615	4.03	5.097+07
	Q-T	61	0.0383	2.26	5.097+07
	H-T	51	0.0224	1.12	5.097+07
A533B(3P)	SSC-1	68	0.0365	2.49	3.842+06
	SSC-2	82	0.0770	5.24	8.420+06
	0-T	73	0.0556	3.68	5.097+07
	Q-T	69	0.0343	2.05	5.097+07
	H-T	53	0.0199	1.01	5.097+07
K Forging	SSC-1	58	0.0270	1.73	3.842+06
	SSC-2	91	0.0569	3.65	8.420+06
	0-T	76	0.0456	2.84	5.097+07
	Q-T	74	0.0273	1.52	5.097+07
	H-T	60	0.0157	0.73	5.097+07
A508B(MO)	SSC-1	17	0.0294	1.89	3.842+06
Forging	SSC-2	39	0.0621	3.98	8.420+06
	0-T	27	0.0504	3.11	5.097+07
	Q-T	22	0.0305	1.67	5.097+07
	H-T	17	0.0177	0.82	5.097+07
Weld EC	SSC-1	110	0.0274	1.75	3.842+06
	SSC-2	121	0.0578	3.69	8.420+06
	0-T	117	0.0480	2.97	5.097+07
	Q-T	95	0.0295	1.62	5.097+07
	H-T	89	0.0173	0.80	5.097+07
Weld R	SSC-1	226	0.0370	2.52	3.842+06
	SSC-2	297	0.0782	5.31	8.420+06
	0-T	290	0.0585	3.85	5.097+07
	Q-T	261	0.0370	2.19	5.097+07
	H-T	240	0.0220	1.10	5.097+07

*Consensus Evaluation (CE) values Ref. (Mc85b).

$$\Delta NDTT = 0.48\sqrt{3}\,\mu b \sqrt{\frac{C_o(H/G_o)}{1+\frac{C_1}{G_o^{\,n}}}\left\{1-\exp\left[-C_2\left(1+\frac{C_1}{G_o^{\,n}}\right)G_o t\right]\right\}}\sqrt{d_o^{\,2}+\frac{C_3}{F^m}Ft}$$

$$\cdot\left[1-\left(E_{Cu}/E_{Fe}\right)^2\right]^{1/2}\cdot \arcsin\left(E_{Cu}/E_{Fe}\right) \qquad (13)$$

where from Eq. (2), $E_{Cu}/E_{Fe} = 1 - A \cdot \ln(d/C_4 \cdot b)$ and where the constants C_o, C_1, C_2, and C_3 are determined by fitting the equation to the data. The concentration of chemical species C_c has been incorporated into the constant C_3. Thus, Eq. (13) is applicable only to a single material. The constants n and m may have values of 0, 0.5, or 1.0, which depend on the prevailing microstructure. The ratio E_{Cu}/E_{Fe} accounts for differences in energy of the dislocation in the precipitate and the iron matrix (Equation 2). In Eq. (13) the parameters H, G_o, and F are all spectrum dependent. As stated before, H is associated with vacancy cluster production, G_o is associated with annihilation of clusters by cascade overlap, and F is associated with cluster growth by absorbing free defects.

2.3 Data Tabulation

There were three basic data sets analyzed. The first two sets included research reactor data on ASTM A302 B reference plate F previously used to develop a damage function for low temperature (<240°C) irradiations (Mc69,Se71). This included the physics-dosimetry-metallurgy data base for the low temperature (<116°C) IRL-SSC-SPV tests. The third set is from the PSF-SSC-SPV experiment run at 288°C, which also included ASTM A302B steel from reference plate F (Mc85b). The first two sets had the largest spectral variation that included light water reactor, heavy water reactor, and graphite-moderated reactor spectra. The light water reactor data bases, therefore, included results from three SSC-SPV experiments, see Table HEDL-16.

The neutron spectra used for the low temperature data set was taken from Serpan and Menkes' compilation of neutron spectra (Se74) used in the damage function analysis by McElroy et al. (Mc69) and a reevaluated analysis of the spectra in the SSC-SPV experiment in the Industrial Research Reactor test (IRL-5)(Si82b).

Heinisch and Mann (He84) calculated neutron cross sections for copper that included production of Frenkel pairs (fppa), interstitial clusters (ic), their size (i.e., number of interstitials per cluster) and mobile interstitials (mi), vacancy cluster (vc), their size, and mobile vacancies (mv), and lobe (or subcascade) production. ENDF/B-V nuclear cross section were used in their calculations. These calculations were repeated for this work using iron neutron cross section data based on ENDF/B-V nuclear data. The iron damage cross sections will be reported elsewhere.

The calculated exposure parameters are tabulated in Table HEDL-16. Also included are fluence E > 1 MeV, dpa, irradiation time, irradiation temperature, and ΔNDTT for A302B steel. The PSF parameters are for the spectral set location at the center of the capsule. The actual PSF SSC-SPV data and dpa dose are shown in Table HEDL-17. These values are the consenses evaluation (CE) values from the PSF blind test results (Mc85b).

2.4 Data Analysis and Results

The low-temperature ΔNDTT data were used to determine which set of defect production cross sections discussed in Section 2.3 best fits the defect production parameters H, G_0, and F. The constant C_4 is a obstacle hardening parameter, so it may also be determined from these data. In all analyses, the constant C_2 was driven to a large value which indicated that the site density was saturated; and consequently, C_2 is not important in the correlation. This leaves three constants plus selection of the parameters n and m that control the damage rate effect. After several trial fits to the low-temperature ΔNDTT data on A302 B, the best results were obtained with n = 1 and m = 0. This implies that the thermal annihilation of obstacle sites was controlled by emission of defects and the growth of the obstacles occurred in a sink dominant microstructure.

Table HEDL-18 shows the various combinations of H, G_0, and F that were tried and the respective variance per degree of freedom (σ^2/df). The lowest variance is obtained with the Frenkel pair per atom function (fppa). The function is significantly better than all other combinations tried except the dpa function. The fppa variance was only 15% smaller than the dpa variance. The fppa function is consistent with the damage function unfolded by McElroy et al. (Mc69) using the same data set. Their damage function showed an enhanced low-energy damage component. The low-energy component of the fppa cross section arises because the decreased density of defects in the cascade results in less recombination in the displacement cascade at low primary recoil energies (PKA). The interstitial clusters (ic) and mobile interstitials (mi) show fairly low variance. The interstitials are known to cause loop formation.

TABLE HEDL-16

INTEGRATED DAMAGE EXPOSURE PER ATOM FOR ΔNDTT DETERMINED FROM IRRADIATION EXPERIMENTS

Spectrum	φt > 1 x 10¹⁹	dpa	Frenkel Pairs	Interstitial Clusters	Interstitial Size (I)	Interstitial Mobile	Vacancy Clusters	Vacancy Size (V)	Vacancy Mobile	Lobes	Time (s)	T_{IRR} (°C)	ΔNDTT (A302B) (°C)
CVTR 10-L	0.691	1.87-02	1.07-02	5.10-04	5.1	5.65-03	4.52-04	5.5	4.77-03	4.22-05	2.11+07	<240	133.
LITR C-53	1.44	2.17-02	9.91-03	9.17-04	5.3	2.72-03	6.96-04	6.1	1.60-03	8.14-05	4.85+06	<116	119.
LITR C-53	2.01	3.02-02	1.38-02	1.27-03	5.3	3.78-03	9.67-04	6.1	2.22-03	1.13-04	6.74+06	<116	167.
LITR C-49	1.05	1.53-02	6.89-03	6.82-04	5.3	1.49-03	5.12-04	7.0	6.10-04	5.82-05	4.76+06	<116	114.
LITR C-28	1.37	1.86-02	7.93-03	8.52-04	5.3	1.53-03	6.30-04	7.4	5.47-04	7.77-05	1.91+06	<116	122.
LITR C-48	1.94	2.72-02	1.16-02	1.24-03	5.3	2.28-03	9.22-04	7.4	8.04-04	1.19-04	3.91+06	<116	142.
LITR C-55	2.56	3.53-02	1.51-02	1.61-03	5.3	3.02-03	1.20-03	7.4	1.09-03	1.43-04	6.47+06	<93	161.
BGR W-44	0.816	1.56-02	7.13-03	5.95-04	5.2	1.40-03	4.65-04	6.2	1.40-03	4.65-05	2.50+07	<138	114.
IRL3 4-5/8"	0.232	3.15-03	1.34-03	1.46-04	5.4	2.46-04	1.07-04	7.5	8.27-05	1.37-05	2.44+06	<116	58.
IRL3 5-5/8"	0.175	2.36-03	1.00-03	1.09-04	5.3	1.85-04	8.07-05	7.7	5.94-05	9.99-06	2.44+06	<116	44.
IRL3 6-5/8"	0.126	1.74-03	7.38-04	8.00-05	5.3	1.39-04	5.92-05	7.7	4.49-05	7.11-06	2.44+06	<116	28.
IRL3 7-5/8"	0.0861	1.25-03	5.34-04	5.72-05	5.3	1.04-04	4.25-05	7.7	3.42-05	4.90-06	2.44+06	<116	28.
IRL3 8-5/8"	0.0632	9.39-04	4.04-04	4.27-05	5.3	8.11-05	3.18-05	7.6	2.74-05	3.55-06	2.44+06	<116	19.
LITR C-43	3.21	4.43-02	1.89-02	2.03-03	5.3	3.64-03	1.51-03	7.5	1.26-03	1.85-04	4.36+06	<116	172.
HWCTR Gray Rod	0.616	1.21-02	6.11-03	4.36-04	5.3	2.38-03	3.46-04	5.7	1.83-03	3.83-05	1.72+06	<240	106.
IRL5-1	0.748	1.04-02	4.47-03	4.73-04	5.4	9.02-04	3.51-04	7.0	3.63-04	4.35-05	1.54+07	<116	92
IRL5-2	0.331	4.65-03	1.98-03	2.14-04	5.3	3.71-04	1.58-04	7.6	1.23-04	1.95-05	1.54+07	<116	69
IRL5-3	0.199	2.99-03	1.28-03	1.37-04	5.3	2.43-04	1.02-04	7.8	7.66-05	1.19-05	1.54+07	<116	44
IRL5-4	0.119	2.00-03	8.73-04	8.86-05	5.3	1.94-04	7.90-05	7.6	6.25-05	8.98-06	1.54+07	<116	28
IRL5-5	0.0478	9.87-04	4.31-04	4.37-05	5.2	9.77-05	3.31-05	7.4	3.45-05	3.32-06	1.54+07	<116	11
IRL5-6	0.0200	4.94-04	2.19-04	2.15-05	5.2	5.23-05	1.64-05	7.4	1.92-05	1.49-06	1.54+07	<116	0
IRL5-7	0.0178	4.45-04	1.97-04	1.94-05	5.2	4.71-05	1.48-05	7.4	1.73-05	1.34-06	1.54+07	<116	0
PSF SSC-1	2.64	3.9-02	1.75-02	1.87-03	5.3	3.46-03	1.39-03	7.7	1.12-03	1.54-04	3.84+06	288	*
PSF SSC-2	5.65	8.82-02	3.79-02	4.01-03	5.3	7.56-03	2.99-03	7.7	2.48-03	3.30-04	8.42+06	288	*
PSF 0-T	4.25	6.80-02	2.94-02	3.08-03	5.3	6.09-03	2.30-03	7.5	2.17-03	2.53-04	5.10+07	288	*
PSF 0-T	2.28	4.16-02	1.80-02	1.88-03	5.3	4.74-03	1.41-03	7.7	1.23-03	1.44-04	5.10+07	288	*
PSF H-T	1.09	2.39-02	1.04-02	1.07-03	5.3	2.25-3	8.06-04	7.7	7.42-04	7.52-05	5.10+07	288	*

*See Table HEDL-17.

TABLE HEDL-17

INTEGRATED DAMAGE EXPOSURES FOR ΔNDTT DATA FROM THE PSF EXPERIMENT

Material	Location	ΔNDTT* (°C)	dpa	$\phi t > 1$ MeV (10^{19} n/cm^2)	Time (s)
A302B(F23)	SSC-1	81	0.0400	2.72	3.842+06
	SSC-2	93	0.0844	5.73	8.420+06
	Q-T	78	0.0615	4.03	5.097+07
	Q-T	61	0.0383	2.26	5.097+07
	H-T	51	0.0224	1.12	5.097+07
A533B(3P)	SSC-1	68	0.0365	2.49	3.842+06
	SSC-2	82	0.0770	5.24	8.420+06
	Q-T	73	0.0556	3.68	5.097+07
	Q-T	69	0.0343	2.05	5.097+07
	H-T	53	0.0199	1.01	5.097+07
K Forging	SSC-1	58	0.0270	1.73	3.842+06
	SSC-2	101	0.0569	3.65	8.420+06
	Q-T	76	0.0456	2.84	5.097+07
	Q-T	74	0.0273	1.52	5.097+07
	H-T	60	0.0157	0.73	5.097+07
A508B(MO)	SSC-1	17	0.0294	1.89	3.842+06
Forging	SSC-2	39	0.0621	3.98	8.420+06
	Q-T	27	0.0504	3.11	5.097+07
	Q-T	22	0.0305	1.67	5.097+07
	H-T	17	0.0177	0.82	5.097+07
Weld EC	SSC-1	110	0.0274	1.75	3.342+06
	SSC-2	121	0.0578	3.69	8.420+06
	Q-T	117	0.0480	2.97	5.097+07
	Q-T	95	0.0295	1.62	5.097+07
	H-T	89	0.0173	0.80	5.097+07
Weld R	SSC-1	226	0.0370	2.52	3.842+06
	SSC-2	297	0.0782	5.31	8.420+06
	Q-T	290	0.0585	3.85	5.097+07
	Q-T	261	0.0370	2.19	5.097+07
	H-T	240	0.0220	1.10	5.097+07

*Consensus Evaluation (CE) values Ref. (Mc85b).

The same set of data was fit to an empirical function of the form

$$\Delta NDTT = A(X-X_0)^B \qquad (14)$$

where X is an exposure function (e.g. dpa, fppa etc.) and A, B, and X_0 are fitted parameters. This functional form fits the data fairly well. The best fit was obtained with the dpa and fppa functions. The remaining damage functions, including $\phi t > 1$ MeV, showed only slightly poorer fits to the data. However, the fppa function in Table HEDL-18 shows more than a factor of two improvement over the results with the empirical function shown in Table HEDL-19.

Figure HEDL-16 shows the measured and calculated ΔNDTT for Eq. (13), and Figure HEDL-17 shows measured and calculated ΔNDTT for Eq. (14). The absolute values of the error in the calculated ΔNDTT do not greatly differ between the two plots, but a substantial number of the calculated values in Figure HEDL-16 are shifted onto the exact correlation line when damage rate is considered.

The obstacle size threshold determined from the low temperature A302 B data was 5.76 Å. This is about one half the value deduced by Russell and Brown. However, it is noted they were dealing with larger concentrations of copper and incoherent fcc ε-copper precipitates. In contrast, the irradiation produced obstacles are probably copper vacancy clusters on the order of 6 to 20 Å in diameter. With the constant C_4 determined from the low temperature data used in the analysis of high temperature PSF data, this leaves three constants. However, it is noted that low- and high-temperature damage mechanisms are not necessarily the same. For example, the low-temperature damage mechanism may be nucleation and growth of faulted loops, whereas the high-temperature mechanism could be copper precipitates. In this analysis, the damage mechanism was assumed to be the same at both temperatures. Since the PSF-SSC-SPV experiment included only five damage exposures, this leaves at most, two degrees of freedom with which to choose n and m for Eq. (13).

The variance/degree of freedom for each equation fit to the high-temperature data is tabulated in Table HEDL-20. Two empirical power law functions were used in the analysis. These were

$$\Delta NDTT = AX^B \qquad (15)$$

and

$$\Delta NDTT = AX^{B+C\cdot \ln X} \qquad (16)$$

where X is the damage exposure and A, B, and C are fitted parameters. Eq. (16) is the form used successfully by Guthrie to correlate plate and weld data from pressure vessel surveillance data (Gu85). The remaining equations correspond to various combinations of n and m in Eq. (13).

TABLE HEDL-18

VARIANCE/DEGREE OF FREEDOM FOR EQUATION (13)
AND VARIOUS COMBINATIONS OF SPECTRAL PARAMETERS

H	G_0	G	σ^2/df
dpa	dpa	dpa	0.00919
fppa	fppa	fppa	0.00781
Vc	dpa	mv	0.0339
Ic	dpa	mi	0.0142
lobes	lobes	mv	0.0383

TABLE HEDL-19

VARIANCE/DEGREE OF FREEDOM FOR EQUATION (14)
AND VARIOUS SPECTRAL PARAMETERS

X	σ^2/df
dpa	0.0178
fppa	0.0186
ic	0.0220
lobes	0.0214
mi	0.0367
mv	0.0584
vc	0.0236
$\phi t > 1$	0.0224

The best correlation for A302B is the same form found for the low temperature data. Furthermore, it achieves a factor of ten reduction in variance/degree of freedom over the empirical equations. For the A533B plate and the two forging materials, the empirical equations give the lowest variances. These variances, however, are not to different than those achieved with Eq. (13) with values of n=m=0 for the HSST A533B plate; n=m=1/2 for the K forging; and n=m=0 or 1/2 for the MO forging. Both weld data sets showed a 40% to 50% reduction in variance by including a damage rate effect with m and n equal to one half. This implies the damage evolved in a recombination dominant microstructure similar to an annealed material.

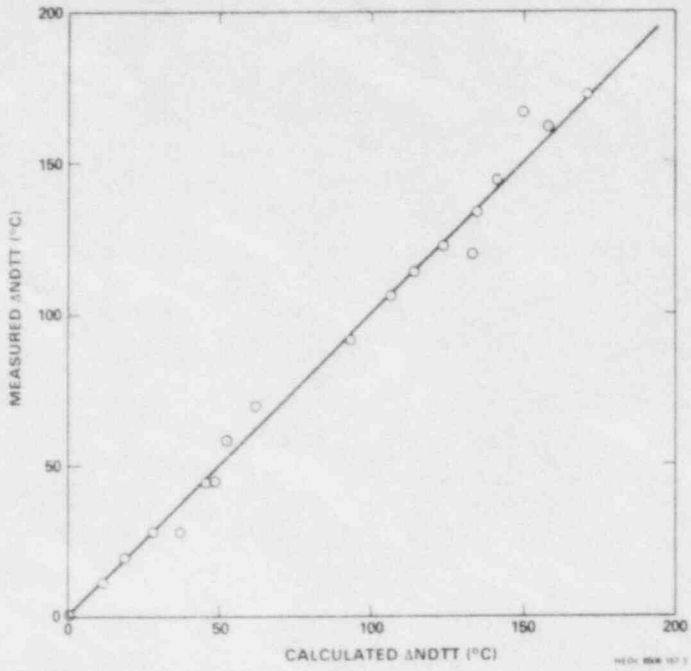

FIGURE HEDL-16. Comparison of Measured and Calculated ΔNDTT Data Using Equation (13) and fppa.

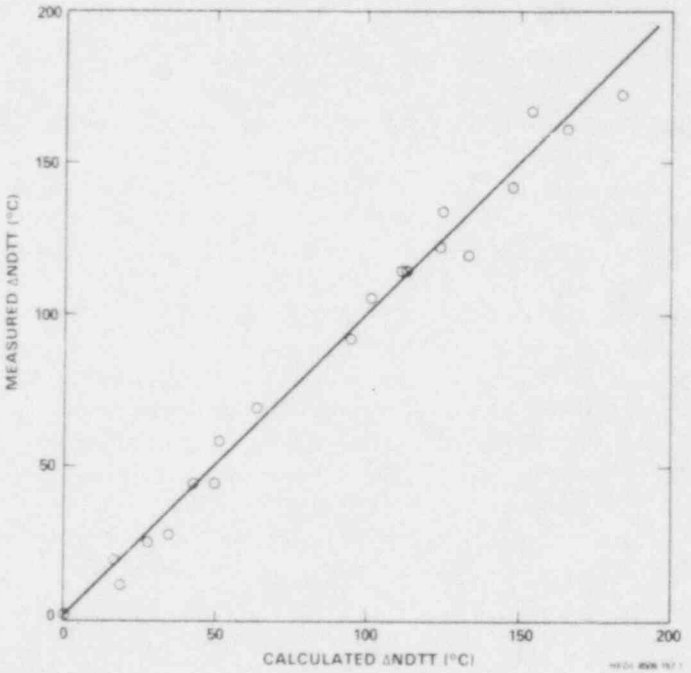

FIGURE HEDL-17. Comparison of Measured and Calculated ΔNDTT Data Using Equation (14) and fppa.

TABLE HEDL-20

VARIANCE/DEGREE OF FREEDOM FOR PSF-SPV DATA

Material \ Eq No. / df	15 3	16 2	13(n=m=0) 2	13(n=m=1/2) 2	13(m=1,n=0) 2
A302B Plate**	0.0156	0.0202	0.0224	0.00381	0.00143*
A533B Plate**	0.00232	0.0016*	0.00204	0.00303	0.00960
K Forging	0.0182*	0.0193	0.0318	0.0216	0.0380
MO Forging	0.0267	0.0182*	0.0388	0.0339	0.0690
EC Weld	0.00467	0.00680	0.00745	0.00288*	0.0138
R Weld**	0.00533	0.00665	0.00970	0.00244*	0.0545

*Lowest σ^2/df for the material.
**ASTM A302B Reference Plate (Ha84,Ha84a); HSST A533B, 03 Reference Plate (Ha84,Ha84a); High-sensitivity British A533B Reference Weld (Da85).

3.0 Discussion

A data correlation improvement better than that achieved by the use of the ASTM E693 dpa standard cross section (As79d) was observed for the low temperature ΔNDTT data on ASTM A302B reference plate steel. The Frenkel pair production cross section, which gave the improved correlation of ΔNDTT with exposure, is based on change in resistivity measurements at 4 K (Si80a). The inference from the resistivity measurements is that they are proportional to the total defect production rate. The resulting damage shows a higher efficiency for retaining damage produced by low energy (<10 keV) PKA recoil events. This is presumably from a low defect density and a low incipient recombination in the cascade. The impact on damage production is that softer spectra, such as in D_2O moderated reactors, will have a higher proportion of defect survival then in harder neutron spectra. Harder spectra such as light water reactors or even harder 14-MeV neutrons do not have, relatively speaking, any additional spectral sensitivity than that shown by the dpa cross section. Frenkel pair damage efficiency is one half that of the calculated standard dpa in bcc iron; however, the two defect cross sections are directly proportional for higher energy PKA recoil events (>10 keV). This is illustrated in Figure HEDL-18, which shows data on change in yield strength in A302 B steel after irradiation in PSF and by 14-MeV [unpublished data from HL Heinisch] neutrons at an irradiation temperature of 288°C. The 14-MeV neutron irradiations were performed at an intermediate damage rate between the SCC and SPV and fall intermediate between the extrapolation of the two PSF data sets. This occurs inspite of the fact that the average dpa cross section for 14-MeV neutrons is about an order of magnitude larger than those for the PSF spectra.

Multiple hardening mechanisms have not been addressed in this work. Smidt and Sprague (Sm73) observed loops, voids, and blackspots in addition to the preirradiation-induced dislocation structure after irradiating A302B and binary metals to 0.8 dpa. This is an order of magnitude higher exposure than data considered here. Much of the preirradiation dislocation structure in their plate material underwent stress relaxation by absorption of point defects. This allows for some dislocation annihilation while the dislocation relocate to a more stable configuration. Smidt and Sprague were not able to resolve irradiation-induced precipitation or clustering such as that observed in field-ion microscopy (Br78).

The copper could potentially act as a precipitate hardening site, or may alter the point defect concentrations by trapping, so as to enhance other microstructural components such as loops. In the latter case, the model used in this analysis may be an over simplification of the irradiation-induced evolution of the microstructure. For example, if irradiation hardening were measureably affected by growth of dislocation loops, Equation (10) would be replaced or supplemented by an equation of the form

$$d_\ell = d_o + \frac{1}{b}\sqrt{\frac{D_v}{F}}\ Ft \qquad (17)$$

where d_ℓ is the loop diameter, b is the Burger's vector, D_v the vacancy diffusion constant, and F is the free defect production rate. Equation 17 is applicable to a recombination dominant microstructure. Comparing Equation 10 and 17 shows that loop growth will be more damage rate sensitive than the precipitate growth. However, from Smidt and Sprague data it appears that significant hardening from loop formation and growth will occur only at dpa exposure higher than of current interest to LWR pressure vessel surveillance programs.

In this analysis of PSF data, it was assumed that dpa was an adequate spectrum effect correlation parameter and the subsequent data scatter could be explained by introducing rate effects. The adequacy of dpa is supported by the fact that the ratio dpa/fppa is constant for all PSF spectra and only fppa gave a better correlation of ΔNDTT than dpa at low irradiation temperatures. The rate effect was introduced by assuming that hardening was caused by an irradiation-induced spherical obstacle that impeded dislocation motion so that no plastic flow was possible, and hence elastic fracture occurred. The obstacles were assumed to be vacancy clusters stabilized by certain chemical elements such as copper, nickel, and/or helium.

The analysis of the PSF did not demonstrate that a single equation consistently gave a superior fit to the data. The A302B and weld steel gave the best fit using the damage rate dependent equation. However, the best fit for A302B steel was with m = 1 and n = 0, which is in contrast to the welds that showed the best fit with m = n = 1/2. If only Equation (13) is considered, the best overall fit occurred with m = n = 1/2 for all steels but the A302B and A533B steels. It is possible that the particular chemistry of

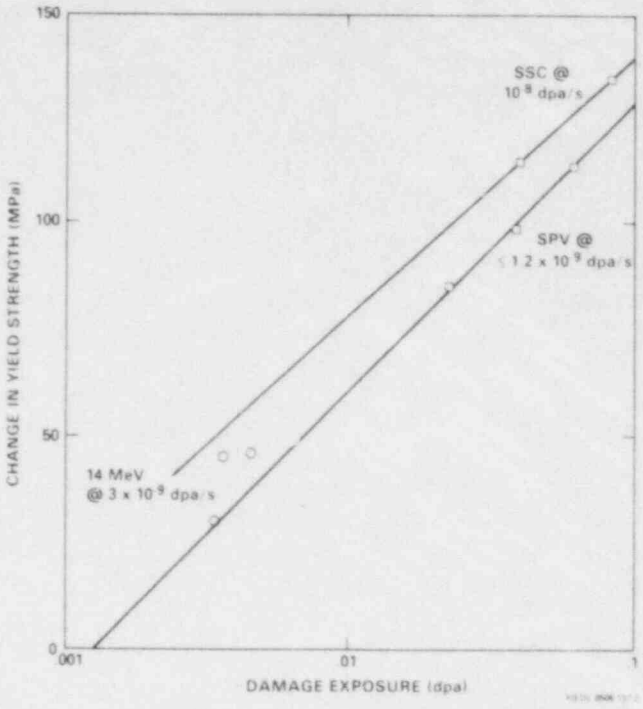

FIGURE HEDL-18. Irradiation-Induced Change Yield Strength in A302B Steel from Irradiation in PSF and 14-MeV Neutrons.

A302B caused a shift in the damage rate dependence and only the low damage rate dependence of A302B was observed. No attempt has been made to determine the chemical compositional dependence of the fitted constants at this time.

The A302B data supported the same rate function at low and high temperatures. Figure HEDL-19 shows the relative rate dependence for both temperatures at 0.03 dpa. The symbols span the damage rate range for the data used. In comparison, the range of damage rates for LWR surveillance capsules is shown by the vertical dashed lines of Figure HEDL-19. Since the damage rate for the vessel walls is lower and the net damage implied is lower, surveillance capsule data should provide a conservative estimate of the condition of the pressure vessel walls made with A302B steel plate at a neutron exposure of 0.03 dpa. However, since only a narrow range of damage rates and chemical composition have been explored, this conclusion is only tenative.

Both weld data sets support the same damage rate dependence in the PSF irradiation. Figure HEDL-20 shows the damage rate dependence of the R and EC weld data at 0.03 dpa. The R weld data show a larger rate variation than the EC weld data. However, the deduced rate dependences agree within 3% to 6% over the damage rate range shown. If this functional dependence is significant, the LWR surveillance data could show a minimum-to-maximum spread in ΔNDTT of 20% for the lower copper ($\leq$0.24 wt%) steels studied herein.

The most significant effect is that the high rate data can potentially be less conservative than lower rate data. That is, it can have a lower property change than low damage rate data. This is illustrated in Figure HEDL-21, which shows measured and calculated ΔNDTT for the R weld material versus dpa. The SSC data (high rate) show lower property change trends than the lower rate SPV data.

The explanation of the curve slope is divided into site density and size effects. At low damage rates the effect of damage rate is most pronounced on the site density. Whereas at high damage rates, the effect of damage rate is also dependent on obstacle size.

The difficulty encountered in this analysis is an obvious lack of experimental data. The three parameter damage rate equation leaves only two degrees of freedom. From that, one must select a rate dependence on the obstacle site density (m) and a rate dependence on growth (n) for Eq. (13). A proper analysis must consider a wider range of spectra, damage rates, and fluence than are offered in the PSF experiment. Furthermore, the effect of chemistry (including helium) variation on neutron exposure and damage rate needs to be explored, see Sections HEDL-A and -F.

4.0 Conclusions

A physically based model for irradiation induced hardening in pressure vessel steels was developed. The model was developed to specifically address damage rate and neutron spectrum effects. The best correlation of low temperatures ΔNDTT data on ASTM A302B Reference plate steel, which had a relatively wide spectrum variation, was obtained with a defect cross section for Frenkel pair production (fppa). This cross section shows an enhanced low-energy defect production relative to high-energy neutrons. The damage rate dependence observed in the data implies that the primary effect is on nucleation of obstacle sites and is associated with thermal emission of point defect from the clusters. The damage rate equation gives over a factor of two reduction in the variance compared to an empirical power law equation.

At high temperatures (288°C) only the PSF data were analysed. It was found that the A302B data were best fit with the same damage rate dependence as found in the low temperature data. The damage rate equation used for the remaining data suggests a recombination dominant microstructure existed during irradiation.

In the case of the R and EC weld data (with 0.23 and 0.24 wt% copper, respectively), the damage rate sensitivity found indicates that accelerated surveillance (or low-flux test reactor) data would be expected to give a conservative end-of-life material condition for these materials. This conservatism may not hold for high damage rate test reactor spectra or at all dpa exposures. The remaining materials (A533B and the two forgings) did not support within data scatter a strong correlation with damage rate. This might imply that chemistry and pre-irradiation microstructure may have a controlling influence in damage rate effects.

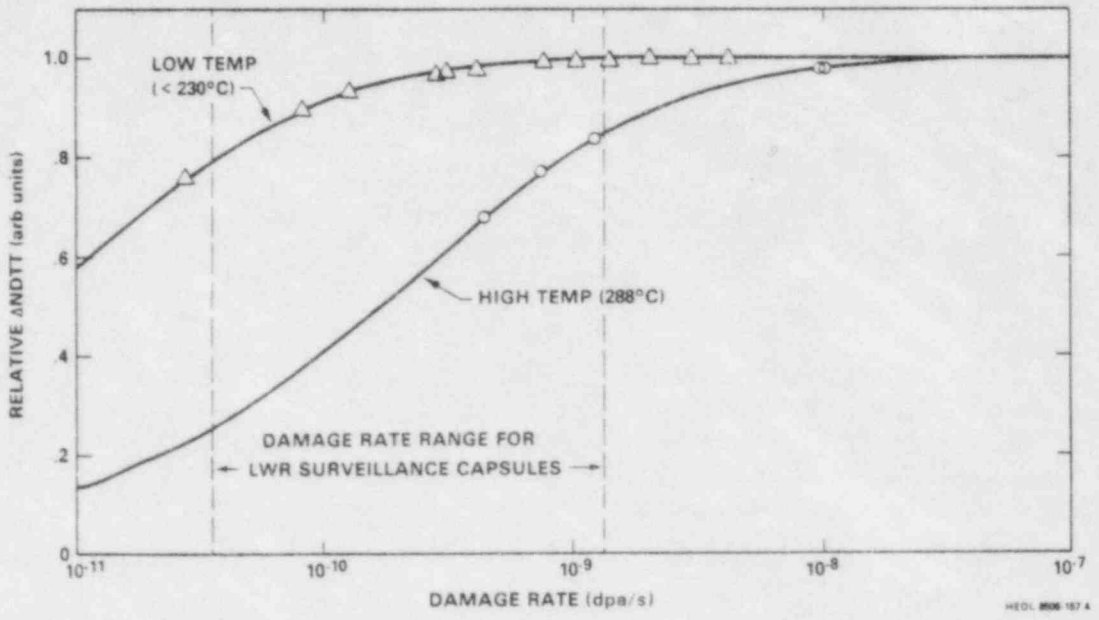

FIGURE HEDL-19. Calculated Damage Rate Sensitivity of A302B Steel for Low- and High-Irradiation Temperatures at 0.03 dpa. The symbols represent where the damage rate for the neutron spectra used in this analysis fall on the calculated curve.

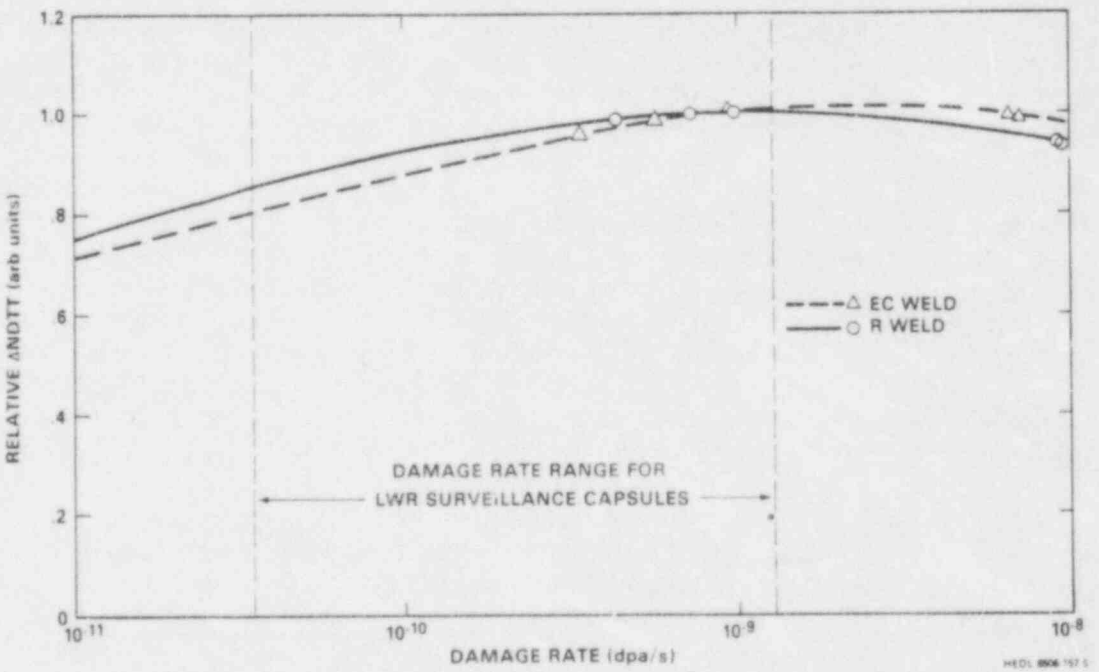

FIGURE HEDL-20. Calculated Damage Rate Sensitivity of EC and R Welds Irradiated in PSF at 0.03 dpa. The symbols represent where the damage rate for the neutron spectra used in this analysis fall on the calculated curve.

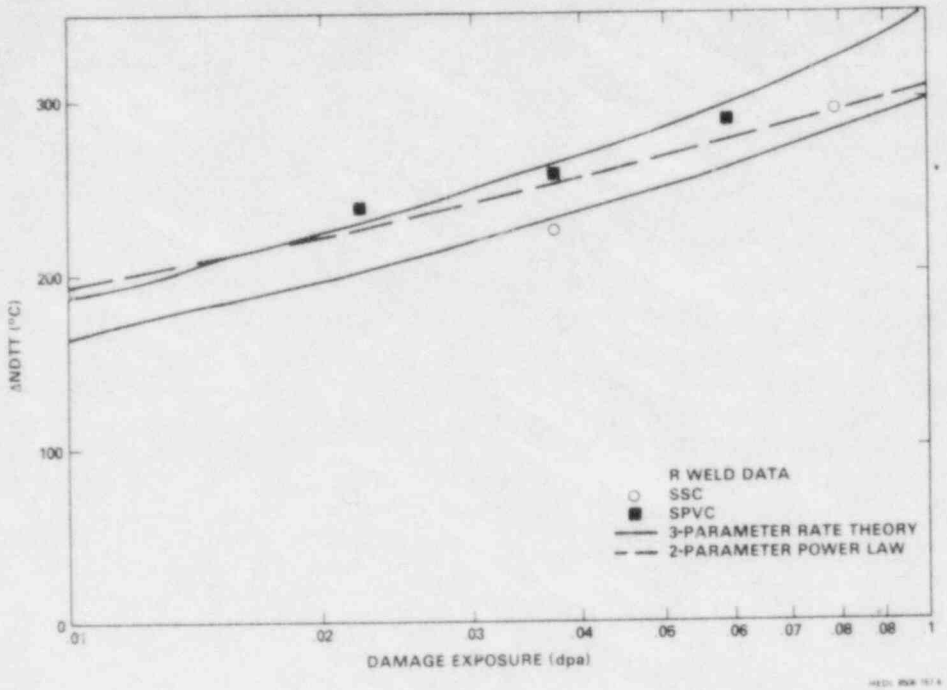

FIGURE HEDL-21. Correlation of ΔNDTT Versus Damage Exposure for Weld Material R Irradiated in PSF.

In general, the existence of damage rate effects will depend on the condition of the material. For a high defect sink density, it is possible that no damage rate effect exists. In fact damage rate effects may become negligible after extended irradiation induces a high density of pcint defect sinks for some materials.

The reader is referred to Section HEDL-F for additional information on a semi-empirical study by McElroy et. al of neutron exposure, flux-spectral, flux-level, and thermal neutron effects using 1) the PSF 2) available PWR and BWR plate and weld and 3) selected plant-specific physics-dosimetry-metallurgy data sets.

Expected Future Accomplishments

Appropriate parts of this work will be extended and incorporated in PSF Experiment physics-dosimetry-metallurgy NUREG reports.

F. TREND CURVE DATA DEVELOPMENT AND TESTING

W. N. McElroy, R. Gold, E. P. Lippincott and R. L. Simons (HEDL), and S. L. Anderson (W-NTD)

Objective

The ultimate objective is to add to the knowledge of the irradiation embrittlement process for Light Water Reactor Pressure Vessel (LWR-PV) steels so that predictive formulas and procedures can be developed for 1) use in pressurized water reactor (PWR) and boiling water reactor (BWR) plant-specific applications and 2) making regulatory decisions regarding the safe operation of power plants during their normal design life (~40 years) and for 3) new life extension (>40 years) programs. The immediate objective of this work is to study, develop and test trend curve model equations and data analysis procedures that include variable terms that account for neutron flux-spectral, flux-level, Ni-Cu, and fluence effects for BWR and PWR plant-specific trend curves. Thermal-intermediate-fast (E > 6 MeV) neutron production of helium, and thermal neutron-induced gamma heating effects were also considered and/or accounted for, as appropriate.

Summary

The PSF Experiment, Gundremmingen BWR surveillance capsule, and existing PWR and BWR surveillance capsule physics-dosimetry-metallurgy Charpy shift data bases have been used to study, develop and test trend curve equations and data analysis procedures that include variable terms that account for neutron flux-spectral, flux-level, chemistry, and fluence effects. Groupings of both lower-Ni (<0.3 wt%) and higher-Ni (>0.4 wt%) pressure vessel steels were studied. The PSF Experiment Code R* (RR&A) weld (0.23% Cu, 1.58% Ni) and the Gundremmingen surveillance capsule weld (0.18% Cu, 0.13% Ni**) Charpy shift property change results were used to determine the constant coefficients for flux-level, chemistry, and fluence-variable terms for selected trend curve equations. Neutron spectral corrections were made using displacements per atom (dpa) in iron to correct for the difference in integral damage rates between the simulated surveillance capsule (SSC), 0-T, 1/4-T, and 1/2-T irradiation positions of the PSF PV mockup. Spectral differences between PSF-SSC and Gundremmingen surveillance capsule irradiation locations were small. Thermal-intermediate-fast (E > 6 MeV) neutron production of helium, and thermal neutron-induced gamma heating effects were considered and accounted for, as appropriate.

An R-residual test was defined and used to provide a measure of the increase or decrease in correlation of existing PWR and BWR Charpy shift surveillance capsule measured and calculated data, with and without corrections for: 1) flux-spectral differences, 2) flux-level and Ni-fluence dependence and 3) the flux-level and copper dependency of the exponent N in power law dependent models.

*High-sensitivity British A533B reference weld (Da85).
**Assumed values pending confirmation.

Procedures for using the derived equations were tested by comparing results obtained with seven Charpy shift trend curve model equations that had been previously developed for weld and plate pressure vessel steels. These seven equations use exposure parameter terms of fluence E > 1 MeV, dpa in iron, and/or thermal-intermediate-fast (E > 6 MeV) neutron production of helium.

Applications of the flux-level correction factor Eq. (6b), derived starting with the Heller and Lowe B&W trend curve model Eq. (4M) and the PSF Experiment (RR&A) Code R weld material results, provided improved Charpy shift calculated-to-experimental (C/E) ratio correlations for data sets with Cu content less than ~0.23 wt% Cu. For Cu wt% greater than ~0.23, some correlations were better and some were worse. In applying the B&W Eq. (4M), a re-normalization of the magnitude of the chemistry term was needed when the Ni wt% was near or outside the 0.54 wt% to 0.70 wt% Ni range of the B&W 25-point weld data base. This data base was used by Heller and Lowe to establish the values of the constants for Eq. (4M). Good results were also achieved by using a modification of the Eq. (4M), which included use of a variable chemistry term for the power law exponent value N, Eq. (16).

Based on the overall consistency of the PSF correlations with the modified Eq. (4M), (6b), (15), and (16), and the results of subsequent PWR and BWR plant-specific applications, it is found that very significant (up to factors of ~4) relative flux-level Charpy shift correction factors could exist and might be required to properly correlate plant-specific surveillance capsule data sets. That is, for sets of surveillance capsule Charpy shift results for materials with similar Cu and Ni chemistry groupings, but irradiated in different flux levels in the range of ~2 x 10^9 n/cm²•s (BWR wall capsule) to ~8 x 10^{11} n/cm²•s (PWR accelerated capsule).

It is further found that, with appropriate modifications, the simpler plant-specific trend curve model equations, such as those established by B&W, can be used very effectively to help sort out different variable effects, such as flux level and its chemistry dependency. In this regard, and as stated by Heller and Lowe: "It is generally viewed as statistically inadvisable to include correlated terms in a regression model because they tend to mask the real effects." This is exactly what was found with the application of the more complex and generic trend curve model equations of Table HEDL-21.

As discussed in Section 4.3.1, for the existing PWR and BWR weld, plate, and forging surveillance capsule physics-dosimetry-metallurgy data base and for the higher-Ni steels, the application of the Eq. (6a) and (7) correction factors provided a strong correlation that supports a Cu-dependent flux-level effect, Figure HEDL-25. Such a dependency was recently suggested by Guthrie (Gu85). For the more limited data for the lower-Ni steels, a significant correlation was not found, Figure HEDL-26. It must be emphasized, however, that these results and conclusions are sensitive to the form of the trend curve model equation used, and they could change with the use of different model equations. Further, in Figure HEDL-27, the addition of PWR data to the PSF data would show that the the damage parameter exponent is more complex than is suggested by just the PSF data.

Based on these results, a simple and preliminary linear Cu dependency for the power law exponent N for the B&W Eq. (4M) was established and was tested using the PSF experiment data base. The result was a significant overall reduction of the standard deviation of fits for the PSF weld Code R; plates, Codes 3PU and F23; and forgings, Codes K and MO, pressure vessel steels.

The Code R material flux-level correction factor, Eq. (6b), was used with the five weld and two plate trend curve model equations to calculate adjusted and model-dependent Charpy shift values for comparison with plant-specific sets of measured data. For some data sets, an improvement in the C/E measured ratio was achieved; while for others sets, there was no improvement or a worsening of results, depending on the Cu-Ni content and trend curve model equation being studied. However, in general, the application of the Eq. (6b) correction factors with the B&W Eq. (4M), or with the Eq. (16) variable term for N, produced results as good or better than the other trend curve model equations of Table HEDL-21. It was concluded, therefore, that the built-in correlations of the existing, and more generic, trend curve model equations have masked the existence of a very real and important flux-level effect.

An independent physically based theoretical study on "Damage Rate and Spectrum Effects in Ferritic Steel ΔNDTT Data" has been completed and the results are reported by R. L. Simons in Section HEDL-E. The results of Simons' study support the conclusions and are consistent with those of the present semi-empirical investigation. New experimental results recently reported by Hawthorne (Ha85) also support the conclusions of this and Simons' studies. Also, recent surveillance data have shown Charpy shifts that are larger than Rev. 2 of Reg. Guide 1.99 by a statistically significant amount.

Additionally, Serpan (Se85) recently stated: "Increasing evidence for a dose rate effect has come from MEA this year, in the form of results from experiments that demonstrate greater embrittlement at low fluxes than previously anticipated (Ha85). This evidence has been so pronounced in reactor surveillance data that Revision 2 of Reg. Guide 1.99 on Radiation Damage to Reactor Vessel Materials has dropped the test reactor data and now includes only power reactor data which has the low flux-higher embrittlement characteristic."

It is important to understand that Serpan's statement is only partially correct, since it applies only to selected PV steels. That is, the correctness of the statement is dependent on a number of variables, including material properties, neutron exposure, and flux-level. This is demonstrated by the combined results of Sections HEDL-E and -F where it is found that a PV steel may show a decrease, an increase or no change in the measured Charpy Shift with changes in flux level.

As stated in Section HEDL-A: "The existence of a flux-level effect has important implications for the U.S. commercial nuclear power industry, since accelerated locations have almost invariably been used in PV surveillance programs. These accelerated PV surveillance capsules have provided lead factors that have been applied to obtain projections of PV embrittlement. In fact, accelerated PV capsules comprise the largest existing data base for trend curve analyses. Consequently, it is clear that a flux-level effect would imply that some correction would be necessary in the application and interpretation of lead factors. Otherwise, the application of lead factors

could not always ensure a conservative extrapolation. At the same time, it is apparent that any reduction in embrittlement afforded from low leakage cores, which are now being adopted in some U.S. power plants, must be quantified in terms of a flux-level effect, lest the predicted gain be under- or over-estimated."

Results of this and the Sections HEDL-A and -E studies provide insight into the difficulty and complexity of developing any unique solution for the problem of correlating and using both generic and plant-specific trend curve data. It is concluded that the study, development, testing, and application of accepted procedures and data for determining generic and plant-specific trend curves for PWRs and BWRs will continue to be difficult because of the lack of appropriate experimental data, but will remain an important objective of the LWR-PV-SDIP for LWR power plant operators as well as regulatory bodies.

As a result of this research, we have concluded that care must be exercised in future trend curve studies to ensure that all of the important damage processes are adequately represented. Future microstructural investigations should be aimed at comprehensive identification of the possible damage processes and ranking of their relative importance.

Accomplishments and Status

1.0 Introduction

The purpose of this work is to study, develop and test trend curve multiplicative correction factors that account for flux-spectral, flux-level, chemistry, and fluence effects. The PSF Experiment (Ha84,Ha84a,Gu85), Gundremmingen BWR surveillance capsule (Ei77), and existing PWR and BWR surveillance capsule physics-dosimetry-metallurgy Charpy shift data bases have been utilized to develop and test multiplicative correction factor (CF) equations that account for flux-spectral, flux-level, chemistry, and fluence effects for both lower-Ni (<0.3 wt%) and higher-Ni (>0.4 wt%) pressure vessel steels.

Based on an iterative procedure, the PSF Experiment Code R (RR&A) weld (0.23% Cu, 1.58% Ni) and the Gundremmingen surveillance program weld (0.18% Cu, 0.13% Ni, assumed) Charpy shift results were used to determine constant coefficients for flux-level, chemistry, and Ni-fluence correction factor equations. Using the PSF data base, linear equations were established to represent the flux-level and Cu dependency of the power law exponent N for the B&W Eq. (4) trend curve model equation, Table HEDL-21. Procedures for using the derived CF equations and the flux-level and Cu dependency of N were then established and tested by comparison of the results obtained with seven Charpy shift trend curve equations that had been previously developed for weld and plate pressure vessel steels.

An R-residual test was defined and used to provide a measure of the increase or decrease in correlation of existing PWR and BWR Charpy shift surveillance capsule measured and calculated data, with and without corrections for: 1) flux-spectral differences, 2) flux-level and Ni-fluence dependence and 3) the flux-level and Cu dependency of N.

TABLE HEDL-21

SELECTED PWR AND BWR PLATE AND WELD METAL CHARPY SHIFT TREND CURVE EQUATIONS*

Eq. 1M [Ref. (Gu84 and Gu84a)] (Guthrie Weld - dpa)

$$\Delta T = (553.8 \cdot Cu - 286.8\sqrt{Cu \cdot Ni} + 247.4 \cdot Ni) \cdot (dpa/0.016)^N$$

$$N = 0.2625 - 0.0350 \log_e (dpa/0.016)$$

dpa = Displaced atoms in iron.

Eq. 2M [Ref. (Gu84)] (Guthrie Weld - Fluence, E > 1 MeV)

$$\Delta T = (624.0 \cdot Cu - 333.1\sqrt{Cu \cdot Ni} + 251.2 \cdot Ni) \cdot (F1)^N$$

$$N = 0.2819 - 0.0490 \log_e (F1)$$

F1 = Fast Fluence (E > 1.0 MeV).

Eq. 3M [Ref. (Gu84)] (Guthrie Plate - Fluence, E > 1 MeV)

$$\Delta T = \left[-38.4 + 555.6 \cdot Cu \cdot \tanh\left(\frac{0.353 \cdot Ni}{Cu}\right)\right] \cdot (F1)^N$$

$$N = 0.2661 - 0.0449 \log_e (F1)$$

F1 = Fast Fluence (E > 1.0 MeV).

Eq. 4M [Ref. (He84a)] (Heller and Lowe Weld - Fluence, E > 1 MeV)

$$\Delta T = -4.66 + (-18.17 + 61.88 \cdot Ni + 49.12 \cdot Cu) \cdot (F1/5.0 \times 10^{19})^N$$

$$N = 0.326$$

F1 = Fast Fluence (E > 1.0 MeV).

Eq. 5M [Ref. (Pe84)] (Odette Weld - Fluence, E > 1 MeV)

$$\Delta T = 360 \cdot Cu \left\{1 + 1.38\left[erf\left(\frac{0.3 \cdot Ni - Cu}{Cu}\right) + 1\right]\right\} \cdot \left[1 - \exp(-F1/0.11)\right]^{1.36} \cdot (F1)^N$$

$$N = 0.18$$

F1 = Fast Fluence (E > 1.0 MeV).

Eq. 6M [Ref. (Pe84)] (Odette Plate - Fluence, E > 1 MeV)

$$\Delta T = 388.8 \cdot Cu \left[1 + 0.33\ erf\left(\frac{0.77 \cdot Ni - Cu}{Cu}\right) + 1\right] \cdot (F1)^N$$

$$N = 0.28$$

F1 = Fast Fluence (E > 1.0 MeV).

Eq. 7M [Ref. (Mc84h)] (Modified Eq. 5M With a Combination of Exposure Parameters: dpa; and Fluences of Thermal, Intermediate, Fast > 6 MeV Neutrons for Calculating Helium Production from Boron and Steel)

$$\Delta T = 295.4 \cdot Cu \left\{1 + 2.17\left[erf\left(\frac{0.24 \cdot Ni - Cu}{Cu}\right) + 1\right]\right\} \cdot \left[1 - \exp(D/0.50)\right]^{0.329} \cdot (D)^N$$

$$N = 0.198$$

$$D = (dpa/0.016) + 15.962 \cdot (8 \cdot 80 + 0.1321 \cdot F6)$$; Dose term.

$$80 = 1 - \exp\left[-(0.02457 \cdot T + 0.000256 \cdot I)\right]$$; Boron burn-out term.

B = Boron content in the steel.

dpa = Displaced atoms in iron.

T = Thermal fluence (E < 0.4 MeV); I = intermediate energy fluence (0.4 eV < E < 1.0 MeV); F1 = Fast fluence (E > 1.0 MeV); and F6 = Fast fluence (E > 6.0 MeV).

*ΔT is the 41-J Charpy shift in °F; Cu and Ni concentrations are in wt%; B content is in wt ppm of natural boron; F1, F6, T, and I are in units of 10^{19} n/cm² = 1; and dpa is in units of displacements per atom of iron.

Background information on reference physics-dosimetry data and trend curve data development, testing, and applications is provided in Section 2.0. The applicable conditions and basis for the present study are discussed and delineated in Sections 3.0 and 4.0. Results and conclusions are presented in Section 4.0. Other work of interest and/or related to this study are reported in Sections HEDL-A through HEDL-E of this progress report.

2.0 Background

2.1 Damage Analysis Studies

As discussed in the 1984 Annual Report (Mc85a) and as a part of the LWR-PV-SDIP, statistically based data correlation studies have been made by HEDL and other program participants using existing PWR and BWR physics-dosimetry-metallurgical data in anticipation of the analysis of new fracture toughness and embrittlement data from the BSR-HSST, SUNY-NSTF, ORR-PSF, and other experiments. The reader is referred to Refs (Ma83b,Mc84,Mc85a,Mc84h,Gu84, Gu84a,Gu84b,Pe84,Ra84) for additional information and appropriate references.

2.2 NRC Physics-Dosimetry Compendium

The NRC physics-dosimetry compendium (Mc85c) is a collation of information and data developed from available research and commercial light water reactor vessel surveillance program (RVSP) documents and related surveillance capsule reports. The data represents the results of the HEDL (Simons) least-squares FERRET-SAND II Code re-evaluation of exposure units and values for 47 PWR and BWR surveillance capsules for W, B&W, CE, and GE power plants (see Figure HEDL-22). Using a consistent set of auxiliary data and dosimetry-adjusted reactor physics results, the revised fluence values (Table HEDL-22) for $E > 1$ MeV averaged 25% higher than the originally reported values. The range of fluence values (new/old) was from a low of 0.80 to a high of 2.38.

These HEDL-derived FERRET-SAND II exposure parameter values are being used for NRC-supported HEDL and other PWR and BWR trend curve data development and testing studies. These studies are providing results to support Revision 2 of Regulatory Guide 1.99. The information in the compendium is also being made available to the ASTM E10 Committee, to the Metal Properties Council (MPC) Subcommittee 6 on Materials for Nuclear Reactors, and to others developing improved data bases and trend curves. These curves are used by the utilities and by the NRC to account for neutron radiation damage in setting pressure/temperature limits, in making fracture analysis, and in predicting neutron-induced changes in reactor PV steel fracture toughness and embrittlement during the vessel's service life.

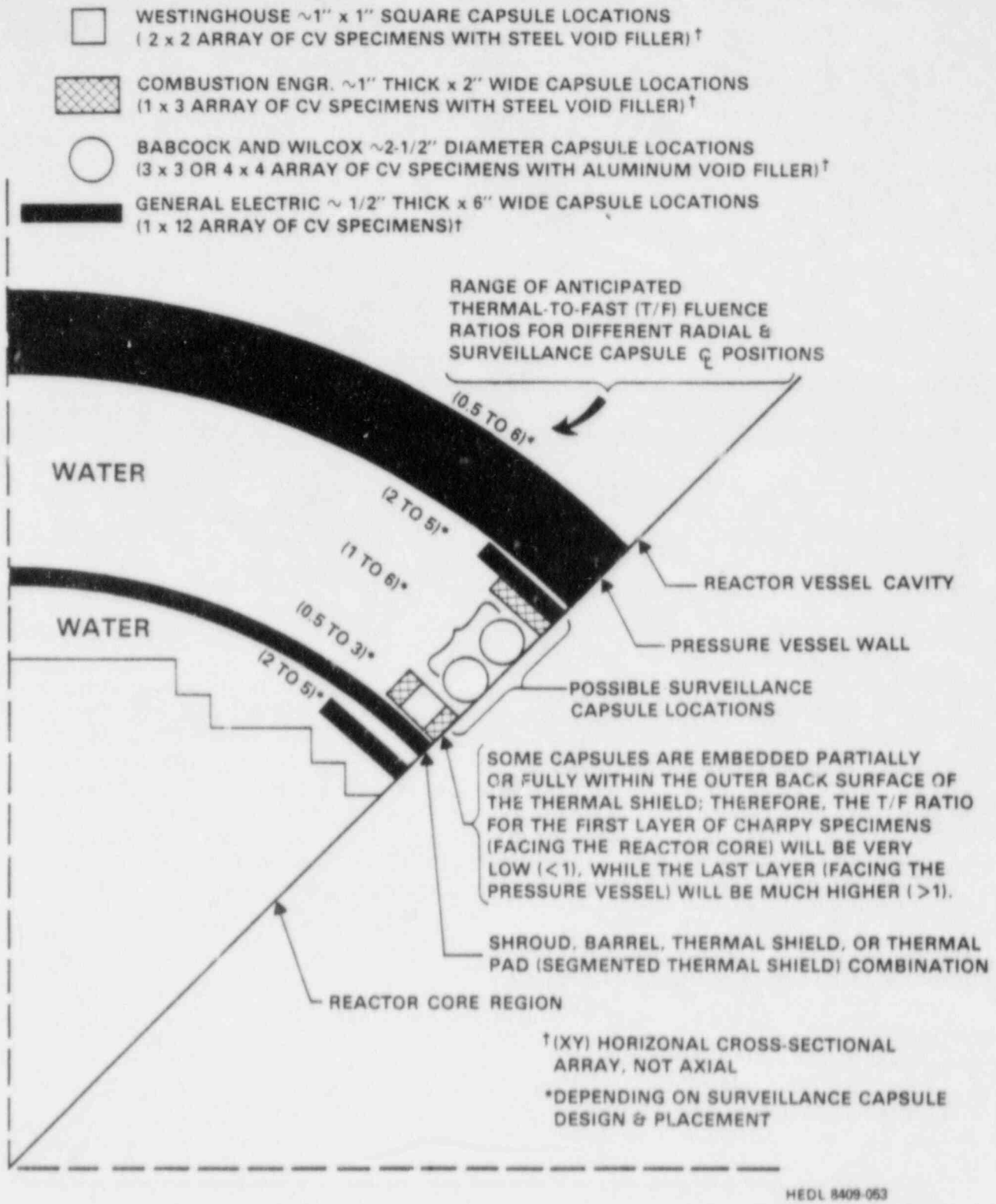

FIGURE HEDL-22. Schematic Representation of In-Vessel Surveillance Capsule Designs and Locations for Operating PWRs and BWRs.

TABLE HEDL-22

RE-EVALUATED EXPOSURE VALUES AND THEIR UNCERTAINTIES FOR LWR-PV SURVEILLANCE CAPSULES

Plant	Unit	Cap-sule	Service Lab*	Biblio Ref	Fluence (ϕt > 1 MeV) (n/cm^2) Old	Fluence (ϕt > 1 MeV) (n/cm^2) New [% (1σ)]	New/Old	Fluence (E < 0.414 eV) (n/cm^2)	dpa [% (1σ)]	New dpa/ϕt	dpa/s	hpa (appb)†	Exposure** Time (s)
Westinghouse						***							
Conn. Yankee		A	BMI	(Ir70)	2.08 E+18	3.16 E+18 (12)	1.53	2.54 E+18 (18)	0.00482 (12)	1.52 E-21	9.06 E-11	6	5.233 E+07
Conn. Yankee		F	BMI	(Pe77)	4.04 E+18	6.06 E+18 (24)	1.50	5.43 E+18 (32)	0.00949 (27)	1.56 E-21	1.24 E-10	13	7.651 E+07
Conn. Yankee		H	W	(Ya67)	1.79 E+19	2.00 E+19 (24)	1.12	2.33 E+19 (19)	0.0324 (27)	1.62 E-21	1.36 E-10	52	2.390 E+08
San Onofre		A	SwRI	(No71)	1.20 E+19	2.86 E+19 (22)	2.38	2.05 E+19 (23)	0.0485 (27)	1.70 E-21	8.35 E-10	43	5.824 E+07
San Onofre		D	SwRI	(No72)	2.36 E+19	5.62 E+19 (26)	2.38	3.76 E+19 (23)	0.0944 (29)	1.68 E-21	1.06 E-09	80	8.881 E+07
San Onofre		F	W	(Ya79)	5.14 E+19	5.73 E+19 (14)	1.11	2.99 E+19 (28)	0.0955 (20)	1.67 E-21	3.92 E-10	73	2.438 E+08
Turkey Point	3	S	SwRI	(No79)	1.41 E+19	1.62 E+19 (24)	1.15	1.34 E+19 (24)	0.0255 (27)	1.57 E-21	2.33 E-10	33	1.095 E+08
Turkey Point	3	T	W	(Ya75)	5.68 E+18	7.01 E+18 (10)	1.23	5.12 E+18 (58)	0.0109 (12)	1.55 E-21	4.73 E-10	14	2.302 E+07
Turkey Point	4	S	SwRI	(No79)	1.25 E+19	1.31 E+19 (25)	1.05	1.31 E+19 (25)	0.0213 (27)	1.63 E-21	1.97 E-10	37	1.079 E+08
Turkey Point	4	T	SwRI	(No76)	6.05 E+18	7.54 E+18 (13)	1.25	8.40 E+18 (21)	0.0130 (13)	1.72 E-21	3.48 E-10	20	3.728 E+07
H. B. Robinson	2	S	W	(Yo73)	3.02 E+18	3.91 E+18 (24)	1.29	8.81 E+18 (18)	0.00615 (27)	1.57 E-21	1.06 E-10	19	4.209 E+07
H. B. Robinson	2	W	SwRI	(No76b)	4.51 E+18	7.24 E+18 (22)	1.61	8.96 E+18 (20)	0.0119 (25)	1.59 E-21	1.08 E-10	21	1.050 E+08
Surry	1	T	BMI	(Pe75)	2.50 E+18	2.86 E+18 (9)	1.14	3.57 E+18 (20)	0.00449 (12)	1.57 E-21	1.33 E-10	8	3.378 E+07
Surry	2	X	BMI	(Pe75a)	3.02 E+18	3.03 E+18 (11)	1.00	3.64 E+18 (20)	0.00473 (13)	1.56 E-21	1.28 E-10	9	3.687 E+07
North Anna	1	V	B&W	(Lo81d)	2.49 E+18	2.72 E+18 (9)	1.09	5.80 E+18 (14)	0.00411 (11)	1.51 E-21	1.15 E-10	11	3.570 E+07
Beznau	2	R	EIR	( )	1.70 E+19	1.34 E+19 (9)	1.27	2.27 E+19 (21)	0.0198 (11)	1.48 E-21	1.16 E-10	49	1.714 E+08
Pr. Island	1	V	W	(Da77)	5.21 E+18	6.03 E+18 (11)	1.16	9.21 E+18 (21)	0.0102 (16)	1.69 E-21	2.41 E-10	20	4.248 E+07
Pr. Island	2	V	W	(Y...1)	5.49 E+18	6.74 E+18 (10)	1.23	9.75 E+18 (26)	0.0117 (13)	1.74 E-21	2.67 E-10	21	4.394 E+07
R. E. Ginna	1	R	W	(Ya74)	7.60 E+18	1.17 E+19 (10)	1.54	1.84 E+19 (25)	0.0215 (14)	1.83 E-21	2.59 E-10	38	8.328 E+07
R. E. Ginna	1	V	W	(Ma73a)	4.90 E+18	5.93 E+18 (14)	1.21	1.37 E+19 (59)	0.0102 (22)	1.72 E-21	2.20 E-10	29	4.612 E+07
Kewaunee		V	W	(Ya77)	5.59 E+18	6.41 E+18 (10)	1.15	1.23 E+19 (23)	0.0114 (13)	1.78 E-21	2.82 E-10	26	4.057 E+07
Point Beach	1	S	W	(Ya76)	7.05 E+18	8.45 E+18 (10)	1.20	1.20 E+19 (19)	0.0146 (13)	1.73 E-21	1.25 E-10	27	1.163 E+08
Point Beach	1	R	W	(Ya78)	2.22 E+19	2.29 E+19 (10)	1.37	2.85 E+19 (22)	0.0408 (13)	1.78 E-21	2.50 E-10	61	1.632 E+08
Point Beach	2	V	BMI	(Pe75b)	4.74 E+18	7.28 E+18 (11)	1.54	1.09 E+19 (18)	0.0121 (13)	1.66 E-21	2.52 E-10	23	4.805 E+07
Point Beach	2	T	W	(Da78a)	9.45 E+18	9.40 E+18 (10)	0.99	1.48 E+19 (21)	0.0157 (12)	1.67 E-21	1.44 E-10	32	1.087 E+08
Point Beach	2	R	W	(Ya79a)	2.01 E+19	2.52 E+19 (10)	1.25	4.71 E+19 (26)	0.0460 (14)	1.83 E-21	2.81 E-10	93	1.640 E+08
D. C. Cook	1	T	SwRI	(No77b)	1.80 E+18	2.71 E+18 (22)	1.51	3.26 E+19 (19)	0.00445 (25)	1.64 E-21	1.12 E-10	77	3.991 E+07
Indian Point	2	T	SwRI	(No77a)	2.02 E+18	3.28 E+18 (22)	1.62	4.01 E+18 (44)	0.00537 (27)	1.64 E-21	1.20 E-10	91	4.473 E+07
Indian Point	3	T	W	(Da79)	2.92 E+18	3.23 E+18 (22)	1.11	3.13 E+18 (21)	0.00520 (25)	1.61 E-21	1.23 E-10	74	4.211 E+07
Zion	1	T	BMI	(Pe78)	1.80 E+18	3.04 E+18 (10)	1.69	3.17 E+18 (21)	0.00488 (12)	1.61 E-21	1.29 E-10	82	3.789 E+07
Zion	1	U	W	(Ya81a)	8.92 E+18	1.01 E+19 (10)	1.13	8.87 E+18 (24)	0.0166 (13)	1.64 E-21	1.47 E-10	21	1.123 E+08
Zion	2	U	BMI	(Pe78)	2.00 E+18	2.80 E+18 (9)	1.40	3.80 E+18 (15)	0.00446 (12)	1.59 E-21	1.11 E-10	10	4.007 E+07
Salem	1	T	W	(Ya80)	2.56 E+18	2.84 E+18 (22)	1.11	3.26 E+18 (19)	0.00460 (25)	1.62 E-21	1.34 E-10	7	3.426 E+07

*BMI = Battelle Memorial Institute; W = Westinghouse; SwRI = Southwest Research Institute; CE = Combustion Engineering; ET = Effects Technology; B&W = Babcock and Wilcox; EIR = Eidg. Institute für Reaktorforschung.

**Equivalent constant power level exposure time.

***3.16 E+18 (12) means 3.16×10^{18} with a 12% (1σ) uncertainty.

†Calculated for A302B steel with a nominal concentration of 0.55 appm boron present.

TABLE HEDL-22 (Cont'd)

Plant	Unit	Capsule	Service Lab*	Biblio Ref	Fluence (at > 1 MeV) (n/cm²) Old	New [% (1σ)]	New/Old	Fluence (E < 0.414 eV) (n/cm²)	dpa [% (1σ)]	New dpa/φt	dpa/s	hpa (appb)†	Exposure** Time (s)
Combustion Engineering													
Palisades		A240	BMI	(Pe79b)	4.40 E+19	6.06 E+19 (23)	1.38	7.26 E+19 (61)	0.0972 (28)	1.60 E-21	1.36 E-09	170	7.130 E+07
Fort Calhoun		W225	CE	(By80)	5.10 E+18	5.83 E+18 (14)	1.14	3.09 E+19 (60)	0.00879 (18)	1.51 E-21	1.07 E-10	63	8.191 E+07
Maine Yankee		1	ET	(Wu75)	1.30 E+19	1.76 E+19 (19)	1.35	3.00 E+19 (29)	0.0285 (23)	1.62 E-21	1.03 E-09	62	2.777 E+07
Maine Yankee		2	W	(Ya81b)	8.84 E+19	7.73 E+19 (13)	0.87	1.20 E+20 (23)	0.121 (18)	1.57 E-21	8.38 E-10	230	1.446 E+08
Maine Yankee		W263	BMI	(Pe80)	7.10 E+18	5.67 E+18 (17)	0.82	2.67 E+19 (21)	0.00843 (14)	1.49 E-21	5.83 E-11	55	1.446 E+08
Babcock & Wilcox													
Oconee	1	F	B&W	(Lo75)	8.70 E+17	6.98 E+17 (21)	0.80	1.00 E+18 (13)	0.000959 (19)	1.37 E-21	3.65 E-11	3	2.629 E+07
Oconee	1	E	B&W	(Lo77)	1.50 E+18	1.50 E+18 (10)	1.00	2.61 E+18 (15)	0.00208 (10)	1.39 E-21	4.01 E-11	7	5.186 E+07
Oconee	2	C	B&W	(Lo77a)	9.43 E+17	1.01 E+18 (10)	1.07	1.55 E+18 (15)	0.00148 (11)	1.47 E-21	3.88 E-11	4	3.802 E+07
Oconee	3	A	B&W	(Lo77b)	7.39 E+17	8.05 E+17 (10)	1.09	1.34 E+18 (11)	0.00113 (11)	1.40 E-21	3.79 E-11	3	2.983 E+07
Three Mile Is.	1	E	B&W	(Lo77c)	1.07 E+18	1.09 E+18 (9)	1.02	1.90 E+18 (11)	0.0015! (9)	1.39 E-21	3.75 E-11	5	4.036 E+07
Arkansas Nuclear	1	E	B&W	(Lo77d)	7.27 E+17	8.18 E+17 (8)	1.13	6.32 E+17 (9)	0.00117 (8)	1.43 E-21	3.92 E-11	2	2.981 E+07
General Electric													
Dresden	3	4G14	W	(Ya82)	2.06 E+19	1.86 E+19 (17)	0.89	1.51 E+20 (62)	0.0285 (17)	1.53 E-21	3.35 E-10	290	8.483 E+07
Dresden	3	4G15	W	(Ya82)	1.50 E+19	1.35 E+19 (17)	0.89	1.19 E+20 (62)	0.0209 (17)	1.55 E-21	2.46 E-10	240	8.483 E+07
Dresden	3	4G16	W	(Ya82)	1.20 E+19	1.08 E+19 (17)	0.89	9.70 E+19 (62)	0.0168 (17)	1.55 E-21	1.98 E-10	200	8.483 E-07
Dresden	3	4G17	W	(Ya82)	5.16 E+18	4.51 E+18 (17)	0.89	5.20 E+19 (62)	0.00733 (18)	1.63 E-21	8.64 E-11	120	8.438 E+07
Quad Cities	1	3G5	W	(Ya81c)	4.04 E+19	4.23 E+19 (17)	1.61	2.41 E+20 (62)	0.0604 (17)	1.43 E-21	4.85 E-10	400	1.243 E+08
Quad Cities	1	3G6	W	(Ya81c)	3.08 E+19	3.12 E+19 (17)	1.61	1.92 E+20 (62)	0.0450 (17)	1.44 E-21	3.62 E-10	340	1.243 E+08
Quad Cities	1	3G7	W	(Ya81c)	2.37 E+19	2.47 E+19 (17)	1.61	1.54 E+20 (62)	0.0356 (17)	1.44 E-21	2.86 E-10	290	1.253 E+08
Quad Cities	1	3G8	W	(Ya81c)	1.24 E+19	1.17 E+19 (17)	1.61	1.03 E+20 (62)	0.0180 (17)	1.54 E-21	1.45 E-10	210	1.243 E+08
Quad Cities	2	3G14	W	(Ya82a)	4.14 E+19	4.28 E+19 (16)	1.03	2.45 E+20 (62)	0.0611 (17)	1.43 E-21	4.29 E-10	400	1.422 E+08
Quad Cities	2	3G15	W	(Ya82a)	3.48 E+19	3.60 E+19 (16)	1.03	2.13 E+20 (62)	0.0516 (17)	1.43 E-21	3.63 E-10	370	1.422 E+08
Quad Cities	2	3G16	W	(Ya82a)	2.43 E+19	2.52 E+19 (16)	1.03	1.55 E+20 (62)	0.0362 (17)	1.44 E-21	2.54 E-10	290	1.422 E+08
Quad Cities	2	3G17	W	(Ya82a)	2.32 E+19	2.37 E+19 (17)	1.03	1.49 E+20 (62)	0.0342 (17)	1.44 E-21	2.41 E-10	290	1.422 E+08
							Avg 1.25						

*BMI = Battelle Memorial Institute; W = Westinghouse; SwRI = Southwest Research Institute; CE = Combustion Engineering; ET = Effects Technology; B&W = Babcock and Wilcox; EIR = Eidg. Institute für Reaktorforschung.

**Equivalent constant power level exposure time.

***3.16 E+18 (12) means 3.16×10^{18} with a 12% (1σ) uncertainty.

†Calculated for A302B steel with a nominal concentration of 0.55 appm boron present.

The status of the development and application of new advancements in LWR-PV-SDIP, such as cavity physics-dosimetry for improving the reliability of current and end-of-life (EOL) predictions on the metallurgical conditions of pressure vessels and their support structures, is discussed with appropriate referencing to the current literature, Federal and NRC regulations and rules, and the new series of 21 ASTM LWR Surveillance Standards. Application of established ASTM standards is expected to permit the reporting of measured materials property changes and neutron exposures to an accuracy and precision within bounds of 10% to 30%, depending on the measured metallurgical variable and neutron environment.

2.3 Regulatory Guide 1.99, Revision 2

In Ref (Ra84), Randall discusses the basis for Revision 2 of Reg. Guide 1.99. As stated, the Guide is being updated to reflect recent studies of the physical basis for neutron radiation damage and efforts to correlate damage to chemical composition and fluence. Revision 2 contains several significant changes. Welds and base metal are treated separately. Nickel content is added as a variable, and phosphorus is removed. The exponent in the fluence factor is reduced, especially at high fluences; and guidance is given for calculating attenuation of damage through the vessel wall.

For PV wall neutron fluence attenuation predictions, the preliminary results of the PSF (Mc85a) comparisons lie within 10% but reaffirm slight deficiencies in the iron cross sections first brought to light by the PCA and PSF startup experiment comparisons (Mc81,Wi83), which show increasing disagreement the further into the PV one goes.

In the planned Revision 2 of Reg. Guide 1.99 (Ra84), the equation used for PV wall fluence attenuation by Randall is

$$\text{Fluence}(x) = \text{Fluence}(\text{Surface}) \cdot e^{-0.24x}, \qquad (1)$$

where x is the depth in the wall in inches, measured from the inside surface. This equation is based on transport calculations by Guthrie et al. (Gu82,Gu82a) for the dpa attenuation through an 8.0-inch vessel wall. These calculations did not account for the deficiencies in the iron cross sections mentioned above.

It has been recently noted by Fabry that the $^6Li(n,\alpha)$ spectrometry data (DeLeeuw, Mc81) in PCA are consistent with gas proton recoil spectrometry (Rogers, Mc81) and silicon damage measurements (DeLeeuw, Mc81), and they indicate larger proportions of neutrons below 1.0 MeV than predicted by ENDF/B-IV; the discrepancy is on the order of 20%, in the same direction as nuclear research emulsion (NRE) results reported by Roberts, Gold, and Preston in Ref (Mc85a), Section 2.2.1.1, "NRE Measurements." This confirmed result does affect the dpa/ϕ > 1 MeV transverse predictions through the reactor PV planned for use in Reg. Guide 1.99, Revision 2 (Ra84), and may adversely impinge upon eventual crack-arrest considerations in the safety analysis of ASME-III designed vessels. It is recommended, therefore, that:

1) A new simultaneous evaluation of all experimental data in PCA, the NESDIP replica, and the Mol Iron Shell Benchmarks should be performed, including the French damage monitor results obtained during the PSF startup program,

2) Integral measurements using NRE as well as higher threshold-energy sensors [such as $^{58}Ni(n,p)$, $^{64}Zn(n,p)$, or $^{27}Al(n,\alpha)$] should be performed in the Mol Iron Shell Benchmarks, and

3) Continuous gamma-ray spectrometry experiments should be conducted in the NESDIP benchmark, Phase 3, to resolve inelastic gamma-rays produced by fast neutron interactions in iron and thereby test the inelastic neutron transport cross section of iron.

2.4 Trend Curve Data Development and Testing

2.4.1 HEDL Studies

In Refs (Gu84b) and (Mc84h), the effects of changes in different variables and use of different exposure parameter models for predicting the Charpy shift for the 30-point PSF weld, plate, and forging data base and a 30-point PWR weld data base are discussed in considerable detail.

The main comments and conclusions of G. L. Guthrie's study (Gu84b), based on the use of PSF and test reactor data, are:

1) In surveying the previously existing data available for the alloys in the PSF experiment, it has become apparent that the fluence exponent is dependent on temperature and flux level. For A302B alloy, the PWR surveillance data fell consistently below the higher flux-level LITR data and showed a lower value for the fluence exponent. The overall scatter of the existing data is such that it is not clear that Charpy tests or K_{IC} tests can be used to uncover fine details in mechanisms.

2) Because of the possible rate effect (which was predicted by G. R. Odette in his PSF Blind Test submission), the PWR surveillance trend-curve laws cannot be expected to work as well in the PSF as might be expected from their stated standard deviations.

3) In applying existing Charpy shift laws to the PSF C_V data, we find that the largest observed shift occurred for the RR&A A533B weld (Code R), which had a high Ni content (1.58%) -- well outside the range of the data base used to develop the HEDL PWR Charpy shift equations (Gu84). A comparison of the HEDL equation applications and the Hawthorne values for ΔT_{CV30} are given in Ref (Gu84). The overall deviation is 31.6°F or 17.6°C (1σ). This is more than the standard deviation of the fit to the original data base and is due to the facts that 1) the Code R specimen is outside the recommended chemistry range, and 2) the rate effect has caused

the predictions for ΔT_{cv30} to be biased low. The values in Ref (Gu84) should not be compared to blind test predictions since no use was made of SSC-1 results to guide the calculations and no correction has been attempted for rate effects.

4) There appears to be a rate effect in the PSF Charpy and compression data. The fluence exponent appears to increase with increased flux and appears to decrease with increased Cu.

5) The similarity of the spectra at the separate irradiation positions severely limits the possible comments about damage functions.

6) No extra thermal neutron effect, beyond that already represented in the ASTM dpa cross section, was identifiable in the PSF data.

The main comments and conclusions of the study by McElroy et al. (Mc84h), based on the use of PSF, PWR, and BWR data, are:

1) There is a significant improvement (reduction) in the standard deviation of the fit for weld Charpy shift trend curves that includes the effect of low-energy thermal neutrons. For the 30-point weld data set, improvements of the amounts observed could occur at a frequency of ~4% by chance.

2) A knowledge of the actual boron content of PV steels and the use of a trend curve that employs an exposure parameter dose term, including the total production of dpa in iron and helium, could make significant improvements in lowering the standard deviation of the fit for the existing PWR surveillance capsule metallurgical weld data base.

3) Based on the trend curve model that includes the effect of thermal neutrons, for both PWR and BWR power plants, up to about 80% of the SS-clad/PV steel wall interface and surveillance capsule specimen dose term values could be attributed to helium production in PV steels, depending on the particular surveillance capsule design, Charpy specimen placement, steel boron content, and power plant operating conditions.

4) Existing PWR and BWR surveillance capsule derived embrittlement trend curves [based on the use of just fast fluence (E > 1 MeV) or dpa for the exposure term] cannot be expected to give reliable predictions of the combined fast and thermal neutron contributions to the Charpy shift at the SS-clad/PV steel wall interface, 1/4-T, 1/2-T, 3/4-T, or 0-T locations. [It is noted that the PSF experiment provides physics-dosimetry-metallurgy data for predicting the Charpy shift in PV steels at deep in-wall locations, such as the 1/4-T, 1/2-T, and 3/4-T positions, where the T/F ratios are in the very low range of ~0.14 to ~0.53. However, even for these very low ratios, helium from both boron and steel high energy (n,α) reactions may still contribute 5% to 30% to the exposure parameter dose term value.]

5) None of the Charpy shift trend curve equations studied [see Table 1 of Ref (Mc84h)] except perhaps the one based on the use of an exposure parameter of fluence E > 0.1 MeV, appears to properly bound all the six PV steel observed PSF damage gradient curves. Based on the French simulated PV-wall DOMPAC Experiment (Mc84,Al83), Alberman concluded that for low temperature (<100°C) irradiations, fast fluence (E > 1 MeV) is too "optimistic" and is not, therefore, a conservative neutron exposure parameter. He also concluded that, at low temperature, 95% of the measured damage (based on tungsten and graphite DM results) comes from neutrons with energy E > 0.1 MeV. This led him to conclude that the exposure parameter, fluence (E > 0.1 MeV), is perhaps "pessimistic" but has the advantage of being the lower threshold of all (displacement) damage models. Thus it takes into account all neutrons that create (displacement) damage.

6) The plant specific weld data sets used in the PWR and BWR data base studies, except for one, do not support a saturation effect at high fluences above ~1 x 10^{19} n/cm² (E > 1 MeV). Consequently, the existing Reg. Guide 1.99 (Re77) upper bound (truncated) trend curve model shape (or plant specific curves) may have to be used for high fluence embrittlement predictions for PV steel welds, and perhaps forgings and plates.

7) Any significant thermal neutron contribution to PV steel embrittlement is, most probably, a result of (n,α) reactions in boron-10 rather than by neutron-induced $Fe(n,\gamma)$ recoil reactions.

8) It appears that the current ASTM E693 dpa cross section should not be used to correlate highly thermalized light or heavy water moderated power or test reactor irradiation effects data because it significantly overestimates the low-energy thermal neutron dpa contribution.

9) The PV-wall SS-clad/PV steel interface surface T/F ratio for PWR and BWR power plants is expected to be in the range of 2 to 6 on the basis of surveillance capsule measurements, Westinghouse transport calculations, GE measurements, and the PSF experiment physics-dosimetry results.

10) Individual Charpy specimens (with natural boron content of ~0.4 up to perhaps 5 wt ppm) in PWR and BWR surveillance capsules will be subject to neutron exposures with T/F ratios in the range of ~0.5 to 5, depending on the surveillance capsule design, its placement, and the reactor operating conditions. The T/F variation for individual Charpy specimens, therefore, could be an important parameter for the correlation of a set of Charpy specimen results and derived ΔRT_{NDT} values.

11) From this study, that of Grant and Earp (Gr84), and others discussed in Ref (Mc84h), a final conclusion is: the PSF experiment and PWR and BWR surveillance program results clearly show that comparison of the effects of radiation damage on yield strength, hardness, RT_{NDT}, and USE will be needed to aid in improving and refining our knowledge of trend curves and PV wall damage gradients. Implicit in this are the current observations that the establishment of separate trend curves for welds, forgings, and plates will give increased understanding and accuracy in projections of the present and future metallurgical condition of PV steels.

2.4.2 Heller and Lowe's B&W Study

In Ref (He84a), Heller and Lowe discuss the development of a new B&W trend curve model equation for the RT_{NDT} shift for submerged-arc weld metals, made with Cu-plated wire and Linde 80* flux. These metals are of greatest importance to B&W 177-FA plants. Previously, there had been an insufficient data base to permit the evaluation of this material exclusively. The main comments and conclusions of their study, based on the use of a significant number of new data from reactor vessel material surveillance capsules, are:

1) Only results from weld metals made by B&W were used. Thus, the B&W data base (26 weld points) should be as free of errors as practical, considering the available sources. The measurement errors within this data base are expected to be small, and a high degree of confidence is placed on the validity of the predicted values from the model, as long as extrapolation beyond the data range is avoided.

2) A linear additive model of the chemical elements (Ni, Cu, etc.) terms was assumed. The stepwise regression procedure subsequently selected variables for inclusion, solely on the basis of the maximum reduction in the residual sum of squares from the addition terms.

3) Results of the analysis indicated that Ni and fluence should be selected into the shift model. No other variables were found to be statistically significant. The results were unaltered when the atypical weld was excluded from the data.

4) At the suggestion of the NRC, Cu was included in the B&W model, subsequent to the stepwise procedure; however, the logarithmic form of the equation [Eq. (4M), Table HEDL-21, Section 3.4] was used without the Cu term to evaluate the power of the fluence component and was found to be 0.326. The multiple correlation coefficient for this model is 0.86, and the uncertainty of prediction (σ) is $\sim$28°F.

5) Recent publications indicate that no consensus can be arrived at for the optimum set of chemical composition terms to be included in a shift prediction model. The reason for this lack of consensus is that the statistical significance of a model depends largely on the data set used. Consequently, the choice of model terms is best determined by a combination of statistical and physical considerations. For instance, silicon has been found to be significant in some B&W and other data. On the otherhand, the models suggested by the NRC exclude this element.

*Registered trademark of Union Carbide, New York, NY.

At the same time, these NRC models suggest that a term of Cu times Ni is significant for predicting the shift. Analyses on the B&W data do not substantiate this and show that, in fact, Cu is insignificant irrespective of the presence of Ni. There is independent support by Oak Ridge studies, stating that Cu times Ni is not significant in some welds. To further complicate matters, Reg. Guide 1.99 (Rev. 1) considers Cu and phosphorous, whereas the screening criteria for thermal shock is based on Cu times Ni.

6) Conclusions of generic significance may be misleading unless a systematic variation in key chemical elements is carried out with the corresponding effects on shift properly noted. The data base and the subjectivity of the physical trends that influence the results and that are reflected in the statistical conclusions may not be conclusive without such an analysis. Thus, we caution that conclusions of this study are not generic.

7) In a comparison of the observed versus predicted shifts using the B&W model equation, and except at the end points, the model has no specific bias since the points are evenly spread about the 45-degree line, especially in the 35° to 200°F shift range. The lack of data at the ends causes some bias in the unconservative direction. Extrapolation beyond the data base is therefore not advisable.

2.4.3 Other Studies

As discussed in previous annual reports and as a part of the LWR-PV-SDIP Program, statistically based (as well as other) physics-dosimetry-metallurgy data analysis and correlation studies using power and research reactor data are being made by ORNL, MEA, HEDL, UCSB, and other program participants. The reader is referred to Sections 2.3.1 and 2.3.2 of Ref (Mc85) and the Proceeding of the 5th ASTM-EURATOM Symposium for more information on the ORNL, MEA, HEDL, UCSB, and other studies.

3.0 General Considerations

3.1 Plant-Specific Trend Curves and Trend Curve Variables

In spite of considerable research that has been conducted over the years on neutron-induced embrittlement of pressure vessel steels, the details and subtleties of this phenomenon still continue to unfold. As stated elsewhere, the complexity of this phenomenon can not be over emphasized, see Section HEDL-A and Refs (Gu85,Ka84).

In Chapter HEDL-A, Gold and McElroy discuss and question the validity of the assumption of the separability of the variables for the chemistry and exposure dose dependence of ΔRT_{NDT}. Further insight into the physical plausibility of this assumption is provided by a heuristic extension of Odette's treatment of microvoid density (Pe84). This extension involved the introduction of a term for microvoid stabilization by chemical variables such as Cu, Ni, and/or He in such a way as to prevent or deter annealing.

The derived equation provides some very simple physical implications. Namely, the extended time-dependent representation of the microvoid density does not satisfy any separability criterion, and the saturated microvoid density (N_{mv}) depends on the exposure, on flux-level and chemistry variables. Also, the saturation value should increase with increasing content of Cu, Ni, and/or He. In Section HEDL-E, Simons shows that a flux-level effect exists and is material dependent for a 0.05 to 0.24 wt% Cu range.

This flux-level effect illustrates a general limitation of trend curve analysis that arises through the inadequacy of the data base. Data bases used for trend curve analysis have various origins. Surveillance capsule measurements comprise the largest available data pool and have, therefore, been used most extensively. However, none of these data bases represents the specific conditions of radiation exposure that exist within an actual pressure vessel. As a consequence, trend curves developed by least-squares analyses of these data bases can systematically deviate from the radiation damage that actually accrues in a PV. This systematic deviation stems from the inability of the data base to truly represent the irradiation conditions that actually arise in the PV of operating power plants.

3.2 Grant and Earp's Trend Curve Material Type and Chemistry Variable Effects Study

Grant and Earp have reported on a study of methods for extending the life of a PWR reactor vessel after long exposure to fast neutron radiation (Gr84). As a part of this study, they evaluated candidate explanatory models for changes in the yield strength of low alloy steel used in nuclear reactor vessels. The most important results were qualitative, the models that proved to be the best within the class examined indicated useful parameterizations for the prediction of changes in yield strength. It was the selected parameterizations that were of primary interest to Grant and Earp, not the fits themselves. The fits did provide a relative measure of model quality that was important to model selection, but it was emphasized that selection of a model was based on its relative quality, not an absolute predictive capability. These models were established on the basis of heuristic reasoning and can be of some use in identifying possible physical damage mechanisms of interest, but do not otherwise possess physical significance.

Because of the small size of the data base, regression models with five or more parameters tended to be unstable; i.e., there was an increasing possibility that the results for these models were due to statistical fluctuation. In order to avoid such problems, it was decided that a regression variable should

show a consistent qualitative contribution to any model in which it appeared; this criterion, called consistency in trend by Grant and Earp, was the requirement that a regressor either act to enhance radiation damage or mitigate it, regardless of the other parameters in the model; i.e., in general, only first order effects would be included in the selection of a model.

The regressor variables considered by Grant and Earp were material type: forging, plate, and weld. It was noted that the average change in yield strength from irradiation for these material types were, respectively, 30.75 MPa, 106.39 MPa, and 193.33 MPa. This indicates grouping according to material type with weld material being most and forging being least susceptible. This led to the study of single-intercept models; i.e., forging, plate, and weld materials were considered in separate groupings.

The model selection was performed by an exhaustive study. There was a large amount of data that required careful examination. Previous work was used as a benchmark in assessing the results of the regressions. There was at least one finding that was not well supported by previous work, that is that manganese content proved to be a valuable parameter. The irradiation specimens used in the study received a fluence of 1.8 to 3.0 x 10^{19} n/cm^2, and were not corrected for the variation in fluence since the fluence dependence of the yield strength change for this range was assumed to be weak. The derived best three term linear regression model took the form

$$\Delta YS = X_1 + X_2 \cdot Mn + X_3 \cdot Cu \cdot Ni, \qquad (2)$$

where the Xs are constants and values of the chemistry terms are given in wt%. The Cu·Ni term was suggested by previous work on nil-ductility transition temperature and, as a term in a mathematical model, is justified by the same perturbational arguments used to select the linear regression model. Interpreted in this manner, this cross product term is a second order term of a non-linear chemistry dependence of the yield strength. Grant and Earp further state that the Ni contribution to damage appears to become important at about a one-to-one Ni/Cu ratio, and within certain Cu and fluence ranges, damage is found to increase directly as the Ni/Cu ratio increases to 6. At this latter ratio, the Cu atom can be surrounded on all orthogonal axes by Ni atoms.

For their study and a single-intercept model, at the five- and six-term level, the best models included the terms Mn, P, Mo, Cu·Ni, Cu, Si, Mn/(10C).

For a three-intercept model, equations of the form

$$\Delta YS = X_1 \cdot I_{Plate} + X_2 \cdot I_{Forg.} + X_3 \cdot I_{weld} + X_4 \cdot P + X_5 \cdot Cu \cdot Ni \qquad (3)$$

and

$$\Delta YS = X_1 \cdot I_{Plate} + X_2 \cdot I_{Forg.} + X_3 \cdot I_{weld} + X_4 \cdot Si + X_5 \cdot (Mn/10C) \quad (4)$$

were derived. The terms I_{Plate}, $I_{Forg.}$ and I_{Weld} are indicator variables and are 1 if the specimen belongs to the respective material category and 0 if not.

Each material category (Plate, Forging, and Weld) differed substantially in behavior. These difference are not adequately explained by residual chemistry alone. Grant and Earp considered the three intercept models examined in their study as promising and represent a reasonable compromise in the grouped/ungrouped model types. The implication of the three-intercept model is that the response of the chemical constituents of steel is the same across categories, and differences between categories are due to non-chemical factors that are constant within each material type and may be represented by a separate intercept term for each material.

The results of the Grant and Earp study suggest that plate, forgings, and welds should be treated as separate material type groupings. For the discussion that follows and the preliminary results and conclusions of Section 4.0, only a single power reactor plate (base metal) and two power reactor weld groupings were used. Future studies, however, should include a third grouping for forging material. The data base for the single plate and first weld grouping is that developed for NRC and reported by Randall, Guthrie, and Simons (Gu84). The data base for the second weld grouping is that reported by Heller and Lowe and developed for B&W 177-FA plants (He84a), see Section 2.4.2.

3.3 Trend Curve Ni-Fluence Dependency

At the October 1984, Geestacht ASTM-EURATOM Symposium, G. Odette reported on his trend curve studies and discussed an additive Ni-enhanced microvoid growth term for Charpy shift trend curves. He proposed a term of the form

$$\Delta T_{Ni} = (X_1 + X_2 \cdot Ni) \sqrt{\phi t - \phi t_o} \cdot \begin{pmatrix} \text{EXPONENTIAL} \\ \text{Ni ACTIVATION} \\ \text{ENERGY TERM} \end{pmatrix} \quad (5)$$

where X_1 and X_2 are constants, ϕt is the neutron fluence ($E > 1$ MeV), and ϕt_o is an assigned fluence value in the range near or above $\sim 1 \times 10^{19}$ n/cm^2. A modification of this equation was formulated for the present study, and the Gundremmingen surveillance capsule Charpy shift results were used to establish values for the constant coefficients, see Section 3.4.

3.4 Trend Curve Flux-Level and Ni-Fluence Correction Factor Equations

Using information given by the Grant and Earp and Odette studies and the previously documented results of Randall (Ra84), Guthrie (Gu84,Gu85), Odette (Pe84), McElroy et al. (Mc84h), and Heller and Lowe (He84a), the following three equations were established for providing relative multiplicative correction factors for flux-level and Ni-fluence effects:

$$CF\ (\text{Flux-level}) = -0.1098340 \cdot \ln(\text{Flux}) + 1.460000 \tag{6a}$$

$$CF\ (\text{Flux-level}) = 0.03227076 \cdot [\ln(\text{Flux})]^2 - 0.2282117 \cdot \ln(\text{Flux}) + 0.9797073 \tag{6b}$$

where "Flux" is given in units of 10^{11} n/cm²•s and

$$CF\ (\text{Ni-fluence}) = (1 + 0.0720467 \cdot \text{Ni}) \times [1 + 0.137520 \cdot (\text{Fluence}-0.55)^{3/4}] \tag{7}$$

and fluence is given in units of 10^{19} n/cm². Eqs. (6a), (6b), and (7) were derived using fluence (E > 1 MeV) as the exposure parameter. In future studies, dpa will be used as the exposure parameter.

The final adjusted forms of the equations and values of constants were derived using the PSF Experiment Code R Weld (0.23% Cu, 1.58% Ni) and the Gundremmingen surveillance capsule weld (0.18% Cu, 0.13% Ni, assumed) Charpy shift results. Mathematical separability of the flux-level and Ni-fluence dependencies was assumed for this study. This assumption allowed separate comparisons to be made of the PSF Code R material shifts to define the constants for Eqs. (6a) and (6b) and of the Gundremmingen weld material to define the constants and power law values for Eq. (7).

The above procedure effected a cancellation of the relative effects of chemistry for each weld material; however, subsequent iterative adjustments to both sets of constants for Eqs. (6a), (6b) and (7) were made by the combined evaluation of all results. The possible benefit of using these flux-level and Ni-fluence correction terms was tested by the application of Eqs. (6a), (6b) and (7) CFs to five existing weld and two plate trend curve equations developed by Guthrie (Gu84), McElroy (Mc84b), Heller and Lowe (He84a) and Odette (Pe84). For reference purposes, these five weld equations, together with the two plate (or base metal) equations, are defined in Table HEDL-21. Eq. (7M*) is a modification of Odette's weld Eq. (5M), developed by McElroy, Guthrie, and Simons, and its exposure term is discussed in Ref (Mc84h). Eq. (7M) makes use of a combination of exposure parameter terms involving dpa and thermal-intermediate-fast (E > 6 MeV) fluences, which account for helium production from both boron and steel.

*Equations referenced from Table HEDL-21 are coded with an "M" for Model to distinguish them from the equations in the text.

Eq. (1M) is Guthries' weld Eq. (2M) but modified to use dpa instead of fluence (E > 1 MeV). Eq. (3M) is Guthrie's plate equation, Eq. (4M) is Heller and Lowe's weld equation, and Eqs. (5M) and (6M) are Odette's weld and plate equations, respectively. Eqs. (2M), (3M), (4M), (5M), and (6M) all make use of fluence (E > 1 MeV) as the exposure parameter.

A code named "Equations All" (EQ.ALL) was developed to calculate Charpy shift values for all seven Table HEDL-21 trend curve models as well as to make corrections for flux-spectral, flux-level, Ni-fluence, power law N, and Cu dependency effects and compare the corrected and uncorrected results. To perform this last step, a R-residual data correlation test was established, see Sections 4.1 and 4.2.

Using the EQ.ALL Code, the Eqs. (1M) and (4M) C/E PSF Code R weld Charpy shift results (Tables HEDL-23a through -23d) were used to determine the constants for Eqs. (6a) and (6b). Tables HEDL-23a through -23d give the C/E and experimental-minus-calculated (E-C) Charpy shift values for the seven Table HEDL-21 trend curve model Eqs. (1M) through (7M). As a coding simplification, the "M" designation is not shown in the EQ.ALL computer output listing of results for Tables HEDL-23a through -23d or subsequent tables in this report.

At this time, the full significance of the 11%, 19%, 29%, 15%, and 16% differences in the C/E ratios [between the SSC (avg of SSC-1 & SSC-2 results) and 1/2-T locations] for the five weld Eqs. (1M), (2M), (4M), (5M), and (7M), respectively, has not been determined. For this investigation, it has been assumed that these differences are, primarily, associated with a flux level and chemistry rather than, say, a combined flux-level and thermal-fluence effect. Another comment is that the use of the Eq. (1M) trend curve model to establish the constants for Eq. (6a) may be in serious error, with a resulting significant under-estimation of the flux-level effect; e.g., when Eq. (4M) is used, the observed effect is ~30%, or three times as large. In this latter case, a simple chemistry term re-normalization (division by 1.484) of the Eq. (4M) C/E high ratio results, Table HEDL-23b, was used to yield acceptable starting (without correction for flux-level and Ni-fluence dependency) ratios of 1.15, 1.13, 1.02, 0.954, and 0.815 for the SSC-1, SSC-2, 0-T, 1/4-T, and 1/2-T locations, respectively, see Table HEDL-23c. Such a re-normalization is justified because the B&W Eq. (4M) trend curve model was developed for a very limited range of Ni-concentrations [0.54 wt% to 0.70 wt% Ni; well below the 1.58 wt% Ni of the Code R material.]

For Tables HEDL-23a, -23b, -23c, and -23d, and all subsequent tables of the EQ.ALL Code printout, the following terms and definitions apply:

C =	Calculated Charpy shift (°F), using Eqs. (1M) through (7M)
E =	Measured Charpy shift [$C_V(F)$] (°F)
Flu. =	Fast fluence (F1), E > 1.0 MeV (10^{19} n/cm² = 1)
Flux =	Fast flux level, E > 1.0 MeV (10^{11} n/cm²-s = 1)
T/F =	Thermal neutron (E < 0.4 eV) to fast neutron (E > 1.0 MeV) flux-level ratio
$C_V(F)$ =	Measured Charpy shift (°F)
Cu% =	Steel copper content (wt%)
Ni% =	Steel nickel content (wt%)

CF = For the J^{th} capsule (data point); the averaged value of the combined correction factor for all capsules (data points) used to correct the i^{th} trend curve equation "without corrections" to the i^{th} Equation "with corrections," for flux-level and/or Ni-fluence effects

L3 = L4•L5

L4 = $-0.1098340 \cdot \ln(\text{Flux}) + 1.460000$ for Eq. (1M)

L5 = $1 + 0.137520 \cdot (\text{Fl} - 0.55)^{0.75}$ for Eq. (1M)

L6 = $1 + 0.0720467 \cdot \text{Ni}$ for Eq. (1M)

L4 = $0.03227076 \cdot [\ln(\text{Flux})]^2 - 0.2282117 \cdot \ln(\text{Flux}) + 0.9797073$ for Eq. (4M)

L5 = L6 = 1.0 for Eqs. (4M)

M = Number of capsule data points "J"

$$R = \frac{\Sigma\,(E-C)^2 \text{uncorrected} - \Sigma\,(E-C)^2 \text{corrected}}{\Sigma\,(E-C)^2 \text{ corrected}/n}, \qquad \text{[see Eq. (11)]}$$

The use of Eq. (1M) was required to correct for dpa neutron spectral differences between the SSC, 0-T, 1/4-T, and 1/2-T locations of the PSF Experiment, Table HEDL-23a. This correction [a maximum of ∿5% (for a 40% dpa spectral difference between SSC and the 1/2-T location) when the ∿0.3 power law dependency of the shift in the 1 to 4 x 10^{19} n/cm² range is considered] was required before determining the value of the constants that would account for an additional 10% to 15% Code R material measured flux-level effect; i.e., the difference between the observed C/E Charpy shift ratios for the SSC, 0-T, 1/4-T, and 1/2-T Charpy specimen locations after correcting for spectral and Ni-fluence effects. This correction was not made when Eq. (4M) was used to determine the constant values for Eq. (6b), since an equation like Eq. (4M) (based on dpa) had not been developed by Heller and Lowe.

Using a similar procedure (Tables HEDL-24a and -24b), the Gundremmingen low-fluence (∿0.55, 1.0, and 3.0 x 10^{19} n/cm²) surveillance capsule C/E ratios (close to unity) were compared with the high fluence (∿22.5 x 10^{19} n/cm²) value of ∿0.61 to establish the values for the power law and constants for Eq. (7), after using Eq. (1M) for correcting for flux-level and spectral differences. A separate correction equation for Ni-fluence dependency was not derived for Eq. (4M), since its power law value was derived by Heller and Lowe using just Ni and fluence variables without Cu, and its use was to be restricted to the fluence range below ∿ 8 x 10^{19} n/cm².

The results of subsequent iterative adjustments to Eqs. (6a) and (7) by the combined evaluation of the PSF and Gundremmingen C/E ratios are shown in Table HEDL-25. Clearly, there is an improvement in the combined in-group and cross-group relative C/E ratio correlations for the PSF and Gundremmingen data sets. Because of concern about the quality of the Gundremmingen physics-dosimetry data base and the values used for the different variables in this study, there appeared to be little, if any, justification for further adjustments to the constants of Eqs. (6a) and (7) in an attempt to remove the ∿10% remaining bias between the Code R PSF and Gundremmingen weld results, see Table HEDL-25b.

Without the large measured Charpy shifts (and the associated small relative uncertainties) for the Code R material, little significance, normally, might have been attributed to the observed 10% to 30% differences between the SSC and 1/2-T C/E ratios [Table HEDL-23a, Eqs. (1M), (2M), (4M), (5M), and (7M)]. Even now, there still remain unanswered questions about the general applicability and meaning of these Code R high-Ni steel PSF results.

The Eqs. (6a), (6b), and (7) flux-level and Ni-fluence correction factors have been used in an investigation of their application and usefulness for improving the correlation of: 1) the PSF data base and 2) two existing plate and weld PWR and BWR surveillance capsule physics-dosimetry-metallurgy data bases, and 3) selected plant-specific data sets. The results and conclusions of this work are presented in Section 4.0.

4.0 DATA ANALYSIS PROCEDURES, RESULTS AND CONCLUSIONS

4.1 Data Analysis Approach and Results - Regulatory Guide 1.99, Revision 2

To show that the calculative procedures given in Revision 2 of Reg. Guide 1.99 are faithful to the data base, they were used by Randall (Ra84) to calculate a Charpy shift value based on the Cu, Ni, and fluence variable values for each data point in the Guthrie data base. The residual [experimentally (E) measured minus calculated (C) value] was then plotted versus fluence, Cu and Ni content. Scatter about the zero residual axis was fairly well balanced between overprediction and underprediction. Another purpose of providing the residual plots was to demonstrate that the blending of Guthrie's and Odette's results to obtain the calculative procedures for the guide had not invalidated the use of twice the standard deviation from the Guthrie's regression analysis to provide a suitable margin. The "two-sigma" limits, margin = $\pm$56°F for welds and equals $\pm$34°F for base metal, plotted on the residual figures, did indeed show that only one weld and two base metal data points would be underpredicted if the margin on ΔRT_{NDT} were made twice the standard deviation.

As given in the guide, the adjusted reference temperature (ART) is represented by the equation

$$ART = \text{Initial } RT_{NDT} + \Delta RT_{NDT} + \text{Margin}, \qquad (8)$$

where:

RT_{NDT} = Reference temperature, nil-ductility transition (°F).

Initial RT_{NDT} = Reference temperature for the unirradiated material.

ΔRT_{NDT} = Adjustment of reference temperature, Charpy shift; i.e., the temperature shift (measured at the 30 ft-lb level) in the average Charpy curve for the irradiated material relative to that for the unirradiated material.

Margin = Quantity (°F) that is to be added to obtain conservative, upperbound values of ART, and is given as

$$\text{Margin} = 2\sqrt{\sigma_0^2 + \sigma_\Delta^2} \qquad (9)$$

where σ_0 is the standard deviation on the initial RT_{NDT} when a generic mean value is used, and σ_Δ is the standard deviation on ΔRT_{NDT}.

Since Guthrie found only a small difference in the constants of the fluence factors for welds and base metal, the fluence factor used by Randall for both in the guide was $\exp(0.28 - 0.10 \log_{10}\phi t)$, which falls between the Guthrie curves [Eqs. (2M) and (3M) of Table HEDL-21] for weld and base metal. As Randall indicates, the fluence factor for welds derived by Odette (Pe84), gives agreement with that obtained by Guthrie except at fluences below 1.5×10^{19}, where the Odette fluence factor drops off sharply. For base metal, Odette used a uniform slope of 0.28, which agrees with that found by Guthrie at 10^{19} n/cm².

The equation for PV wall fluence attenuation selected by Randall for the Reg. Guide, Eq. (1), was combined with an 0.28 power law fluence dependence for the Charpy shift to obtain the result:

$$\Delta RT_{NDT} = [\Delta RT_{NDT} \text{ surface}]\, e^{-0.067x} \qquad (10)$$

where x is the depth in the PV wall, in inches, measured from the inside surface.

4.2 Data Analysis Approach and Results - HEDL Studies

4.2.1 R-Residual Test - Present Study

Randall's study of residuals for Reg. Guide 1.99, Rev. 2, were based entirely on comparisons to Guthrie's Eqs. (2M) and (3M), Table HEDL-21. The data analysis procedure adopted for the present study was to compare E-C and C/E values for a larger number (seven) of trend curve model equations, Table HEDL-21, developed by Guthrie, Odette, McElroy, Simons, and Heller and Lowe. Thus, a larger number of possible plant-specific trend curves, as well as the more generic averaged curves developed for use in Reg. Guide 1.99, Revision 2, could be studied and evaluated. Rather than using plots of individual (E-C) residual data points for seven equations, a cumbersome procedure, it was decided to define and use a R-residual test as the measure of "increased" or "decreased" correlation, with and without corrections for the following variables:

a) Neutron spectra (dpa)
b) Thermal-intermediate-fast (E > 6 MeV) neutron production of helium (from boron and steel)
c) Flux level and flux-level Cu dependency of the power law value N
d) Ni-fluence dependence

The R-residual test is represented by the equation,

$$R = \frac{\Sigma\ (E-C)^2\ \text{uncorrected} - \Sigma\ (E-C)^2\ \text{corrected}}{\Sigma\ (E-C)^2\ \text{corrected}/n} \qquad (11)$$

where E and C are the experimentally measured and calculated Charpy shifts (°F) and n is the number of data points in selected subsets for: 1) the PSF Experiment, 2) four Gundremmingen surveillance capsules, 3) the Randall-Guthrie-Simons PWR and BWR physics-dosimetry-metallurgy data base, 4) the B&W data base, or 5) selected plant-specific data sets. Larger and positive values of R are a reflection of the approach to unity for the C/E ratios, and indicate increased (improved) correlation resulting from a correction for one or more of the variables a) through d). A negative value of R indicates a decrease (worsing) in correlation associated with the application of one or more of the variables and any of the seven trend curve model equations.

4.2.2 Guthrie's PSF Analysis Procedures and Results

In Ref (Gu85), Guthrie discusses his observations on a Cu or Ni dependence for the Charpy shift equation power law value of N in PWR surveillance capsule data. He states:

> "*Past HEDL attempts (Gu81) at finding a Cu or Ni dependence for N in PWR surveillance capsule data showed no Ni dependence and a very slight indication of a Cu-dependence for N. The apparent Cu dependence for N in the PSF surveillance location can be seen in Figure HEDL-23 using either the data derived by Stallmann (St84b) or that derived by Hawthorne (Ha84, Ha84a), but the Cu dependence of the N value in the PV wall of the PSF is only apparent from Hawthorne's values for the Charpy shifts (see Figure HEDL-24). Values of N found using Hawthorne's data show higher N values at low Cu concentrations and lower N values at high Cu concentration for both the PV wall and surveillance capsule locations in the PSF, with a stronger Cu dependence for the surveillance capsule location. This trend fits in with the previous information found from power reactor data analysis (Gu81).*
>
> *Using Hawthorne's values for the Charpy ΔTs and the HEDL values for dpa, we find that least-squares fits give*
>
> $$N_{SSC} \sim 1.11 - 3.9 \cdot (\text{wt\% Cu}) \qquad (12a)$$

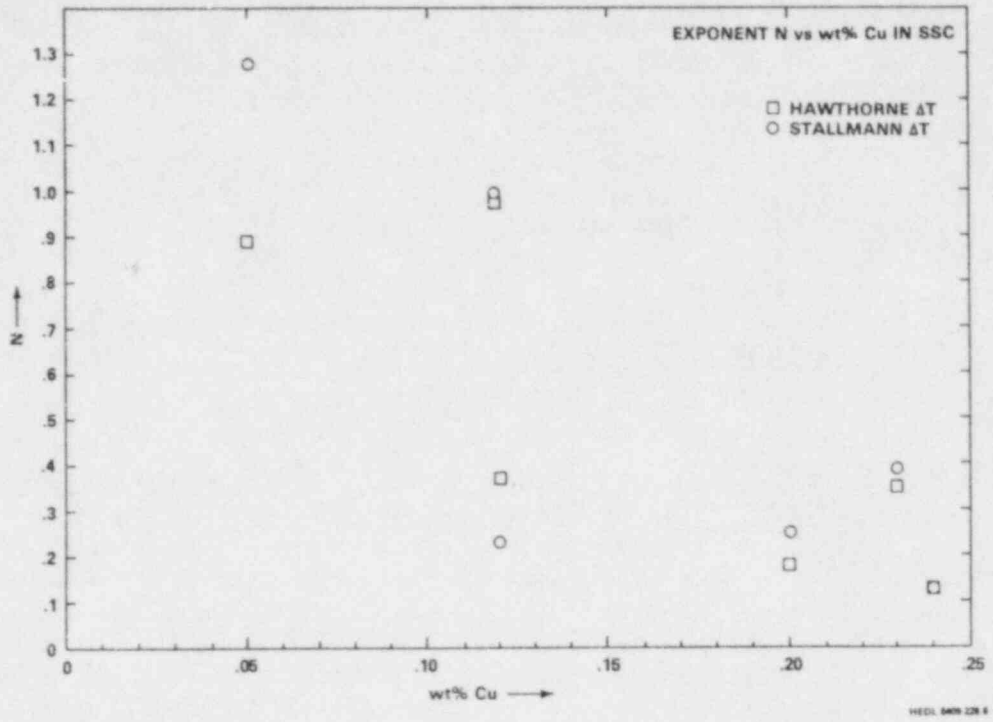

FIGURE HEDL-23. Exponent N Versus wt% Copper in SSC. (Guthrie)

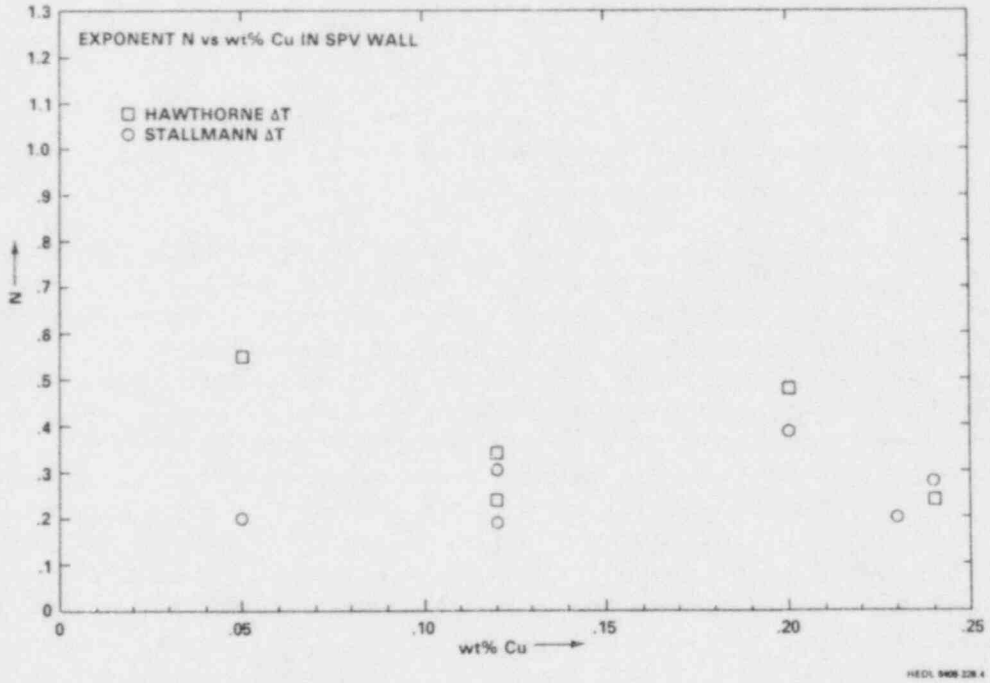

FIGURE HEDL-24. Exponent N Versus wt% Copper in the SPV Wall. (Guthrie)

$$N_{SPV} \sim 0.52 - 1.1 \bullet (\text{wt\% Cu}) \quad . \qquad (12b)$$

From previous work (Gu81) with PWR surveillance capsules, the derivative of N with respect to Cu was found to be approximately -0.36. This leads to an apparent relationship as shown in Table HEDL-26. The difference between dN/d(%Cu) for the SPV and power reactor surveillance cases is small and not unambiguously identifiable.*

We (Guthrie) have recently (Gu83a,Gu83c,Gu84) been working with trend curve laws of the type

$$\Delta T = f(\text{chem}) \bullet (\phi t)^{A} + B \ln(\phi t). \qquad (13)$$

One way to modify such a law to make the exponent Cu dependent and flux dependent (weakly) is to use

$$\Delta T = f(\text{chem}) \bullet (\phi t)^{N} \qquad (14a)$$

where:

$$N = A + B \bullet Cu \bullet \ln(\text{flux}) + C \bullet \ln(\text{fluence}). \qquad (14b)$$

In Eq. (14), it is presumed that B and C are constants while A might be very weakly flux dependent.

Details of the conclusions rest on the values chosen for the Charpy transition temperatures. In fact, the existence or nonexistence of the effects may depend on the values chosen. Unfortunately, the choice of a Charpy transition temperature is not clear cut. Furthermore, there may be some inconsistencies between the PSF N values for Alloy F and those found from data already existing for Alloy F (Gu85)."

4.2.3 Data Analysis and Adjustment Procedures - Present Study

The procedures for using and applying the Eqs. (6a), (6b), and (7) [variables (c) and (d)] correction factors are based on an extension of the results of the modeling studies of Guthrie, Heller and Lowe, Odette, Randall, Grant and Earp. Further, no attempt was made to separate the PWR and BWR base metal data bases into plate and forging material groupings, as had been done by Grant and Earp for their study and by others for the PSF Experiment (He84,He84a,

*The relationship was found to be N = 0.26 - 0.36•(wt% Cu).

TABLE HEDL-26

DERIVATIVE OF EXPONENT N WITH RESPECT TO COPPER

	dN/d (%Cu)	Flux	1/Flux
PSF SSC Data	-3.9	6×10^{12}	1.6×10^{-13}
PSF SPV Data	-1.1	4×10^{11}	2.5×10^{-12}
Power Reactor Surveillance Data	-0.36	1×10^{11}	1.0×10^{-11}

Gu84d,Gu85,Mc84h); only the plate (base metal) and weld groupings were used. The use of a third, forging grouping, should, however, be considered for future investigations.

For the chemistry term, the selected models, Eqs. (1M) - (7M), Table HEDL-21, only include first and second order terms for the Cu and Ni chemistry variables. The effects of other chemistry variables, therefore, are not addressed in the present investigation. Further, none of these seven equations currently include a variable or separate correction term for flux-level dependence.

Normally, little success would be expected in accurately determining the constants A, B, and C for Eq. (14), because of the poor quality of most existing PWR and BWR data bases. That is, there is an increasing chance that any regression analysis used to determine these values of the constants would produce unreliable results because of statistical fluctuations.

It is for this reason that a more plant-specific analysis approach was adopted for accounting for the flux-spectral, flux-level and any associated copper dependency. To accomplish this required the sorting out of the effects of a number of variables, including the trend curve model and those associated with chemistry and material type (plate forging, and weld). The approach selected to establish flux-spectral, flux-level, Cu, and/or Ni-fluence dependent multiplicative correction factor equations was outlined and discussed in Section 3.4. The analytical procedures established for using these equations, with one or more of the Table HEDL-21 trend curve equations, will now be considered.

4.2.3.1 Copper and Sulfur Dependencies - Procedure for Evaluation of Flux-Level Effect

To study the flux-level effect and its Cu dependency, Cu groupings of selected subsets of the PWR and BWR weld and plate material data bases that had small ranges of Cu concentration were used. This was done for three groupings of Ni concentration; lower-Ni (0.06 wt% to 0.30 wt%); and higher-Ni (0.49 wt% to 0.78 wt%) and higher-Ni (0.54 wt% to 0.70 wt%). The first two groupings were

for the NRC plate and weld data bases, while the third was for the B&W 177-FA plant weld data base.

Based on Grant and Earp's work, these three groupings may have been too broad in their Ni range, particularily for the lower-Ni (0.06 wt% to 0.30 wt%) because of their statement that the Ni contribution to damage appears to become important at about a one-to-one Ni/Cu ratio; and within certain Cu and fluence ranges, damage is found to increase directly as the Ni/Cu ratio increases to 6. Inclusion of these conditions, at this time, would require further subgroupings of an already limited PWR and BWR data base. A Cu-Ni cross product type chemistry dependency is used in most of the trend curve model equations, Table HEDL-21. Future investigations of the present type, however, should consider groupings with smaller ranges of Ni concentration. The results of the Heller and Lowe study strongly support this conclusion; i.e., the results of the investigation indicated that only Ni and fluence should be selected into their shift model; since no other variables were found to be statistically significant.

Another concern for the separation and evaluation of the many variable effects being considered here, is the determination of the part that sulfur may play in removing Cu from solution. Fisher et al. (Fa84) have recently stated that: "The observation of Cu precipitates in thermally aged plate together with $Cu_{1.8}S$ particles in all weld specimens leads to an analysis of the in-reactor hardening in terms of radiation-enhanced precipitation of free Cu during long-term aging in the reactor. A good correlation is obtained between the yield stress changes and $[\text{free Cu}]^{1/2}$, which suggests that copper-related hardening is the operative mechanism and that the radiation damage contribution is small following an in-reactor period of ~12 years at 220°C to a dose of 1.5 x 10^{19} n/cm² (E > 1 MeV)." The good correlation was achieved by correcting for Cu that had been precipitated as $Cu_{1.8}S$. It is likely, therefore, that future investigations of the type reported here, should consider replacing the Cu variable term wt% with free Cu wt%. This has not been tried for the present study because of the unavailability of quantitative information on the free Cu content of the PV steels utilized for this study.

4.2.3.2 Commentary on Evaluation of Trend Curve Model Equations and Variable Effects

With reference to Sections 3.4 and 4.2.1, the discussion and definition of terms and equations, and the results obtained from the EQ.ALL Code printout (Tables HEDL-23a through -23d), some further commentary is needed about the use and interpretation of the R-residual results for Eqs. (1M) through (7M), with and without corrections for flux-spectral, flux-level, Cu, and/or Ni-fluence dependencies.

For the PSF Code R weld results, the Table HEDL-23b "R" values for the weld Eqs. (1M), (2M), (5M), and (7M) are all high, in the range of ~3.3 to ~7.6. This shows that the application of the Eqs. (6a) and (7) flux-level and Ni-fluence correction factors produce a significant improvement in the correlation (lowering of the standard deviation of the fit) for the five PSF data points (J = 1 to 5) for four of the five weld trend curve equations. It is apparent,

however, that the Eq. (4M) trend curve model does not provide a good representation for this particular five data point subset, which is being used to represent a plant-specific set of surveillance data obtained from five idealized surveillance capsule locations, i.e., at the SSC-1, SSC-2, 0-T, 1/4-T, and 1/2-T positions.

As discussed in Section 3.4, this is simply a reflection of the fact that a different set of constants for Eq. (6a) should be used that provides different flux-level correction factors. To handle this problem, a separate equation [Eq. (6b)] was derived for use with Eq. (4M), with the requirement that a re-normalization of the magnitude of the chemistry term could be required, in general, or when the Ni wt% was near or outside the 0.54 wt% to 0.70 wt% Ni range.

The importance of the form of the trend curve model equation and use of different exposure parameters is further illustrated by observing that there is little to be gained in the use of Eq. (1M) over (2M); i.e, the use of dpa instead of fast fluence (E > 1 MeV) as the exposure parameter. The reason for this is that the R values are about the same (in the 6.4 to 6.9 range for Eq. (1M) to (1M) and (2M) to (2M); and in the 1.4 to 1.7 range for Eq. (2) to (1). This is not the case, however, when Eqs. (5M) and (7M) are used to represent these five data points. Here, as with Eqs. (1M) and (2M), the R values are high ($\sim$7.6 and $\sim$3.3) for Eqs. (5M) and (7M), respectively, after correcting for flux-level and Ni-fluence effects. As can be seen, a further and still significant improvement in correlation is achieved by changing to an exposure parameter that accounts for spectral (dpa) as well as helium production from boron and steel. The resulting R values for making this change from the Eq. (5M) fast fluence (E > 1 MeV) to the Eq. (7M) dpa plus helium production exposure parameters are $\sim$5 and $\sim$10, respectively, with and without corrections for flux-level and Ni-fluence dependencies. Based on the use of the Eqs. (5M) and (7M) trend curve models, therefore, a significant data correlation improvement appears to have been achieved by including 1) neutron spectral (dpa), 2) helium production, 3) flux-level, and 4) Ni-fluence effects. On the other hand, if Eqs. (1M) and (2M) are used, little, if any significant improvement is apparent by including just the dpa instead of the fluence (E > 1.0 MeV) exposure parameter.

The significance of the above discussion is that a code, such as EQ.ALL, can be used in a very systematic manner to study and make individual corrections for different variable effects for plant-specific trend curves and data sets. The result is that correlations, previously thought impossible, may be extracted from some of the existing PWR and BWR surveillance capsule physics-dosimetry-metallurgy data bases. More will be said on this subject in Section 4.3.

With these thoughts in mind, the EQ.ALL procedures and steps for applying a flux-level dependency for the power law exponent N for Eq. (4M) to calculate re-normalized flux-level and/or Ni-fluence correction factors for the seven Table HEDL-21 trend curve equations is presented in Section 4.3.2, after first discussing the flux-level effect copper dependency in Section 4.3.1.

4.3 Results of Present Study

4.3.1 Flux-Level Effect Copper Dependency

As discussed in Section 4.2.3.1, Cu groupings of selected subsets of the PWR and BWR weld and plate material data bases (that had small ranges of Cu wt%) were used for evaluating a possible flux-level Cu dependency. The upper and lower bounds of these ranges are identified by the vertical bars in Figures HEDL-25 and -26. The R-residual test is defined by Eq. (11) and was discussed in Section 4.2.1. Using Eqs. (1M), (6a), and (7), the R values for the data subsets are plotted in Figures HEDL-25 and -26 versus Cu wt% for higher Ni (0.49% wt% to 0.75 wt%) and lower Ni (0.06 wt% to 0.30 wt%), respectively.

The results of linear least-squares straightline fits to the two sets of data are shown by the solid lines. The number of data points (surveillance capsule charpy shift values) used in each Cu subset is shown by the number in parentheses next to each plotted point.

Concern was expressed in Section 4.2.3.1 about the part that sulfur could play in removing Cu from solution. Because of this concern, as well as the effect of phosphorus in low Cu steels, it was assumed that a fraction of the Cu would be tied-up as $Cu_{1.8}S$ particles, and, therefore would not be available to contribute to the steel embrittlement process. Data points that fell below the 0.1 wt% Cu vertical dashed lines in Figures HEDL-25 and -26, therefore, were not used for the least-squares straightline fits.

For the existing PWR and BWR weld, plate, and forging surveillance capsule physics-dosimetry-metallurgy data base, and for the higher-Ni steels, the application of the Eqs. (6a) and (7) flux-level and Ni-fluence correction factors with Eq. (1M) provided a strong correlation that supports a Cu-dependent flux-level effect. On the other hand, for the lower-Ni steels, a significant correlation was not found.

These Cu-flux-level dependency results are sensitive to the form of the trend curve model equation used [Eqs. (1M) through (7M)] and will have some variation with the use of different data bases and model equations. For example, the R-residual test results using the B&W Eq. (4M), with the Eq. (6b) flux-level correction factor are plotted as "Xs" in Figure HEDL-25. Results for four data subset groupings of Cu [0.21 to 0.23; 0.25 to 0.28; 0.30 to 0.33; and 0.35 to 0.36 wt%] taken from the B&W 25-point weld data base are shown. The trend of improved correlation (below ~0.25 wt% Cu) with decreasing Cu concentration is apparent.

The EQ.ALL Code results for the lowest and highest Cu groupings are presented in Tables HEDL-27 and -28, respectively. The Eq. (6b) CF values range from a low of 0.893 to a high of 1.31 for the 0.21 to 0.23 Cu grouping; and from a low of 0.887 to a high of 1.17 for the 0.35 to 0.36 Cu grouping.

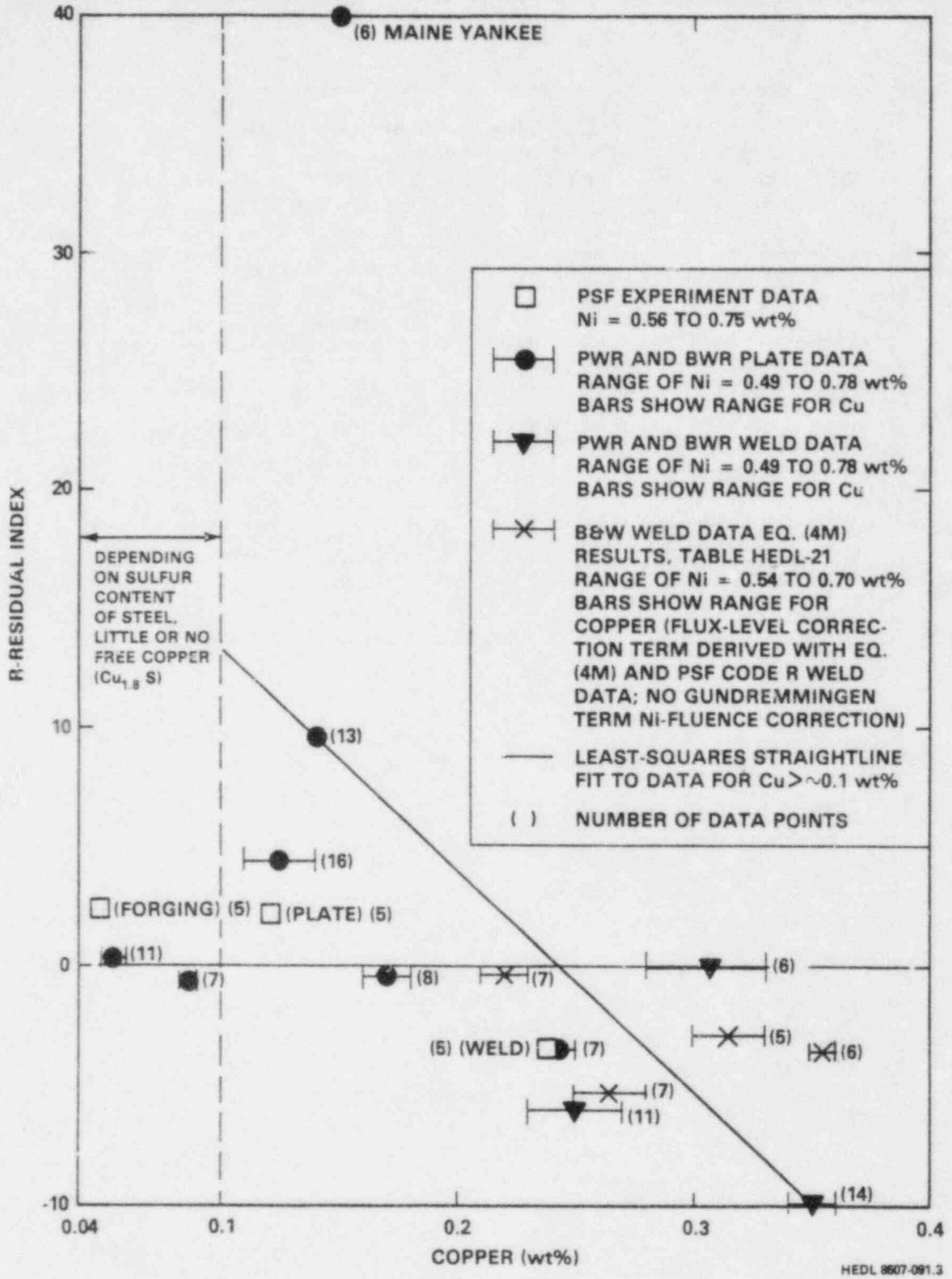

FIGURE HEDL-25. Residual (R) Versus wt% Copper for Steels with Higher Nickel (0.49 wt% to 0.75 wt%).

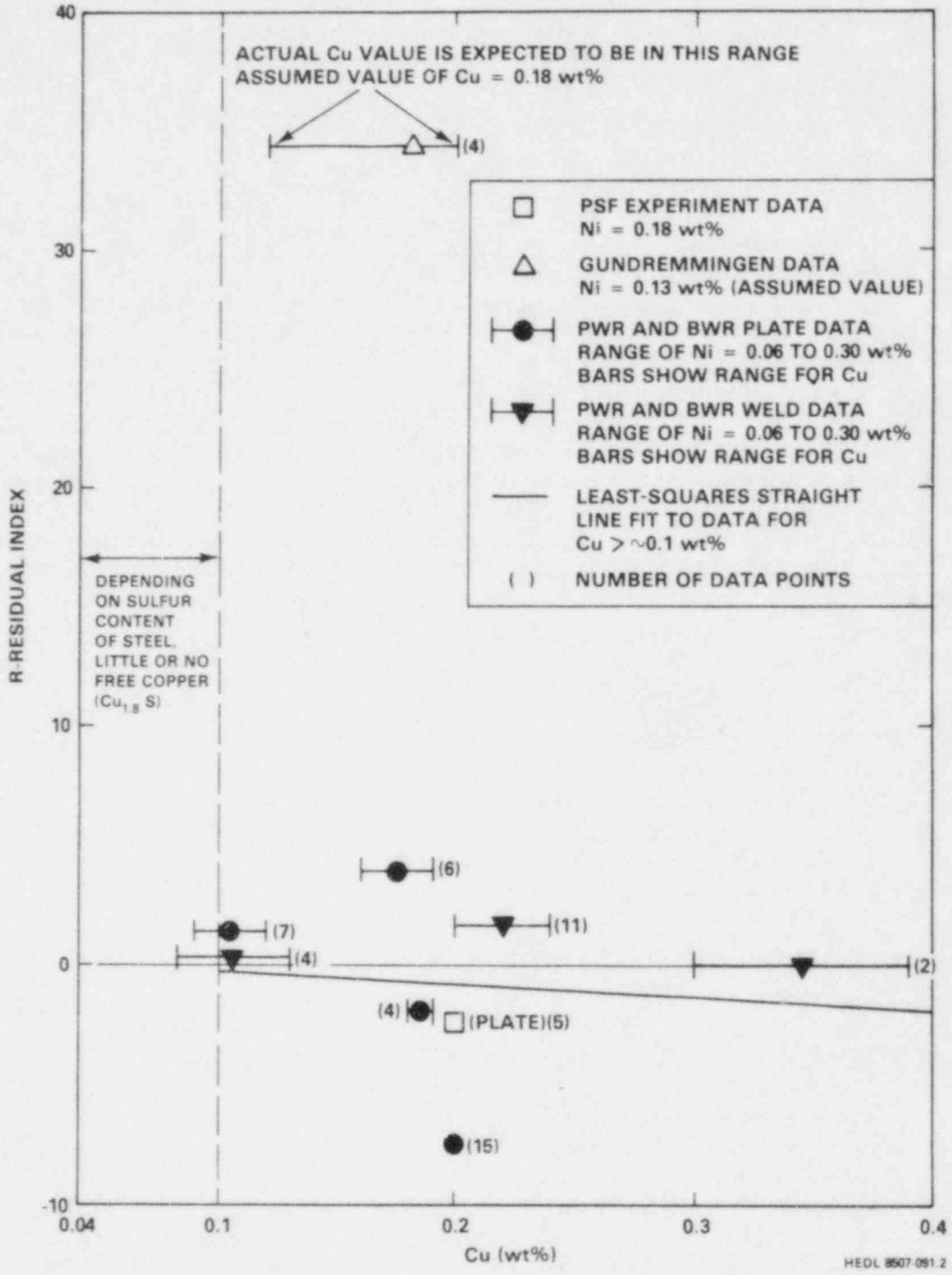

FIGURE HEDL-26. Residual (R) Versus wt% Copper for Steels with Lower Nickel (0.06 wt% to 0.30 wt%).

4.3.2 Development and Testing Using the PSF Experiment Physics-Dosimetry-Metallurgy Data Base

4.3.2.1 PSF Testing Results

4.3.2.1.1 Analytical Procedures and Equations

Using the EQ.ALL Code; the B&W trend curve model Eq. (4M), and the PSF Code R weld derived flux-level correction factor Eq. (6b); and a PSF Experiment-derived linear equation, Eq. (16), to represent the flux-level Cu dependency of the Eq (4M) power law exponent N value; a set of analytical procedures and equations were established and tested using the PSF Experiment Physics-dosimetry-metallurgy data base.

For this study it was assumed that the only significant independent variables are Ni and Cu chemistry terms, fluence (E > 1 MeV), flux level, and flux-level Cu dependency. For other studies and future work, however, the use of the dpa exposure parameter term is essential, particularly when higher values of the exponent N (~0.5 to 0.9) are encountered, and because of the need to predict Charpy shifts from the inside to the outside surface of the pressure vessel, as well as for the evaluation of the effect of the neutron exposure on the embrittlement of ex-vessel support structures. Also, the most appropriate chemistry dependence of the flux-level effect still remains to be established and accounted for in the data correlation and subsequent application steps. In addition, thermal neutron-induced helium production and gamma-heating effects must be addressed, and these effects need to be quantified.

With this analytical procedure, the Charpy shift C/E ratio is represented by the relationship

$$(C/E)_J = [Eq.(4M)]\cdot(CF_J)/(CV_J\cdot NF) \qquad (15)$$

where the analytical form for Eq. (4M) is given in Table HEDL-21. Eq. (15) is also used with Table HEDL-21 Equations (1M), (2M), (3M), (5M), and (7M), but with NF set equal to unity. In Eq. (15), Cv_J is the measured Charpy shift value for the J^{th} data point; and CF_J, as defined by Eq. (6b), but used here, is the EQ.ALL derived value of the flux-level correction factor for the J^{th} data point for a plant-specific surveillance capsule set of data, J = 1 .... N. NF is a re-normalization factor, the average value of the Eq. (15) calculated C/E ratios for the input data set, without correction for flux-level; i.e., initially all the CF_J values are set equal to unity to obtain the value of NF. NF simply re-normalizes the B&W Eq. (4M) results to account for any initial plant-specific data set bias in the predicted versus measured Charpy shifts using this equation; for applications both within and outside the range of Cu and Ni concentrations found in the B&W 177-FA plant weld data base. It also

removes other C/E ratio bias from inadequacies of Eq. (4M) to properly model other variable effects, such as the actual fluence dependence of the power law value of 0.326; this is discussed in Section 4.3.2.1.3.

4.3.2.1.2 PSF Testing Results - Using Equation (15)

The results of the testing of these EQ.ALL Code analytical procedures using the PSF Experiment data base is considered next. The results are presented in Tables HEDL-29 through -34 for two weld materials [A533B-weld, Code R; A533B weld, Code EC], two plate materials [A533B Plate (HSST), Code 3PU; A302B Plate (ASTM), Code F23], and two forgings materials [A508 Forging, Code K; A508 Forging, Code MO]. As before, the "Table HEDL-XXa and -XXb" designations signify results with and without corrections for flux-level effects. For all "EQ.4" [Eq. (4M)] results presented in these tables, the C/E ratio results are based on the use of Eq. (15).

The things to be compared in these tables are: 1) the "EQ.4" results with the EQ.1, EQ.2, EQ.5, and EQ.7 results for weld materials and 2) the "EQ.4" results with EQ.3 and EQ.6 for plate and forging materials. It is important to look at the relative R-residual values and standard deviations of the fits for all PSF weld, plate, and forgings. When this is done, it is found that the single Eq. (15) and EQ.ALL Code results are equally as good or better for most materials. Furthermore, even though there are specific exceptions, there appears to be an observed overall systematic decrease in the C/E ratios for results between the SSC, 0-T, 1/4-T, and 1/2-T locations, consistent with the Code R weld results and the variations in flux level between the 30 data points.

Because of the much smaller magnitude (~200°F) of the observed measured shifts for the Code EC, 3PU, F23, K, and MO materials, there is a much higher absolute and relative uncertainty associated with these results as compared with the Code R weld material, with its measured shifts in the 400 to 520°F range. For this reason, it is believed that, at least, the Code R data are reliable and that the Eq. (4M) and EQ.ALL-derived flux-level correction factor Eq. (6b) can be used, with reasonable confidence, to predict and quantify plant-specific relative surveillance capsule to surveillance capsule flux-level correction factors for this as well as other materials that show an increase in embrittlement with a decrease in flux-level.

4.3.2.1.3 PSF Testing Results - Using Equations (15) and (16)

As discussed in Section 4.3.1, for the existing PWR and BWR weld, plate, and forging surveillance capsule physics-dosimetry-metallurgy data base and for the higher-Ni steels, the application of the Eq. (6a) and (7) correction factors provided a strong correlation that supports a Cu-dependent flux-level effect, Figure HEDL-25. Such a dependency was recently suggested by Guthrie (Gu85). Figure HEDL-27 shows this dependency for the PSF-SSC data base used for the present study. For the more limited data for the lower-Ni steels, a

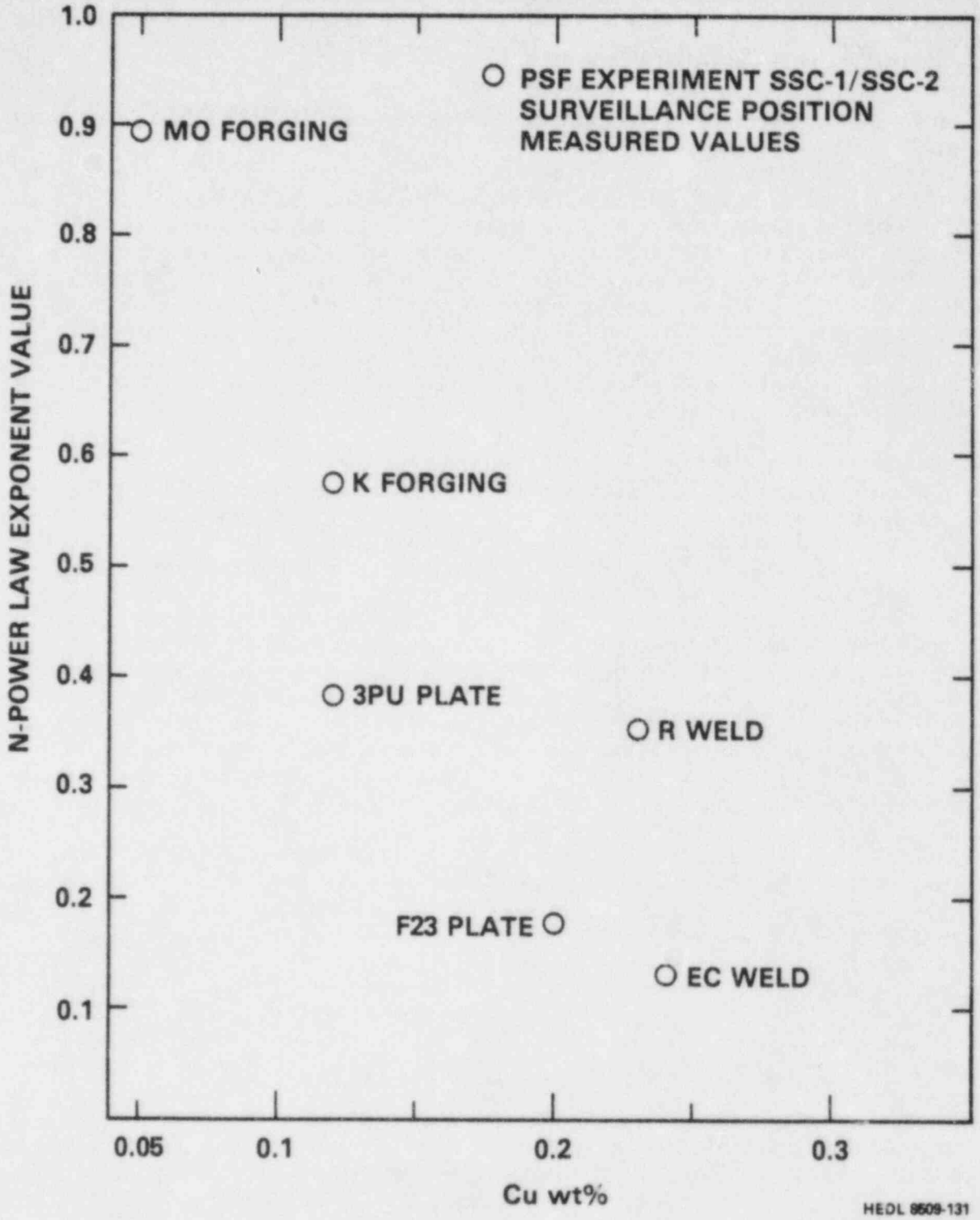

FIGURE HEDL-27. PSF-Measured Values of N Versus Copper wt% for Forging, Plate, and Weld Materials for the SSC Surveillance Capsule Position.

significant correlation was not found, Figure HEDL-26. It must be emphasized, however, that these results and conclusions are sensitive to the form of the trend curve model equation used, and they will change with the use of different model equations.

Based on these results, a simple and preliminary linear Cu chemistry dependency for the power law exponent for the B&W EQ. (4M) was established and tested using the PSF experiment data base. The result was an overall reduction of the standard deviation (SD) of fits for the PSF weld, Code R; plates, Codes 3PU and F23; forgings, Codes K and MO pressure vessel steels; i.e., 9.2 to 4.2°F, 9.4 to 8.2°F, 36.0 to 25.5°F; and 20.8 to 17.4°F, and 15.0 to 10.6°F, respectively. The Code EC weld SD did not decrease, but showed a small increase, from 25.5 to 26.2°F. The R-residual values were 852, -3.7, 20.0, -0.9, 2.6, and -2.8, respectively. Thus, only half of the six PSF materials showed a significant improvement with the use of Eqs. (6b) and (16). This suggests that the actual material and chemistry dependency of N is much more complex than that represented by just a linear function of Cu, Eq. (16), see Section HEDL-E.

For the above results, the power law exponent N (used with the B&W Eq. (4M) and that was selected on the basis of Guthrie's study of the PSF Experiment results) was

$$N = 0.7170 - 1.7\ (\text{Cu wt\%}). \qquad (16)$$

The value of -1.7, was arbitrarily selected on the low side, between the values of -3.9 and -1.1, as reported by Guthrie for the PSF SSC and SPV wall block locations, see Section 4.2.2. The detailed results of the use of Eq. (16) with Eq. (15) are presented in Tables HEDL-35 through -40 for the two welds, two plates, and two forging materials. The things to be compared in these tables are the same as those discussed previously for the EQ.ALL Code results for Eq. (15).

The important result here is that the introduction of a variable term for N, Eq. (16), in Eq. (15) to replace the fixed power law exponent value of 0.326 has produced some very significant reductions in the standard deviations of the fits for the PSF Experiment data base.

For applications to PWR and BWR plant-specific sets of data, Section 4.3.3, no use of the PSF-derived Eq. (16) linear Cu dependency of N was made. This was not done because much more study of the PSF results would be needed to define the combined effects of flux-spectra, flux-level, and chemistry in determining the value of N. It seemed unreasonable, on the basis of Tables HEDL-35 through -40 R-residual test results, and the Grant-Earp and Heller-Lowe studies that the chemistry term could be as simple as that given by Eq. (16). This conclusion is supported by the results of Simon's study, Section HEDL-E.

4.3.2.2 Implications from PSF Test Results

Using results from Tables HEDL-29 through -40, another observation of interest is that the relative flux-level multiplicative correction factors, in going

from the SSC-1 or SSC-2 to the PV surface, 1/4-T, and 1/2-T locations are approximately 1.11, 1.21, and 1.40, respectively. This would suggest that the relative correction factor between a surveillance capsule and the 3/4-T location of a pressure vessel could be up to about 1.5 to 2.0; i.e., the application of a measured and correlated plant-specific set of surveillance capsule Charpy shift data points for projections to the 3/4-T location could require an increase in the predicted Charpy shift value up to about ∿1.5, depending on the material and its chemistry. For the surface and 1/4-T locations, the corresponding correction factors could be up to ∿1.1 and 1.2, respectively.

For PV support structure embrittlement projections based on low-temperature test reactor results, the use of even higher correction factors, in the range up to 2 or higher, might be required for some PV steels, again depending on the material and its chemistry.

In conclusion, the application of new data analysis procedures for determining and applying relative flux-level multiplicative correction factors for PV weld, plate and forging materials has been tested using the 30-point PSF Experiment physics-dosimetry-metallurgy data base. Results of this study support the existence of a significant flux-level effect for PV and support structure steel embrittlement. From these and the results of Simon's study, Section HEDL-E, it is found that a PV steel may show a decrease, an increase, or no change in the measure Charpy Shift with changes in flux level.

The application of these new procedures for selected sets of PWR and BWR surveillance capsule results is considered in Section 4.3.3.

4.3.3 PWR and BWR Applications - Using Equations (15) and (6b)

The analysis procedures developed and tested in Section 4.3.2 will now be applied to the study and evaluation of several PWR and one BWR plant specific surveillance capsule data sets. The plants studied are: 1) Maine Yankee (weld), 2) Palisades (weld and plate), 3) Point Beach 1 (weld), 4) Point Beach 2 (weld), 5) Indian Point 2 and 3 (weld), 6) Nine Mile Point 1 (plate) (BWR).

The EQ.ALL results of the application of the Eq. (15), (6b), and (4M) trend curve model are given in Tables HEDL-41 through -46. The things to be compared in these tables are the same as those discussed in Section 4.3.2 and need not be repeated here.

As with the PSF Experiment results of Section 4.3.2, and considering the much larger uncertainties associated with these PWR and BWR surveillance capsule data, there is an observed overall very good consistency for most of the Tables HEDL-41 to -46 results. This supports the existence of a significant, and previously unobserved, flux-level effect for PWR and BWR surveillance capsule plant-specific data bases. More detailed discussions and comments about these EQ.ALL results, for the seven power plants, are presented in the following subsections.

4.3.3.1 Maine Yankee (Weld) Results

The standard deviation of the fit (SD) improves significantly for EQ.4 and worsens for EQ.1, EQ.2, EQ.5, and EQ.7 with the flux-level corrections, see Table HEDL-41. The relative difference in flux-level correction factors (CF) between the accelerated (AC) and wall (W) capsule locations is ∿1.8. Assuming that EQ.4 results are qualitatively correct, the more generic EQ.1, EQ.2, EQ.5, and EQ.7 trend curve models appear to have masked a very significant and previously unobserved power reactor data base flux-level effect. It is important to understand that the EQ.1, EQ.2, EQ.5, and EQ.7 models were originally established with these three MY data points, as well as a number of other power reactor data points, with a wide range of flux levels from about 0.3 to 9 x 10^{11} n/cm² s. It is not surprising, therefore, that the starting C/E ratios (without correction for flux level differences) are very near unity. On the basis of the study of other power reactor data points with a wide range of flux levels from about 1 to 70 x 10^{11} n/cm²•s), it is now believed that these more generic trend curve models have erroneously forced the correlation of the flux-level dependency to appear as part of the chemistry and fluence dependencies. It is also apparent that the Code R derived flux-level dependency [Equations (15) and (6b)] produces an over-correction for the MY weld material.

4.3.3.2 Palisades (Weld) Results

The (SD) of the fit improves significantly for EQ.4 and worsens for the other weld equations with flux-level corrections, see Table HEDL-42. The relative difference in flux-level CFs between the AC and wall capsule locations is ∿1.7. These results are, therefore, essentially the same as were found for Maine Yankee.

Also for the Code R material used to establish the Eq. (6b) flux-level correction factors for Eq. (4M), its chemistry (0.23% Cu, 1.58% Ni) is closer to the PAL Chemistry (0.24% Cu, 0.95% Ni) than it is to the MY chemistry (0.36% Cu, 0.78% Ni). Consequently, the PAL correlation could be better, which it is, than that obtained for MY. It is important to note here, however, that the Code R derived Eq. (6b) cannot be expected to properly represent the flux-level dependency for all material and chemistry variations, see Section HEDL-E.

It is also now believed, that at least a large part of the previously identified thermal neutron-effect (Mc84h) is associated more with flux-level and temperature variations than with the production of helium in PV steels. This conclusion is based on the comparison of the R-residual test results of Table HEDL-42b for EQ 5 to EQ. 7 "without flux-level correction (R = 11.7)" and "and with flux-level correction (R = 0.055)". What is observed here is that these particular Palisades plant-specific results can be correlated equally well with a flux-level correction factor (R = 7.9) or with a thermal neutron correction factor (R = 11.7).

4.3.3.3 Point Beach 1 (Weld) Results

The (SD) of the fit improves significantly for all weld EQs. with flux-level corrections, see Table HEDL-43. The "R and S" capsules have the largest relative difference in flux level CFs, a value of ~1.16 for a factor of ~2 change in flux-level. Of particular interest here is the observation that the so called "saturation" of damage previously suggested (St79a) by the Table HEDL-43a uncorrected results could be just as easily explained and associated with a flux-level effect; i.e., the capsule "S" measured Charpy shift value of 165°F is about 16% higher than it would have been if the capsule had been irradiated in the factor of two higher flux environment of capsule R. If this proves to be true, then much more care must be taken in the determination of the exact placement of surveillance capsules and the measurement of the local flux-level and neutron field perturbations.

4.3.3.4 Point Beach 2 (Weld) Results

The (SD) of the fit is lowest for EQ.4, without and with, corrections for a flux level effect, see Table HEDL-44. However, none of the five weld equations, EQ.1, EQ.2, EQ.4, EQ.5, and EQ.7, provide a clear cut advantage or disadvantage for use in improving the correlation of this particular PWR plant-specific set of Charpy shift data. This suggests that the Code R, Equation (6b), flux-level dependency is not correct for the Point Beach 2 weld material.

4.3.3.5 Indian Point 2 and 3 (Weld) Results

The (SD) of the fit improves significantly for all weld EQs with flux-level corrections, see Table HEDL-45. The relative difference in flux level CFs, a value of 1.17, is consistent with similar values found for MY, Palisades, and PB1.

4.3.3.6 Palisades, Indian Point 3, and Nine Mile Point 1 (BWR) (Plate) Results

A four-point data set material-specific grouping with about the same Cu (medium copper) and Ni concentrations (high nickel) was selected to evaluate a recent, and very low flux-level BWR (Nine Mile Point 1) (plate) wall capsule result with a rather high and unexpected measured Charpy shift. The results are shown in Table HEDL-46. The standard deviation of the fit improved rather dramatically for the EQ.4 flux-level corrected results, while it worsened, somewhat for the more generic plate equations, EQ.3 and EQ.6.

The relative difference in flux-level CFs between the BWR (wall) and Palisades (AC) surveillance capsules is ~3.7, an extremely high value. What is interesting here, is that the Eq. (6b) derived correction factor of 1.86, Table HEDL-46b produces a corrected C/E ratio value of 1.06 as compared with the uncorrected value of 0.574 for EQ.4. Certainly, this almost exact correlation is partly fortuitous, since the fluence value is so low (0.047×10^{19} n/cm^2) for this BWR wall capsule data point compared with that of the PSF Experiment (~1 to 6 $\times 10^{19}$ n/cm^2). Further, it is known that the actual BWR (wall) capsule temperature could be as much as ~40°F below 550°F, which was the irradiation temperature for the PSF Experiment Code R material.

It might also be noted that although the Ni contents are quite different, the BWR wall data point material Cu content is about the same as that of the Code R material.

4.4 Conclusions

The PWR and BWR plant-specific surveillance capsule results of Sections 4.3.3, together with the PSF results of Section 4.3.2, support the existence of a material dependent flux-level effect for pressure vessel and support structure steels. It is expected that the chemistry part of this dependency will include terms for Cu, Ni, and other minor alloying constituents of PV steels; further, different microstructural dependencies will exist for forgings, plates, and welds.

It is concluded that the existing and more generic trend curve model equations have, inadvertently, masked the existence of this very real and important flux-level effect. In order to quantify this effect, however, it will be necessary to quantify and separate out the effects of other environmental variables; namely: Spectrum, temperature, and the contribution of thermal-intermediate-fast neutrons to displacement damage and the production of helium. Implicit in the above is the need to also separate out the effects of the non-environmental variables associated with the microstructure, chemistry, time-at-temperature, annealing, etc, as discussed in Section HEDL-A.

As just indicated, the existing trend curves do not account for the observed flux-level effect and there may be other physical processes and/or damage mechanisms which contribute to the damage of pressure vessel steels under certain conditions; e.g., phosphorus in the presence of low copper concentrations, nitrogen impact on copper precipitation, etc. Any agreement between measured data and trend curve predictions, which do not adequately represent the important microstructural damage processes could be fortuitous. The exception to such fortuitous agreememt could be limited to certain variable ranges where some processes may be of less relative importance.

As stated in Section HEDL-A: "The existence of a flux-level effect has important implications for the U.S. commercial nuclear power industry, since accelerated locations have almost invariably been used in PV surveillance programs. These accelerated PV surveillance capsules have provided lead factors

that have been applied to obtain projections of PV embrittlement. In fact, accelerated PV capsules comprise the largest existing data base for trend curve analyses. Consequently, it is clear that a flux-level effect would imply that some correction would be necessary in the application and interpretation of lead factors. Otherwise, the application of lead factors could not always ensure a conservative extrapolation. At the same time, it is apparent that any reduction in embrittlement afforded from low leakage cores, which are now being adopted in some U.S. power plants, must be quantified in terms of a flux-level effect, lest the predicted gain be under-or over-estimated."

An independent physically based theoretical study on "Damage Rate and Spectrum Effects in Ferritic Steel ΔNDTT Data" has been completed and the results are reported by R. L. Simons in Section HEDL-E. The results of Simons' study support the conclusions and are consistent with those of the present semi-empirical investigation.

Additional support for the validity of the conclusions of this, Simons' Section, and Gold and McElroys' Section HEDL-A comes from information presented by Serpan (Se85) and Hawthorne (Ha85) at the 13th Water Reactor Safety Research Information Meeting held at NBS in October 1985. Serpan states: "Increasing evidence for a dose rate effect has come from MEA this year, in the form of results from experiments that demonstrate greater embrittlement at low fluxes than previously anticipated (Ha85). This evidence has been so pronounced in reactor surveillance data that Revision 2 of Reg. Guide 1.99 on Radiation Damage to Reactor Vessel Materials has dropped the test reactor data and now includes only power reactor data which has the low flux-higher embrittlement characteristic."

It is important to understand that Serpan's statement is only partially correct, since it applies only to selected PV steels. That is, the correctness of the statement is dependent on a number of variables, including material properties, neutron exposure, and flux-level. This is demonstrated by the combined results of Sections HEDL-E and -F where it is found that a PV steel may show a decrease, an increase or no change in the measured Charpy Shift with changes in flux level.

Expected Future Accomplishments

Appropriate parts of this work will be extended and incorporated in PSF Experiment physics-dosimetry-metallurgy NUREG reports.

TABLE HEDL-23a

PSF RESULTS WITHOUT CORRECTION FOR FLUX-LEVEL
AND NICKEL-FLUENCE EFFECTS USING
EQUATION (1M) DERIVED EQUATIONS (6a) AND (7)

*** RESULTS FOR SEVEN EQUATIONS WITH NO CORRECTIONS FOR FLUX LEVEL AND NI-FLUENCE EFFECTS ***

CALCULATE TO MEASURED (C/E) CHARPY SHIFT(DEG.F) VALUES FOR SELECTED TREND CURVE EQNS.

J	CAPSULE		EQ.1	EQ.2	EQ.3	EQ.4	EQ.5	EQ.6	EQ.7	FLU.	FLUX	T/F	Cv(F)	CU%	NI%	CF
1	SSC1	R	1.04	1.06	.609	1.71	.874	.480	.970	2.52	65.1	.68	400	.23	1.58	.927
2	SSC2	R	.922	.932	.524	1.68	.768	.455	.862	5.31	66.7	.65	520	.23	1.58	1.08
3	OT	R	.888	.895	.507	1.53	.732	.420	.935	3.85	7.41	4.31	515	.23	1.58	1.24
4	1/4T	R	.910	.896	.514	1.42	.739	.401	.829	2.19	4.22	.53	461	.23	1.58	1.17
5	1/2T	R	.869	.811	.472	1.21	.700	.354	.769	1.1	2.12	.16	430	.23	1.58	1.12

MEASURED - CALCULATED (E-C) CHARPY SHIFT(DEG.F) VALUES FOR SELECTED TREND CURVE EQNS.

J	CAPSULE		EQ.1	EQ.2	EQ.3	EQ.4	EQ.5	EQ.6	EQ.7	FLU.	FLUX	T/F	Cv(F)	CU%	NI%	CF
1	SSC1	R	-19.	-25.	156.	-286	50.3	207.	11.8	2.52	65.1	.68	400	.23	1.58	.927
2	SSC2	R	40.5	34.8	247.	-356	120.	283.	71.2	5.31	66.7	.65	520	.23	1.58	1.08
3	OT	R	57.4	53.9	253.	-273	137.	298.	33.1	3.85	7.41	4.31	515	.23	1.58	1.24
4	1/4T	R	41.1	47.9	223.	-194	120.	276.	78.3	2.19	4.22	.53	461	.23	1.58	1.17
5	1/2T	R	55.9	81.2	226.	-92.	128.	277.	98.9	1.1	2.12	.16	430	.23	1.58	1.12

AVE VALUE OF COMBINED ((SUM L3)/N;L3=L4*L5) CORRECTION FACTOR FOR ALL CAPSULES=1.478
CORRECTION FACTOR'S AVERAGE VALUES: L4 = 1.184 L5 = 1.259 L6 = 1.114

SUM OF SQUARES (E-C) FOR EACH OF THE SEVEN EQUATIONS =
EQ1= 10163.483 EQ2= 13685.679 EQ3= 251413.196 EQ4= 330616.541 EQ5= 66918.388

EQ6= 365646.793 EQ7= 22254.58

STANDARD DEVIATION OF FIT FOR EACH OF THE SEVEN EQUATIONS =
EQ1= 45.085 EQ2= 52.318 EQ3= 224.238 EQ4= 257.145 EQ5= 115.688 EQ6= 270.424 EQ7= 66.715

TABLE HEDL-23b

PSF RESULTS WITH CORRECTION FOR FLUX-LEVEL
AND NICKEL-FLUENCE EFFECTS USING
EQUATION (1M) DERIVED EQUATIONS (6a) AND (7)

**** RESULTS FOR SEVEN EQUATIONS WITH CORRECTIONS FOR FLUX LEVEL AND NI-FLUENCE EFFECTS ****

CALCULATE TO MEASURED (C/E) CHARPY SHIFT(DEG.F) VALUES FOR SELECTED TREND CURVE EQNS.

J	CAPSULE		EQ.1	EQ.2	EQ.3	EQ.4	EQ.5	EQ.6	EQ.7	FLU.	FLUX	T/F	Cu(F)	CU%	NI%	CF
1	SSC1	R	.973	.986	.565	1.59	.810	.445	.899	2.52	65.1	.68	400	.23	1.58	.927
2	SSC2	R	1.00	1.01	.569	1.83	.835	.494	.937	5.31	66.7	.65	520	.23	1.58	1.08
3	QT	R	1.10	1.11	.634	1.91	.915	.525	1.16	3.85	7.41	4.31	515	.23	1.58	1.24
4	1/4T	R	1.07	1.05	.606	1.67	.870	.471	.976	2.19	4.22	.53	461	.23	1.58	1.17
5	1/2T	R	.982	.915	.533	1.37	.791	.400	.869	1.1	2.12	.16	430	.23	1.58	1.12

MEASURED - CALCULATED (E-C) CHARPY SHIFT(DEG.F) VALUES FOR SELECTED TREND CURVE EQNS.

J	CAPSULE		EQ.1	EQ.2	EQ.3	EQ.4	EQ.5	EQ.6	EQ.7	FLU.	FLUX	T/F	Cu(F)	CU%	NI%	CF
1	SSC1	R	10.6	5.38	173.	-236	75.7	221.	40.0	2.52	65.1	.68	400	.23	1.58	.927
2	SSC2	R	-.84	-6.9	223.	-432	85.6	262.	32.5	5.31	66.7	.65	520	.23	1.58	1.08
3	QT	R	-56.	-60.	188.	-470	43.5	244.	-66.	3.85	7.41	4.31	515	.23	1.58	1.24
4	1/4T	R	-33.	-25.	181.	-310	59.7	243.	10.7	2.19	4.22	.53	461	.23	1.58	1.17
5	1/2T	R	7.51	36.1	200.	-160	89.8	257.	56.1	1.1	2.12	.16	430	.23	1.58	1.12

AVE VALUE OF COMBINED ((SUM L3)/N;L3=L4+L5) CORRECTION FACTOR FOR ALL CAPSULES=1.478
CORRECTION FACTOR'S AVERAGE VALUES: L4 = 1.184 L5 = 1.25? L6 = 1.114

SUM OF SQUARES (E-C) FOR EACH OF SEVEN EQUATIONS =
EQ1= 4465.838 EQ2= 5730.098 EQ3= 189119.773 EQ4= 586234.897 EQ5= 26612.764

EQ6= 303631.876 EQ7= 13486.703

STANDARD DEVIATION OF FIT FOR EACH OF SEVEN EQUATIONS =
EQ1= 29.886 EQ2= 33.853 EQ3= 194.484 EQ4= 342.417 EQ5= 72.956 EQ6= 246.427 EQ7= 51.936

THE R VALUES FOR EACH OF SEVEN EQUATIONS =

FOR I=1 TO 7 : EQN(I)*WITHOUT TO EQN(I)*WITH FLUX LEVEL & NI - FLUENCE CORRECTIONS =
EQ1= 6.379 EQ2= 6.942 EQ3= 1.647 EQ4= -2.18 EQ5= 7.573 EQ6= 1.021 EQ7= 3.251

THE R VALUES FOR EQN.2 TO EQN.1 AND FOR EQN.5 TO EQN.7 =

NO FLUX LEVEL & NI-FLUENCE CORRECTIONS: EQ7 TO EQ1= 1.733
WITH FLUX LEVEL & NI-FLUENCE CORRECTIONS: EQ2 TO EQ1= 1.415
NO FLUX LEVEL & NI-FLUENCE CORRECTIONS: EQ5 TO EQ7= 10.035
WITH FLUX LEVEL & NI-FLUENCE CORRECTIONS: EQ5 TO EQ7= 4.666

TABLE HEDL-23c

PSF RESULTS WITHOUT CORRECTION FOR FLUX-LEVEL USING EQUATION (4M) DERIVED EQUATION (6b)

********** RESULTS FOR SEVEN EQUATIONS WITH NO CORRECTION FOR FLUX LEVEL EFFECT **********

CALCULATE TO MEASURED (C/E) CHARPY SHIFT(DEG.F) VALUES FOR SELECTED TREND CURVE EQNS.

J	CAPSULE		EQ.1	EQ.2	EQ.3	EQ.4	EQ.5	EQ.6	EQ.7	FLU.	FLUX	T/F	Cv(F)	CU%	NI%	CF
1	SSC1	R	1.04	1.06	.609	1.15	.874	.480	.970	2.52	65.1	.68	400	.23	1.58	.872
2	SSC2	R	.922	.932	.524	1.13	.768	.455	.862	5.31	66.7	.65	520	.23	1.58	.874
3	OT	R	.888	.895	.507	1.02	.732	.420	.935	3.85	7.41	4.31	515	.23	1.58	.965
4	1/4T	R	.910	.896	.514	.954	.739	.401	.829	2.19	4.22	.53	461	.23	1.58	1.06
5	1/2T	R	.869	.811	.472	.815	.700	.354	.769	1.1	2.12	.16	430	.23	1.58	1.22

MEASURED - CALCULATED (E-C) CHARPY SHIFT(DEG.F) VALUES FOR SELECTED TREND CURVE EQNS.

J	CAPSULE		EQ.1	EQ.2	EQ.3	EQ.4	EQ.5	EQ.6	EQ.7	FLU.	FLUX	T/F	Cv(F)	CU%	NI%	CF
1	SSC1	R	-19.	-25.	156.	-61.	50.3	207.	11.8	2.52	65.1	.68	400	.23	1.58	.872
2	SSC2	R	40.5	34.8	247.	-69.	120.	283.	71.2	5.31	66.7	.65	520	.23	1.58	.874
3	OT	R	57.4	53.9	253.	-15.	137.	298.	33.1	3.85	7.41	4.31	515	.23	1.58	.965
4	1/4T	R	41.1	47.9	223.	20.7	120.	276.	78.3	2.19	4.22	.53	461	.23	1.58	1.06
5	1/2T	R	55.9	81.2	226.	79.2	128.	277.	98.9	1.1	2.12	.16	430	.23	1.58	1.22

AVE VALUE OF COMBINED ((SUM L3)/N;L3=L4*L5) CORRECTION FACTOR FOR ALL CAPSULES=.675
CORRECTION FACTOR'S AVERAGE VALUES: L4 = .675 L5 = 1 L6 = 1

SUM OF SQUARES (E-C) FOR EACH OF THE SEVEN EQUATIONS =
EQ1= 10163.483 EQ2= 13685.679 EQ3= 251413.196 EQ4= 15442.692 EQ5= 66918.388

EQ6= 36646.793 EQ7= 22254.58

STANDARD DEVIATION OF FIT FOR EACH OF THE SEVEN EQUATIONS =
EQ1= 45.085 EQ2= 52.318 EQ3= 224.238 EQ4= 55.575 EQ5= 115.688 EQ6= 270.424 EQ7= 66.715

TABLE HEDL-23d

PSF RESULTS WITH CORRECTION FOR FLUX-LEVEL USING EQUATION (4M) DERIVED EQUATION (6b)

********** RESULTS FOR SEVEN EQUATIONS WITH CORRECTION FOR FLUX LEVEL EFFECT **********

CALCULATE TO MEASURED (C/E) CHARPY SHIFT(DEG.F) VALUES FOR SELECTED TREND CURVE EQNS.

J	CAPSULE		EQ.1	EQ.2	EQ.3	EQ.4	EQ.5	EQ.6	EQ.7	FLU.	FLUX	T/F	Cu(F)	CU%	NI%	CF
1	SSC1	R	.916	.928	.532	1.00	.763	.419	.846	2.52	65.1	.68	400	.23	1.58	.872
2	SSC2	R	.806	.815	.458	.990	.672	.398	.754	5.31	66.7	.65	520	.23	1.58	.874
3	OT	R	.857	.864	.490	.993	.707	.405	.903	3.85	7.41	4.31	515	.23	1.58	.965
4	1/4T	R	.968	.952	.547	1.01	.786	.426	.882	2.19	4.22	.53	461	.23	1.58	1.06
5	1/2T	R	1.06	.992	.578	.998	.857	.433	.942	1.1	2.12	.16	430	.23	1.58	1.22

MEASURED - CALCULATED (E-C) CHARPY SHIFT(DEG.F) VALUES FOR SELECTED TREND CURVE EQNS.

J	CAPSULE		EQ.1	EQ.2	EQ.3	EQ.4	EQ.5	EQ.6	EQ.7	FLU.	FLUX	T/F	Cu(F)	CU%	NI%	CF
1	SSC1	R	33.5	28.5	187.	-2.4	94.7	232.	61.2	2.52	65.1	.68	400	.23	1.58	.872
2	SSC2	R	100.	95.8	281.	4.85	170.	312.	127.	5.31	66.7	.65	520	.23	1.58	.874
3	OT	R	73.2	69.8	262.	3.17	150.	305.	49.7	3.85	7.41	4.31	515	.23	1.58	.965
4	1/4T	R	14.6	21.7	208.	-7.0	98.4	264.	54.1	2.19	4.22	.53	461	.23	1.58	1.06
5	1/2T	R	-27.	3.21	181.	.723	61.4	243.	24.8	1.1	2.12	.16	430	.23	1.58	1.22

AVE VALUE OF COMBINED ((SUM L3)/N;L3=L4*L5) CORRECTION FACTOR FOR ALL CAPSULES=.675
CORRECTION FACTOR'S AVERAGE VALUES: L4 = .675 L5 = 1 L6 = 1

SUM OF SQUARES (E-C) FOR EACH OF SEVEN EQUATIONS =
EQ1= 17622.364 EQ2= 15357.68 EQ3= 259752.959 EQ4= 90.116 EQ5= 74158.686

EQ6= 374529.675 EQ7= 26061.1

STANDARD DEVIATION OF FIT FOR EACH OF SEVEN EQUATIONS =
EQ1= 59.367 EQ2= 55.421 EQ3= 227.927 EQ4= 4.245 EQ5= 121.786 EQ6= 273.689 EQ7= 72.196

THE R VALUES FOR EACH OF SEVEN EQUATIONS =

FOR I=1 TO 7 ; ********** EQN(I)*WITHOUT TO EQN(I)*WITH CORRECTION FOR FLUX LEVEL =
EQ1= -2.116 EQ2= -.544 EQ3= -.161 EQ4= 851.825 EQ5= -.488 EQ6= -.119 EQ7= -.73

THE R VALUES FOR EQN.2 TO EQN.1 AND FOR EQN.5 TO EQN.7 =

NO FLUX LEVEL CORRECTION **********: EQ2 TO EQ1= 1.733
WITH FLUX LEVEL CORRECTION **********: EQ2 TO EQ1= -.643
NO FLUX LEVEL CORRECTION **********: EQ5 TO EQ7= 10.035
WITH FLUX LEVEL CORRECTION **********: EQ5 TO EQ7= 9.228

TABLE HEDL-24a

GUNDREMMINGEN RESULTS WITHOUT CORRECTION FOR FLUX-LEVEL AND NICKEL-FLUENCE EFFECTS

*** RESULTS FOR SEVEN EQUATIONS WITH NO CORRECTIONS FOR FLUX LEVEL AND NI-FLUENCE EFFECTS ***

CALCULATE TO MEASURED (C/E) CHARPY SHIFT(DEG.F) VALUES FOR SELECTED TREND CURVE EQNS.

J	CAPSULE		EQ.1	EQ.2	EQ.3	EQ.4	EQ.5	EQ.6	EQ.7	FLU.	FLUX	T/F	Cv(F)	CU%	NI%	CF
1	GUND	A	1.03	1.08	.969	-.14	1.09	.966	1.07	.55	1.3	2	72	.18	.13	.780
2	GUND	B	1.04	1.12	.991	-.14	1.04	.981	1.07	1.1	3.7	2	86	.18	.13	.788
3	GUND	C	.978	1.06	.917	-.13	.940	.972	.984	3	2.4	2	115	.18	.13	.953
4	GUND	D	.606	.650	.526	-.10	.664	.840	.697	22.5	18	2	234	.18	.13	1.50

MEASURED - CALCULATED (E-C) CHARPY SHIFT(DEG.F) VALUES FOR SELECTED TREND CURVE EQNS.

J	CAPSULE		EQ.1	EQ.2	EQ.3	EQ.4	EQ.5	EQ.6	EQ.7	FLU.	FLUX	T/F	Cv(F)	CU%	NI%	CF
1	GUND	A	-2.2	-6.2	2.17	82.6	-6.9	2.44	-5.6	.55	1.3	2	72	.18	.13	.780
2	GUND	B	-4.1	-10.	.713	98.1	-4.2	1.54	-6.6	1.1	3.7	2	86	.18	.13	.788
3	GUND	C	2.49	-6.9	9.44	129.	6.83	3.15	1.78	3	2.4	2	115	.18	.13	.953
4	GUND	D	92.1	81.8	110.	258.	78.5	37.3	70.7	22.5	18	2	234	.18	.13	1.50

AVE VALUE OF COMBINED ((SUM L3)/N;L3=L4*L5) CORRECTION FACTOR FOR ALL CAPSULES=1.833
CORRECTION FACTOR'S AVERAGE VALUES: L4 = 1.313 L5 = 1.438 L6 = 1.007

SUM OF SQUARES (E-C) FOR EACH OF THE SEVEN EQUATIONS =
EQ1= 8527.771 EQ2= 6905.854 EQ3= 12357.516 EQ4= 100216.263 EQ5= 6282.476

EQ6= 1415.494 EQ7= 5079.41

STANDARD DEVIATION OF FIT FOR EACH OF THE SEVEN EQUATIONS =
EQ1= 46.173 EQ2= 41.551 EQ3= 55.582 EQ4= 158.285 EQ5= 39.631 EQ6= 18.812 EQ7= 35.635

TABLE HEDL-24b

GUNDREMMINGEN RESULTS WITH CORRECTION FOR FLUX-LEVEL AND NICKEL-FLUENCE EFFECTS

**** RESULTS FOR SEVEN EQUATIONS WITH CORRECTIONS FOR FLUX LEVEL AND NI-FLUENCE EFFECTS ****

CALCULATE TO MEASURED (C/E) CHARPY SHIFT(DEG.F) VALUES FOR SELECTED TREND CURVE EQNS.

J	CAPSULE	EQ.1	EQ.2	EQ.3	EQ.4	EQ.5	EQ.6	EQ.7	FLU.	FLUX	T/F	Cv(F)	CU%	NI%	CF
1	GUND A	.805	.849	.757	-.11	.856	.754	.842	.55	1.3	2	72	.18	.13	.780
2	GUND B	.826	.885	.782	-.11	.828	.774	.849	1.1	3.7	2	86	.18	.13	.788
3	GUND C	.932	1.01	.875	-.12	.896	.927	.938	3	2.4	2	115	.18	.13	.953
4	GUND D	.913	.979	.793	-.15	1.00	1.26	1.05	22.5	18	2	234	.18	.13	1.50

MEASURED - CALCULATED (E-C) CHARPY SHIFT(DEG.F) VALUES FOR SELECTED TREND CURVE EQNS.

J	CAPSULE	EQ.1	EQ.2	EQ.3	EQ.4	EQ.5	EQ.6	EQ.7	FLU.	FLUX	T/F	Cv(F)	CU%	NI%	CF
1	GUND A	14.0	10.8	17.4	80.2	10.3	17.6	11.3	.55	1.3	2	72	.18	.13	.780
2	GUND B	14.8	9.85	18.7	95.5	14.7	19.3	12.9	1.1	3.7	2	86	.18	.13	.788
3	GUND C	7.72	-1.3	14.3	129.	11.8	8.35	7.05	3	2.4	2	115	.18	.13	.953
4	GUND D	20.3	4.78	48.2	271.	-.26	-62.	-12.	22.5	18	2	234	.18	.13	1.50

AVE VALUE OF COMBINED ((SUM L3)/N;L3=L4*L5) CORRECTION FACTOR FOR ALL CAPSULES=1.833
CORRECTION FACTOR'S AVERAGE VALUES: L4 = 1.313 L5 = 1.438 L6 = 1.007

SUM OF SQUARES (E-C) FOR EACH OF SEVEN EQUATIONS =
EQ1= 889.729 EQ2= 239.567 EQ3= 3190.478 EQ4= 105764.2 EQ5= 465.882

EQ6= 4639.407 EQ7= 491.549

STANDARD DEVIATION OF FIT FOR EACH OF SEVEN EQUATIONS =
EQ1= 14.914 EQ2= 7.739 EQ3= 28.242 EQ4= 162.607 EQ5= 10.792 EQ6= 34.057 EQ7= 11.085

THE R VALUES FOR EACH OF SEVEN EQUATIONS =

FOR I=1 TO 7 ; EQN(I)*WITHOUT TO EQN(I)*WITH FLUX LEVEL & NI - FLUENCE CORRECTIONS =
EQ1= 34.339 EQ2= 111.305 EQ3= 11.493 EQ4= -.21 EQ5= 49.941 EQ6= -2.78 EQ7= 37.334

THE R VALUES FOR EQN.2 TO EQN.1 AND FOR EQN.5 TO EQN.7 =

NO FLUX LEVEL & NI-FLUENCE CORRECTIONS: EQ2 TO EQ1= -.761
WITH FLUX LEVEL & NI-FLUENCE CORRECTIONS: EQ2 TO EQ1= -2.923
NO FLUX LEVEL & NI-FLUENCE CORRECTIONS: EQ5 TO EQ7= .947
WITH FLUX LEVEL & NI-FLUENCE CORRECTIONS: EQ5 TO EQ7= -.209

TABLE HEDL-25a

COMBINED PSF AND GUNDREMMINGEN RESULTS WITHOUT CORRECTION FOR FLUX-LEVEL AND NICKEL-FLUENCE EFFECTS

*** RESULTS FOR SEVEN EQUATIONS WITH NO CORRECTIONS FOR FLUX LEVEL AND NI-FLUENCE EFFECTS ***

CALCULATE TO MEASURED (C/E) CHARPY SHIFT(DEG.F) VALUES FOR SELECTED TREND CURVE EQNS.

J	CAPSULE		EQ.1	EQ.2	EQ.3	EQ.4	EQ.5	EQ.6	EQ.7	FLU.	FLUX	T/F	Cv(F)	CU%	NI%	CF
1	GUND	A	1.03	1.08	.969	-.14	1.09	.966	1.07	.55	1.3	2	72	.18	.13	.875
2	GUND	B	1.04	1.12	.991	-.14	1.04	.981	1.07	1.1	3.7	2	86	.18	.13	.883
3	1/2T	R	.869	.811	.472	1.21	.700	.354	.769	1.1	2.12	.16	430	.23	1.58	1.02
4	GUND	C	.978	1.06	.917	-.13	.940	.972	.984	3	2.4	2	115	.18	.13	1.06
5	1/4T	R	.910	.896	.514	1.42	.739	.401	.829	2.19	4.22	.53	461	.23	1.58	1.06
6	OT	R	.888	.895	.507	1.53	.732	.420	.935	3.85	7.41	4.31	515	.23	1.58	1.12
7	GUND	D	.606	.650	.526	-.10	.664	.840	.697	22.5	18	2	234	.18	.13	1.68
8	SSC1	R	1.04	1.06	.609	1.71	.874	.480	.970	2.52	65.1	.68	400	.23	1.58	.837
9	SSC2	R	.922	.932	.524	1.68	.768	455	.862	5.31	66.7	.65	520	.23	1.58	.981

MEASURED - CALCULATED (E-C) CHARPY SHIFT(DEG.F) VALUES FOR SELECTED TREND CURVE EQNS.

J	CAPSULE		EQ.1	EQ.2	EQ.3	EQ.4	EQ.5	EQ.6	EQ.7	FLU.	FLUX	T/F	Cv(F)	CU%	NI%	CF
1	GUND	A	-2.2	-6.2	2.17	82.6	-6.9	2.44	-5.6	.55	1.3	2	72	.18	.13	.875
2	GUND	B	-4.1	-10.	.713	98.1	-4.2	1.54	-6.6	1.1	3.7	2	86	.18	.13	.883
3	1/2T	R	55.9	81.2	226.	-92.	128.	277.	98.9	1.1	2.12	.16	430	.23	1.58	1.02
4	GUND	C	2.49	-6.9	9.44	129.	6.83	3.15	1.78	3	2.4	2	115	.18	.13	1.06
5	1/4T	R	41.1	47.9	223.	-194	120.	276.	78.3	2.19	4.22	.53	461	.23	1.58	1.06
6	OT	R	57.4	53.9	253.	-273	137.	298.	33.1	3.85	7.41	4.31	515	.23	1.58	1.12
7	GUND	D	92.1	81.8	110.	258.	78.5	37.3	70.7	22.5	18	2	234	.18	.13	1.68
8	SSC1	R	-19.	-25.	156.	-286	50.3	207.	11.8	2.52	65.1	.68	400	.23	1.58	.837
9	SSC2	R	40.5	34.8	247.	-356	120.	283.	71.2	5.31	66.7	.65	520	.23	1.58	.981

AVE VALUE OF COMBINED ((SUM L3)/N;L3=L4*L5) CORRECTION FACTOR FOR ALL CAPSULES=1.635
CORRECTION FACTOR'S AVERAGE VALUES: L4 = 1.241 L5 = 1.339 L6 = 1.066

SUM OF SQUARES (E-C) FOR EACH OF THE SEVEN EQUATIONS =
EQ1= 18691.253 EQ2= 20591.534 EQ3= 263770.712 EQ4= 430832.804 EQ5= 73200.864

EQ6= 367062.286 EQ7= 27333.989

STANDARD DEVIATION OF FIT FOR EACH OF THE SEVEN EQUATIONS =
EQ1= 45.572 EQ2= 47.833 EQ3= 171.195 EQ4= 218.793 EQ5= 90.186 EQ6= 201.952 EQ7= 55.11

TABLE HEDL-25b

COMBINED PSF AND GUNDREMMINGEN RESULTS WITH CORRECTIO.. FOR FLUX-LEVEL AND NICKEL-FLUENCE EFFECTS

**** RESULTS FOR SEVEN EQUATIONS WITH CORRECTIONS FOR FLUX LEVEL AND NI-FLUENCE EFFECTS ****

CALCULATE TO MEASURED (C/E) CHARPY SHIFT(DEG.F) VALUES FOR SELECTED TREND CURVE EQNS.

J	CAPSULE		EQ.1	EQ.2	EQ.3	EQ.4	EQ.5	EQ.6	EQ.7	FLU.	FLUX	T/F	Cv(F)	CU%	NI%	CF
1	GUND	A	.902	.951	.848	-.12	.959	.845	.943	.55	1.3	2	72	.18	.13	.875
2	GUND	B	.926	.992	.876	-.12	.927	.867	.952	1.1	3.7	2	86	.18	.13	.883
3	1/2T	R	.887	.827	.482	1.24	.71~	.361	.785	1.1	2.12	.16	430	.23	1.58	1.02
4	GUND	C	1.04	1.13	.980	-.13	1.00	1.03	1.05	3	2.4	2	115	.18	.13	1.06
5	1/4T	R	.968	.952	.547	1.51	.786	.426	.882	2.19	4.22	.53	461	.23	1.58	1.06
6	QT	R	1.00	1.01	.572	1.72	.827	.474	1.05	3.85	7.41	4.31	515	.23	1.58	1.12
7	GUND	D	1.02	1.09	.889	-.17	1.12	1.41	1.17	22.5	18	2	234	.18	.13	1.68
8	SSC1	R	.879	.891	.510	1.43	.732	.402	.813	2.52	65.1	.68	400	.23	1.58	.837
9	SSC2	R	.905	.915	.514	1.65	.754	.447	.847	5.31	66.7	.65	520	.23	1.58	.981

MEASURED - CALCULATED (E-C) CHARPY SHIFT(DEG.F) VALUES FOR SELECTED TREND CURVE EQNS.

J	CAPSULE		EQ.1	EQ.2	EQ.3	EQ.4	EQ.5	EQ.6	EQ.7	FLU.	FLUX	T/F	Cv(F)	CU%	NI%	CF
1	GUND	A	7.02	3.48	10.8	81.2	2.88	11.1	4.05	.55	1.3	2	72	.18	.13	.875
2	GUND	B	6.31	.678	10.6	96.7	6.20	11.3	4.12	1.1	3.7	2	86	.18	.13	.883
3	1/2T	R	48.2	74.1	222.	-103	122.	274.	92.1	1.1	2.12	.16	430	.23	1.58	1.02
4	GUND	C	-5.2	-15.	2.22	131.	-.57	-4.4	-5.9	3	2.4	2	115	.18	.13	1.06
5	1/4T	R	14.5	21.7	208.	-236	98.4	264.	54.1	2.19	4.22	.53	461	.23	1.58	1.06
6	QT	R	-1.4	-5.4	219.	-375	88.9	270.	-28.	3.85	7.41	4.31	515	.23	1.58	1.12
7	GUND	D	-5.4	-22.	25.8	275.	-28.	-98.	-41.	22.5	18	2	234	.18	.13	1.68
8	SSC1	R	48.2	43.4	195.	-175	107.	238.	74.7	2.52	65.1	.68	400	.23	1.58	.837
9	SSC2	R	49.3	43.8	252.	-340	127.	287.	79.5	5.31	66.7	.65	520	.23	1.58	.981

AVE VALUE OF COMBINED ((SUM L3)/N;L3=L4*L5) CORRECTION FACTOR FOR ALL CAPSULES=1.635
CORRECTION FACTOR'S AVERAGE VALUES: L4 = 1.241 L5 = 1.339 L6 = 1.066

SUM OF SQUARES (E-C) FOR EACH OF SEVEN EQUATIONS =
EQ1= 7450.527 EQ2= 10570.548 EQ3= 244407.383 EQ4= 463048.348 EQ5= 61222.917

EQ6= 367994.811 EQ7= 25985.421

STANDARD DEVIATION OF FIT FOR EACH OF SEVEN EQUATIONS =
EQ1= 28.772 EQ2= 34.271 EQ3= 164.792 EQ4= 226.826 EQ5= 82.478 EQ6= 202.209 EQ7= 53.733

THE R VALUES FOR EACH OF SEVEN EQUATIONS =

FOR I=1 TO 7 : EQN(I)*WITHOUT TO EQN(I)*WITH FLUX LEVEL & NI - FLUENCE CORRECTIONS =
EQ1= 13.578 EQ2= 8.532 EQ3= .713 EQ4= -.626 EQ5= 1.761 EQ6= -.023 EQ7= .467

THE R VALUES FOR EQN.2 TO EQN.1 AND FOR EQN.5 TO EQN.7 =

NO FLUX LEVEL & NI-FLUENCE CORRECTIONS: EQ2 TO EQ1= .915
WITH FLUX LEVEL & NI-FLUENCE CORRECTIONS: EQ2 TO EQ1= 3.769
NO FLUX LEVEL & NI-FLUENCE CORRECTIONS: EQ5 TO EQ7= 15.102
WITH FLUX LEVEL & NI-FLUENCE CORRECTIONS: EQ5 TO EQ7= 12.204

TABLE HEDL-27a

B&W DATA BASE RESULTS WITHOUT CORRECTION FOR FLUX-LEVEL EFFECT FOR AN 0.21 TO 0.23 COPPER GROUPING USING EQUATION (6b)

********** RESULTS FOR SEVEN EQUATIONS WITH NO CORRECTION FOR FLUX LEVEL EFFECT **********

CALCULATE TO MEASURED (C/E) CHARPY SHIFT(DEG.F) VALUES FOR SELECTED TREND CURVE EQNS.

J	CAPSULE		EQ.1	EQ.2	EQ.3	EQ.4	EQ.5	EQ.6	EQ.7	FLU.	FLUX	T/F	Cv(F)	CU%	NI%	CF
1	DBESS	F	.792	.799	.759	.816	.947	.697	.820	.229	.27	1.67	127	.21	.63	1.31
2	PB1	R	1.11	1.16	1.11	1.17	1.10	.995	1.11	2.17	1.4	1.24	165	.21	.57	.893
3	PB1	S	.885	.919	.888	.858	.931	.765	.913	.851	.73	1.42	165	.21	.57	1.03
4	PB1	V	1.00	1.02	1.00	.953	1.12	.895	1.10	.35	1.29	2.31	110	.21	.57	.910
5	REG1	R	.995	1.04	1.04	.968	1.01	.899	1.02	1.17	1.4	1.58	165	.23	.56	.893
6	REG	T	1.20	1.26	1.26	1.21	1.20	1.10	1.21	1.75	.73	1.42	150	.23	.56	1.03
7	REG	V	.969	1.00	1.02	.910	1.05	.878	1.06	.598	1.29	2.31	140	.23	.56	.910

MEASURED - CALCULATED (E-C) CHARPY SHIFT(DEG.F) VALUES FOR SELECTED TREND CURVE EQNS.

J	CAPSULE		EQ.1	EQ.2	EQ.3	EQ.4	EQ.5	EQ.6	EQ.7	FLU.	FLUX	T/F	Cv(F)	CU%	NI%	CF
1	DBESS	F	26.3	25.4	30.5	23.3	19.3	38.4	22.7	.229	.27	1.67	127	.21	.63	1.31
2	PB1	R	-19.	-27.	-18.	-28.	-17.	.754	-18.	2.17	1.4	1.24	165	.21	.57	.893
3	PB1	S	18.8	13.2	18.3	23.3	11.3	38.6	14.3	.851	.73	1.42	165	.21	.57	1.03
4	PB1	V	-.54	-3.0	-.29	5.13	-13.	11.4	-11.	.35	1.29	2.31	110	.21	.57	.910
5	REG1	R	.725	-6.9	-8.1	5.18	-2.8	16.5	-4.0	1.17	1.4	1.58	165	.23	.56	.893
6	REG	T	-31.	-40.	-40.	-32.	-30.	-16.	-32.	1.75	.73	1.42	150	.23	.56	1.03
7	REG	V	4.28	-.90	-3.2	12.5	-7.8	16.9	-8.5	.598	1.29	2.31	140	.23	.56	.910

AVE VALUE OF COMBINED ((SUM L3)/N;L3=L4*L5) CORRECTION FACTOR FOR ALL CAPSULES=1.015
CORRECTION FACTOR'S AVERAGE VALUES: L4 = 1.015 L5 = 1 L6 = 1

SUM OF SQUARES (E-C) FOR EACH OF THE SEVEN EQUATIONS =
EQ1= 2425.451 EQ2= 3290.516 EQ3= 3301.862 EQ4= 3215.34 EQ5= 1975.03

EQ6= 3924.592 EQ7= 2364.134

STANDARD DEVIATION OF FIT FOR EACH OF THE SEVEN EQUATIONS =
EQ1= 18.614 EQ2= 21.681 EQ3= 21.719 EQ4= 21.432 EQ5= 16.797 EQ6= 23.678 EQ7= 18.378

TABLE HEDL-27b

B&W DATA BASE RESULTS WITH CORRECTION FOR FLUX-LEVEL EFFECT FOR AN 0.21 TO 0.23 COPPER GROUPING USING EQUATION (6b)

********** RESULTS FOR SEVEN EQUATIONS WITH CORRECTION FOR FLUX LEVEL EFFECT **********

CALCULATE TO MEASURED (C/E) CHARPY SHIFT(DEG.F) VALUES FOR SELECTED TREND CURVE EQNS.

J	CAPSULE		EQ.1	EQ.2	EQ.3	EQ.4	EQ.5	EQ.6	EQ.7	FLU.	FLUX	T/F	Cv(F)	CU%	NI%	CF
1	DBESS	F	1.04	1.05	.998	1.07	1.11	.916	1.07	.229	.27	1.67	127	.21	.63	1.31
2	PB1	R	.998	1.04	.992	1.04	.985	.889	.994	2.17	1.4	1.24	165	.21	.57	.893
3	PB1	S	.920	.955	.923	.892	.968	.796	.949	.851	.73	1.42	165	.21	.57	1.03
4	PB1	V	.914	.935	.912	.867	1.02	.815	1.00	.35	1.29	2.31	110	.21	.57	.910
5	REG1	R	.889	.930	.937	.865	.908	.803	.915	1.17	1.4	1.58	165	.23	.56	.893
6	REG	T	1.25	1.31	1.31	1.26	1.25	1.15	1.26	1.75	.73	1.42	150	.23	.56	1.03
7	REG	V	.882	.916	.931	.828	.961	.799	.965	.598	1.29	2.31	140	.23	.56	.910

MEASURED - CALCULATED (E-C) CHARPY SHIFT(DEG.F) VALUES FOR SELECTED TREND CURVE EQNS.

J	CAPSULE		EQ.1	EQ.2	EQ.3	EQ.4	EQ.5	EQ.6	EQ.7	FLU.	FLUX	T/F	Cv(F)	CU%	NI%	CF
1	DBESS	F	-5.3	-6.4	.188	-9.2	-14.	10.5	-10.	.229	.27	1.67	127	.21	.63	1.31
2	PB1	R	.169	-7.3	1.23	-8.1	2.41	18.2	.935	2.17	1.4	1.24	165	.21	.57	.893
3	PB1	S	13.1	7.28	12.6	17.7	5.26	33.6	8.41	.851	.73	1.42	165	.21	.57	1.03
4	PB1	V	9.38	7.10	9.60	14.5	-2.6	20.3	-.85	.35	1.29	2.31	110	.21	.57	.910
5	REG1	R	18.2	11.4	10.3	22.2	15.0	32.3	13.9	1.17	1.4	1.58	165	.23	.56	.893
6	REG	T	-38.	-47.	-47.	-40.	-37.	-22.	-39.	1.75	.73	1.42	150	.23	.56	1.03
7	REG	V	16.4	11.7	9.58	23.9	5.44	28.0	4.81	.598	1.29	2.31	140	.23	.56	.910

AVE VALUE OF COMBINED ((SUM L3)/N;L3=L4*L5) CORRECTION FACTOR FOR ALL CAPSULES=1.015
CORRECTION FACTOR'S AVERAGE VALUES: L4 = 1.015 L5 = 1 L6 = 1

SUM OF SQUARES (E-C) FOR EACH OF SEVEN EQUATIONS =
EQ1= 2366.255 EQ2= 2753.66 EQ3= 2729.509 EQ4= 3353.666 EQ5= 1914.136

EQ6= 4340.983 EQ7= 1976.564

STANDARD DEVIATION OF FIT FOR EACH OF SEVEN EQUATIONS =
EQ1= 18.386 EQ2= 19.834 EQ3= 19.747 EQ4= 21.888 EQ5= 16.536 EQ6= 24.903 EQ7= 16.804

THE R VALUES FOR EACH OF SEVEN EQUATIONS =

FOR I=1 TO 7 : ********** EQN(I)*WITHOUT TO EQN(I)*WITH CORRECTION FOR FLUX LEVEL =
EQ1= .175 EQ2= 1.365 EQ3= 1.468 EQ4= -.289 EQ5= .223 EQ6= -.671 EQ7= 1.373

THE R VALUES FOR EQN.2 TO EQN.1 AND FOR EQN.5 TO EQN.7 =

NO FLUX LEVEL CORRECTION **********: EQ2 TO EQ1= 2.497
WITH FLUX LEVEL CORRECTION **********: EQ2 TO EQ1= 1.146
NO FLUX LEVEL CORRECTION **********: EQ5 TO EQ7= -1.152
WITH FLUX LEVEL CORRECTION **********: EQ5 TO EQ7= -.221

TABLE HEDL-28a

B&W DATA BASE RESULTS WITHOUT CORRECTION FOR FLUX-LEVEL EFFECT FOR AN 0.35 TO 0.36 COPPER GROUPING USING EQUATION (6b)

********** RESULTS FOR SEVEN EQUATIONS WITH NO CORRECTION FOR FLUX LEVEL EFFECT **********

CALCULATE TO MEASURED (C/E) CHARPY SHIFT(DEG.F) VALUES FOR SELECTED TREND CURVE EQNS.

J	CAPSULE		EQ.1	EQ.2	EQ.3	EQ.4	EQ.5	EQ.6	EQ.7	FLU.	FLUX	T/F	Cv(F)	CU%	NI%	CF
1	OC2	A	1.28	1.34	1.56	1.18	1.43	1.28	1.34	.337	.27	1.67	114	.36	.58	1.17
2	OC2	C	2.06	2.04	2.38	1.99	1.56	2.32	2.01	.101	.27	1.53	45	.36	.58	1.17
3	ZION1	T	1.23	1.28	1.48	1.12	1.37	1.24	1.20	.306	.8	1.04	112	.35	.57	.912
4	ZION1	U	1.01	1.07	1.22	.952	1.04	.978	1.00	1.02	.9	.88	199	.35	.57	.887
5	ZION2	U	.923	.962	1.11	.848	1.02	.936	.932	.282	.7	1.36	145	.35	.57	.941
6	SUR1	T	.879	.907	1.03	.922	.973	.870	.876	.288	.85	1.25	167	.35	.7	.899

MEASURED - CALCULATED (E-C) CHARPY SHIFT(DEG.F) VALUES FOR SELECTED TREND CURVE EQNS.

J	CAPSULE		EQ.1	EQ.2	EQ.3	EQ.4	EQ.5	EQ.6	EQ.7	FLU.	FLUX	T/F	Cv(F)	CU%	NI%	CF
1	OC2	A	-32.	-38.	-63.	-21.	-49.	-32.	-38.	.337	.27	1.67	114	.36	.58	1.17
2	OC2	C	-47.	-47.	-62.	-44.	-25.	-59.	-45.	.101	.27	1.53	45	.36	.58	1.17
3	ZION1	T	-25.	-31.	-54.	-14.	-41.	-26.	-23.	.306	.8	1.04	112	.35	.57	.912
4	ZION1	U	-1.9	-14.	-45.	9.50	-9.3	4.33	-.03	1.02	.9	.88	199	.35	.57	.887
5	ZION2	U	11.0	5.50	-16.	21.9	-3.2	9.18	9.74	.282	.7	1.36	145	.35	.57	.941
6	SUR1	T	20.1	15.4	-5.9	12.9	4.48	21.6	20.5	.288	.85	1.25	167	.35	.7	.899

AVE VALUE OF COMBINED ((SUM L3)/N;L3+L4*L5) CORRECTION FACTOR FOR ALL CAPSULES=1.131
CORRECTION FACTOR'S AVERAGE VALUES: L4 = 1.131 L5 = 1 L6 = 1

SUM OF SQUARES (E-C) FOR EACH OF THE SEVEN EQUATIONS =
EQ1= 4535.204 EQ2= 5256.637 EQ3= 13364.187 EQ4= 3387.016 EQ5= 5003.359

EQ6= 5880.342 EQ7= 4638.154

STANDARD DEVIATION OF FIT FOR EACH OF THE SEVEN EQUATIONS =
EQ1= 27.493 EQ2= 29.599 EQ3= 47.195 EQ4= 23.759 EQ5= 28.877 EQ6= 31.306 EQ7= 27.803

TABLE HEDL-28b

B&W DATA BASE RESULTS WITH CORRECTION FOR FLUX-LEVEL EFFECT FOR AN 0.35 TO 0.36 COPPER GROUPING USING EQUATION (6b)

********** RESULTS FOR SEVEN EQUATIONS WITH CORRECTION FOR FLUX LEVEL EFFECT **********

CALCULATE TO MEASURED (C/E) CHARPY SHIFT(DEG.F) VALUES FOR SELECTED TREND CURVE EQNS.

J	CAPSULE		EQ.1	EQ.2	EQ.3	EQ.4	EQ.5	EQ.6	EQ.7	FLU.	FLUX	T/F	Cv(F)	CU%	NI%	CF
1	OC2	A	1.51	1.58	1.83	1.39	1.69	1.51	1.58	.337	.27	1.67	114	.36	.58	1.17
2	OC2	C	2.43	2.41	2.81	2.34	1.84	2.73	2.37	.101	.27	1.53	45	.36	.58	1.17
3	ZION1	T	1.12	1.17	1.35	1.03	1.25	1.13	1.10	.306	.8	1.04	112	.35	.57	.912
4	ZION1	U	.896	.954	1.09	.845	.929	.868	.887	1.02	.9	.88	199	.35	.57	.887
5	ZION2	U	.869	.905	1.04	.798	.962	.882	.878	.282	.7	1.36	145	.35	.57	.941
6	SUR1	T	.791	.816	.931	.829	.875	.782	.788	.288	.85	1.25	167	.35	.7	.899

MEASURED - CALCULATED (E-C) CHARPY SHIFT(DEG.F) VALUES FOR SELECTED TREND CURVE EQNS.

J	CAPSULE		EQ.1	EQ.2	EQ.3	EQ.4	EQ.5	EQ.6	EQ.7	FLU.	FLUX	T/F	Cv(F)	CU%	NI%	CF
1	OC2	A	-58.	-66.	-95.	-45.	-79.	-58.	-66.	.337	.27	1.67	114	.36	.58	1.17
2	OC2	C	-64.	-63.	-81.	-60.	-38.	-78.	-61.	.101	.27	1.53	45	.36	.58	1.17
3	ZION1	T	-13.	-19.	-40.	-3.4	-28.	-14.	-11.	.306	.8	1.04	112	.35	.57	.912
4	ZION1	U	20.5	9.04	-18.	30.7	14.0	26.2	22.3	1.02	.9	.88	199	.35	.57	.887
5	ZION2	U	18.6	13.6	-7.2	29.1	5.38	17.1	17.6	.282	.7	1.36	145	.35	.57	.941
6	SUR1	T	34.8	30.6	11.3	28.3	20.7	36.2	35.2	.288	.85	1.25	167	.35	.7	.899

AVE VALUE OF COMBINED ((SUM L3)/N;L3=L4*L5) CORRECTION FACTOR FOR ALL CAPSULES=1.131
CORRECTION FACTOR'S AVERAGE VALUES: L4 = 1.131 L5 = 1 L6 = 1

SUM OF SQUARES (E-C) FOR EACH OF SEVEN EQUATIONS =
EQ1= 9760.569 EQ2= 10043.463 EQ3= 17970.21 EQ4= 8349.09 EQ5= 9195.176

EQ6= 12053.629 EQ7= 10389.989

STANDARD DEVIATION OF FIT FOR EACH OF SEVEN EQUATIONS =
EQ1= 40.333 EQ2= 40.913 EQ3= 54.727 EQ4= 37.303 EQ5= 39.148 EQ6= 44.821 EQ7= 41.613

THE R VALUES FOR EACH OF SEVEN EQUATIONS =

FOR I=1 TO 7 : ********** EQN(I)*WITHOUT TO EQN(I)*WITH CORRECTION FOR FLUX LEVEL =
EQ1= -3.212 EQ2= -2.86 EQ3= -1.538 EQ4= -3.566 EQ5= -2.735 EQ6= -3.073 EQ7= -3.322

THE R VALUES FOR EQN.2 TO EQN.1 AND FOR EQN.5 TO EQN.7 =

NO FLUX LEVEL CORRECTION **********: EQ2 TO EQ1= .954
WITH FLUX LEVEL CORRECTION **********: EQ2 TO EQ1= .174
NO FLUX LEVEL CORRECTION **********: EQ5 TO EQ7= .472
WITH FLUX LEVEL CORRECTION **********: EQ5 TO EQ7= -.69

TABLE HEDL-29a

PSF CODE R WELD RESULTS WITHOUT CORRECTION FOR FLUX-LEVEL EFFECT USING EQUATION (4M) DERIVED EQUATION (6b)

********** RESULTS FOR SEVEN EQUATIONS WITH NO CORRECTION FOR FLUX LEVEL EFFECT **********

CALCULATE TO MEASURED (C/E) CHARPY SHIFT(DEG.F) VALUES FOR SELECTED TREND CURVE EQNS.

J	CAPSULE		EQ.1	EQ.2	EQ.3	EQ.4	EQ.5	EQ.6	EQ.7	FLU.	FLUX	T/F	Cv(F)	CU%	NI%	CF
1	SSC1	R	1.04	1.06	.609	1.13	.874	.480	.970	2.52	65.1	.68	400	.23	1.58	.872
2	SSC2	R	.922	.932	.524	1.11	.768	.455	.862	5.31	66.7	.65	520	.23	1.58	.874
3	OT	R	.888	.895	.507	1.01	.732	.420	.935	3.85	7.41	4.31	515	.23	1.58	.965
4	1/4T	R	.910	.896	.514	.938	.739	.401	.829	2.19	4.22	.53	461	.23	1.58	1.06
5	1/2T	R	.869	.811	.472	.801	.700	.354	.769	1.1	2.12	.16	430	.23	1.58	1.22

MEASURED - CALCULATED (E-C) CHARPY SHIFT(DEG.F) VALUES FOR SELECTED TREND CURVE EQNS.

J	CAPSULE		EQ.1	EQ.2	EQ.3	EQ.4	EQ.5	EQ.6	EQ.7	FLU.	FLUX	T/F	Cv(F)	CU%	NI%	CF
1	SSC1	R	-19.	-25.	156.	-53.	50.3	207.	11.8	2.52	65.1	.68	400	.23	1.58	.872
2	SSC2	R	40.5	34.8	247.	-58.	120.	283.	71.2	5.31	66.7	.65	520	.23	1.58	.874
3	OT	R	57.4	53.9	253.	-5.8	137.	298.	33.1	3.85	7.41	4.31	515	.23	1.58	.965
4	1/4T	R	41.1	47.9	223.	28.4	120.	276.	78.3	2.19	4.22	.53	461	.23	1.58	1.06
5	1/2T	R	55.9	81.2	226.	85.3	128.	277.	98.9	1.1	2.12	.16	430	.23	1.58	1.22

AVE VALUE OF COMBINED ((SUM L2)/N;L3=L4*L5) CORRECTION FACTOR FOR ALL CAPSULES=.675
CORRECTION FACTOR'S AVERAGE VALUES: L4 = .675 L5 = 1 L6 = 1

SUM OF SQUARES (E-C) FOR EACH OF THE SEVEN EQUATIONS =
EQ1= 10163.483 EQ2= 13685.679 EQ3= 251413.196 EQ4= 14410.759 EQ5= 66918.388

EQ6= 365646.793 EQ7= 22254.58

STANDARD DEVIATION OF FIT FOR EACH OF THE SEVEN EQUATIONS =
EQ1= 45.085 EQ2= 52.318 EQ3= 224.238 EQ4= 53.686 EQ5= 115.688 EQ6= 270.424 EQ7= 66.715

TABLE HEDL-29b

PSF CODE R WELD RESULTS WITH CORRECTION FOR FLUX-LEVEL EFFECT USING EQUATION (4M) DERIVED EQUATION (6b)

********** RESULTS FOR SEVEN EQUATIONS WITH CORRECTION FOR FLUX LEVEL EFFECT **********

CALCULATE TO MEASURED (C/E) CHARPY SHIFT(DEG.F) VALUES FOR SELECTED TREND CURVE EQNS.

J	CAPSULE		EQ.1	EQ.2	EQ.3	EQ.4	EQ.5	EQ.6	EQ.7	FLU.	FLUX	T/F	Cv(F)	CU%	NI%	CF
1	SSC1	R	.916	.928	.532	.988	.763	.419	.846	2.52	65.1	.68	400	.23	1.58	.872
2	SSC2	R	.806	.815	.458	.973	.672	.398	.754	5.31	66.7	.65	520	.23	1.58	.874
3	OT	R	.857	.864	.490	.976	.707	.405	.903	3.85	7.41	4.31	515	.23	1.58	.965
4	1/4T	R	.968	.952	.547	.997	.786	.426	.882	2.19	4.22	.53	461	.23	1.58	1.06
5	1/2T	R	1.06	.992	.578	.980	.857	.433	.942	1.1	2.12	.16	430	.23	1.58	1.22

MEASURED - CALCULATED (E-C) CHARPY SHIFT(DEG.F) VALUES FOR SELECTED TREND CURVE EQNS.

J	CAPSULE		EQ.1	EQ.2	EQ.3	EQ.4	EQ.5	EQ.6	EQ.7	FLU.	FLUX	T/F	Cv(F)	CU%	NI%	CF
1	SSC1	R	33.5	28.5	187.	4.55	94.7	232.	61.2	2.52	65.1	.68	400	.23	1.58	.872
2	SSC2	R	100.	95.8	281.	13.7	170.	312.	127.	5.31	66.7	.65	520	.23	1.58	.874
3	OT	R	73.2	69.8	262.	12.0	150.	305.	49.7	3.85	7.41	4.31	515	.23	1.58	.965
4	1/4T	R	14.6	21.7	208.	1.07	98.4	264.	54.1	2.19	4.22	.53	461	.23	1.58	1.06
5	1/2T	R	-27.	3.21	181.	8.21	61.4	243.	24.8	1.1	2.12	.16	430	.23	1.58	1.22

AVE VALUE OF COMBINED ((SUM L3)/N;L3=L4*L5) CORRECTION FACTOR FOR ALL CAPSULES=.675
CORRECTION FACTOR'S AVERAGE VALUES: L4 = .675 L5 = 1 L6 = 1

SUM OF SQUARES (E-C) FOR EACH OF SEVEN EQUATIONS =
EQ1= 17622.364 EQ2= 15357.68 EQ3= 259752.959 EQ4= 425.317 EQ5= 74158.686

EQ6= 374529.675 EQ7= 26061.1

STANDARD DEVIATION OF FIT FOR EACH OF SEVEN EQUATIONS =
EQ1= 59.367 EQ2= 55.421 EQ3= 227.927 EQ4= 9.22[illegible] EQ5= 121.786 EQ6= 273.689 EQ7= 72.196

THE R VALUES FOR EACH OF SEVEN EQUATIONS =

FOR I=1 TO 7 : ********** EQN(I)*WITHOUT TO EQN(I)*WITH CORRECTION FOR FLUX LEVEL =
EQ1= -2.116 EQ2= -.544 EQ3= -.161 EQ4= 164.412 EQ5= -.488 EQ6= -.119 EQ7= -.73

THE R VALUES FOR EQN.2 TO EQN.1 AND FOR EQN.5 TO EQN.7 =

NO FLUX LEVEL CORRECTION **********: EQ2 TO EQ1= 1.733
WITH FLUX LEVEL CORRECTION **********: EQ2 TO EQ1= -.643
NO FLUX LEVEL CORRECTION **********: EQ5 TO EQ7= 10.035
WITH FLUX LEVEL CORRECTION **********: EQ5 TO EQ7= 9.228

TABLE HEDL-30a

PSF CODE EC WELD RESULTS WITHOUT CORRECTION FOR FLUX-LEVEL EFFECT USING EQUATION (4M) DERIVED EQUATION (6b)

********** RESULTS FOR SEVEN EQUATIONS WITH NO CORRECTION FOR FLUX LEVEL EFFECT **********

CALCULATE TO MEASURED (C/E) CHARPY SHIFT(DEG.F) VALUES FOR SELECTED TREND CURVE EQNS.

J	CAPSULE	EQ.1	EQ.2	EQ.3	EQ.4	EQ.5	EQ.6	EQ.7	FLU.	FLUX	T/F	Cv(F)	CU%	NI%	CF
1	SSC1 EC	1.05	1.07	1.06	.936	1.02	.908	1.01	1.75	45.2	1.07	194	.24	.64	.829
2	SSC2 EC	1.10	1.13	1.10	1.08	1.05	1.01	1.06	3.69	46.4	1.03	214	.24	.64	.830
3	OT EC	1.11	1.13	1.11	1.05	1.06	.997	1.09	2.97	5.72	1.33	205	.24	.64	.974
4	1/4T EC	1.22	1.20	1.19	1.04	1.15	1.02	1.12	1.62	3.12	.24	169	.24	.64	1.09
5	1/2T EC	1.14	1.05	1.05	.872	1.07	.884	1.03	.8	1.54	.14	160	.24	.64	1.27

MEASURED - CALCULATED (E-C) CHARPY SHIFT(DEG.F) VALUES FOR SELECTED TREND CURVE EQNS.

J	CAPSULE	EQ.1	EQ.2	EQ.3	EQ.4	EQ.5	EQ.6	EQ.7	FLU.	FLUX	T/F	Cv(F)	CU%	NI%	CF
1	SSC1 EC	-9.8	-14.	-11.	12.3	-4.0	17.7	-3.8	1.75	45.2	1.07	194	.24	.64	.829
2	SSC2 EC	-22.	-28.	-21.	-18.	-12.	-3.2	-14.	3.69	46.4	1.03	214	.24	.64	.830
3	OT EC	-23.	-28.	-22.	-11.	-12.	.597	-18.	2.97	5.72	1.33	205	.24	.64	.974
4	1/4T EC	-38.	-35.	-33.	-7.9	-26.	-3.4	-21.	1.62	3.12	.24	169	.24	.64	1.09
5	1/2T EC	-22.	-8.6	-8.9	20.3	-11.	18.4	-4.8	.8	1.54	.14	160	.24	.64	1.27

AVE VALUE OF COMBINED ((SUM L3)/N;L3=L4*L5) CORRECTION FACTOR FOR ALL CAPSULES=.697
CORRECTION FACTOR'S AVERAGE VALUES: L4 = .697 L5 = 1 L6 = 1

SUM OF SQUARES (E-C) FOR EACH OF THE SEVEN EQUATIONS =
EQ1= 3128.139 EQ2= 3114.14 EQ3= 2306.153 EQ4= 1124.437 EQ5= 1171.916

EQ6= 677.007 EQ7= 1065.896

STANDARD DEVIATION OF FIT FOR EACH OF THE SEVEN EQUATIONS =
EQ1= 25.013 EQ2= 24.957 EQ3= 21.476 EQ4= 14.996 EQ5= 15.31 EQ6= 11.636 EQ7= 14.601

TABLE HEDL-30b

PSF CODE EC WELD RESULTS WITH CORRECTION FOR FLUX-LEVEL EFFECT USING EQUATION (4M) DERIVED EQUATION (6b)

********** RESULTS FOR SEVEN EQUATIONS WITH CORRECTION FOR FLUX LEVEL EFFECT **********

CALCULATE TO MEASURED (C/E) CHARPY SHIFT(DEG.F) VALUES FOR SELECTED TREND CURVE EQNS.

J	CAPSULE	EQ.1	EQ.2	EQ.3	EQ.4	EQ.5	EQ.6	EQ.7	FLU.	FLUX	T/F	Cv(F)	CU%	NI%	CF
1	SSC1 EC	.871	.889	.879	.776	.847	.753	.846	1.75	45.2	1.07	194	.24	.64	.829
2	SSC2 EC	.917	.941	.914	.903	.879	.343	.888	3.69	46.4	1.03	214	.24	.64	.830
3	OT EC	1.08	1.10	1.08	1.03	1.03	.972	1.06	2.97	5.72	1.33	205	.24	.64	.974
4	1/4T EC	1.33	1.32	1.30	1.14	1.26	1.11	1.22	1.62	3.12	.24	169	.24	.64	1.09
5	1/2T EC	1.45	1.34	1.34	1.11	1.36	1.12	1.31	.8	1.54	.14	160	.24	.64	1.27

MEASURED - CALCULATED (E-C) CHARPY SHIFT(DEG.F) VALUES FOR SELECTED TREND CURVE EQNS.

J	CAPSULE	EQ.1	EQ.2	EQ.3	EQ.4	EQ.5	EQ.6	EQ.7	FLU.	FLUX	T/F	Cv(F)	CU%	NI%	CF
1	SSC1 EC	24.8	21.3	23.3	43.2	29.6	47.7	29.8	1.75	45.2	1.07	194	.24	.64	.829
2	SSC2 EC	17.6	12.5	18.2	20.5	25.8	33.5	23.9	3.69	46.4	1.03	214	.24	.64	.830
3	OT EC	-17.	-22.	-16.	-6.2	-7.3	5.72	-13.	2.97	5.72	1.33	205	.24	.64	.974
4	1/4T EC	-57.	-54.	-51.	-24.	-44.	-19.	-38.	1.62	3.12	.24	169	.24	.64	1.09
5	1/2T EC	-72.	-54.	-55.	-17.	-58.	-20.	-49.	.8	1.54	.14	160	.24	.64	1.27

AVE VALUE OF COMBINED ((SUM L3)/N;L3=L4*L5) CORRECTION FACTOR FOR ALL CAPSULES=.697
CORRECTION FACTOR'S AVERAGE VALUES: L4 = .697 L5 = 1 L6 = 1

SUM OF SQUARES (E-C) FOR EACH OF SEVEN EQUATIONS =
EQ1= 9749.456 EQ2= 7015.135 EQ3= 6888.483 EQ4= 3241.309 EQ5= 7012.387

EQ6= 4222.199 EQ7= 5612.769

STANDARD DEVIATION OF FIT FOR EACH OF SEVEN EQUATIONS =
EQ1= 44.158 EQ2= 37.457 EQ3= 37.117 EQ4= 25.461 EQ5= 37.45 EQ6= 29.059 EQ7= 33.505

THE R VALUES FOR EACH OF SEVEN EQUATIONS =

FOR I=1 TO 7 ; ********** EQN(I)*WITHOUT TO EQN(I)*WITH CORRECTION FOR FLUX LEVEL =
EQ1= -3.396 EQ2= -2.78 EQ3= -3.326 EQ4= -3.265 EQ5= -4.164 EQ6= -4.198 EQ7= -4.05

THE R VALUES FOR EQN.2 TO EQN.1 AND FOR EQN.5 TO EQN.7 =

NO FLUX LEVEL CORRECTION **********: EQ2 TO EQ1= -.022
WITH FLUX LEVEL CORRECTION **********: EQ2 TO EQ1= -1.402
NO FLUX LEVEL CORRECTION **********: EQ5 TO EQ7= .497
WITH FLUX LEVEL CORRECTION **********: EQ5 TO EQ7= 1.247

TABLE HEDL-31a

PSF CODE 3PU PLATE RESULTS WITHOUT CORRECTION FOR FLUX-LEVEL EFFECT USING EQUATION (4M) DERIVED EQUATION (6b)

********** RESULTS FOR SEVEN EQUATIONS WITH NO CORRECTION FOR FLUX LEVEL EFFECT **********

CALCULATE TO MEASURED (C/E) CHARPY SHIFT(DEG.F) VALUES FOR SELECTED TREND CURVE EQNS.

J	CAPSULE	EQ.1	EQ.2	EQ.3	EQ.4	EQ.5	EQ.6	EQ.7	FLU.	FLUX	T/F	Cv(F)	CU%	NI%	CF
1	SSC13PU	1.43	1.46	.912	1.08	1.37	.908	1.39	2.49	64.3	.67	110	.12	.56	.864
2	SSC23PU	1.23	1.26	.769	1.04	1.18	.843	1.21	5.24	65.9	.64	146	.12	.56	.866
3	OT 3PU	1.27	1.28	.793	1.00	1.20	.826	1.40	3.68	7.08	4.32	135	.12	.56	.964
4	1/4T3PU	1.26	1.24	.780	.900	1.17	.763	1.20	2.05	3.95	.53	124	.12	.56	1.06
5	1/2T3PU	1.45	1.36	.863	.922	1.35	.817	1.34	1.01	1.94	.17	95	.12	.56	1.23

MEASURED - CALCULATED (E-C) CHARPY SHIFT(DEG.F) VALUES FOR SELECTED TREND CURVE EQNS.

J	CAPSULE	EQ.1	EQ.2	EQ.3	EQ.4	EQ.5	EQ.6	EQ.7	FLU.	FLUX	T/F	Cv(F)	CU%	NI%	CF
1	SSC13PU	-48.	-51.	9.58	-9.2	-41.	10.0	-43.	2.49	64.3	.67	110	.12	.56	.864
2	SSC23PU	-34.	-38.	33.6	-7.2	-26.	22.8	-31.	5.24	65.9	.64	146	.12	.56	.866
3	OT 3PU	-36.	-39.	27.8	-1.0	-27.	23.4	-54.	3.68	7.08	4.32	135	.12	.56	.964
4	1/4T3PU	-32.	-30.	27.2	12.3	-22.	29.3	-25.	2.05	3.95	.53	124	.12	.56	1.06
5	1/2T3PU	-43.	-34.	13.0	7.34	-33.	17.3	-33.	1.01	1.94	.17	95	.12	.56	1.23

AVE VALUE OF COMBINED ((SUM L3)/N;L3=L4*L5) CORRECTION FACTOR FOR ALL CAPSULES=.681
CORRECTION FACTOR'S AVERAGE VALUES: L4 = .681 L5 = 1 L6 = 1

SUM OF SQUARES (E-C) FOR EACH OF THE SEVEN EQUATIONS =
EQ1= 7802.127 EQ2= 7781.49 EQ3= 2912.446 EQ4= 345.833 EQ5= 4785.792

EQ6= 2333.1 EQ7= 7539.688

STANDARD DEVIATION OF FIT FOR EACH OF THE SEVEN EQUATIONS =
EQ1= 39.502 EQ2= 39.45 EQ3= 24.135 EQ4= 8.317 EQ5= 30.938 EQ6= 21.601 EQ7= 38.832

TABLE HEDL-31b

PSF CODE 3PU PLATE RESULTS WITH CORRECTION FOR FLUX-LEVEL EFFECT USING EQUATION (4M) DERIVED EQUATION (6b)

********** RESULTS FOR SEVEN EQUATIONS WITH CORRECTION FOR FLUX LEVEL EFFECT **********

CALCULATE TO MEASURED (C/E) CHARPY SHIFT(DEG.F) VALUES FOR SELECTED TREND CURVE EQNS.

J	CAPSULE	EQ.1	EQ.2	EQ.3	EQ.4	EQ.5	EQ.6	EQ.7	FLU.	FLUX	T/F	Cv(F)	CU%	NI%	CF
1	SSC13PU	1.24	1.26	.789	.937	1.18	.786	1.20	2.49	64.3	.67	110	.12	.56	.864
2	SSC23PU	1.07	1.09	.666	.909	1.02	.730	1.05	5.24	65.9	.64	146	.12	.56	.866
3	OT 3PU	1.22	1.24	.765	.971	1.15	.796	1.35	3.68	7.08	4.32	135	.12	.56	.964
4	1/4T3PU	1.34	1.33	.832	.960	1.25	.815	1.28	2.05	3.95	.53	124	.12	.56	1.06
5	1/2T3PU	1.79	1.68	1.06	1.14	1.67	1.01	1.66	1.01	1.94	.17	95	.12	.56	1.23

MEASURED - CALCULATED (E-C) CHARPY SHIFT(DEG.F) VALUES FOR SELECTED TREND CURVE EQNS.

J	CAPSULE	EQ.1	EQ.2	EQ.3	EQ.4	EQ.5	EQ.6	EQ.7	FLU.	FLUX	T/F	Cv(F)	CU%	NI%	CF
1	SSC13PU	-26.	-29.	23.1	6.90	-20.	23.5	-22.	2.49	64.3	.67	110	.12	.56	.864
2	SSC23PU	-10.	-13.	48.6	13.2	-3.8	39.3	-7.5	5.24	65.9	.64	146	.12	.56	.866
3	OT 3PU	-30.	-32.	31.6	3.82	-21.	27.4	-47.	3.68	7.08	4.32	135	.12	.56	.964
4	1/4T3PU	-42.	-41.	20.7	4.83	-31.	22.9	-35.	2.05	3.95	.53	124	.12	.56	1.06
5	1/2T3PU	-75.	-65.	-6.4	-13.	-64.	-1.0	-63.	1.01	1.94	.17	95	.12	.56	1.23

AVE VALUE OF COMBINED ((SUM L3)/N;L3=L4*L5) CORRECTION FACTOR FOR ALL CAPSULES=.681
CORRECTION FACTOR'S AVERAGE VALUES: L4 = .681 L5 = 1 L6 = 1

SUM OF SQUARES (E-C) FOR EACH OF SEVEN EQUATIONS =
EQ1= 9362.993 EQ2= 8112.011 EQ3= 4381.311 EQ4= 442.492 EQ5= 6032.51

EQ6= 3380.91 EQ7= 8105.583

STANDARD DEVIATION OF FIT FOR EACH OF SEVEN EQUATIONS =
EQ1= 43.274 EQ2= 40.279 EQ3= 29.602 EQ4= 9.407 EQ5= 34.735 EQ6= 26.003 EQ7= 40.263

THE R VALUES FOR EACH OF SEVEN EQUATIONS =

FOR I=1 TO 7 ; ********** EQN(I)*WITHOUT TO EQN(I)*WITH CORRECTION FOR FLUX LEVEL =
EQ1= -.834 EQ2= -.204 EQ3= -1.676 EQ4= -1.092 EQ5= -1.033 EQ6= -1.55 EQ7= -.349

THE R VALUES FOR EQN.2 TO EQN.1 AND FOR EQN.5 TO EQN.7 =

NO FLUX LEVEL CORRECTION **********: EQ2 TO EQ1= -.013
WITH FLUX LEVEL CORRECTION **********: EQ2 TO EQ1= -.668
NO FLUX LEVEL CORRECTION **********: EQ5 TO EQ7= -1.826
WITH FLUX LEVEL CORRECTION **********: EQ5 TO EQ7= -1.279

TABLE HEDL-32a

PSF CODE F23 PLATE RESULTS WITHOUT CORRECTION FOR FLUX-LEVEL EFFECT USING EQUATION (4M) DERIVED EQUATION (6b)

********** RESULTS FOR SEVEN EQUATIONS WITH NO CORRECTION FOR FLUX LEVEL EFFECT **********

CALCULATE TO MEASURED (C/E) CHARPY SHIFT(DEG.F) VALUES FOR SELECTED TREND CURVE EQNS.

J	CAPSULE	EQ.1	EQ.2	EQ.3	EQ.4	EQ.5	EQ.6	EQ.7	FLU.	FLUX	T/F	Cv(F)	CU%	NI%	CF
1	SSC1F23	.841	.918	.862	1.10	.825	.847	.801	2.72	70.3	.66	148	.2	.18	.879
2	SSC2F23	.838	.912	.839	1.24	.826	.914	.811	5.73	72	.63	169	.2	.18	.880
3	OT F23	.923	1.00	.930	1.27	.897	.959	1.00	4.03	7.76	4.29	146	.2	.18	.960
4	1/4TF23	1.01	1.07	1.01	1.26	.968	.976	.951	2.26	4.35	.52	122	.2	.18	1.05
5	1/2TF23	1.21	1.22	1.17	1.34	1.15	1.08	1.11	1.12	2.16	.16	90	.2	.18	1.22

MEASURED - CALCULATED (E-C) CHARPY SHIFT(DEG.F) VALUES FOR SELECTED TREND CURVE EQNS.

J	CAPSULE	EQ.1	EQ.2	EQ.3	EQ.4	EQ.5	EQ.6	EQ.7	FLU.	FLUX	T/F	Cv(F)	CU%	NI%	CF
1	SSC1F23	23.4	12.0	20.4	-15.	25.8	22.5	29.3	2.72	70.3	.66	148	.2	.18	.879
2	SSC2F23	27.3	14.7	27.1	-41.	29.3	14.4	31.8	5.73	72	.63	169	.2	.18	.880
3	OT F23	11.2	-.12	10.2	-40.	14.9	5.94	-.29	4.03	7.76	4.29	146	.2	.18	.960
4	1/4TF23	-1.4	-8.8	-1.2	-31.	3.87	2.88	5.96	2.26	4.35	.52	122	.2	.18	1.05
5	1/2TF23	-19.	-20.	-15.	-31.	-14.	-7.8	-10.	1.12	2.16	.16	90	.2	.18	1.22

AVE VALUE OF COMBINED ((SUM L3)/N;L3=L4*L5) CORRECTION FACTOR FOR ALL CAPSULES=.674
CORRECTION FACTOR'S AVERAGE VALUES: L4 = .674 L5 = 1 L6 = 1

SUM OF SQUARES (E-C) FOR EACH OF THE SEVEN EQUATIONS =
EQ1= 1814.899 EQ2= 850.124 EQ3= 1492.252 EQ4= 5621.376 EQ5= 1966.921

EQ6= 821.912 EQ7= 2019.93

STANDARD DEVIATION OF FIT FOR EACH OF THE SEVEN EQUATIONS =
EQ1= 19.052 EQ2= 13.039 EQ3= 17.276 EQ4= 33.53 EQ5= 19.834 EQ6= 12.821 EQ7= 20.099

TABLE HEDL-32b

PSF CODE F23 PLATE RESULTS WITH CORRECTION FOR FLUX-LEVEL EFFECT USING EQUATION (4M) DERIVED EQUATION (6b)

********** RESULTS FOR SEVEN EQUATIONS WITH CORRECTION FOR FLUX LEVEL EFFECT **********

CALCULATE TO MEASURED (C/E) CHARPY SHIFT(DEG.F) VALUES FOR SELECTED TREND CURVE EQNS.

J	CAPSULE	EQ.1	EQ.2	EQ.3	EQ.4	EQ.5	EQ.6	EQ.7	FLU.	FLUX	T/F	Cv(F)	CU%	NI%	CF
1	SSC1F23	.739	.807	.757	.973	.725	.745	.704	2.72	70.3	.66	148	.2	.18	.879
2	SSC2F23	.738	.803	.739	1.09	.727	.805	.714	5.73	72	.63	169	.2	.18	.880
3	OT F23	.886	.961	.893	1.22	.862	.921	.962	4.03	7.76	4.29	146	.2	.18	.960
4	1/4TF23	1.07	1.13	1.07	1.33	1.02	1.03	1.00	2.26	4.35	.52	122	.2	.18	1.05
5	1/2TF23	1.48	1.49	1.42	1.64	1.41	1.32	1.35	1.12	2.16	.16	90	.2	.18	1.22

MEASURED - CALCULATED (E-C) CHARPY SHIFT(DEG.F) VALUES FOR SELECTED TREND CURVE EQNS.

J	CAPSULE	EQ.1	EQ.2	EQ.3	EQ.4	EQ.5	EQ.6	EQ.7	FLU.	FLUX	T/F	Cv(F)	CU%	NI%	CF
1	SSC1F23	38.4	28.4	35.8	3.97	40.6	37.6	43.7	2.72	70.3	.66	148	.2	.18	.879
2	SSC2F23	44.2	33.1	44.0	-16.	45.9	32.8	48.2	5.73	72	.63	169	.2	.18	.880
3	OT F23	16.5	5.65	15.5	-33.	20.1	11.4	5.49	4.03	7.76	4.29	146	.2	.18	.960
4	1/4TF23	-8.7	-16.	-8.5	-40.	-3.0	-4.1	-.86	2.26	4.35	.52	122	.2	.18	1.05
5	1/2TF23	-43.	-44.	-38.	-58.	-37.	-29.	-32.	1.12	2.16	.16	90	.2	.18	1.22

AVE VALUE OF COMBINED ((SUM L3)/N;L3=L4*L5) CORRECTION FACTOR FOR ALL CAPSULES=.674
CORRECTION FACTOR'S AVERAGE VALUES: L4 = .674 L5 = 1 L6 = 1

SUM OF SQUARES (E-C) FOR EACH OF SEVEN EQUATIONS =
EQ1= 5719.9 EQ2= 4198.761 EQ3= 5023.836 EQ4= 6473.49 EQ5= 5552.836

EQ6= 3516.944 EQ7= 5309.119

STANDARD DEVIATION OF FIT FOR EACH OF SEVEN EQUATIONS =
EQ1= 33.823 EQ2= 28.978 EQ3= 31.698 EQ4= 35.982 EQ5= 33.325 EQ6= 26.521 EQ7= 32.586

THE R VALUES FOR EACH OF SEVEN EQUATIONS =

FOR I=1 TO 7 : ********** EQN(I)*WITHOUT TO EQN(I)*WITH CORRECTION FOR FLUX LEVEL =
EQ1= -3.414 EQ2= -3.988 EQ3= -3.515 EQ4= -.658 EQ5= -3.229 EQ6= -3.931 EQ7= -3.098

THE R VALUES FOR EQN.2 TO EQN.1 AND FOR EQN.5 TO EQN.7 =

NO FLUX LEVEL CORRECTION **********: EQ2 TO EQ1= -2.658
WITH FLUX LEVEL CORRECTION **********: EQ2 TO EQ1= -1.33
NO FLUX LEVEL CORRECTION **********: EQ5 TO EQ7= -.131
WITH FLUX LEVEL CORRECTION **********: EQ5 TO EQ7= .23

TABLE HEDL-33a

PSF CODE K FORGING RESULTS WITHOUT CORRECTION FOR FLUX-LEVEL EFFECT USING EQUATION (4M) DERIVED EQUATION (6b)

********** RESULTS FOR SEVEN EQUATIONS WITH NO CORRECTION FOR FLUX LEVEL EFFECT **********

CALCULATE TO MEASURED (C/E) CHARPY SHIFT(DEG.F) VALUES FOR SELECTED TREND CURVE EQNS.

J	CAPSULE		EQ.1	EQ.2	EQ.3	EQ.4	EQ.5	EQ.6	EQ.7	FLU.	FLUX	T/F	Cv(F)	CU%	NI%	CF
1	SSC1	K	2.13	2.12	.887	1.11	1.60	.820	1.89	1.73	44.7	1.06	110	.12	.96	.821
2	SSC2	K	1.61	1.61	.662	.931	1.19	.658	1.42	3.65	45.9	1.01	169	.12	.96	.822
3	OT	K	2.01	2.00	.826	1.11	1.48	.797	1.80	2.84	5.47	1.33	130	.12	.96	.972
4	1/4T	K	1.68	1.61	.677	.837	1.22	.622	1.41	1.52	2.93	.24	140	.12	.96	1.09
5	1/2T	K	2.03	1.83	.774	.903	1.48	.701	1.68	.729	1.4	.15	101	.12	.96	1.28

MEASURED - CALCULATED (E-C) CHARPY SHIFT(DEG.F) VALUES FOR SELECTED TREND CURVE EQNS.

J	CAPSULE		EQ.1	EQ.2	EQ.3	EQ.4	EQ.5	EQ.6	EQ.7	FLU.	FLUX	T/F	Cv(F)	CU%	NI%	CF
1	SSC1	K	-124	-123	12.4	-12.	-66.	19.7	-98.	1.73	44.7	1.06	110	.12	.96	.821
2	SSC2	K	-103	-103	57.0	11.5	-32.	57.7	-72.	3.65	45.9	1.01	169	.12	.96	.822
3	OT	K	-131	-130	22.5	-14.	-62.	26.2	-104	2.84	5.47	1.33	130	.12	.96	.972
4	1/4T	K	-95.	-86.	45.1	22.8	-32.	52.9	-57.	1.52	2.93	.24	140	.12	.96	1.09
5	1/2T	K	-104	-83.	22.7	9.76	-49.	30.1	-68.	.729	1.4	.15	101	.12	.96	1.28

AVE VALUE OF COMBINED ((SUM L3)/N;L3=L4*L5) CORRECTION FACTOR FOR ALL CAPSULES=.704
CORRECTION FACTOR'S AVERAGE VALUES: L4 = .704 L5 = 1 L6 = 1

SUM OF SQUARES (E-C) FOR EACH OF THE SEVEN EQUATIONS =
EQ1= 63599.206 EQ2= 57795.664 EQ3= 6480.953 EQ4= 1120.615 EQ5= 12822.014

EQ6= 8115.166 EQ7= 33909.375

STANDARD DEVIATION OF FIT FOR EACH OF THE SEVEN EQUATIONS =
EQ1= 112.782 EQ2= 107.513 EQ3= 36.003 EQ4= 14.971 EQ5= 50.64 EQ6= 40.287 EQ7= 82.352

TABLE HEDL-33b

PSF CODE K FORGING RESULTS WITH CORRECTION FOR FLUX-LEVEL EFFECT USING EQUATION (4M) DERIVED EQUATION (6b)

********** RESULTS FOR SEVEN EQUATIONS WITH CORRECTION FOR FLUX LEVEL EFFECT **********

CALCULATE TO MEASURED (C/E) CHARPY SHIFT(DEG.F) VALUES FOR SELECTED TREND CURVE EQNS.

J	CAPSULE		EQ.1	EQ.2	EQ.3	EQ.4	EQ.5	EQ.6	EQ.7	FLU.	FLUX	T/F	Cv(F)	CU%	NI%	CF
1	SSC1	K	1.75	1.74	.728	.914	1.31	.674	1.55	1.73	44.7	1.06	110	.12	.96	.821
2	SSC2	K	1.32	1.32	.544	.766	.980	.541	1.17	3.65	45.9	1.01	169	.12	.96	.822
3	QT	K	1.95	1.94	.804	1.08	1.44	.776	1.75	2.84	5.47	1.33	130	.12	.96	.972
4	1/4T	K	1.84	1.77	.742	.917	1.34	.681	1.54	1.52	2.93	.24	140	.12	.96	1.09
5	1/2T	K	2.62	2.35	.997	1.16	1.91	.903	2.16	.729	1.4	.15	101	.12	.96	1.28

MEASURED - CALCULATED (E-C) CHARPY SHIFT(DEG.F) VALUES FOR SELECTED TREND CURVE EQNS.

J	CAPSULE		EQ.1	EQ.2	EQ.3	EQ.4	EQ.5	EQ.6	EQ.7	FLU.	FLUX	T/F	Cv(F)	CU%	NI%	CF
1	SSC1	K	-82.	-82.	29.8	9.41	-34.	35.8	-61.	1.73	44.7	1.06	110	.12	.96	.821
2	SSC2	K	-54.	-55.	76.9	39.5	3.34	77.4	-29.	3.65	45.9	1.01	169	.12	.96	.822
3	QT	K	-124	-123	25.4	-10.	-57.	29.0	-98.	2.84	5.47	1.33	130	.12	.96	.972
4	1/4T	K	-117	-108	36.0	11.5	-48.	44.5	-76.	1.52	2.93	.24	140	.12	.96	1.09
5	1/2T	K	-163	-137	.268	-16.	-92.	9.73	-117	.729	1.4	.15	101	.12	.96	1.28

AVE VALUE OF COMBINED ((SUM L3)/N;L3=L4*L5) CORRECTION FACTOR FOR ALL CAPSULES=.704
CORRECTION FACTOR'S AVERAGE VALUES: L4 = .704 L5 = 1 L6 = 1

SUM OF SQUARES (E-C) FOR EACH OF SEVEN EQUATIONS =
EQ1= 66074.286 EQ2= 55645.931 EQ3= 8767.155 EQ4= 2173.33 EQ5= 15467.716

EQ6= 10214.697 EQ7= 33962.829

STANDARD DEVIATION OF FIT FOR EACH OF SEVEN EQUATIONS =
EQ1= 114.956 EQ2= 105.495 EQ3= 41.874 EQ4= 20.849 EQ5= 55.62 EQ6= 45.199 EQ7= 82.417

THE R VALUES FOR EACH OF SEVEN EQUATIONS =

FOR I=1 TO 7 ; ********** EQN(I)*WITHOUT TO EQN(I)*WITH CORRECTION FOR FLUX LEVEL =
EQ1= -.187 EQ2= .193 EQ3= -1.304 EQ4= -2.422 EQ5= -.855 EQ6= -1.028 EQ7= -8E-03

THE R VALUES FOR EQN.2 TO EQN.1 AND FOR EQN.5 TO EQN.7 =

NO FLUX LEVEL CORRECTION **********: EQ2 TO EQ1= -.456
WITH FLUX LEVEL CORRECTION **********: EQ2 TO EQ1= -.789
NO FLUX LEVEL CORRECTION **********: EQ5 TO EQ7= -3.109
WITH FLUX LEVEL CORRECTION **********: EQ5 TO EQ7= -2.723

TABLE HEDL-34a

PSF CODE MO FORGING RESULTS WITHOUT CORRECTION FOR FLUX-LEVEL EFFECT USING EQUATION (4M) DERIVED EQUATION (6b)

********** RESULTS FOR SEVEN EQUATIONS WITH NO CORRECTION FOR FLUX LEVEL EFFECT **********

CALCULATE TO MEASURED (C/E) CHARPY SHIFT(DEG.F) VALUES FOR SELECTED TREND CURVE EQNS.

J	CAPSULE	EQ.1	EQ.2	EQ.3	EQ.4	EQ.5	EQ.6	EQ.7	FLU.	FLUX	T/F	Cv(F)	CU%	NI%	CF
1	SSC1 MO	5.07	5.07	.432	.970	2.10	1.07	2.66	1.89	48.8	1.04	36	.05	.75	.834
2	SSC2 MO	3.01	3.02	.253	.654	1.23	.678	1.58	3.98	50	1	70	.05	.75	.835
3	OT MO	4.52	4.50	.379	.931	1.84	.985	2.39	3.11	5.99	1.32	45	.05	.75	.970
4	1/4T MO	5.11	4.92	.421	.926	2.06	1.03	2.54	1.67	3.21	.24	36	.05	.75	1.08
5	1/2T MO	6.47	5.85	.507	1.02	2.61	1.22	3.16	.821	1.58	.14	25	.05	.75	1.26

MEASURED - CALCULATED (E-C) CHARPY SHIFT(DEG.F) VALUES FOR SELECTED TREND CURVE EQNS.

J	CAPSULE	EQ.1	EQ.2	EQ.3	EQ.4	EQ.5	EQ.6	EQ.7	FLU.	FLUX	T/F	Cv(F)	CU%	NI%	CF
1	SSC1 MO	-146	-146	20.4	1.07	-39.	-2.5	-59.	1.89	48.8	1.04	36	.05	.75	.834
2	SSC2 MO	-141	-141	52.2	24.1	-16.	22.4	-40.	3.98	50	1	70	.05	.75	.835
3	OT MO	-158	-157	27.9	3.09	-38.	.661	-62.	3.11	5.99	1.32	45	.05	.75	.970
4	1/4T MO	-148	-141	20.8	2.64	-38.	-1.2	-55.	1.67	3.21	.24	36	.05	.75	1.08
5	1/2T MO	-136	-121	12.3	-.50	-40.	-5.5	-54.	.821	1.58	.14	25	.05	.75	1.26

AVE VALUE OF COMBINED ((SUM L3)/N;L3=L4*L5) CORRECTION FACTOR FOR ALL CAPSULES=.695
CORRECTION FACTOR'S AVERAGE VALUES: L4 = .695 L5 = 1 L6 = 1

SUM OF SQUARES (E-C) FOR EACH OF THE SEVEN EQUATIONS =
EQ1= 107138.928 EQ2= 101112.896 EQ3= 4510.478 EQ4= 603.497 EQ5= 6401.282

EQ6= 545.117 EQ7= 15218.006

STANDARD DEVIATION OF FIT FOR EACH OF THE SEVEN EQUATIONS =
EQ1= 146.382 EQ2= 142.206 EQ3= 30.035 EQ4= 10.986 EQ5= 35.781 EQ6= 10.441 EQ7= 55.169

TABLE HEDL-34b

PSF CODE MO FORGING RESULTS WITH CORRECTION FOR FLUX-LEVEL EFFECT
USING EQUATION (4M) DERIVED EQUATION (6b)

********** RESULTS FOR SEVEN EQUATIONS WITH CORRECTION FOR FLUX LEVEL EFFECT **********

CALCULATE TO MEASURED (C/E) CHARPY SHIFT(DEG.F) VALUES FOR SELECTED TREND CURVE EQNS.

J	CAPSULE	EQ.1	EQ.2	EQ.3	EQ.4	EQ.5	EQ.6	EQ.7	FLU.	FLUX	T/F	Cv(F)	CU%	NI%	CF
1	SSC1 MO	4.23	4.23	.361	.809	1.76	.894	2.22	1.89	48.8	1.04	36	.05	.75	.834
2	SSC2 MO	2.51	2.52	.211	.546	1.03	.567	1.32	3.98	50	1	70	.05	.75	.835
3	OT MO	4.38	4.36	.368	.903	1.79	.956	2.32	3.11	5.99	1.32	45	.05	.75	.970
4	1/4T MO	5.57	5.36	.459	1.00	2.24	1.12	2.76	1.67	3.21	.24	36	.05	.75	1.08
5	1/2T MO	8.21	7.43	.644	1.29	3.31	1.55	4.02	.821	1.58	.14	25	.05	.75	1.26

MEASURED - CALCULATED (E-C) CHARPY SHIFT(DEG.F) VALUES FOR SELECTED TREND CURVE EQNS.

J	CAPSULE	EQ.1	EQ.2	EQ.3	EQ.4	EQ.5	EQ.6	EQ.7	FLU.	FLUX	T/F	Cv(F)	CU%	NI%	CF
1	SSC1 MO	-116	-116	22.9	6.84	-27.	3.80	-43.	1.89	48.8	1.04	36	.05	.75	.834
2	SSC2 MO	-106	-106	55.1	31.7	-2.5	30.2	-22.	3.98	50	1	70	.05	.75	.835
3	OT MO	-152	-151	28.4	4.32	-35.	1.96	-59.	3.11	5.99	1.32	45	.05	.75	.970
4	1/4T MO	-164	-157	19.4	-.35	-44.	-4.5	-63.	1.67	3.21	.24	36	.05	.75	1.08
5	1/2T MO	-180	-160	8.89	-7.3	-57.	-13.	-75.	.821	1.58	.14	25	.05	.75	1.26

AVE VALUE OF COMBINED ((SUM L3)/N;L3=L4*L5) CORRECTION FACTOR FOR ALL CAPSULES=.695
CORRECTION FACTOR'S AVERAGE VALUES; L4 = .695 L5 = 1 L6 = 1

SUM OF SQUARES (E-C) FOR EACH OF SEVEN EQUATIONS =
EQ1= 107752.035 EQ2= 98375.783 EQ3= 4836.588 EQ4= 1126.438 EQ5= 7380.292

EQ6= 1146.695 EQ7= 15781.759

STANDARD DEVIATION OF FIT FOR EACH OF SEVEN EQUATIONS =
EQ1= 146.801 EQ2= 140.411 EQ3= 31.102 EQ4= 15.01 EQ5= 38.42 EQ6= 15.144 EQ7= 56.181

THE R VALUES FOR EACH OF SEVEN EQUATIONS =

FOR I=1 TO 7 ; ********** EQN(I)*WITHOUT TO EQN(I)*WITH CORRECTION FOR FLUX LEVEL =
EQ1= -.028 EQ2= .129 EQ3= -.337 EQ4= -2.321 EQ5= -.663 EQ6= -1.23 EQ7= -.179

THE R VALUES FOR EQN.2 TO EQN.1 AND FOR EQN.5 TO EQN.7 =

NO FLUX LEVEL CORRECTION **********; EQ2 TO EQ1= -.281
WITH FLUX LEVEL CORRECTION **********; EQ2 TO EQ1= -.426
NO FLUX LEVEL CORRECTION **********; EQ5 TO EQ7= -2.897
WITH FLUX LEVEL CORRECTION **********; EQ5 TO EQ7= -2.662

TABLE HEDL-35a

EQUATION (15) PSF CODE R WELD RESULTS WITHOUT CORRECTION* FOR FLUX-LEVEL COPPER DEPENDENCY USING EQUATION (16)

********** RESULTS FOR SEVEN EQUATIONS WITH NO CORRECTION FOR FLUX LEVEL EFFECT **********

CALCULATE TO MEASURED (C/E) CHARPY SHIFT(DEG.F) VALUES FOR SELECTED TREND CURVE EQNS.

J	CAPSULE		EQ.1	EQ.2	EQ.3	EQ.4	EQ.5	EQ.6	EQ.7	FLU.	FLUX	T/F	Cu(F)	CU%	NI%	CF
1	SSC1	R	1.04	1.06	.609	1.15	.874	.480	.970	2.52	65.1	.68	400	.23	1.58	.872
2	SSC2	R	.922	.932	.524	1.13	.768	.455	.862	5.31	66.7	.65	520	.23	1.58	.874
3	OT	R	.888	.895	.507	1.02	.732	.420	.935	3.85	7.41	4.31	515	.23	1.58	.965
4	1/4T	R	.910	.896	.514	.954	.739	.401	.829	2.19	4.22	.53	461	.23	1.58	1.06
5	1/2T	R	.869	.811	.472	.815	.700	.354	.769	1.1	2.12	.16	430	.23	1.58	1.22

MEASURED - CALCULATED (E-C) CHARPY SHIFT(DEG.F) VALUES FOR SELECTED TREND CURVE EQNS.

J	CAPSULE		EQ.1	EQ.2	EQ.3	EQ.4	EQ.5	EQ.6	EQ.7	FLU.	FLUX	T/F	Cu(F)	CU%	NI%	CF
1	SSC1	R	-19.	-25.	156.	-61.	50.3	207.	11.8	2.52	65.1	.68	400	.23	1.58	.872
2	SSC2	R	40.5	34.8	247.	-69.	120.	283.	71.2	5.31	66.7	.65	520	.23	1.58	.874
3	OT	R	57.4	53.9	253.	-15.	137.	298.	33.1	3.85	7.41	4.31	515	.23	1.58	.965
4	1/4T	R	41.1	47.9	223.	20.7	120.	276.	78.3	2.19	4.22	.53	461	.23	1.58	1.06
5	1/2T	R	55.9	81.2	226.	79.2	128.	277.	98.9	1.1	2.12	.16	430	.23	1.58	1.22

AVE VALUE OF COMBINED ((SUM L3)/N;L3=L4*L5) CORRECTION FACTOR FOR ALL CAPSULES=.675
CORRECTION FACTOR'S AVERAGE VALUES: L4 = .675 L5 = 1 L6 = 1

SUM OF SQUARES (E-C) FOR EACH OF THE SEVEN EQUATIONS =
EQ1= 10163.483 EQ2= 13685.679 EQ3= 251413.196 EQ4= 15442.692 EQ5= 66918.388

EQ6= 365646.793 EQ7= 22254.58

STANDARD DEVIATION OF FIT FOR EACH OF THE SEVEN EQUATIONS =
EQ1= 45.085 EQ2= 52.318 EQ3= 224.238 EQ4= 55.575 EQ5= 115.688 EQ6= 270.424 EQ7= 66.715

*EQ (6a)

NOTE: For comparing the Code R weld results of the EQ.ALL code using just the Eq.(6a) flux-level correction with the same results, but with the addition of the flux-level Cu dependency (Eq. (16), the std deviation of the fits in Tables HEDL-29b and -35b for Eq. (4M) must be used; these values are 9.233 and 4.245, respectively. This same procedure must be followed for the Codes EC, 3PU, F23, K, and MO steels, Tables HEDL-30 through -34 and Tables HEDL-36 through -40.

TABLE HEDL-35b

EQUATION (15) PSF CODE R WELD RESULTS WITH CORRECTION* FOR FLUX-LEVEL COPPER DEPENDENCY USING EQUATION (16)

********** RESULTS FOR SEVEN EQUATIONS WITH CORRECTION FOR FLUX LEVEL EFFECT **********

CALCULATE TO MEASURED (C/E) CHARPY SHIFT(DEG.F) VALUES FOR SELECTED TREND CURVE EQNS.

J	CAPSULE		EQ.1	EQ.2	EQ.3	EQ.4	EQ.5	EQ.6	EQ.7	FLU.	FLUX	T/F	Cv(F)	CU%	NI%	CF
1	SSC1	R	.916	.928	.532	1.00	.763	.419	.846	2.52	65.1	.68	400	.23	1.58	.872
2	SSC2	R	.806	.815	.458	.990	.672	.398	.754	5.31	66.7	.65	520	.23	1.58	.874
3	OT	R	.857	.864	.490	.993	.707	.405	.903	3.85	7.41	4.31	515	.23	1.58	.965
4	1/4T	R	.968	.952	.547	1.01	.786	.426	882	2.19	4.22	.53	461	.23	1.58	1.06
5	1/2T	R	1.06	.992	.578	.998	.857	.433	.942	1.1	2.12	.16	430	.23	1.58	1.22

MEASURED - CALCULATED (E-C) CHARPY SHIFT(DEG.F) VALUES FOR SELECTED TREND CURVE EQNS.

J	CAPSULE		EQ.1	EQ.2	EQ.3	EQ.4	EQ.5	EQ.6	EQ.7	FLU.	FLUX	T/F	Cv(F)	CU%	NI%	CF
1	SSC1	R	33.5	28.5	187.	-2.4	94.7	232.	61.2	2.52	65.1	.68	400	.23	1.58	.872
2	SSC2	R	100.	95.8	281.	4.85	170.	312.	127.	5.31	66.7	.65	520	.23	1.58	.874
3	OT	R	73.2	69.8	262.	3.17	150.	305.	49.7	3.85	7.41	4.31	515	.23	1.58	.965
4	1/4T	R	14.6	21.7	208.	-7.0	98.4	264.	54.1	2.19	4.22	.53	461	.23	1.58	1.06
5	1/2T	R	-27.	3.21	181.	.723	61.4	243.	24.8	1.1	2.12	.16	430	.23	1.58	1.22

AVE VALUE OF COMBINED ((SUM L3)/N;L3=L4*L5) CORRECTION FACTOR FOR ALL CAPSULES=.675
CORRECTION FACTOR'S AVERAGE VALUES: L4 = .675 L5 = 1 L6 = 1

SUM OF SQUARES (E-C) FOR EACH OF SEVEN EQUATIONS =
EQ1= 17622.364 EQ2= 15357.68 EQ3= 259752.959 EQ4= 90.116 EQ5= 74158.686
EQ6= 374529.675 EQ7= 26061.1

STANDARD DEVIATION OF FIT FOR EACH OF SEVEN EQUATIONS =
EQ1= 59.367 EQ2= 55.421 EQ3= 227.927 EQ4= 4.245 EQ5= 121.786 EQ6= 273.689 EQ7= 72.196

THE R VALUES FOR EACH OF SEVEN EQUATIONS =

FOR I=1 TO 7 : ********** EQN(I)*WITHOUT TO EQN(I)*WITH CORRECTION FOR FLUX LEVEL =
EQ1= -2.116 EQ2= -.544 EQ3= -.161 EQ4= 851.825 EQ5= -.488 EQ6= -.119 EQ7= -.73

THE R VALUES FOR EQN.2 TO EQN.1 AND FOR EQN.5 TO EQN.7 =

NO FLUX LEVEL CORRECTION **********: EQ2 TO EQ1= 1.733
WITH FLUX LEVEL CORRECTION **********: EQ2 TO EQ1= -.643
NO FLUX LEVEL CORRECTION **********: EQ5 TO EQ7= 10.035
WITH FLUX LEVEL CORRECTION **********: EQ5 TO EQ7= 9.228

*Eq. (6a)

TABLE HEDL-36a

EQUATION (15) PSF CODE EC WELD RESULTS WITHOUT CORRECTION*
FOR FLUX-LEVEL COPPER DEPENDENCY USING EQUATION (16)

********** RESULTS FOR SEVEN EQUATIONS WITH NO CORRECTION FOR FLUX LEVEL EFFECT **********

CALCULATE TO MEASURED (C/E) CHARPY SHIFT(DEG.F) VALUES FOR SELECTED TREND CURVE EQNS.

J	CAPSULE	EQ.1	EQ.2	EQ.3	EQ.4	EQ.5	EQ.6	EQ.7	FLU.	FLUX	T/F	Cv(F)	CU%	NI%	CF
1	SSC1 EC	1.05	1.07	1.06	.938	1.02	.908	1.01	1.75	45.2	1.07	194	.24	.64	.829
2	SSC2 EC	1.10	1.13	1.10	1.07	1.05	1.01	1.06	3.69	46.4	1.03	214	.24	.64	.830
3	OT EC	1.11	1.13	1.11	1.04	1.06	.997	1.09	2.97	5.72	1.33	205	.24	.64	.974
4	1/4T EC	1.22	1.20	1.19	1.05	1.15	1.02	1.12	1.62	3.12	.24	169	.24	.64	1.09
5	1/2T EC	1.14	1.05	1.05	.887	1.07	.884	1.03	.8	1.54	.14	160	.24	.64	1.27

MEASURED - CALCULATED (E-C) CHARPY SHIFT(DEG.F) VALUES FOR SELECTED TREND CURVE EQNS.

J	CAPSULE	EQ.1	EQ.2	EQ.3	EQ.4	EQ.5	EQ.6	EQ.7	FLU.	FLUX	T/F	Cv(F)	CU%	NI%	CF
1	SSC1 EC	-9.8	-14.	-11.	11.9	-4.0	17.7	-3.8	1.75	45.2	1.07	194	.24	.64	.829
2	SSC2 EC	-22.	-28.	-21.	-16.	-12.	-3.2	-14.	3.69	46.4	1.03	214	.24	.64	.830
3	OT EC	-23.	-28.	-22.	-10.	-12.	.597	-18.	2.97	5.72	1.33	205	.24	.64	.974
4	1/4T EC	-38.	-35.	-33.	-8.6	-26.	-3.4	-21.	1.62	3.12	.24	169	.24	.64	1.09
5	1/2T EC	-22.	-8.6	-8.9	18.0	-11.	18.4	-4.8	.8	1.54	.14	160	.24	.64	1.27

AVE VALUE OF COMBINED ((SUM L3)/N;L3=L4*L5) CORRECTION FACTOR FOR ALL CAPSULES=.697
CORRECTION FACTOR'S AVERAGE VALUES: L4 = .697 L5 = 1 L6 = 1

SUM OF SQUARES (E-C) FOR EACH OF THE SEVEN EQUATIONS =
EQ1= 3128.139 EQ2= 3114.14 EQ3= 2306.153 EQ4= 918.567 EQ5= 1171.916

EQ6= 677.007 EQ7= 1065.896

STANDARD DEVIATION OF FIT FOR EACH OF THE SEVEN EQUATIONS =
EQ1= 25.013 EQ2= 24.957 EQ3= 21.476 EQ4= 13.554 EQ5= 15.31 EQ6= 11.636 EQ7= 14.601

*Eq. (6a)

TABLE HEDL-36b

EQUATION (15) PSF CODE EC WELD RESULTS WITH CORRECTION*
FOR FLUX-LEVEL COPPER DEPENDENCY USING EQUATION (16)

********** RESULTS FOR SEVEN EQUATIONS WITH CORRECTION FOR FLUX LEVEL EFFECT **********

CALCULATE TO MEASURED (C/E) CHARPY SHIFT(DEG.F) VALUES FOR SELECTED TREND CURVE EQNS.

J	CAPSULE	EQ.1	EQ.2	EQ.3	EQ.4	EQ.5	EQ.6	EQ.7	FLU.	FLUX	T/F	Cu(F)	CU%	NI%	CF
1	SSC1 EC	.871	.889	.879	.778	.847	.753	.046	1.75	45.2	1.07	194	.24	.64	.829
2	SSC2 EC	.917	.941	.914	.894	.879	.843	.888	3.69	46.4	1.03	214	.24	.64	.830
3	OT EC	1.08	1.10	1.08	1.02	1.03	.972	1.06	2.97	5.72	1.33	205	.24	.64	.974
4	1/4T EC	1.33	1.32	1.30	1.14	1.26	1.11	1.22	1.62	3.12	.24	169	.24	.64	1.09
5	1/2T EC	1.45	1.34	1.34	1.12	1.36	1.12	1.31	.8	1.54	.14	160	.24	.64	1.27

MEASURED - CALCULATED (E-C) CHARPY SHIFT(DEG.F) VALUES FOR SELECTED TREND CURVE EQNS.

J	CAPSULE	EQ.1	EQ.2	EQ.3	EQ.4	EQ.5	EQ.6	EQ.7	FLU.	FLUX	T/F	Cu(F)	CU%	NI%	CF
1	SSC1 EC	24.8	21.3	23.3	42.9	29.6	47.7	29.8	1.75	45.2	1.07	194	.24	.64	.829
2	SSC2 EC	17.6	12.5	18.2	22.6	25.8	33.5	23.9	3.69	46.4	1.03	214	.24	.64	.830
3	OT EC	-17.	-22.	-16.	-4.7	-7.3	5.72	-13.	2.97	5.72	1.33	205	.24	.64	.974
4	1/4T EC	-57.	-54.	-51.	-25.	-44.	-19.	-38.	1.62	3.12	.24	169	.24	.64	1.09
5	1/2T EC	-72.	-54.	-55.	-20.	-58.	-20.	-49.	.8	1.54	.14	160	.24	.64	1.27

AVE VALUE OF COMBINED ((SUM L3)/N;L3=L4*L5) CORRECTION FACTOR FOR ALL CAPSULES=.697
CORRECTION FACTOR'S AVERAGE VALUES: L4 = .697 L5 = 1 L6 = 1

SUM OF SQUARES (E-C) FOR EACH OF SEVEN EQUATIONS =
EQ1= 9749.456 EQ2= 7015.135 EQ3= 6888.483 EQ4= 3428.738 EQ5= 7012.387

EQ6= 4222.199 EQ7= 5612.769

STANDARD DEVIATION OF FIT FOR EACH OF SEVEN EQUATIONS =
EQ1= 44.158 EQ2= 37.457 EQ3= 37.117 EQ4= 26.187 EQ5= 37.45 EQ6= 29.059 EQ7= 33.505

THE R VALUES FOR EACH OF SEVEN EQUATIONS =

FOR I=1 TO 7 : ********** EQN(I)*WITHOUT TO EQN(I)*WITH CORRECTION FOR FLUX LEVEL =
EQ1= -3.396 EQ2= -2.78 EQ3= -3.326 EQ4= -3.66 EQ5= -4.164 EQ6= -4.198 EQ7= -4.05

THE R VALUES FOR EQN.2 TO EQN.1 AND FOR EQN.5 TO EQN.7 =

NO FLUX LEVEL CORRECTION **********: EQ2 TO EQ1= -.022
WITH FLUX LEVEL CORRECTION **********: EQ2 TO EQ1= -1.402
NO FLUX LEVEL CORRECTION **********: EQ5 TO EQ7= .497
WITH FLUX LEVEL CORRECTION **********: EQ5 TO EQ7= 1.247

*Eq. (6a)

TABLE HEDL-37a

EQUATION (15) PSF CODE 3PU WELD RESULTS WITHOUT CORRECTION*
FOR FLUX-LEVEL COPPER DEPENDENCY USING EQUATION (16)

********** RESULTS FOR SEVEN EQUATIONS WITH NO CORRECTION FOR FLUX LEVEL EFFECT **********

CALCULATE TO MEASURED (C/E) CHARPY SHIFT(DEG.F) VALUES FOR SELECTED TREND CURVE EQNS.

J	CAPSULE	EQ.1	EQ.2	EQ.3	EQ.4	EQ.5	EQ.6	EQ.7	FLU.	FLUX	T/F	Cv(F)	CU%	NI%	CF
1	SSC13PU	1.43	1.46	.912	1.04	1.37	.908	1.39	2.49	64.3	.67	110	.12	.56	.864
2	SSC23PU	1.23	1.26	.769	1.17	1.18	.843	1.21	5.24	65.9	.64	146	.12	.56	.866
3	OT 3PU	1.27	1.28	.793	1.05	1.20	.826	1.40	3.68	7.08	4.32	135	.12	.56	.964
4	1/4T3PU	1.26	1.24	.780	.838	1.17	.763	1.20	2.05	3.95	.53	124	.12	.56	1.06
5	1/2T3PU	1.45	1.36	.863	.745	1.35	.817	1.34	1.01	1.94	.17	95	.12	.56	1.23

MEASURED - CALCULATED (E-C) CHARPY SHIFT(DEG.F) VALUES FOR SELECTED TREND CURVE EQNS.

J	CAPSULE	EQ.1	EQ.2	EQ.3	EQ.4	EQ.5	EQ.6	EQ.7	FLU.	FLUX	T/F	Cv(F)	CU%	NI%	CF
1	SSC13PU	-48.	-51.	9.58	-5.3	-41.	10.0	-43.	2.49	64.3	.67	110	.12	.56	.864
2	SSC23PU	-34.	-38.	33.6	-25.	-26.	22.8	-31.	5.24	65.9	.64	146	.12	.56	.866
3	OT 3PU	-36.	-39.	27.8	-6.9	-27.	23.4	-54.	3.68	7.08	4.32	135	.12	.56	.964
4	1/4T3PU	-32.	-30.	27.2	20.0	-22.	29.3	-25.	2.05	3.95	.53	124	.12	.56	1.06
5	1/2T3PU	-43.	-34.	13.0	24.1	-33.	17.3	-33.	1.01	1.94	.17	95	.12	.56	1.23

AVE VALUE OF COMBINED ((SUM L3)/N;L3=L4*L5) CORRECTION FACTOR FOR ALL CAPSULES=.681
CORRECTION FACTOR'S AVERAGE VALUES: L4 = .681 L5 = 1 L6 = 1

SUM OF SQUARES (E-C) FOR EACH OF THE SEVEN EQUATIONS =
EQ1= 7802.127 EQ2= 7781.49 EQ3= 2912.446 EQ4= 1691.101 EQ5= 4785.792

EQ6= 2333.1 EQ7= 7539.688

STANDARD DEVIATION OF FIT FOR EACH OF THE SEVEN EQUATIONS =
EQ1= 39.502 EQ2= 39.45 EQ3= 24.135 EQ4= 18.391 EQ5= 30.938 EQ6= 21.601 EQ7= 38.832

*Eq. (6a)

TABLE HEDL-37b

EQUATION (15) PSF CODE 3PU WELD RESULTS WITH CORRECTION*
FOR FLUX-LEVEL COPPER DEPENDENCY USING EQUATION (16)

********** RESULTS FOR SEVEN EQUATIONS WITH CORRECTION FOR FLUX LEVEL EFFECT **********

CALCULATE TO MEASURED (C/E) CHARPY SHIFT(DEG.F) VALUES FOR SELECTED TREND CURVE EQNS.

J	CAPSULE	EQ.1	EQ.2	EQ.3	EQ.4	EQ.5	EQ.6	EQ.7	FLU.	FLUX	T/F	Cv(F)	CU%	NI%	CF
1	SSC13PU	1.24	1.26	.789	.906	1.18	.786	1.20	2.49	64.3	.67	110	.12	.56	.864
2	SSC23PU	1.07	1.09	.666	1.01	1.02	.730	1.05	5.24	65.9	.64	146	.12	.56	.866
3	OT 3PU	1.22	1.24	.765	1.01	1.15	.796	1.35	3.68	7.08	4.32	135	.12	.56	.964
4	1/4T3PU	1.34	1.33	.832	.894	1.25	.815	1.28	2.05	3.95	.53	124	.12	.56	1.06
5	1/2T3PU	1.79	1.68	1.06	.922	1.67	1.01	1.66	1.01	1.94	.17	95	.12	.56	1.23

MEASURED - CALCULATED (E-C) CHARPY SHIFT(DEG.F) VALUES FOR SELECTED TREND CURVE EQNS.

J	CAPSULE	EQ.1	EQ.2	EQ.3	EQ.4	EQ.5	EQ.6	EQ.7	FLU.	FLUX	T/F	Cv(F)	CU%	NI%	CF
1	SSC13PU	-26.	-29.	23.1	10.2	-20.	23.5	-22.	2.49	64.3	.67	110	.12	.56	.864
2	SSC23PU	-10.	-13.	48.6	-2.2	-3.8	39.3	-7.5	5.24	65.9	.64	146	.12	.56	.866
3	OT 3PU	-30.	-32.	31.6	-1.8	-21.	27.4	-47.	3.68	7.08	4.32	135	.12	.56	.964
4	1/4T3PU	-42.	-41.	20.7	13.0	-31.	22.9	-35.	2.05	3.95	.53	124	.12	.56	1.06
5	1/2T3PU	-75.	-65.	-6.4	7.32	-64.	-1.0	-63.	1.01	1.94	.17	95	.12	.56	1.23

AVE VALUE OF COMBINED ((SUM L3)/N;L3=L4*L5) CORRECTION FACTOR FOR ALL CAPSULES=.681
CORRECTION FACTOR'S AVERAGE VALUES: L4 = .681 L5 = 1 L6 = 1

SUM OF SQUARES (E-C) FOR EACH OF SEVEN EQUATIONS =
EQ1= 9362.993 EQ2= 8112.011 EQ3= 4381.311 EQ4= 337.648 EQ5= 6032.51

EQ6= 3380.91 EQ7= 8105.583

STANDARD DEVIATION OF FIT FOR EACH OF SEVEN EQUATIONS =
EQ1= 43.274 EQ2= 40.279 EQ3= 29.602 EQ4= 8.218 EQ5= 34.735 EQ6= 26.003 EQ7= 40.263

THE R VALUES FOR EACH OF SEVEN EQUATIONS =

FOR I=1 TO 7 : ********** EQN(I)*WITHOUT TO EQN(I)*WITH CORRECTION FOR FLUX LEVEL =
EQ1= -.834 EQ2= -.204 EQ3= -1.676 EQ4= 20.042 EQ5= -1.033 EQ6= -1.55 EQ7= -.349

THE R VALUES FOR EQN.2 TO EQN.1 AND FOR EQN.5 TO EQN.7 =

NO FLUX LEVEL CORRECTION **********: EQ2 TO EQ1= -.013
WITH FLUX LEVEL CORRECTION **********: EQ2 TO EQ1= -.668
NO FLUX LEVEL CORRECTION **********: EQ5 TO EQ7= -1.826
WITH FLUX LEVEL CORRECTION **********: EQ5 TO EQ7= -1.279

*Eq. (6a)

TABLE HEDL-38a

EQUATION (15) PSF CODE F23 PLATE RESULTS WITHOUT CORRECTION*
FOR FLUX-LEVEL COPPER DEPENDENCY USING EQUATION (16)

********** RESULTS FOR SEVEN EQUATIONS WITH NO CORRECTION FOR FLUX LEVEL EFFECT **********

CALCULATE TO MEASURED (C/E) CHARPY SHIFT(DEG.F) VALUES FOR SELECTED TREND CURVE EQNS.

J	CAPSULE	EQ.1	EQ.2	EQ.3	EQ.4	EQ.5	EQ.6	EQ.7	FLU.	FLUX	T/F	Cv(F)	CU%	NI%	CF
1	SSC1F23	.841	.918	.862	1.02	.825	.847	.801	2.72	70.3	.66	148	.2	.18	.879
2	SSC2F23	.838	.912	.839	1.19	.826	.914	.811	5.73	72	.63	169	.2	.18	.880
3	OT F23	.923	1.00	.930	1.20	.897	.959	1.00	4.03	7.76	4.29	146	.2	.18	.960
4	1/4TF23	1.01	1.07	1.01	1.15	.968	.976	.951	2.26	4.35	.52	122	.2	.18	1.05
5	1/2TF23	1.21	1.22	1.17	1.18	1.15	1.08	1.11	1.12	2.16	.16	90	.2	.18	1.22

MEASURED - CALCULATED (E-C) CHARPY SHIFT(DEG.F) VALUES FOR SELECTED TREND CURVE EQNS.

J	CAPSULE	EQ.1	EQ.2	EQ.3	EQ.4	EQ.5	EQ.6	EQ.7	FLU.	FLUX	T/F	Cv(F)	CU%	NI%	CF
1	SSC1F23	23.4	12.0	20.4	-3.4	25.8	22.5	29.3	2.72	70.3	.66	148	.2	.18	.879
2	SSC2F23	27.3	14.7	27.1	-33.	29.3	14.4	31.8	5.73	72	.63	169	.2	.18	.880
3	OT F23	11.2	-.12	10.2	-30.	14.9	5.94	-.29	4.03	7.76	4.29	146	.2	.18	.960
4	1/4TF23	-1.4	-8.8	-1.2	-18.	3.87	2.88	5.96	2.26	4.35	.52	122	.2	.18	1.05
5	1/2TF23	-19.	-20.	-15.	-17.	-14.	-7.8	-10.	1.12	2.16	.16	90	.2	.18	1.22

AVE VALUE OF COMBINED ((SUM L3)/N;L3=L4*L5) CORRECTION FACTOR FOR ALL CAPSULES=.674
CORRECTION FACTOR'S AVERAGE VALUES: L4 = .674 L5 = 1 L6 = 1

SUM OF SQUARES (E-C) FOR EACH OF THE SEVEN EQUATIONS =
EQ1= 1814.899 EQ2= 850.124 EQ3= 1492.252 EQ4= 2688.065 EQ5= 1966.921

EQ6= 821.912 EQ7= 2019.93

STANDARD DEVIATION OF FIT FOR EACH OF THE SEVEN EQUATIONS =
EQ1= 19.052 EQ2= 13.039 EQ3= 17.276 EQ4= 23.186 EQ5= 19.834 EQ6= 12.821 EQ7= 20.099

*Eq. (6a)

TABLE HEDL-38b

EQUATION (15) PSF CODE F23 PLATE RESULTS WITH CORRECTION*
FOR FLUX-LEVEL COPPER DEPENDENCY USING EQUATION (16)

********** RESULTS FOR SEVEN EQUATIONS WITH CORRECTION FOR FLUX LEVEL EFFECT **********

CALCULATE TO MEASURED (C/E) CHARPY SHIFT(DEG.F) VALUES FOR SELECTED TREND CURVE EQNS.

J	CAPSULE	EQ.1	EQ.2	EQ.3	EQ.4	EQ.5	EQ.6	EQ.7	FLU.	FLUX	T/F	Cv(F)	CU%	NI%	CF
1	SSC1F23	.739	.807	.757	.899	.725	.745	.704	2.72	70.3	.66	148	.2	.18	.879
2	SSC2F23	.738	.803	.739	1.05	.727	.805	.714	5.73	72	.63	169	.2	.18	.880
3	OT F23	.886	.961	.893	1.16	.862	.921	.962	4.03	7.76	4.29	146	.2	.18	.960
4	1/4TF23	1.07	1.13	1.07	1.22	1.02	1.03	1.00	2.26	4.35	.52	122	.2	.18	1.05
5	1/2TF23	1.48	1.49	1.42	1.45	1.41	1.32	1.35	1.12	2.16	.16	90	.2	.18	1.22

MEASURED - CALCULATED (E-C) CHARPY SHIFT(DEG.F) VALUES FOR SELECTED TREND CURVE EQNS.

J	CAPSULE	EQ.1	EQ.2	EQ.3	EQ.4	EQ.5	EQ.6	EQ.7	FLU.	FLUX	T/F	Cv(F)	CU%	NI%	CF
1	SSC1F23	38.4	28.4	35.8	14.8	40.6	37.6	43.7	2.72	70.3	.66	148	.2	.18	.879
2	SSC2F23	44.2	33.1	44.0	-9.0	45.9	32.8	48.2	5.73	72	.63	169	.2	.18	.880
3	OT F23	16.5	5.65	15.5	-23.	20.1	11.4	5.49	4.03	7.76	4.29	146	.2	.18	.960
4	1/4TF23	-8.7	-16.	-8.5	-27.	-3.0	-4.1	-.86	2.26	4.35	.52	122	.2	.18	1.05
5	1/2TF23	-43.	-44.	-38.	-40.	-37.	-29.	-32.	1.12	2.16	.16	90	.2	.18	1.22

AVE VALUE OF COMBINED ((SUM L3)/N;L3=L4*L5) CORRECTION FACTOR FOR ALL CAPSULES=.674
CORRECTION FACTOR'S AVERAGE VALUES: L4 = .674 L5 = 1 L6 = 1

SUM OF SQUARES (E-C) FOR EACH OF SEVEN EQUATIONS =
EQ1= 5719.9 EQ2= 4198.761 EQ3= 5023.836 EQ4= 3252.834 EQ5= 5552.836

EQ6= 3516.944 EQ7= 5309.119

STANDARD DEVIATION OF FIT FOR EACH OF SEVEN EQUATIONS =
EQ1= 33.823 EQ2= 28.978 EQ3= 31.698 EQ4= 25.506 EQ5= 33.325 EQ6= 26.521 EQ7= 32.586

THE R VALUES FOR EACH OF SEVEN EQUATIONS =

FOR I=1 TO 7 ; ********** EQN(I)*WITHOUT TO EQN(I)*WITH CORRECTION FOR FLUX LEVEL =
EQ1= -3.414 EQ2= -3.988 EQ3= -3.515 EQ4= -.868 EQ5= -3.229 EQ6= -3.831 EQ7= -3.098

THE R VALUES FOR EQN.2 TO EQN.1 AND FOR EQN.5 TO EQN.7 =

NO FLUX LEVEL CORRECTION **********: EQ2 TO EQ1= -2.658
WITH FLUX LEVEL CORRECTION **********: EQ2 TO EQ1= -1.33
NO FLUX LEVEL CORRECTION **********: EQ5 TO EQ7= -.131
WITH FLUX LEVEL CORRECTION **********: EQ5 TO EQ7= .23

*Eq. (6a)

TABLE HEDL-39a

EQUATION (15) PSF CODE K FORGING RESULTS WITHOUT CORRECTION* FOR FLUX-LEVEL COPPER DEPENDENCY USING EQUATION (16)

********** RESULTS FOR SEVEN EQUATIONS WITH NO CORRECTION FOR FLUX LEVEL EFFECT **********

CALCULATE TO MEASURED (C/E) CHARPY SHIFT(DEG.F) VALUES FOR SELECTED TREND CURVE EQNS.

J	CAPSULE		EQ.1	EQ.2	EQ.3	EQ.4	EQ.5	EQ.6	EQ.7	FLU.	FLUX	T/F	Cv(F)	CU%	NI%	CF
1	SSC1	K	2.13	2.12	.887	1.07	1.60	.820	1.89	1.73	44.7	1.06	110	.12	.96	.821
2	SSC2	K	1.61	1.61	.662	1.04	1.19	.658	1.42	3.65	45.9	1.01	169	.12	.96	.822
3	OT	K	2.01	2.00	.826	1.18	1.48	.797	1.80	2.84	5.47	1.33	130	.12	.96	.972
4	1/4T	K	1.68	1.61	.677	.791	1.22	.622	1.41	1.52	2.93	.24	140	.12	.96	1.09
5	1/2T	K	2.03	1.83	.774	.738	1.48	.701	1.68	.729	1.4	.15	101	.12	.96	1.28

MEASURED - CALCULATED (E-C) CHARPY SHIFT(DEG.F) VALUES FOR SELECTED TREND CURVE EQNS.

J	CAPSULE		EQ.1	EQ.2	EQ.3	EQ.4	EQ.5	EQ.6	EQ.7	FLU.	FLUX	T/F	Cv(F)	CU%	NI%	CF
1	SSC1	K	-124	-123	12.4	-8.7	-66.	19.7	-98.	1.73	44.7	1.06	110	.12	.96	.821
2	SSC2	K	-103	-103	57.0	-7.4	-32.	57.7	-72.	3.65	45.9	1.01	169	.12	.96	.822
3	OT	K	-131	-130	22.5	-24.	-62.	26.2	-104	2.84	5.47	1.33	130	.12	.96	.972
4	1/4T	K	-95.	-86.	45.1	29.1	-32.	52.9	-57.	1.52	2.93	.24	140	.12	.96	1.09
5	1/2T	K	-104	-83.	22.7	26.4	-49.	30.1	-68.	.729	1.4	.15	101	.12	.96	1.28

AVE VALUE OF COMBINED ((SUM L3)/N;L3=L4*L5) CORRECTION FACTOR FOR ALL CAPSULES=.704
CORRECTION FACTOR'S AVERAGE VALUES: L4 = .704 L5 = 1 L6 = 1

SUM OF SQUARES (E-C) FOR EACH OF THE SEVEN EQUATIONS =
EQ1= 63599.206 EQ2= 57795.664 EQ3= 6480.953 EQ4= 2281.026 EQ5= 12822.014

EQ6= 8115.166 EQ7= 33909.375

STANDARD DEVIATION OF FIT FOR EACH OF THE SEVEN EQUATIONS =
EQ1= 112.782 EQ2= 107.513 EQ3= 36.003 EQ4= 21.359 EQ5= 50.64 EQ6= 40.287 EQ7= 82.352

*Eq. (6a)

TABLE HEDL-39b

EQUATION (15) PSF CODE K FORGING RESULTS WITH CORRECTION*
FOR FLUX-LEVEL COPPER DEPENDENCY USING EQUATION (16)

********** RESULTS FOR SEVEN EQUATIONS WITH CORRECTION FOR FLUX LEVEL EFFECT **********

CALCULATE TO MEASURED (C/E) CHARPY SHIFT(DEG.F) VALUES FOR SELECTED TREND CURVE EQNS.

J	CAPSULE		EQ.1	EQ.2	EQ.3	EQ.4	EQ.5	EQ.6	EQ.7	FLU.	FLUX	T/F	Cv(F)	CU%	NI%	CF
1	SSC1	K	1.75	1.74	.728	.887	1.31	.674	1.55	1.73	44.7	1.06	110	.12	.96	.821
2	SSC2	K	1.32	1.32	.544	.858	.980	.541	1.17	3.65	45.9	1.01	169	.12	.96	.822
3	OT	K	1.95	1.94	.804	1.15	1.44	.776	1.75	2.84	5.47	1.33	130	.12	.96	.972
4	1/4T	K	1.84	1.77	.742	.867	1.34	.681	1.54	1.52	2.93	.24	140	.12	.96	1.09
5	1/2T	K	2.62	2.35	.997	.950	1.41	.903	2.16	.729	1.4	.15	101	.12	.96	1.28

MEASURED - CALCULATED (E-C) CHARPY SHIFT(DEG.F) VALUES FOR SELECTED TREND CURVE EQNS.

J	CAPSULE		EQ.1	EQ.2	EQ.3	EQ.4	EQ.5	EQ.6	EQ.7	FLU.	FLUX	T/F	Cv(F)	CU%	NI%	CF
1	SSC1	K	-82.	-82.	29.8	12.4	-34.	35.8	-61.	1.73	44.7	1.06	110	.12	.96	.821
2	SSC2	K	-54.	-55.	76.9	23.9	3.34	77.4	-29.	3.65	45.9	1.01	169	.12	.96	.822
3	OT	K	-124	-123	25.4	-20.	-57.	29.0	-98.	2.84	5.47	1.33	130	.12	.96	.972
4	1/4T	K	-117	-108	36.0	18.5	-48.	44.5	-76.	1.52	2.93	.24	140	.12	.96	1.09
5	1/2T	K	-163	-137	.268	4.97	-92.	9.73	-117	.729	1.4	.15	101	.12	.96	1.28

AVE VALUE OF COMBINED ((SUM L3)/N;L3=L4*L5) CORRECTION FACTOR FOR ALL CAPSULES=.704
CORRECTION FACTOR'S AVERAGE VALUES: L4 = .704 L5 = 1 L6 = 1

SUM OF SQUARES (E-C) FOR EACH OF SEVEN EQUATIONS =
EQ1= 66074.286 EQ2= 55645.931 EQ3= 8767.155 EQ4= 1509.577 EQ5= 15467.716

EQ6= 10214.697 EQ7= 33962.829

STANDARD DEVIATION OF FIT FOR EACH OF SEVEN EQUATIONS =
EQ1= 114.956 EQ2= 105.495 EQ3= 41.874 EQ4= 17.376 EQ5= 55.62 EQ6= 45.199 EQ7= 82.417

THE R VALUES FOR EACH OF SEVEN EQUATIONS =

FOR I=1 TO 7 : ********** EQN(I)*WITHOUT TO EQN(I)*WITH CORRECTION FOR FLUX LEVEL =
EQ1= -.187 EQ2= .193 EQ3= -1.304 EQ4= 2.555 EQ5= -.855 EQ6= -1.028 EQ7= -8E-03

THE R VALUES FOR EQN.2 TO EQN.1 AND FOR EQN.5 TO EQN.7 =

NO FLUX LEVEL CORRECTION **********: EQ2 TO EQ1= -.456
WITH FLUX LEVEL CORRECTION **********: EQ2 TO EQ1= -.789
NO FLUX LEVEL CORRECTION **********: EQ5 TO EQ7= -3.109
WITH FLUX LEVEL CORRECTION **********: EQ5 TO EQ7= -2.723

*Eq. (6a)

TABLE HEDL-40a

EQUATION (15) PSF CODE MO FORGING RESULTS WITHOUT CORRECTION* FOR FLUX-LEVEL COPPER DEPENDENCY USING EQUATION (16)

********** RESULTS FOR SEVEN EQUATIONS WITH NO CORRECTION FOR FLUX LEVEL EFFECT **********

CALCULATE TO MEASURED (C/E) CHARPY SHIFT(DEG.F) VALUES FOR SELECTED TREND CURVE EQNS.

J	CAPSULE	EQ.1	EQ.2	EQ.3	EQ.4	EQ.5	EQ.6	EQ.7	FLU.	FLUX	T/F	Cv(F)	CU%	NI%	CF
1	SSC1 MO	5.07	5.07	.432	.946	2.10	1.07	2.66	1.89	48.8	1.04	36	.05	.75	.834
2	SSC2 MO	3.01	3.02	.253	.818	1.23	.670	1.58	3.98	50	1	70	.05	.75	.835
3	OT MO	4.52	4.50	.379	1.07	1.84	.985	2.39	3.11	5.99	1.32	45	.05	.75	.970
4	1/4T MO	5.11	4.92	.421	.865	2.06	1.03	2.54	1.67	3.21	.24	36	.05	.75	1.08
5	1/2T MO	6.47	5.85	.507	.727	2.61	1.22	3.16	.821	1.58	.14	25	.05	.75	1.26

MEASURED - CALCULATED (E-C) CHARPY SHIFT(DEG.F) VALUES FOR SELECTED TREND CURVE EQNS.

J	CAPSULE	EQ.1	EQ.2	EQ.3	EQ.4	EQ.5	EQ.6	EQ.7	FLU.	FLUX	T/F	Cv(F)	CU%	NI%	CF
1	SSC1 MO	-146	-146	20.4	1.94	-39.	-2.5	-59.	1.89	48.8	1.04	36	.05	.75	.834
2	SSC2 MO	-141	-141	52.2	12.6	-16.	22.4	-40.	3.98	50	1	70	.05	.75	.835
3	OT MO	-158	-157	27.9	-3.3	-38.	.661	-62.	3.11	5.99	1.32	45	.05	.75	.970
4	1/4T MO	-148	-141	20.8	4.85	-38.	-1.2	-55.	1.67	3.21	.24	36	.05	.75	1.08
5	1/2T MO	-136	-121	12.3	6.80	-40.	-5.5	-54.	.821	1.58	.14	25	.05	.75	1.26

AVE VALUE OF COMBINED ((SUM L3)/N;L3=L4*L5) CORRECTION FACTOR FOR ALL CAPSULES=.695
CORRECTION FACTOR'S AVERAGE VALUES: L4 = .695 L5 = 1 L6 = 1

SUM OF SQUARES (E-C) FOR EACH OF THE SEVEN EQUATIONS =
EQ1= 107138.928 EQ2= 101112.896 EQ3= 4510.478 EQ4= 245.588 EQ5= 6401.282

EQ6= 545.117 EQ7= 15218.006

STANDARD DEVIATION OF FIT FOR EACH OF THE SEVEN EQUATIONS =
EQ1= 146.382 EQ2= 142.206 EQ3= 30.035 EQ4= 7.008 EQ5= 35.781 EQ6= 10.441 EQ7= 55.169

*Eq. (6a)

TABLE HEDL-40b

EQUATION (15) PSF CODE MO FORGING RESULTS WITH CORRECTION*
FOR FLUX-LEVEL COPPER DEPENDENCY USING EQUATION (16)

********** RESULTS FOR SEVEN EQUATIONS WITH CORRECTION FOR FLUX LEVEL EFFECT **********

CALCULATE TO MEASURED (C/E) CHARPY SHIFT(DEG.F) VALUES FOR SELECTED TREND CURVE EQNS.

J	CAPSULE	EQ.1	EQ.2	EQ.3	EQ.4	EQ.5	EQ.6	EQ.7	FLU.	FLUX	T/F	Cv(F)	CU%	NI%	CF
1	SSC1 MO	4.23	4.23	.361	.789	1.76	.894	2.22	1.89	48.8	1.04	36	.05	.75	.834
2	SSC2 MO	2.51	2.52	.211	.684	1.03	.567	1.32	3.98	50	1	70	.05	.75	.835
3	OT MO	4.38	4.36	.368	1.04	1.79	.956	2.32	3.11	5.99	1.32	45	.05	.75	.970
4	1/4T MO	5.57	5.36	.459	.942	2.24	1.12	2.76	1.67	3.21	.24	36	.05	.75	1.08
5	1/2T MO	8.21	7.43	.644	.923	3.31	1.55	4.02	.821	1.58	.14	25	.05	.75	1.26

MEASURED - CALCULATED (E-C) CHARPY SHIFT(DEG.F) VALUES FOR SELECTED TREND CURVE EQNS.

J	CAPSULE	EQ.1	EQ.2	EQ.3	EQ.4	EQ.5	EQ.6	EQ.7	FLU.	FLUX	T/F	Cv(F)	CU%	NI%	CF
1	SSC1 MO	-116	-116	22.9	7.56	-27.	3.80	-43.	1.89	48.8	1.04	36	.05	.75	.834
2	SSC2 MO	-106	-106	55.1	22.0	-2.5	30.2	-22.	3.98	50	1	70	.05	.75	.835
3	OT MO	-152	-151	28.4	-1.9	-35.	1.96	-59.	3.11	5.99	1.32	45	.05	.75	.970
4	1/4T MO	-164	-157	19.4	2.05	-44.	-4.5	-63.	1.67	3.21	.24	36	.05	.75	1.08
5	1/2T MO	-180	-160	8.89	1.90	-57.	-13.	-75.	.821	1.58	.14	25	.05	.75	1.26

AVE VALUE OF COMBINED ((SUM L3)/N;L3=L4*L5) CORRECTION FACTOR FOR ALL CAPSULES=.695
CORRECTION FACTOR'S AVERAGE VALUES: L4 = .695 L5 = 1 L6 = 1

SUM OF SQUARES (E-C) FOR EACH OF SEVEN EQUATIONS =
EQ1= 107752.035 EQ2= 98575.783 EQ3= 4836.588 EQ4= 557.05 EQ5= 7380.292

EQ6= 1146.695 EQ7= 15781.759

STANDARD DEVIATION OF FIT FOR EACH OF SEVEN EQUATIONS =
EQ1= 146.801 EQ2= 140.411 EQ3= 31.102 EQ4= 10.555 EQ5= 38.42 EQ6= 15.144 EQ7= 56.181

THE R VALUES FOR EACH OF SEVEN EQUATIONS =

FOR I=1 TO 7 : ********** EQN(I)*WITHOUT TO EQN(I)*WITH CORRECTION FOR FLUX LEVEL =
EQ1= -.028 EQ2= .129 EQ3= -.337 EQ4= -2.796 EQ5= -.663 EQ6= -2.623 EQ7= -.179

THE R VALUES FOR EQN.2 TO EQN.1 AND FOR EQN.5 TO EQN.7 =

NO FLUX LEVEL CORRECTION **********: EQ2 TO EQ1= -.281
WITH FLUX LEVEL CORRECTION **********: EQ2 TO EQ1= -.426
NO FLUX LEVEL CORRECTION **********: EQ5 TO EQ7= -2.897
WITH FLUX LEVEL CORRECTION **********: EQ5 TO EQ7= -2.662

*Eq. (6a)

TABLE HEDL-41a

MAINE YANKEE (MY) SURVEILLANCE CAPSULE WELD RESULTS
WITHOUT CORRECTION FOR FLUX-LEVEL EFFECT
USING EQUATION (4M) DERIVED EQUATION (6b)

********** RESULTS FOR SEVEN EQUATIONS WITH NO CORRECTION FOR FLUX LEVEL EFFECT **********

CALCULATED TO MEASURED (C/E) CHARPY SHIFT(DEG.F) VALUES FOR SELECTED TREND CURVE EQNS.

J	CAPSULE	EQ.1	EQ.2	EQ.3	EQ.4	EQ.5	EQ.6	EQ.7	FLU.	FLUX	T/F	Cv(F)	CU%	NI%	CF
1	MY 1AC	1.02	1.04	1.15	.965	.986	.939	1.02	1.76	6.34	1.7	270	.36	.78	.777
2	MY 2AC	1.02	1.06	1.12	1.23	1.00	1.11	1.05	7.73	5.35	1.55	345	.36	.78	.799
3	MY W263	.901	.924	1.04	.804	.970	.831	1.08	.567	.39	4.71	222	.36	.78	1.42

MEASURED - CALCULATED (E-C) CHARPY SHIFT(DEG.F) VALUES FOR SELECTED TREND CURVE EQNS.

J	CAPSULE	EQ.1	EQ.2	EQ.3	EQ.4	EQ.5	EQ.6	EQ.7	FLU.	FLUX	T/F	Cv(F)	CU%	NI%	CF
1	MY 1AC	-6.3	-12.	-42.	9.40	3.63	16.4	-6.0	1.76	6.34	1.7	270	.36	.78	.777
2	MY 2AC	-9.1	-21.	-44.	-80.	-2.6	-38.	-19.	7.73	5.35	1.55	345	.36	.78	.799
3	MY W263	21.7	16.7	-9.3	43.3	6.46	37.3	-17.	.567	.39	4.71	222	.36	.78	1.42

AVE VALUE OF COMBINED ((SUM L3)/N;L3=L4*L5) CORRECTION FACTOR FOR ALL CAPSULES=.86
CORRECTION FACTOR'S AVERAGE VALUES: L4 = .86 L5 = 1 L6 = 1

SUM OF SQUARES (E-C) FOR EACH OF THE SEVEN EQUATIONS =
EQ1= 997.739 EQ2= 879.441 EQ3= 3915.224 EQ4= 8371.054 EQ5= 62.119

EQ6= 3165.404 EQ7= 721.809

STANDARD DEVIATION OF FIT FOR EACH OF THE SEVEN EQUATIONS =
EQ1= 14.115 EQ2= 17.122 EQ3= 36.126 EQ4= 52.824 EQ5= 4.55 EQ6= 32.483 EQ7= 15.511

TABLE HEDL-41b

MAINE YANKEE (MY) SURVEILLANCE CAPSULE WELD RESULTS WITH CORRECTION FOR FLUX-LEVEL EFFECT USING EQUATION (4M) DERIVED EQUATION (6b)

********** RESULTS FOR SEVEN EQUATIONS WITH CORRECTION FOR FLUX LEVEL EFFECT **********

CALCULATE TO MEASURED (C/E) CHARPY SHIFT(DEG.F) VALUES FOR SELECTED TREND CURVE EQNS.

J	CAPSULE	EQ.1	EQ.2	EQ.3	EQ.4	EQ.5	EQ.6	EQ.7	FLU.	FLUX	T/F	Cv(F)	CU%	NI%	CF
1	MY 1AC	.795	.813	.900	.750	.766	.729	.794	1.76	6.34	1.7	270	.36	.78	.777
2	MY 2AC	.821	.848	.903	.985	.806	.889	.844	7.73	5.35	1.55	345	.36	.78	.799
3	MY W263	1.28	1.31	1.48	1.14	1.38	1.18	1.53	.567	.39	4.71	222	.36	.78	1.42

MEASURED - CALCULATED (E-C) CHARPY SHIFT(DEG.F) VALUES FOR SELECTED TREND CURVE EQNS.

J	CAPSULE	EQ.1	EQ.2	EQ.3	EQ.4	EQ.5	EQ.6	EQ.7	FLU.	FLUX	T/F	Cv(F)	CU%	NI%	CF
1	MY 1AC	55.1	50.4	26.9	67.4	62.9	72.9	55.4	1.76	6.34	1.7	270	.36	.78	.777
2	MY 2AC	61.7	52.1	33.2	4.99	66.8	38.0	53.7	7.73	5.35	1.55	345	.36	.78	.799
3	MY W263	-62.	-70.	-107	-32.	-84.	-40.	-119	.567	.39	4.71	222	.36	.78	1.42

AVE VALUE OF COMBINED ((SUM L3)/N;L3=L4*L5) CORRECTION FACTOR FOR ALL CAPSULES=.86
CORRECTION FACTOR'S AVERAGE VALUES: L4 = .86 L5 = 1 L6 = 1

SUM OF SQUARES (E-C) FOR EACH OF SEVEN EQUATIONS =
EQ1= 10807.143 EQ2= 10170.68 EQ3= 13295.16 EQ4= 5611.638 EQ5= 15602.248

EQ6= 8419.961 EQ7= 20216.784

STANDARD DEVIATION OF FIT FOR EACH OF SEVEN EQUATIONS =
EQ1= 60.02 EQ2= 58.226 EQ3= 66.571 EQ4= 43.25 EQ5= 72.116 EQ6= 52.978 EQ7= 82.091

THE R VALUES FOR EACH OF SEVEN EQUATIONS =

FOR I=1 TO 7 : ********** EQN(I)*WITHOUT TO EQN(I)*WITH CORRECTION FOR FLUX LEVEL =
EQ1= -2.834 EQ2= -2.741 EQ3= -2.117 EQ4= 1.475 EQ5= -2.988 EQ6= -1.872 EQ7= -2.893

THE R VALUES FOR EQN.2 TO EQN.1 AND FOR EQN.5 TO EQN.7 =

NO FLUX LEVEL CORRECTION **********: EQ2 TO EQ1= 1.414
WITH FLUX LEVEL CORRECTION **********: EQ2 TO EQ1= -.177
NO FLUX LEVEL CORRECTION **********: EQ5 TO EQ7= -2.742
WITH FLUX LEVEL CORRECTION **********: EQ5 TO EQ7= -.685

TABLE HEDL-42a

PALISADES (PAL) SURVEILLANCE CAPSULE WELD RESULTS WITHOUT CORRECTION FOR FLUX-LEVEL EFFECT USING EQUATION (4M) DERIVED EQUATION (6b)

********** RESULTS FOR SEVEN EQUATIONS WITH NO CORRECTION FOR FLUX LEVEL EFFECT **********

CALCULATE TO MEASURED (C/E) CHARPY SHIFT(DEG.F) VALUES FOR SELECTED TREND CURVE EQNS.

J	CAPSULE	EQ.1	EQ.2	EQ.3	EQ.4	EQ.5	EQ.6	EQ.7	FLU.	FLUX	T/F	Cv(F)	CU%	NI%	CF
1	PAL 1AC	.945	.953	.785	1.18	.911	.732	.958	6.06	8.5	1.2	350	.24	.95	.749
2	PALWALL	.801	.810	.694	.813	.807	.546	.931	1.09	.695	4.81	290	.24	.95	1.25

MEASURED - CALCULATED (E-C) CHARPY SHIFT(DEG.F) VALUES FOR SELECTED TREND CURVE EQNS.

J	CAPSULE	EQ.1	EQ.2	EQ.3	EQ.4	EQ.5	EQ.6	EQ.7	FLU.	FLUX	T/F	Cv(F)	CU%	NI%	CF
1	PAL 1AC	19.1	16.2	75.1	-66.	31.1	93.6	14.3	6.06	8.5	1.2	350	.24	.95	.749
2	PALWALL	57.5	55.0	88.5	54.0	55.8	131.	19.7	1.09	.695	4.81	290	.24	.95	1.25

AVE VALUE OF COMBINED ((SUM L3)/N;L3=L4*L5) CORRECTION FACTOR FOR ALL CAPSULES=.853
CORRECTION FACTOR'S AVERAGE VALUES: L4 = .853 L5 = 1 L6 = 1

SUM OF SQUARES (E-C) FOR EACH OF THE SEVEN EQUATIONS =
EQ1= 3678.71 EQ2= 3299.704 EQ3= 13491.058 EQ4= 7313.304 EQ5= 4086.667

EQ6= 26048.697 EQ7= 596.635

STANDARD DEVIATION OF FIT FOR EACH OF THE SEVEN EQUATIONS =
EQ1= 42.888 EQ2= 40.618 EQ3= 82.131 EQ4= 60.47 EQ5= 45.203 EQ6= 114.124 EQ7= 17.272

TABLE HEDL-42b

PALISADES (PAL) SURVEILLANCE CAPSULE WELD RESULTS WITH CORRECTION FOR FLUX-LEVEL EFFECT USING EQUATION (4M) DERIVED EQUATION (6b)

********** RESULTS FOR SEVEN EQUATIONS WITH CORRECTION FOR FLUX LEVEL EFFECT **********

CALCULATE TO MEASURED (C/E) CHARPY SHIFT(DEG.F) VALUES FOR SELECTED TREND CURVE EQNS.

J	CAPSULE	EQ.1	EQ.2	EQ.3	EQ.4	EQ.5	EQ.6	EQ.7	FLU.	FLUX	T/F	Cv(F)	CU%	NI%	CF
1	PAL IAC	.708	.714	.588	.891	.682	.548	.718	6.06	8.5	1.2	350	.24	.95	.749
2	PALWALL	1.00	1.01	.868	1.01	1.00	.683	1.16	1.09	.695	4.81	290	.24	.95	1.25

MEASURED - CALCULATED (E-C) CHARPY SHIFT(DEG.F) VALUES FOR SELECTED TREND CURVE EQNS.

J	CAPSULE	EQ.1	EQ.2	EQ.3	EQ.4	EQ.5	EQ.6	EQ.7	FLU.	FLUX	T/F	Cv(F)	CU%	NI%	CF
1	PAL IAC	102.	99.9	144.	38.1	111.	157.	98.5	6.06	8.5	1.2	350	.24	.95	.749
2	PALWALL	-.74	-3.8	38.0	-5.1	-2.8	91.6	-48.	1.09	.695	4.81	290	.24	.95	1.25

AVE VALUE OF COMBINED ((SUM L3)/N;L3=L4*L5) CORRECTION FACTOR FOR ALL CAPSULES=.853
CORRECTION FACTOR'S AVERAGE VALUES: L4 = .853 L5 = 1 L6 = 1

SUM OF SQUARES (E-C) FOR EACH OF SEVEN EQUATIONS =
EQ1= 10429.65 EQ2= 10011.207 EQ3= 22201.345 EQ4= 1479.698 EQ5= 12348.948

EQ6= 33352.431 EQ7= 12019.962

STANDARD DEVIATION OF FIT FOR EACH OF SEVEN EQUATIONS =
EQ1= 72.21 EQ2= 70.75 EQ3= 105.36 EQ4= 27.2 EQ5= 78.578 EQ6= 129.136 EQ7= 77.524

THE R VALUES FOR EACH OF SEVEN EQUATIONS =

FOR I=1 TO 7 ; ********** EQN(I)*WITHOUT TO EQN(I)*WITH CORRECTION FOR FLUX LEVEL =
EQ1= -1.294 EQ2= -1.341 EQ3= -.785 EQ4= 7.885 EQ5= -1.338 EQ6= -.438 EQ7= -1.901

THE R VALUES FOR EQN.2 TO EQN.1 AND FOR EQN.5 TO EQN.7 =

NO FLUX LEVEL CORRECTION **********: EQ2 TO EQ1= -.206
WITH FLUX LEVEL CORRECTION **********: EQ2 TO EQ1= -.08
NO FLUX LEVEL CORRECTION **********: EQ5 TO EQ7= 11.699
WITH FLUX LEVEL CORRECTION **********: EQ5 TO EQ7= .055

TABLE HEDL-43a

POINT BEACH 1 (PB1) SURVEILLANCE CAPSULE WELD RESULTS WITHOUT CORRECTION FOR FLUX-LEVEL EFFECT USING EQUATION (4M) DERIVED EQUATION (6b)

********** RESULTS FOR SEVEN EQUATIONS WITH NO CORRECTION FOR FLUX LEVEL EFFECT **********

CALCULATE TO MEASURED (C/E) CHARPY SHIFT(DEG.F) VALUES FOR SELECTED TREND CURVE EQNS.

J	CAPSULE		EQ.1	EQ.2	EQ.3	EQ.4	EQ.5	EQ.6	EQ.7	FLU.	FLUX	T/F	Cv(F)	CU%	NI%	CF
1	PB1	R	1.11	1.16	1.11	1.18	1.10	.995	1.11	2.17	1.4	1.24	165	.21	.57	.942
2	PB1	S	.885	.919	.888	.864	.931	.765	.913	.851	.73	1.42	165	.21	.57	1.09
3	PB1	V	1.00	1.02	1.00	.959	1.12	.895	1.10	.35	1.29	2.31	110	.21	.57	.960

MEASURED - CALCULATED (E-C) CHARPY SHIFT(DEG.F) VALUES FOR SELECTED TREND CURVE EQNS.

J	CAPSULE		EQ.1	EQ.2	EQ.3	EQ.4	EQ.5	EQ.6	EQ.7	FLU.	FLUX	T/F	Cv(F)	CU%	NI%	CF
1	PB1	R	-1?.	-27.	-18.	-30.	-17.	.754	-18.	2.17	1.4	1.24	165	.21	.57	.942
2	PB1	S	18.8	13.2	18.3	22.4	11.3	38.6	14.3	.851	.73	1.42	165	.21	.57	1.09
3	PB1	V	-.54	-3.0	-.29	4.43	-13.	11.4	-11.	.35	1.29	2.31	110	.21	.57	.960

AVE VALUE OF COMBINED ((SUM L3)/N;L3=L4*L5) CORRECTION FACTOR FOR ALL CAPSULES=.962
CORRECTION FACTOR'S AVERAGE VALUES: L4 = .962 L5 = 1 L6 = 1

SUM OF SQUARES (E-C) FOR EACH OF THE SEVEN EQUATIONS =
EQ1= 736.8 EQ2= 967.67? EQ3= 673.078 EQ4= 1430.142 EQ5= 605.061

EQ6= 1623.641 EQ7= 692.56

STANDARD DEVIATION OF FIT FOR EACH OF THE SEVEN EQUATIONS =
EQ1= 15.672 EQ2= 17.96 EQ3= 14.979 EQ4= 21.834 EQ5= 14.202 EQ6= 23.264 EQ7= 15.194

TABLE HEDL-43b

POINT BEACH 1 (PB1) SURVEILLANCE CAPSULE WELD RESULTS WITH CORRECTION FOR FLUX-LEVEL EFFECT USING EQUATION (4M) DERIVED EQUATION (6b)

********** RESULTS FOR SEVEN EQUATIONS WITH CORRECTION FOR FLUX LEVEL EFFECT **********

CALCULATE TO MEASURED (C/E) CHARPY SHIFT(DEG.F) VALUES FOR SELECTED TREND CURVE EQNS.

J	CAPSULE		EQ.1	EQ.2	EQ.3	EQ.4	EQ.5	EQ.6	EQ.7	FLU.	FLUX	T/F	Cu(F)	CU%	NI%	CF
1	PB1	R	1.05	1.10	1.04	1.1[illegible]	1.03	.938	1.04	2.17	1.4	1.24	165	.21	.57	.942
2	PB1	S	.971	1.00	.974	.947	1.02	.840	1.00	.851	.73	1.42	165	.21	.57	1.09
3	PB1	V	.965	.987	.963	.921	1.08	.860	1.06	.35	1.29	2.31	110	.21	.57	.960

MEASURED - CALCULATED (E-C) CHARPY SHIFT(DEG.F) VALUES FOR SELECTED TREND CURVE EQNS.

J	CAPSULE		EQ.1	EQ.2	EQ.3	EQ.4	EQ.5	EQ.6	EQ.7	FLU.	FLUX	T/F	Cu(F)	CU%	NI%	CF
1	PB1	R	-8.9	-16.	-7.[illegible]	-18.	-6.5	10.1	-8.1	2.17	1.4	1.24	165	.21	.57	.942
2	PB1	S	4.71	-1.4	4.18	8.60	-3.5	26.3	-.24	.851	.73	1.42	165	.21	.57	1.09
3	PB1	V	3.82	1.41	4.05	8.60	-8.8	15.3	-6.9	.35	1.29	2.31	110	.21	.57	.960

AVE VALUE OF COMBINED ((SUM L3)/N;L3=L4*L5) CORRECTION FACTOR FOR ALL CAPSULES= .962
CORRECTION FACTOR'S AVERAGE VALUES: L4 = .962 L5 = 1 L6 = 1

SUM OF SQUARES (E-C) FOR EACH OF SEVEN EQUATIONS =
EQ1= 116.866 EQ2= 290.501 EQ3= 95.046 EQ4= 507.666 EQ5= 133.894

EQ6= 1035.519 EQ7= 114.958

STANDARD DEVIATION OF FIT FOR EACH OF SEVEN EQUATIONS =
EQ1= 6.241 EQ2= 9.84 EQ3= 5.629 EQ4= 13.009 EQ5= 6.681 EQ6= 18.579 EQ7= 6.19

THE R VALUES FOR EACH OF SEVEN EQUATIONS =

FOR I=1 TO 7 : ********** EQN(I)*WITHOUT TO EQN(I)*WITH CORRECTION FOR FLUX LEVEL =
EQ1= 15.914 EQ2= 6.993 EQ3= 18.245 EQ4= 5.451 EQ5= 10.557 EQ6= 1.704 EQ7= 15.073

THE R VALUES FOR EQN.2 TO EQN.1 AND FOR EQN.5 TO EQN.7 =

NO FLUX LEVEL CORRECTION **********: EQ2 TO EQ1= .94
WITH FLUX LEVEL CORRECTION **********: EQ2 TO EQ1= 4.457
NO FLUX LEVEL CORRECTION **********: EQ5 TO EQ7= -.379
WITH FLUX LEVEL CORRECTION **********: EQ5 TO EQ7= .494

TABLE HEDL-44a

POINT BEACH 2 (PB2) SURVEILLANCE CAPSULE WELD RESULTS WITHOUT CORRECTION FOR FLUX-LEVEL EFFECT USING EQUATION (4M) DERIVED EQUATION (6b)

********** RESULTS FOR SEVEN EQUATIONS WITH NO CORRECTION FOR FLUX LEVEL EFFECT **********

CALCULATE TO MEASURED (C/E) CHARPY SHIFT(DEG.F) VALUES FOR SELECTED TREND CURVE EQNS.

J	CAPSULE		EQ.1	EQ.2	EQ.3	EQ.4	EQ.5	EQ.6	EQ.7	FLU.	FLUX	T/F	Cv(F)	CU%	NI%	CF
1	PB2	R	.895	.941	.956	.980	.877	.847	.912	2.54	1.54	1.87	235	.25	.59	.953
2	PB2	T	1.10	1.15	1.19	1.10	1.15	1.00	1.14	.947	.86	1.57	150	.25	.59	1.09
3	PB2	V	.934	.974	1.01	.922	.997	.852	.969	.733	1.52	1.5	165	.25	.59	.956

MEASURED - CALCULATED (E-C) CHARPY SHIFT(DEG.F) VALUES FOR SELECTED TREND CURVE EQNS.

J	CAPSULE		EQ.1	EQ.2	EQ.3	EQ.4	EQ.5	EQ.6	EQ.7	FLU.	FLUX	T/F	Cv(F)	CU%	NI%	CF
1	PB2	R	24.5	13.7	10.2	4.53	28.7	35.8	20.6	2.54	1.54	1.87	235	.25	.59	.953
2	PB2	T	-15.	-23.	-29.	-15.	-22.	-1.0	-21.	.947	.86	1.57	150	.25	.59	1.09
3	PB2	V	10.8	4.13	-2.1	12.8	.358	24.3	5.11	.733	1.52	1.5	165	.25	.59	.956

AVE VALUE OF COMBINED ((SUM L3)/N;L3=L4*L5) CORRECTION FACTOR FOR ALL CAPSULES=.931
CORRECTION FACTOR'S AVERAGE VALUES: L4 = .931 L5 = 1 L6 = 1

SUM OF SQUARES (E-C) FOR EACH OF THE SEVEN EQUATIONS =
EQ1= 971.175 EQ2= 762.037 EQ3= 993.3 EQ4= 435.459 EQ5= 1339.1

EQ6= 1880.246 EQ7= 924.966

STANDARD DEVIATION OF FIT FOR EACH OF THE SEVEN EQUATIONS =
EQ1= 17.992 EQ2= 15.938 EQ3= 18.196 EQ4= 12.048 EQ5= 21.127 EQ6= 25.035 EQ7= 17.559

TABLE HEDL-44b

POINT BEACH 2 (PB2) SURVEILLANCE CAPSULE WELD RESULTS WITH CORRECTION FOR FLUX-LEVEL EFFECT USING EQUATION (4M) DERIVED EQUATION (6b)

********** RESULTS FOR SEVEN EQUATIONS WITH CORRECTION FOR FLUX LEVEL EFFECT **********

CALCULATE TO MEASURED (C/E) CHARPY SHIFT(DEG.F) VALUES FOR SELECTED TREND CURVE EQNS.

J	CAPSULE		EQ.1	EQ.2	EQ.3	EQ.4	EQ.5	EQ.6	EQ.7	FLU.	FLUX	T/F	Cv(F)	CU%	NI%	CF
1	PB2	R	.853	.897	.911	.934	.836	.807	.869	2.54	1.54	1.87	235	.25	.59	.953
2	PB2	T	1.20	1.26	1.30	1.20	1.25	1.09	1.24	.947	.86	1.57	150	.25	.59	1.09
3	PB2	V	.893	.932	.968	.881	.954	.814	.926	.733	1.52	1.5	165	.25	.59	.956

MEASURED - CALCULATED (E-C) CHARPY SHIFT(DEG.F) VALUES FOR SELECTED TREND CURVE EQNS.

J	CAPSULE		EQ.1	EQ.2	EQ.3	EQ.4	EQ.5	EQ.6	EQ.7	FLU.	FLUX	T/F	Cv(F)	CU%	NI%	CF
1	PB2	R	34.4	24.0	20.7	15.2	38.3	45.1	30.6	2.54	1.54	1.87	235	.25	.59	.953
2	PB2	T	-30.	-39.	-46.	-30.	-38.	-14.	-37.	.947	.86	1.57	150	.25	.59	1.09
3	PB2	V	17.5	11.1	5.14	19.5	7.57	30.5	12.1	.733	1.52	1.5	165	.25	.59	.956

AVE VALUE OF COMBINED ((SUM L3)/N;L3=L4*L5) CORRECTION FACTOR FOR ALL CAPSULES=.931
CORRECTION FACTOR'S AVERAGE VALUES: L4 = .931 L5 = 1 L6 = 1

SUM OF SQUARES (E-C) FOR EACH OF SEVEN EQUATIONS =
EQ1= 2441.787 EQ2= 2248.485 EQ3= 2571.656 EQ4= 1564.204 EQ5= 2995.071

EQ6= 3188.284 EQ7= 2476.927

STANDARD DEVIATION OF FIT FOR EACH OF SEVEN EQUATIONS =
EQ1= 28.529 EQ2= 27.377 EQ3= 29.278 EQ4= 22.834 EQ5= 31.597 EQ6= 32.6 EQ7= 28.734

THE R VALUES FOR EACH OF SEVEN EQUATIONS =

FOR I=1 TO 7 : ********** EQN(I)*WITHOUT TO EQN(I)*WITH CORRECTION FOR FLUX LEVEL =
EQ1= -1.807 EQ2= -1.983 EQ3= -1.841 EQ4= -2.165 EQ5= -1.659 EQ6= -1.231 EQ7= -1.88

THE R VALUES FOR EQN.2 TO EQN.1 AND FOR EQN.5 TO EQN.7 =

NO FLUX LEVEL CORRECTION **********: EQ2 TO EQ1= -.646
WITH FLUX LEVEL CORRECTION **********: EQ2 TO EQ1= -.237
NO FLUX LEVEL CORRECTION **********: EQ5 TO EQ7= 1.343
WITH FLUX LEVEL CORRECTION **********: EQ5 TO EQ7= .628

TABLE HEDL-45a

INDIAN POINT 2 (IP2) AND INDIAN POINT 3 (IP3) SURVEILLANCE CAPSULE WELD RESULTS WITHOUT CORRECTION FOR FLUX-LEVEL EFFECT USING EQUATION (4M) DERIVED EQUATION (6b)

********** RESULTS FOR SEVEN EQUATIONS WITH NO CORRECTION FOR FLUX LEVEL EFFECT **********

CALCULATE TO MEASURED (C/E) CHARPY SHIFT(DEG.F) VALUES FOR SELECTED TREND CURVE EQNS.

J	CAPSULE		EQ.1	EQ.2	EQ.3	EQ.4	EQ.5	EQ.6	EQ.7	FLU.	FLUX	T/F	Cv(F)	CU%	NI%	CF
1	IP3	T	.832	.819	.863	.762	.887	.767	.792	.323	.77	.97	137	.24	.52	1.05
2	IP3	T	.967	.951	1.00	.885	1.02	.891	.919	.323	.77	.97	118	.24	.52	1.05
3	IP2	Y	1.12	1.15	1.14	1.36	1.22	.944	1.17	.589	1.5	1.5	145	.25	.73	.899

MEASURED - CALCULATED (E-C) CHARPY SHIFT(DEG.F) VALUES FOR SELECTED TREND CURVE EQNS.

J	CAPSULE		EQ.1	EQ.2	EQ.3	EQ.4	EQ.5	EQ.6	EQ.7	FLU.	FLUX	T/F	Cv(F)	CU%	NI%	CF
1	IP3	T	22.8	24.6	18.7	32.5	15.4	31.8	28.4	.323	.77	.97	137	.24	.52	1.05
2	IP3	T	3.88	5.69	-.23	13.5	-3.5	12.8	9.48	.323	.77	.97	118	.24	.52	1.05
3	IP2	Y	-17.	-22.	-20.	-52.	-32.	8.01	-24.	.589	1.5	1.5	145	.25	.73	.899

AVE VALUE OF COMBINED ((SUM L3)/N;L3=L4*L5) CORRECTION FACTOR FOR ALL CAPSULES=.992
CORRECTION FACTOR'S AVERAGE VALUES: L4 = .992 L5 = 1 L6 = 1

SUM OF SQUARES (E-C) FOR EACH OF THE SEVEN EQUATIONS =
EQ1= 857.605 EQ2= 1163.406 EQ3= 789.658 EQ4= 3997.9 EQ5= 1332.123

EQ6= 1243.91 EQ7= 1519.04

STANDARD DEVIATION OF FIT FOR EACH OF THE SEVEN EQUATIONS =
EQ1= 16.908 EQ2= 19.693 EQ3= 16.224 EQ4= 36.505 EQ5= 21.072 EQ6= 20.363 EQ7= 22.502

TABLE HEDL-45b

INDIAN POINT 2 (IP2) AND INDIAN POINT 3 (IP3) SURVEILLANCE CAPSULE WELD RESULTS WITH CORRECTION FOR FLUX-LEVEL EFFECT USING EQUATION (4M) DERIVED EQUATION (6b)

********** RESULTS FOR SEVEN EQUATIONS WITH CORRECTION FOR FLUX LEVEL EFFECT **********

CALCULATE TO MEASURED (C/E) CHARPY SHIFT(DEG.F) VALUES FOR SELECTED TREND CURVE EQNS.

J	CAPSULE		EQ.1	EQ.2	EQ.3	EQ.4	EQ.5	EQ.6	EQ.7	FLU.	FLUX	T/F	Cv(F)	CU%	NI%	CF
1	IP3	T	.874	.860	.906	.800	.931	.805	.831	.323	.77	.97	137	.24	.52	1.05
2	IP3	T	1.01	.999	1.05	.929	1.08	.935	.965	.323	.77	.97	118	.24	.52	1.05
3	IP2	Y	1.01	1.04	1.02	1.22	1.10	.850	1.05	.589	1.5	1.5	145	.25	.73	.899

MEASURED - CALCULATED (E-C) CHARPY SHIFT(DEG.F) VALUES FOR SELECTED TREND CURVE EQNS.

J	CAPSULE		EQ.1	EQ.2	EQ.3	EQ.4	EQ.5	EQ.6	EQ.7	FLU.	FLUX	T/F	Cv(F)	CU%	NI%	CF
1	IP3	T	17.1	19.0	12.8	27.2	9.39	26.5	23.0	.323	.77	.97	137	.24	.52	1.05
2	IP3	T	-1.8	.069	-6.1	8.26	-9.6	7.58	4.04	.323	.77	.97	118	.24	.52	1.05
3	IP2	Y	-1.5	-6.0	-4.2	-32.	-15.	21.7	-7.8	.589	1.5	1.5	145	.25	.73	.899

AVE VALUE OF COMBINED ((SUM L3)/N;L3=L4*L5) CORRECTION FACTOR FOR ALL CAPSULES=.992
CORRECTION FACTOR'S AVERAGE VALUES: L4 = .992 L5 = 1 L6 = 1

SUM OF SQUARES (E-C) FOR EACH OF SEVEN EQUATIONS =
EQ1= 300.374 EQ2= 399.772 EQ3= 221.211 EQ4= 1883.405 EQ5= 406.827

EQ6= 1236.918 EQ7= 608.896

STANDARD DEVIATION OF FIT FOR EACH OF SEVEN EQUATIONS =
EQ1= 10.006 EQ2= 11.544 EQ3= 8.587 EQ4= 25.056 EQ5= 11.645 EQ6= 20.305 EQ7= 14.247

THE R VALUES FOR EACH OF SEVEN EQUATIONS =

FOR I=1 TO 7 ; ********** EQN(I)*WITHOUT TO EQN(I)*WITH CORRECTION FOR FLUX LEVEL =
EQ1= 5.565 EQ2= 5.731 EQ3= 7.709 EQ4= 3.368 EQ5= 6.823 EQ6= .017 EQ7= 4.484

THE R VALUES FOR EQN.2 TO EQN.1 AND FOR EQN.5 TO EQN.7 =

NO FLUX LEVEL CORRECTION **********: EQ2 TO EQ1= 1.07
WITH FLUX LEVEL CORRECTION **********: EQ2 TO EQ1= .993
NO FLUX LEVEL CORRECTION **********: EQ5 TO EQ7= -.369
WITH FLUX LEVEL CORRECTION **********: EQ5 TO EQ7= -.996

TABLE HEDL-46a

NINE MILE POINT (BWR), PALISADES (PAL), INDIAN POINT 2 (IP2), AND INDIAN POINT 3 (IP3) SURVEILLANCE CAPSULE PLATE RESULTS WITHOUT CORRECTION FOR FLUX-LEVEL EFFECT USING EQUATION (4M) DERIVED EQUATION (6b)

********** RESULTS FOR SEVEN EQUATIONS WITH NO CORRECTION FOR FLUX LEVEL EFFECT **********

CALCULATE TO MEASURED (C/E) CHARPY SHIFT(DEG.F) VALUES FOR SELECTED TREND CURVE EQNS.

J	CAPSULE	EQ.1	EQ.2	EQ.3	EQ.4	EQ.5	EQ.6	EQ.7	FLU.	FLUX	T/F	Cv(F)	CU%	NI%	CF
1	BWRWALL	.472	.442	.467	.574	.210	.572	.586	.047	.019	4.71	113	TBD	TBD	1.86
2	PALWALL	1.00	1.04	1.09	1.06	1.01	.927	1.15	1.09	.695	4.81	165	.25	.53	.830
3	IP3 T	.891	.877	.923	.872	.949	.821	.847	.323	.77	.97	128	.24	.52	.810
4	PAL 1AC	1.15	1.19	1.20	1.51	1.11	1.20	1.15	6.06	8.5	1.2	205	.25	.53	.497

MEASURED - CALCULATED (E-C) CHARPY SHIFT(DEG.F) VALUES FOR SELECTED TREND CURVE EQNS.

J	CAPSULE	EQ.1	EQ.2	EQ.3	EQ.4	EQ.5	EQ.6	EQ.7	FLU.	FLUX	T/F	Cv(F)	CU%	NI%	CF
1	BWRWALL	59.6	62.9	60.2	48.0	89.2	48.3	46.7	.047	.019	4.71	113	TBD	TBD	1.86
2	PALWALL	-1.2	-6.9	-15.	-10.	-2.9	11.9	-24.	1.09	.695	4.81	165	.25	.53	.830
3	IP3 T	13.6	15.6	9.76	16.3	6.47	22.8	19.4	.323	.77	.97	128	.24	.52	.810
4	PAL 1AC	-31.	-39.	-41.	-105	-23.	-42.	-30.	6.06	8.5	1.2	205	.25	.53	.497

AVE VALUE OF COMBINED ((SUM L3)/N;L3=L4*L5) CORRECTION FACTOR FOR ALL CAPSULES=1.285
CORRECTION FACTOR'S AVERAGE VALUES: L4 = 1.285 L5 = 1 L6 = 1

SUM OF SQUARES (E-C) FOR EACH OF THE SEVEN EQUATIONS =
EQ1= 4750.976 EQ2= 5803.848 EQ3= 5695.141 EQ4= 13906.272 EQ5= 8570.93

EQ6= 4804.505 EQ7= 4146.531

STANDARD DEVIATION OF FIT FOR EACH OF THE SEVEN EQUATIONS =
EQ1= 34.464 EQ2= 38.091 EQ3= 37.733 EQ4= 58.962 EQ5= 46.29 EQ6= 34.657 EQ7= 32.197

TABLE HEDL-46b

NINE MILE POINT (BWR), PALISADES (PAL), INDIAN POINT 2 (IP2), AND INDIAN POINT 3 (IP3) SURVEILLANCE CAPSULE PLATE RESULTS WITH CORRECTION FOR FLUX-LEVEL EFFECT USING EQUATION (4M) DERIVED EQUATION (6b)

********** RESULTS FOR SEVEN EQUATIONS WITH CORRECTION FOR FLUX LEVEL EFFECT **********

CALCULATE TO MEASURED (C/E) CHARPY SHIFT(DEG.F) VALUES FOR SELECTED TREND CURVE EQNS.

J	CAPSULE	EQ.1	EQ.2	EQ.3	EQ.4	EQ.5	EQ.6	EQ.7	FLU.	FLUX	T/F	Cu(F)	CU%	NI%	CF
1	BWRWALL	.878	.823	.869	1.06	.391	1.06	1.09	.047	.019	4.71	113	TBD	TBD	1.86
2	PALWALL	.836	.865	.909	.884	.845	.770	.956	1.09	.695	4.81	165	.25	.53	.830
3	IP3 T	.722	.711	.748	.707	.769	.666	.687	.323	.77	.97	128	.24	.52	.810
4	PAL 1AC	.574	.592	.598	.754	.554	.600	.572	6.06	8.5	1.2	205	.25	.53	.497

MEASURED - CALCULATED (E-C) CHARPY SHIFT(DEG.F) VALUES FOR SELECTED TREND CURVE EQNS.

J	CAPSULE	EQ.1	EQ.2	EQ.3	EQ.4	EQ.5	EQ.6	EQ.7	FLU.	FLUX	T/F	Cu(F)	CU%	NI%	CF
1	BWRWALL	13.7	19.8	14.7	-7.8	68.7	-7.3	-10.	.047	.019	4.71	113	TBD	TBD	1.86
2	PALWALL	26.9	22.1	14.9	19.0	25.5	37.8	7.22	1.09	.695	4.81	165	.25	.53	.830
3	IP3 T	35.4	36.9	32.1	37.4	29.4	42.7	40.0	.323	.77	.97	128	.24	.52	.810
4	PAL 1AC	87.2	83.4	82.3	50.3	91.2	81.8	87.6	6.06	8.5	1.2	205	.25	.53	.497

AVE VALUE OF COMBINED ((SUM L3)/N;L3=L4*L5) CORRECTION FACTOR FOR ALL CAPSULES=1.285
CORRECTION FACTOR'S AVERAGE VALUES; L4 = 1.285 L5 = 1 L6 = 1

SUM OF SQUARES (E-C) FOR EACH OF SEVEN EQUATIONS =
EQ1= 9794.394 EQ2= 9220.532 EQ3= 8251.282 EQ4= 4361.853 EQ5= 14566.27

EQ6= 10017.34 EQ7= 9439.205

STANDARD DEVIATION OF FIT FOR EACH OF SEVEN EQUATIONS =
EQ1= 49.483 EQ2= 48.012 EQ3= 45.418 EQ4= 33.022 EQ5= 60.345 EQ6= 50.043 EQ7= 48.578

THE R VALUES FOR EACH OF SEVEN EQUATIONS =

FOR I=1 TO 7 : ********** EQN(I)*WITHOUT TO EQN(I)*WITH CORRECTION FOR FLUX LEVEL =
EQ1= -2.06 EQ2= -1.482 EQ3= -1.239 EQ4= 8.753 EQ5= -1.646 EQ6= -2.082 EQ7= -2.343

THE R VALUES FOR EQN.2 TO EQN.1 AND FOR EQN.5 TO EQN.7 =

NO FLUX LEVEL CORRECTION **********: EQ2 TO EQ1= .886
WITH FLUX LEVEL CORRECTION **********: EQ2 TO EQ1= -.234
NO FLUX LEVEL CORRECTION **********: EQ5 TO EQ7= 4.268
WITH FLUX LEVEL CORRECTION **********: EQ5 TO EQ7= 2.173

OAK RIDGE NATIONAL LABORATORY

(ORNL)

OAK RIDGE NATIONAL LABORATORY

LIGHT WATER REACTOR PRESSURE VESSEL SIMULATION (LWR-PVS) PROGRAM

F. B. K. Kam

The LWR-PVS program has two major tasks; the first task is concerned primarily with well-defined reproducible benchmark experiments, and the second task deals with ASTM Standards activities.

During this report period, the following work is presented.

- Program Documentation
- Final Phase II and Preliminary Phase III Calculations of the VENUS PWR Mockup Experiment
- NESDIP Transport Calculations for the 0-cm, 20-cm, and 70-cm Cavity Configurations
- Babcock & Wilcox (B&W) SDMF Perturbation Experiment
- The Fifth NRC HSST Series of Metallurgical Irradiations
- ASTM Standards Activities

A. BENCHMARK EXPERIMENTS

Objectives

The objective of the benchmark experiments is to validate, by means of advanced statistical procedures, current methodologies and data bases which are used to predict radiation damage in reactor pressure vessels (RPV).

A.1 PROGRAM DOCUMENTATION

F. B. K. Kam
F. W. Stallmann
L. F. Miller
M. L. Williams
R. E. Maerker

Summary

A list of planned NRC reports is presented in Table S-1. These reports provide supporting documentation for the set of ASTM Standards for Surveillance of LWR Nuclear Reactor Pressure Vessels and Their Support Structures shown in Figure S-1. Table ORNL-1 lists the status of each section for which ORNL has lead responsibility.

Table ORNL-2 lists the ORNL/TM reports and oral presentations that have been published in FY 1985.

Accomplishments and Status

See Tables OPNL-1 and ORNL-2.

TABLE ORNL-1

STATUS OF ORNL'S CONTRIBUTIONS TO PROGRAM DOCUMENTATION

NUREG I.D.	Sect.	Title	Lead Author	Comments and Status*
NUREG/CR-3318 (NUREG No. 1)		PCA DOSIMETRY IN SUPPORT OF THE PSF PHYSICS-DOSIMETRY-METALLURGY EXPER.		
	1.0	Description of Experimental Facility - Summary	L.F. Miller	Completed - 12/14 82
	1.1	Physical Description of PCA 4/12 and 4/12 SSC Configurations	L.F. Miller	Completed - 12/14/82
	5.0	Transport (Neutron and Gamma) Results	F.B.K. Kam	Completed - 5/6/85
	5.1	ORNL Analysis	R.E. Maerker	Completed - 12/14/82
	6.0	Current PCA Specifications for Transport Theory Validation - Summary	F.W. Stallmann	Completed - 12/14/82
	7.1.2	ORNL Results	F.W. Stallmann	Completed - 1/23/84
	7.2.2	ORNL Results	F.W. Stallmann	Completed - 1/23/84
NUREG/CR-3320 Vol. 2 (NUREG No. 2)		PSF STARTUP EXPERIMENT		
	1.0	Description of Experimental Facility - Summary	L.F. Miller	Completed - 1/11/85
	1.1	Physical Description of PSF	L.F. Miller	Completed - 3/83 Revision - 3/22/85
	1.2	Calculated Core Power	L.F. Miller	Completed - 1/11/85

*Completed date indicates the data that the section was mailed to HEDL.

TABLE ORNL-1
(CONTINUED)

NUREG I.D.	Section	Title	Lead Author	Comments and Status*
NUREG/CR-3320		PSF STARTUP EXPERIMENT (Continued)		
	4.0	Transport Calculation Results - Summary (NUREG/CR-2696)	L.F. Miller	Completed - 3/22/85
	4.1	ORNL Analysis (NUREG/CR-2696)	L.F. Miller	Completed - 3/22/85
NUREG/CR-3320 Vol. 1 (NUREG No. 3)		PSF EXPERIMENTS SUMMARY AND BLIND TEST RESULTS		
	1.1	Physical Description of SSC, SPVC, and SVBC - Summary	L.F. Miller	Completed - 1/11/85
	1.2	Temperature Control of SSC and SPVC - Summary	L.F. Miller	Completed - 1/10/85
	2.0	Recommended HEDL-ORNL-MEA Consensus - Physics-Dosimetry-Metallurgy Data Base for the PSF Blind Test	F.W. Stallmann	Draft sent to other participants for review - 3/22/85
	2.1	ORNL Transport Analysis (NUREG/CR-3886)	L.F. Miller	Completed - 3/22/85 Revision - 5/8/85
	2.2	HEDL-ORNL Exposure Parameter Values	F.W. Stallmann	Completed - 5/6/85
	2.3	MEA-HEDL-ORNL Metallurgical Data Base	F.W. Stallmann	Draft sent to other participants for review - 3/22/85

*Completed date indicates the date that the section was mailed to HEDL.

TABLE ORNL-1
(CONTINUED)

NUREG I.D.	Sect.	Title	Lead Author	Comments and Status*
NUREG/CR-3319 (NUREG No. 4)		LWR POWER REACTOR SURVEILLANCE PHYSICS-DOSIMETRY DATA BASE COMPENDIUM		
	5.3	The Use of Adjustment Methods and Related Statistical Analysis of the Evaluation of Pressure Vessel Surveillance Results at ORNL	F.W. Stallmann	Completed - 11/17/82
NUREG/CR-3320 Vol. 3 (NUREG No. 5)		PSF STARTUP EXPERIMENT		
	1.0	Description of Experimental Facility - Summary	L.F. Miller	Completed - 1/10/85
	1.1	Physical Description of the SSC, SPVC, and the SVBC	L.F. Miller	Completed - 1/10/85
	1.2	Positions of Participant Dosimeter Packages	L.F. Miller	Completed - 1/10/85
	1.3	Calculated Core Power Source	L.F. Miller	Completed - 5/6/85
	3.0	Transport Calculation Results - Summary	R.E. Maerker	
	3.1	ORNL Transport Analysis (NUREG/CR-3886)	L.F. Miller	Completed - 5/6/85
	4.2	Consistency of Experimental Data and Derived Exposure Parameters - ORNL	F.W. Stallmann	
	5.1.2	ORNL Analysis (Methodology)	F.W. Stallmann	
	5.2.2	ORNL Analysis (Recommended Integral Parameter Values)	F.W. Stallmann	

*Completed date indicated the date the section was mailed to HEDL.

TABLE ORNL-1
(CONTINUED)

NUREG I.D.	Sect.	Title	Lead Author	Comments and Status*
NUREG/CR-3320 Vol. 4 (NUREG No 6-1)		PSF METALLURGY PROGRAM		
	1.1	Physical Description	L.F. Miller	Completed - 1/11/85
	1.3	Temperature and Temperature Control	L.F. Miller	Completed - 1/10/85
NUREG/CR-3321 (NUREG No. 7)		SERVICE LAB. PROCEDURES VERIFICATION AND SURVEILLANCE CAPSULE PERTURBATIONS		
	1.0	Description of Experimental Facility - Summary	L.F. Miller	
	1.1	Physical Description of PSF	L.F. Miller	Draft being reviewed
	1.2	Core Power/History	L.F. Miller	Draft sent to clearance 4/30/85
	4.1	ORNL Fluxes and Source (2nd SDMF W)	L.F. Miller	
	4.5	ORNL 4th (4/12 SSC) PCA	L.F. Miller	

*Completed date indicates date the section was mailed to HEDL.

TABLE ORNL-1
(CONTINUED)

NUREG I.D.	Sect.	Title	Lead Author	Comments and Status
NUREG/CR-3323 (NUREG Nos. 9-1 and 9-2)		VENUS PWR CORE SOURCE AND AZIMUTHAL LEAD FACTOR EXPERIMENTS AND CALCULATIONAL TESTS		
	7.2	Analysis of the VENUS PWR Engineering Mockup Experiment - Phase I: Source Distribution	M.L. Williams	Completed and sent to A. Fabry - 8/84
	11.2	Phase II: Calculations of the VENUS PWR Mockup Experiment	M.L. Williams	Completed and sent to G. Minsart - 1/2/85
	14.2	Phase III		
NUREG/CR-3324 Vol. 4 (NUREG No. 10-4)		NESTOR DOSIMETRY IMPROVEMENT PROGRAM CAVITY SIMULATION EXPERIMENTS		
	4.2.1	Radial Shield	R.E. Maerker	Information to perform calculations has not been received from AEEW
	4.2.2	Cavity	R.E. Maerker	Information to perform calculations has not been received from AEEW

TABLE ORNL-2

PAPERS AND PUBLICATIONS - FY 1985

1. R. E. Maerker and B. A. Worley, Activity and Fluence Calculations for the Startup and Two-Year Irradiation Experiments Performed at the Poolside Facility, NUREG/CR-3886, ORNL/TM-9265, Nuclear Regulatory Commission, Washington, DC, October 1984.

2. F. W. Stallmann, Determination of Damage Exposure Parameter Values in the PSF Metallurgical Irradiation Experiment, NUREG/CR-3814, ORNL/TM-9166, Nuclear Regulatory Commission, Washington, DC, October 1984.

3. C. A. Baldwin, F. B. K. Kam, and F. W. Stallmann, Neutron Spectral Characterization for the Fifth Heavy Section Steel Technology (HSST) Irradiation Series "Simulator Experiments," NUREG/CR-4031, Vol. 1, ORNL/TM-9423/V1, Nuclear Regulatory Commission, Washington, DC, November 1984.

4. R. E. Maerker, Gamma-Ray Characterization of the Two-Year Irradiation Experiment Performed at the Poolside Facility, NUREG/CR-4039, ORNL/TM-9440, Nuclear Regulatory Commission, Washington, DC, January 1985.

5. F. W. Stallmann, F. B. K. Kam, G. Guthrie, and W. N. McElroy, "LWR Surveillance Dosimetry Improvement Program: PSF Metallurgical Blind Test Results," presented at the 12th Water Reactor Safety Research Information Meeting, October 22-26, 1984 at the National Bureau of Standards, Gaithersburg, MD, NUREG/CP-0058, Vol. 4, January 1985.

6. M. L. Williams, I. Remec, and F. B. K. Kam, Neutron Spectral Characterization for the Fifth Heavy Section Steel Technology (HSST) Irradiation Series, "Neutronics Calculations," NUREG/CR-4031, Vol. 2, ORNL/TM-9423/V2, Nuclear Regulatory Commission, Washington, DC, March 1985.

7. I. Remec, F. W. Stallmann, and F. B. K. Kam, Neutron Spectral Characterization for the Fifth Heavy Section Steel Technology (HSST) Irradiation Series, "Neutronics Exposure Parameters," NUREG/CR-4031, Vol. 3, ORNL/TM-9423/V3, Nuclear Regulatory Commission, Washington, DC, March 1985.

8. L. F. Miller and R. W. Hobbs, Data Acquisition and Control of the HSST Series V Irradiation Experiment at the ORR, NUREG/CR-3872, ORNL/TM-9253, Nuclear Regulatory Commission, Washington, DC, March 1985.

9. F. W. Stallmann, F. B. K. Kam, and C. A. Baldwin, Neutron Exposure Parameters for the Fifth Heavy Section Steel Technology Irradiation Series, NUREG/CR-4284, ORNL/TM-9664, Nuclear Regulatory Commission, Washington, DC (to be published).

A.2 FINAL PHASE II AND PRELIMINARY PHASE III CALCULATIONS OF THE VENUS PWR MOCKUP EXPERIMENT

M. L. Williams
F. B. K. Kam

Summary

Calculated results of Phase I have been completed by CEN/SCK and ORNL. Phase II results have been reported by CEN/SCK, ORNL, and Westinghouse. In general, all three results show good agreement. The following are some of the preliminary conclusions of the results:

1. The core source near the baffle was calculated with transport theory to an accuracy of within 2% for points away from the baffle corner.

2. Near the baffle corners, the agreement between calculation and measurement was within 7%. Thus, the calculational accuracy near the corners is about a factor of three worse than away from the corners, but is still relatively good. In the corner locations, the calculations overpredict the neutron source strength, which is conservative for vessel fluence analysis.

3. The thermal flux in the core near the baffle hardens and reduces the thermal group fission cross section by about 10% at the periphery. It was necessary to use spatially weighted cross sections to obtain good agreement with the measured power shape.

4. The error incurred by transformation of the calculated X-Y source distribution into R-θ coordinates was very small; thus, the usual method of performing the in-core calculations in X-Y and the ex-core in R-θ coordinates was validated.

5. The ex-core calculations show generally good agreement with measured dosimeter activities. For most reactions, the agreement is better than 10%, but the ex-core ^{237}Np results are about 30% lower than the measurements in the water region between the core and the barrel. The other two calculational studies also see this discrepancy. Perhaps, it is caused by photofission effects.

Overall, it appears that present transport methods are able to predict the fission source and ex-core neutron flux accurately in this PWR-type configuration.

Accomplishments and Status

In the last semiannual report, preliminary calculations of ex-core dosimeter activations were reported. These results have now been finalized and are

repeated in Table ORNL-3. Phase II, along with Phase I, of the VENUS project is now completed. The Phase II results and conclusions have been published in a paper entitled "Calculation of the Neutron Source Distribution in the VENUS PWR Mockup Experiment" which will be published in the Proceedings of the Fifth ASTM-EURATOM Symposium on Reactor Dosimetry, held in Geesthacht, Germany, September 24-28, 1984. (Wi84b)

The Phase III portion of the VENUS program has now begun. In Phase III, coupled neutron gamma calculations will be performed and compared with TLD gamma measurements. These calculations are being performed with the 47-neutron/20-gamma group cross-section library SAILOR. This library has been obtained from the Radiation Shielding Information Center, and the appropriate macroscopic cross sections have been mixed. Because the effective "buckling" of the gamma flux is not known, the 3-D synthesis approach, which has been utilized in other studies, will be used. This approach requires performing R-θ (or X-Y), R-Z, and R discrete ordinates calculations. A 3-D distribution can then be synthesized from the two 2-D and one 1-D calculations. Considerable time was spent to determine the most appropriate way to define the R-Z geometry for the VENUS configuration. It was finally decided to model a slice along the zero-degree radius. Within the core, the same mesh as in the X-Y calculations performed in Phase I was adopted, and outside the core, the same mesh as in the R-θ calculations done in Phase II was used. The appropriate models for the R-Z and R coordinate systems were then determined.

The 67-group transport calculations which were done with DOT-IV (Rh79) for the X-Y, R-θ, R-Z, and R are completed. These runs will be combined to give a synthesized expression for the 3-D neutron and gamma fluxes.

The synthesis procedure is as follows. Let $\hat{P} = (X,Y) = (R,\theta)$ = point defined in either the X-Y or R-θ coordinate systems which have been used in the 2-D DOT calculations. Then

$$\tilde{\phi}_g(\hat{P}) = \tilde{\phi}_g(X,Y) = \tilde{\phi}_g(R,\theta) = \text{2-D flux value at } \hat{P} \quad .$$

The value for this flux can be taken either from the X-Y or the R-θ runs. For points inside the core and baffle, one uses the X-Y results, and outside the core, the R-θ results. The 2-D fluxes are computed using a source distribution which has been integrated over Z.

In order to correct the 2-D flux for axial leakage, one multiplies by a correction factor $C_g(P)$, so that

$$\phi_g(\hat{P},Z) = \tilde{\phi}_g(\hat{P})C_g(\hat{P},Z) = \text{synthesized 3-D flux} \quad .$$

The correction factor is obtained by first defining a mapping $\hat{P} \longrightarrow \hat{P}_o$, where $\hat{P}$ is the actual point in the 3-D VENUS configuration, and $\hat{P}_o$ is some "corresponding" point in the R-Z coordinate system. The manner in which R-Z

points (which are defined for a azimuthally uniform model) should be related to the irregularly shaped core baffle is open to debate. A single point has been chosed in the outer baffle of the R-Z model for all points in the actual, irregularly shaped baffle. (Recall that the baffle is represented in the R-Z model as being circular.)

After selecting the appropriate R-Z point $\hat{P}_o$, the correction factor can be computed as

$$\hat{P} \longrightarrow \hat{P}_o$$

$$C_g(\hat{P},Z) = \frac{\phi_{RZ}(\hat{P}_o,Z)}{\phi_R(\hat{P}_o)} \quad .$$

The program which computes the group-dependent correction factors has been written, and the synthesizing of the 3-D neutron and gamma fluxes is now in progress.

TABLE ORNL-3

DOSIMETER ACTIVITY (DPS) BY EXPERIMENT POSITION

	SL No.	Dosimeter Location	$^{115}In(n,n')$ Exp.	$^{115}In(n,n')$ Calc.	$^{115}In(n,n')$ C/E	$^{58}Ni(n,p)$ Exp.	$^{58}Ni(n,p)$ Calc.	$^{58}Ni(n,p)$ C/E	$^{238}U(n,f)$ Exp.	$^{238}U(n,f)$ Calc.	$^{238}U(n,f)$ C/E
Outer Baffle	1	0.909° (-29,+2)	7.83E+8	7.72615E+8	0.98674	5.738E+8	6.21099E+8	1.08243	7.162E+8	7.61287E+8	1.06295
	2	8.13° (-29,-2)	7.37E+8	7.30400E+8	0.99104	5.455E+8	5.86847E+8	1.07579	6.636E+8	7.19648E+8	1.08446
	3	16.78° (-29,-7)	5.98E+8	5.86570E+8	0.98089	4.469E+8	4.69851E+8	1.05135	5.511E+8	5.77716E+8	1.04829
	4	24.72° (-29,-12)	3.52E+8	3.44850E+8	0.97969	2.638E+8	2.70738E+8	1.02630	--	3.37988E+8	--
	5	29.22° (-27,-14)	3.64E+8	3.58174E+8	0.98399	2.764E+8	2.82001E+8	1.02026	3.277E+8	3.51115E+8	1.07145
	6	33.96° (-22,-14)	7.16E+8	6.90520E+8	0.96441	5.148E+8	5.49511E+8	1.06742	6.534E+8	6.78512E+8	1.03843
	7	40.236° (-17,-14)	1.16E+9	1.11503E+9	0.96123	8.376E+8	8.80173E+8	1.05082	1.036E+9	1.09326E+8	1.05525
Center	8	45.0° (+2.5,+2.5)	1.244E+9	1.21996E+9	0.98068	1.017E+9	1.09070E+9	1.07247	1.218E+9	1.12326E+9	1.01199
Inner Baffle	9	45.0° (-1.0,-1.0)	2.27E+9	2.25416E+9	0.993022	1.634E+9	1.79094E+9	1.09971	2.055E+9	2.21647E+9	1.07857
Fuel 3.3/0*	10	45.0° (-3.5,-3.5)	--	3.57798E+9	--	--	3.34502E+9	--	--	3.63750E+9	--
	11	45.0° (-6.5,-6.5)	--	3.85298E+9	--	--	3.64790E+9	--	--	3.92631E+9	--
	12	45.0° (-9.5,-9.5)	--	3.70367E+9	--	--	3.49779E+9	--	--	3.77183E+9	--
	13	45.0° (-12.5,-12.5)	--	2.62518E+9	--	--	2.38058E+9	--	--	2.65386E+9	--
Water	14	45.0° (-16,-16)	--	7.50090E+8	--	--	6.40918E+8	--	7.366E+8	7.48488E+8	1.01613
	15	45.0° (-18,-18)	--	3.78176E+8	--	--	3.48144E+8	--	--	3.84746E+8	--
	16	45.0° (-20,-20)	--	1.97508E+8	--	--	1.92443E+8	--	2.074E+8	2.03862E+8	0.98294
	17	45.0° (-22,-22)	--	1.05654E+8	--	--	1.07490E+8	--	--	1.10186E+8	--
	18	45.0° (-24,-24)	--	6.04573E+7	--	--	6.13120E+7	--	6.607E+7	6.30601E+7	0.95444
Barrel	19	45.0° (-26,-26)	4.50E+7	4.17072E+7	0.92683	4.36E+7	3.61261E+7	0.82858	4.278E+7	4.19434E+7	0.980444

*Weight % ^{235}U/weight % ^{239}Pu.

TABLE ORNL-3

(CONTINUED)

	SL No.	Dosimeter Location	$^{235}U(n,f)$* Exp.	$^{235}U(n,f)$* Calculation 56 Group Act. / 10 Group Act.	$^{235}U(n,f)$* C/E	$^{237}Np(n,f)$ Exp.	$^{237}Np(n,f)$ Calc.	$^{237}Np(n,f)$ C/E	$^{54}Fe(n,p)$ Exp.	$^{54}Fe(n,p)$ Calc.	$^{54}Fe(n,p)$ C/E
	1	0.909° (-29,+2)	--	1.94482E-13 / 1.7436E-13	--	1.009E+9	1.08150E+9	1.0719	--	6.3286E+8	--
	2	8.13° (-29,-2)	--	1.84050E-12 / 1.6484E-13	--	--	1.02271E+9	--	--	5.9791E+8	--
	3	16.78° (-29,-7)	1.354E-13	1.46334E-13 / 1.3193E-13	1.08075 / 0.97438	7.539E+8	8.23250E+8	1.092	--	4.7851E+8	--
Outer Baffle	4	24.72° (-29,-12)	8.736E-14	9.50769E-14 / 8.5524E-14	1.08833 / 0.97898	4.513E+8	4.94982E+8	1.0968	--	2.7506E+8	--
	5	29.22° (-27,-14)	--	1.20619E-13 / 9.8461E-14	--	4.662E+8	5.14402E+8	1.1033	--	2.8663E+8	--
	6	33.96° (-22,-14)	--	2.15570E-13 / 1.7781E-13	--	8.884E+8	9.78648E+8	1.1020	--	5.5927E+8	--
	7	40.236° (-17,-14)	2.625E-13	2.81544E-13 / 2.5E-13	1.07254 / 0.95238	1.468E+9	1.58828E+9	1.0819	--	8.9493E+8	--
Center	8	45.0° (+2.5,+2.5)	--	--	--	1.689E+9	1.63870E+9	0.97022	--	--	--
Inner Baffle	9	45.0° (-1.0,-1.0)	5.128E-13	3.39114E-13 / 3.1722E-13	0.661298 / 0.61861	2.711E+9	3.16830E+9	1.16868	--	7.8293E+9	--
	10	45.0° (-3.5,-3.5)	--	8.52126E-13 / 6.7808E-13	--	3.867E+9	4.41842E+9	1.14259	--	3.4702E+9	--
	11	45.0° (-6.5,-6.5)	--	8.58132E-13 / 6.9571E-13	--	4.219E+9	4.70454E+9	1.11746	--	3.7897E+9	--
Fuel 3.3/0†	12	45.0° (-9.5,-9.5)	--	8.61507E-13 / 6.8141E-13	--	3.990E+9	4.53127E+9	1.13565	--	3.6327E+9	--
	13	45.0° (-12.5,-12.5)	--	4.25370E-13 / 3.7407E-13	--	3.217E+9	3.31724E+9	1.03115	--	2.4609E+9	--
	14	45.0° (-16,-16)	--	8.17394E-13 / 9.3564E-13	--	1.020E+9	1.03450E+9	1.01421	--	6.5803E+8	--
	15	45.0° (-18,-18)	--	9.86577E-13 / 1.2108E-12	--	5.591E+8	5.03565E+8	0.90067	--	3.6053E+8	--
Water	16	45.0° (-20,-20)	--	8.12458E-13 / 8.8241E-13	--	3.680E+8	2.56632E+8	0.69736	--	2.0043E+8	--
	17	45.0° (-22,-22)	--	5.36947E-13 / 4.9822E-13	--	1.646E+8	1.34971E+8	0.81999	--	1.1246E+8	--
	18	45.0° (-24,-24)	--	2.68838E-13 / 1.869E-13	--	1.015E+8	7.70384E+7	0.759	--	6.4135E+7	--
Barrel	19	45.0° (-26,-26)	--	3.05186E-14 / 1.7671E-14	--	5.620E+7	5.68663E+7	1.0119	--	3.7155E+7	--

*Calculated activities have been multiplied by E-24.
†Weight % ^{235}U/weight % ^{239}Pu.

A.3 NESDIP TRANSPORT CALCULATIONS FOR THE 0-CM, 20-CM, and 70-CM CAVITY CONFIGURATIONS

R. E. Maerker
F. B. K. Kam

Accomplishments and Status

The data necessary to perform the calculations have not been sent by John Butler of Atomic Energy Establishment Winfrith (AEEW). C. Z. Serpan expects to clarify the status of agreement between NRC and AEEW during his trip to London in May 1985.

A.4 BABCOCK & WILCOX (B&W) SDMF PERTURBATION EXPERIMENT

F. B. K. Kam

Accomplishments and Status

Frank Walters of B&W has reported that he expects the transport calculations and measurements to be completed in July 1985. The three-dimensional fission source densities were provided by ORNL. The least squares adjustment procedure will be applied to the B&W data at that time.

A.5 THE FIFTH NRC HSST SERIES OF METALLURGICAL IRRADIATIONS

F. W. Stallmann

The Nuclear Regulatory Commission's (NRC's) Heavy Section Steel Technology (HSST) Program is concerned with the investigation of crack-like flaws in reactor pressure vessel steels. In the fifth irradiation series, capsules containing a variety of metallurgical test specimens were irradiated to fluences in the range of $1 \cdot 10^{19}$ to $3 \cdot 10^{19}$ neutrons/cm^2 ($E > 1.0$ MeV). In order to correlate radiation embrittlement to damage fluences, accurate determination of the neutron fluence spectra at the critical location of the test specimen is needed. The part of the neutron spectrum which is responsible for the radiation damage is characterized as "damage exposure parameter." Fluences for energies greater than 1.0 MeV ($F > 1.0$ MeV) is the most widely used parameter; however, current thinking favors displacements per atom (dpa) in iron as better related to the physical mechanism of radiation damage. Fluences for energies greater than 0.1 MeV ($F > 0.1$ MeV) are also considered since neutrons in the 0.1 to 1.0 MeV range are likely to contribute to the damage. In order not to prejudice future investigations, all three damage parameters $F > 1.0$ MeV, $F > 0.1$ MeV, and dpa are considered.

The irradiations are performed at the Oak Ridge Research Reactor (ORR) Poolside Facility (PSF) (Fig. ORNL-1). A preliminary determination of the

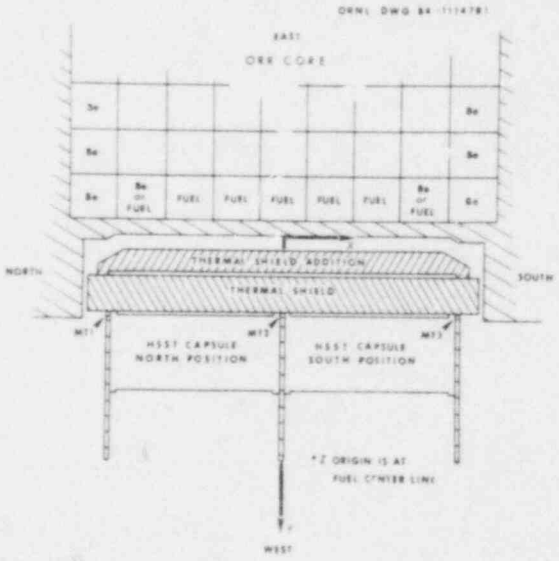

FIGURE ORNL-1. Top View of HSST Irradiation Configuration.

fluence spectra at the irradiation facility has been performed using simulator capsules (Ba84,Wi85,Re85) (Fig. ORNL-2). The results of these determinations were used to calculate approximate irradiation times needed to reach the nominal fluences. However, these fluence predictions may vary by about 30% due to in-core experiments and other changes in fuel management. For this reason, extensive dosimetry was placed in each metallurgical capsule to monitor the actual fluences resulting in damage parameter determinations which are better than 10% at all critical locations of the metallurgical test specimens.

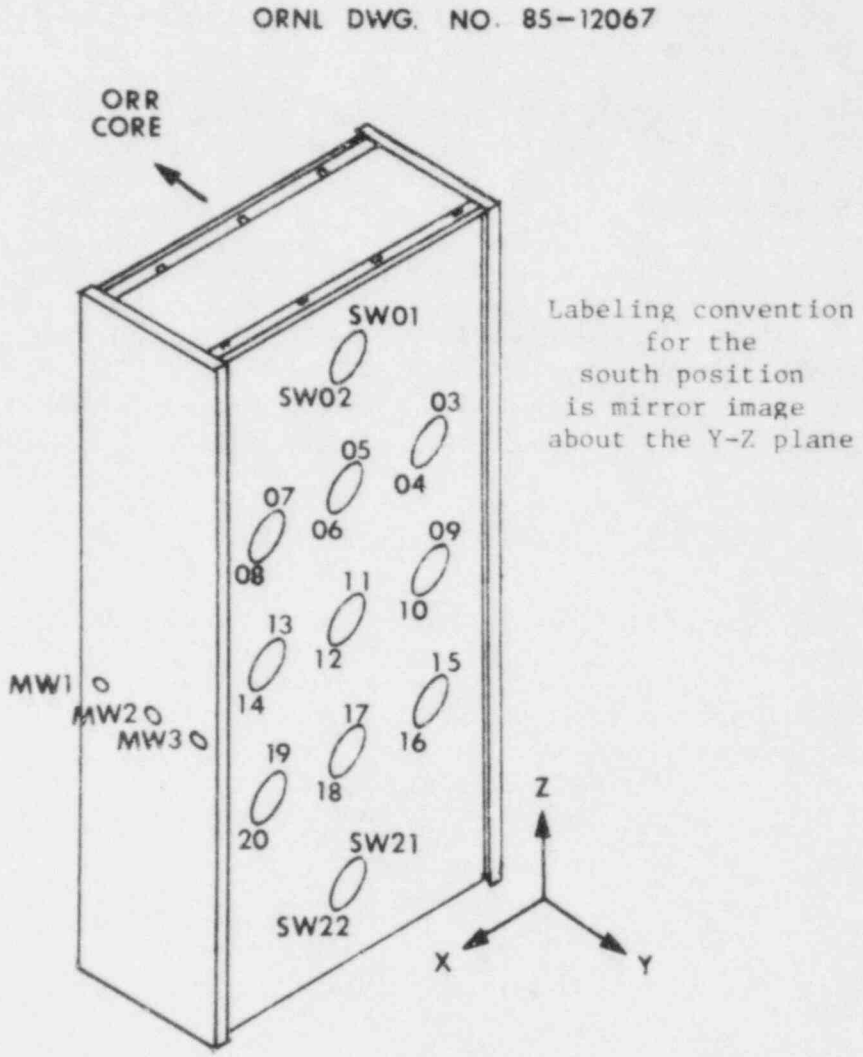

FIGURE ORNL-2. Gradient Wire Labeling Convention for Simulator in the North Position.

The neutron fluence characterization for both the simulator and the metallurgical capsules are obtained from a combination of transport calculations (Wi85) and dosimetry using the LSL-M2* adjustment procedure. The damage parameter values at the locations of the multiple-foil fission/radiometric dosimetry sets (FRDS) and gradient wires (GW) (Figs. ORNL-3 and ORNL-4) were fitted to cosine-exponential curves to obtain a complete spatial map of these values.

For the simulator capsules, the fluence map is described by the formula

$$A(X,Y,Z) = A_0 \cos B_X(X-X_0) \cos B_Z(Z-Z_0)\, e^{-\lambda(Y-Y_0)} \qquad (1)$$

where A is the damage parameter in question. The coefficients for formula (1) are listed in Table ORNL-4.

TABLE ORNL-4

THE FITTING PARAMETER VALUES TO BE USED WITH FORMULA (1) FOR CALCULATION OF THE DAMAGE EXPOSURE PARAMETERS IN THE SIMULATOR BLOCK (30-MW CORE POWER)

Parameter	A_0	B_Z (cm^{-1})	Z_0 (cm)	B_X (cm^{-1})	X_0 (cm)	λ (cm^{-1})	Y_0 (cm)
$^{54}Fe(n,p)^{54}Mn$ reaction rate	1.46×10^{-13} s^{-1}	4.02×10^{-2}	-4.8	4.40×10^{-2}	0.34	-0.2018	18.17
$\phi(E > 1.0$ MeV)	3.57×10^{12} $n/(cm^2\cdot s)$	4.02×10^{-2}	-4.8	4.40×10^{-2}	0.34	-0.1628	18.17
$\phi(E > 0.1$ MeV)	1.66×10^{14} $n/(cm^2\cdot s)$	4.02×10^{-2}	-4.8	4.40×10^{-2}	0.34	-0.1149	18.17
dpa/s of iron	8.75×10^{-8} s^{-1}	4.02×10^{-2}	-4.8	4.40×10^{-2}	0.34	-0.1295	18.17

*F. W. Stallmann, "LSL-M1 and LSL-M2: Two Extensions of the LSL Adjustment Procedure for Including Multiple Spectrum Locations," presented at the Fifth ASTM-EURATOM Symposium on Reactor Dosimetry, Geesthacht, FRG, September 24-28, 1984 (St84a)

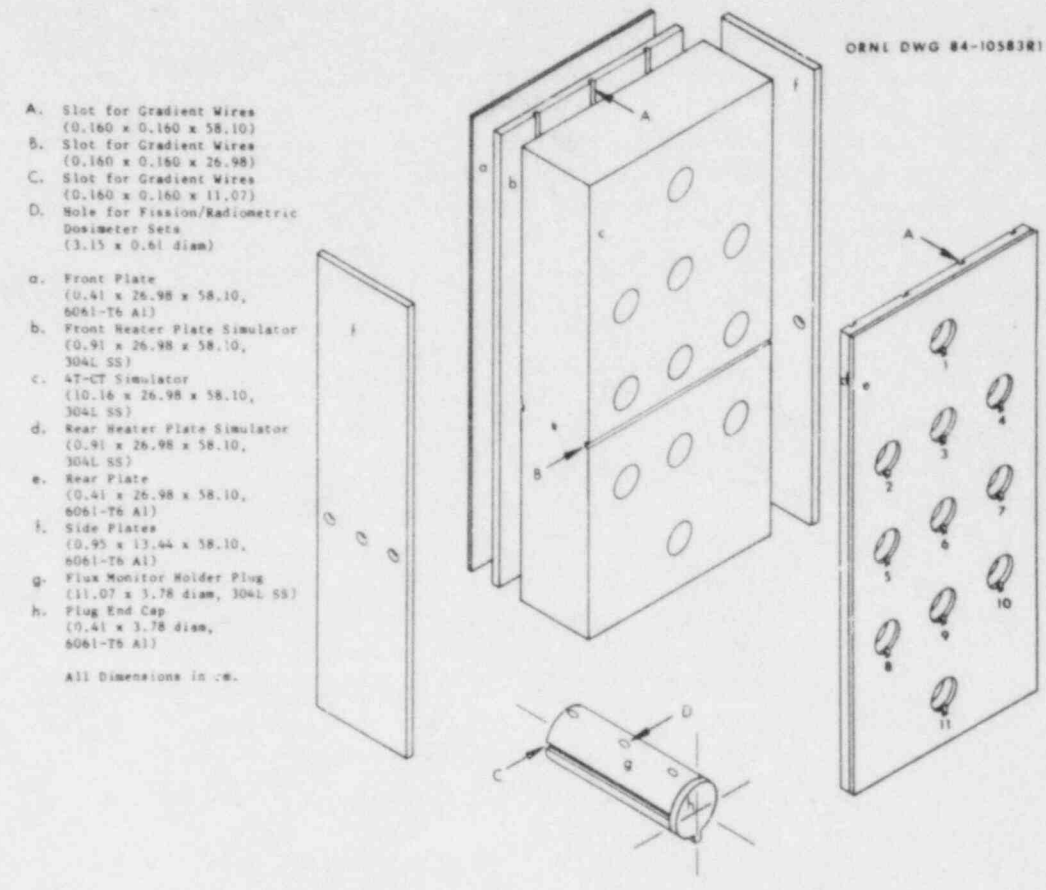

FIGURE ORNL-3. Placement of FRDS and GW Dosimeters in the ORR HSST Simulator Capsule.

The uncertainties in the damage parameter values determined according to formula (1) and Table ORNL-4 are 9%, 13%, and 10% relative standard deviation, respectively, for $F > 1.0$ MeV, $F > 0.1$ MeV, and dpa.

The fluence characterization for the metallurgical capsules is more complex because the capsules are either rotated or shifted at the midpoint of the irradiation to obtain a more uniform exposure. Thus, the exposure map becomes a superposition of two maps [formula (1)] with differing coefficients.

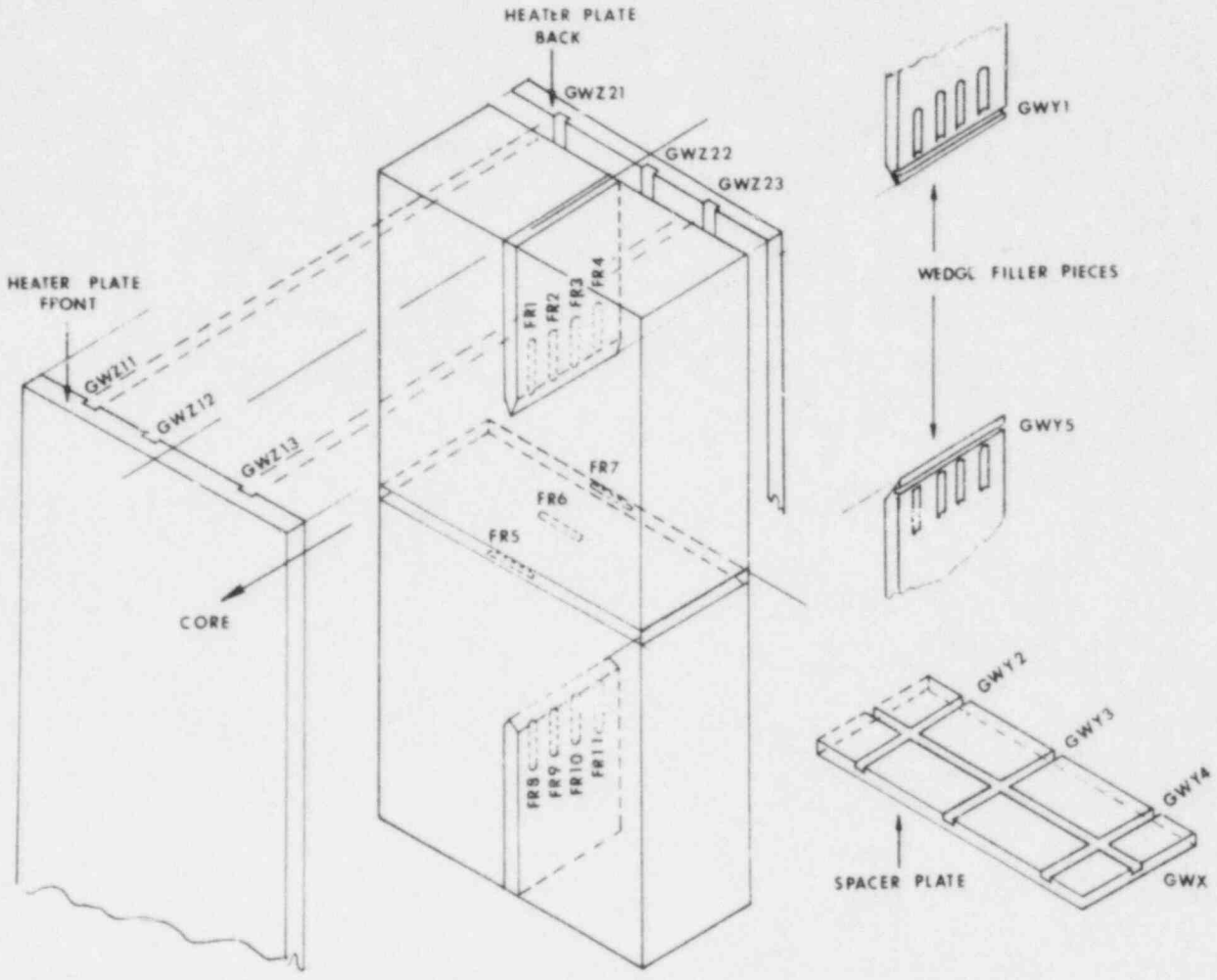

FIGURE ORNL-4. Location of the FRDS and GW Dosimeters in the 4T-CS Metallurgical Capsules.

The characterization of the metallurgical capsules 1 and 2 has been completed.* These capsules contain two 4-in.-thick compact specimens (4T-CS) each, which are rotated around their axes so that each side receives a nearly equal amount of radiation (Fig. ORNL-5). The map in the crack plane X = ±14.76 can be described by a combination of trigonometric and hyperbolic cosine functions.

*F. W. Stallmann, Neutron Exposure Parameters for the Fifth Heavy Section Steel Irradiation Series, NUREG/CR-4284, ORNL/TM-9664, Nuclear Regulatory Commission, Washington, DC, June 1985 (St85a).

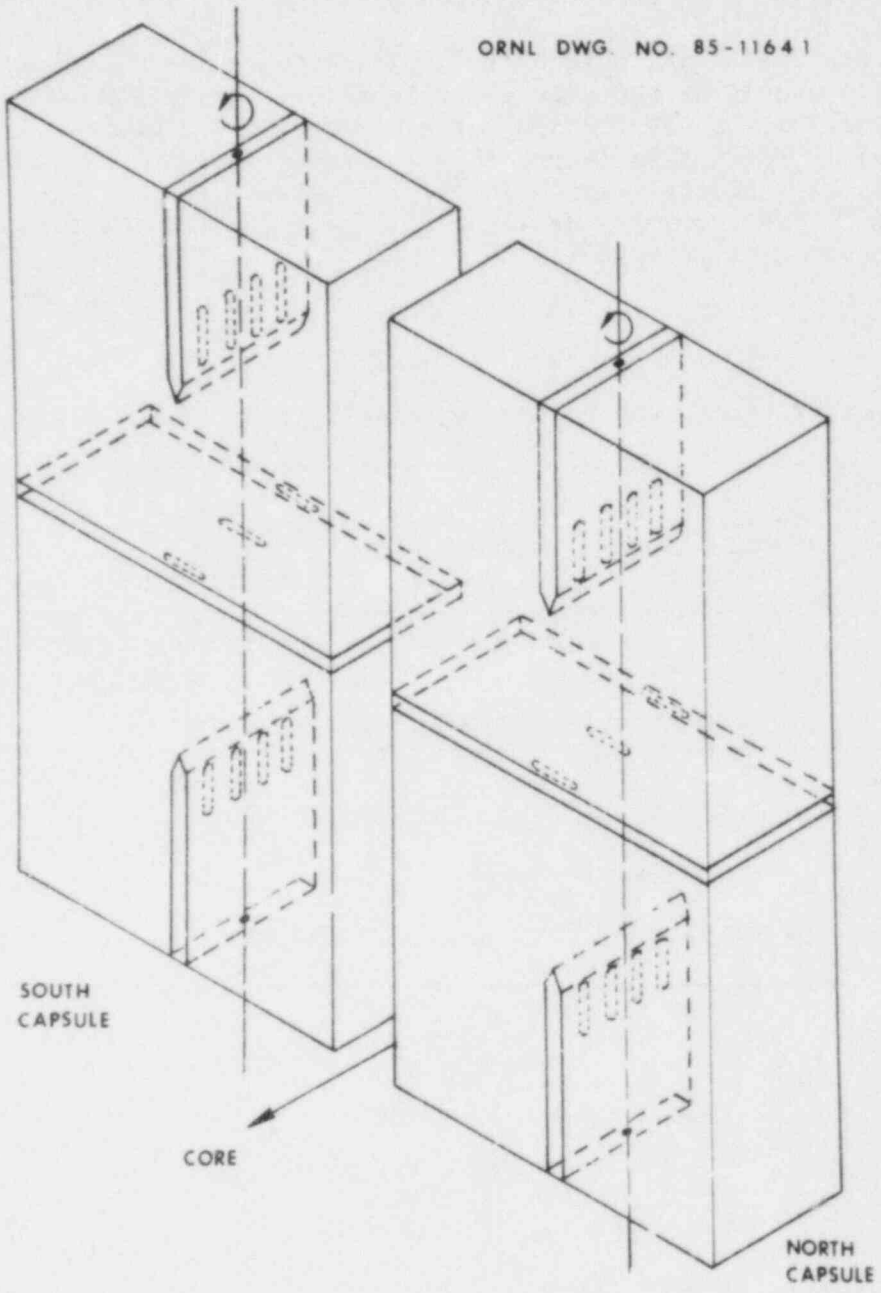

FIGURE ORNL-5. Positioning of the 4T-CS Capsules. Each is rotated around its centerline at the midpoint of irradiation.

$$A(Y,Z) = A_C \cosh\lambda(Y-Y_O) \cos B_Z(Z-Z_O) \quad . \qquad (2)$$

The coefficients are listed in Table ORNL-5. The attenuation coefficients, λ, which theoretically should be the same as in Table ORNL-4 are somewhat smaller in Table ORNL-5 for F > 1.0 MeV and dpa and zero for F > 0.1 MeV, i.e., no change in the Y direction. This is probably a boundary effect and could be predicted from the experimental values in the simulator experiment (Figs. ORNL-6 and ORNL-7). The resulting damage parameter values at the crack tips of the CS are listed in Table ORNL-6.

TABLE ORNL-5

SUMMARY OF FITTING PARAMETERS FOR THE CRACK PLANES [FORMULA (2)]

	A_C		Y_O		λ	B_Z	Z_O
	North	South	North (cm)	South (cm)	(cm^{-1})	(cm^{-1})	(cm)
F>1.0 MeV	1.78*	1.89*	18.51	17.84	0.132	0.0402	-1.77
F>0.1 MeV	11.30*	12.00*	---	---	0.0	0.0414	-1.33
dpa	0.0409	0.0434	18.86	17.13	0.080	0.0410	-1.98

*10^{19} neutrons/cm^2.

TABLE ORNL-6

DAMAGE PARAMETER VALUES AT THE CRACK TIP OF THE 4T-CS

	North		South	
	Top	Bottom	Top	Bottom
X coordinate	-14.76	-14.76	14.76	14.76
Z coordinate	6.82	-14.45	6.82	-14.45
F>1.0 MeV (10^{19} neutrons/cm^2)				
Minimum	1.67	1.54	1.78	1.63
Maximum	2.10	1.94	2.28	2.09
Average	1.80	1.66	1.91	1.75
F>0.1 MeV (10^{19} neutrons/cm^2)				
Average	10.7	9.56	11.3	10.2
dpa				
Minimum	0.0368	0.0348	0.0409	0.0370
Maximum	0.0425	0.0383	0.0462	0.0418
Average	0.0378	0.0358	0.0420	0.0380

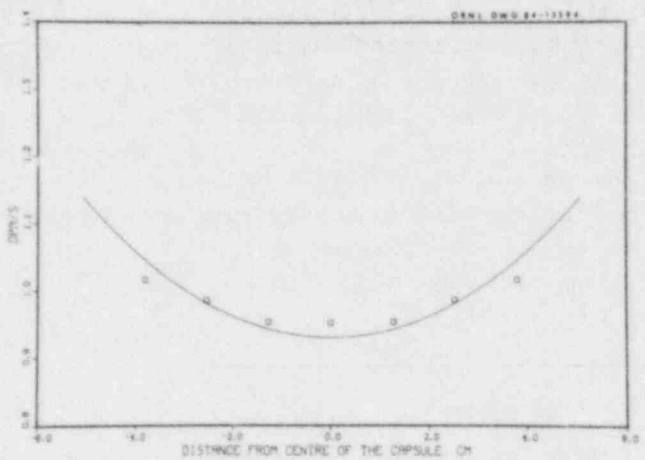

FIGURE ORNL-6. Distribution of F > 0.1 MeV along the Y Axis for the 4T-CS experiment estimated from the simulator experiment. The solid line represents the theoretical prediction [formula (1)], and the squares represent the experimental values.

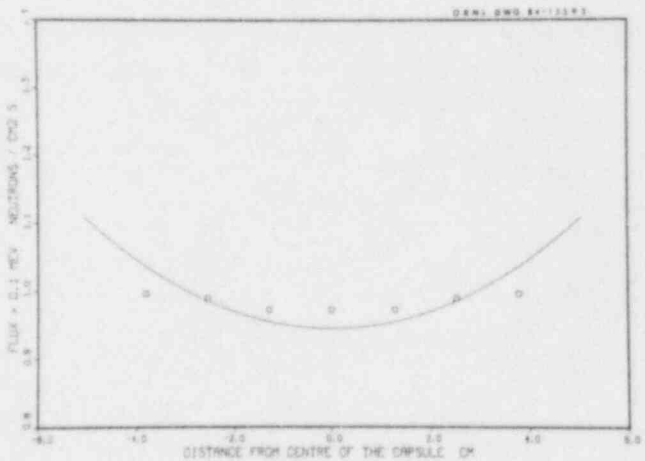

FIGURE ORNL-7. Distribution of dpa along the Y Axis for the 4T-CS experiment estimated from the simulator experiment. The solid line represents the theoretical prediction [formula (1)], and the squares represent the experimental values.

The uncertainties of the values obtained from formula (2) and Table ORNL-5 is reduced to that of the LSL-M2 adjustment procedure. They are listed in Table ORNL-7 in percent relative standard deviation.

TABLE ORNL-7

UNCERTAINTIES OBTAINED FROM THE LSL-M2 PROCEDURE FOR DAMAGE PARAMETER VALUES AT GRADIENT WIRE LOCATIONS

$F > 1.0$ MeV	6.4%
$F > 0.1$ MeV	8.0%
dpa	7.0%

For off-center locations, the formula

$$A(X,Y,Z) = [A_1 \cos B_{X1}(X_1-X_{01})\, e^{\lambda(Y_C-Y)} + A_2 \cos B_{X2}(X_2-X_{02})\, e^{-\lambda(Y_C-Y)}] \times \cos B_Z(Z-Z_0) \quad (3)$$

with $Y_C = 18.30$, the capsule centerline, applies which is a superposition of two functions in formula (1). X_1 is the X coordinate before rotation and X_2 is the same point in the capsule after rotation relative to a fixed coordinate system.

$X_2 = 29.52 - X_1$ for the north side and

$X_2 = -29.52 - X_1$ for the south side.

$X = X_1$ at the start of irradiation.

The coefficients are in Table ORNL-8.

TABLE ORNL-8

SUMMARY OF FITTING PARAMETERS FOR FORMULA (3)

	A_1	A_2	B_{X1} (cm^{-1})	B_{X2} (cm^{-1})	X_{O1} (cm)	X_{O2} (cm)	λ (cm^{-1})	B_Z (cm^{-1})	Z_O (cm^{-1})
F>1.0 MeV	1.14*	1.16*	0.0419	0.0412	0.13	-0.70	0.132	0.0402	-1.77
F>0.1 MeV	7.16*	7.28*	0.0419	0.0412	0.13	-0.70	0.0	0.0414	-1.33
dpa	0.0260	0.0265	0.0419	0.0412	0.13	-0.70	0.080	0.0410	-1.48
$^{54}Fe(n,p)^{54}Mn$	$4.18E^{-7}$	$4.26E^{-7}$	0.0419	0.0412	0.13	-0.70	0.019	0.0396	-1.98

*10^{19} neutrons/cm^2.

The uncertainties for formula (3) are largest since the dosimetry data are insufficient to separate the contributions from the two irradiation intervals. However, they do not exceed 15% relative standard deviation.

A.6 IRRADIATION HISTORY AND NEUTRON SOURCE DISTRIBUTIONS FOR THE SDMF EXPERIMENTS

L. F. Miller and F. B. K. Kam

Summary

Neutron source distributions in the ORR core are obtained for three of the four SDMF experiments. In particular, three-dimensional (3-D) neutron sources calculated by Williams, Maerker, and Worley (personal communications) are obtained for SDMF No. 1 (ORR PSF Startup Experiment), SDMF No. 2 (Westinghouse Perturbation Experiment), and SDMF No. 3 (B&W Perturbation Experiment). Neutronics calculations are not available, however, for the SDMF No. 4 (Radiometric and Advanced Sensor Calibration Program). Distributions for SDMF No. 1 through No. 3 are reported as two 2-D distributions (one horizontal and one vertical). The 2-D distributions are obtained by integrating the 3-D distributions in the appropriate transverse direction.

Accomplishments and Status

The irradiation history of each of the SDMF experiments is provided by Tables ORNL-9 and ORNL-10. The associated core loading specifications are defined by Figures ORNL-8 through ORNL-12.

TABLE ORNL-9

IRRADIATION DATA FOR EACH OF THE SDMF EXPERIMENTS

Event or Description	SDMF Experiment Designation†				
	1	2	3	4 (1st run)	4 (2nd run)
Core Cycle	151-A	152-A	162-B	166-D	166-E
Facility Insertion Date (Time)	10/27/79 (2:26 PM)*	10/31/80 (3:30 PM)	8/26/82 (1:55 PM)	11/23/83 (2:00 PM)	12/9/83 (10:23 AM)
Facility Retraction Date (Time) or Reactor Scram	11/14/79 (8:55 AM)	2/9/80 (3:30 PM)	9/7/82 (8:15 AM)	12/7/83 (3:00 AM)	12/14/83 (1:03 PM)
Megawatt-hours of Exposure	1.26 E+4	6.48 E+3	8.45 E+3	9.68 E+3	3.63 E+3

*See Table 1.2.2.

†SDMF No. 1 - Startup Experiment
SDMF No. 2 - Westinghouse Perturbation Experiment
SDMF No. 3 - B&W Perturbation Experiment
SDMF No. 4 - Radiometric and Advanced Sensor Calibration Program

TABLE ORNL-10

TIMING OF EXPOSURE FOR THE 18-DAY PSF STARTUP INTERLABORATORY DOSIMETRY CHARACTERIZATION (1979)[a,b]

Channel[c]	Total Exposure[d] (s)	Begin Exposure[e]	End Exposure[e]
SSC	1537640	Oct. 27; 2:26:00 PM	Nov. 14; 8:54:50 AM
PVF	1516382	Oct. 27; 8:20:48 PM	idem
1/4-T	1536960	Oct. 27; 2:26:00 PM	Nov. 14; 8:43:00 AM
$1/4\text{-}T_{off}$	1355012	Oct. 29; 4:10:18 PM	Nov. 14; 8:54:50 AM
1/2-T	1513374	Oct. 27: 9:10:56 PM	idem
3/4-T	1512975	Oct. 27; 9:17:37 PM	idem

[a]Average power is 29.6 MW.

[b]Data were obtained from A. Fabry, personal communications.

[c]SSC Simulated surveillance capsule
PVF Pressure vessel front
1/4-T Vessel quarter thickness
$1/4\text{-}T_{off}$: Off-centered vessel quarter thickness
1/2-T: Vessel half thickness
3/4-T: Vessel three-quarter thickness

[d]Time from beginning of exposure (column 3) to end of exposure (column 4) minus 21-minute shutdown period on November 1 from 10:00 AM to 10:21 AM; one hour Daylight Saving Time change added (October 28, 1979).

[e]Local time, Oak Ridge, Tennessee (USA).

ORR CORE

Cycle 151-A

Start October 23, 1979

End November 14, 1979

Core location →	A-3
Element identification →	T-125
Initial ^{235}U mass (g) →	285
^{235}U mass (g) at start of cycle →	221

POOL
WEST

	A-1 Be	A-2 Be	A-3 T-125 241	A-4 T-100 211	A-5 T-136 265	A-6 T-118 209	A-7 T-127 241	A-8 Be	A-9 Be	
	B-1 Be	B-2 T-101 196	B-3 T-137 265	B-4* FZC 004W 77	B-5 T-129 239	B-6* FZC 004Z 77	B-7 T-138 265	B-8 Xe	B-9 Be	
	C-1 Ir	C-2 T-19 208	C-3 Al	C-4 T-42 176	C-5 T-64 176	C-6 T-63 176	C-7 Al	C-8 T-105 214	C-9 Be	
S	D-1 Be	D-2 T-41 157	D-3 T-59 174	D-4* FZC 0051 138	D-5 T-37 157	D-6* FZC 004R 137	D-7 T-76 178	D-8 Be	D-9 Be	N
	E-1 Be	E-2 T-139 265	E-3 Al	E-4 T-4 157	E-5 Al	E-6 T-3 157	E-7 MFE-2	E-8 T-140 265	E-9 Be	
	F-1 Be	F-2 T-17 157	F-3 T-69 165	F-4* FZC 004U 53	F-5 T-124 246	F-6* FZC 004V 49	F-7 T-51 199	F-8 T-28 158	F-9 Be	
	G-1 Be	G-2 Be	G-3 Be	G-4 Be	G-5 Be	G-6 Be	G-7 Be	G-8 Be	G-9 Be	

*Control-rod location

EAST

FIGURE ORNL-8. Core Loading of the ORR for the Startup Experiment (SDMF No. 1).

ORR CORE

Cycle 152-A

Start January 25, 1980

End February 11, 1980

Core location —>	A-3
Element identification —>	T-125
Initial ^{235}U mass (g) —>	285
^{235}U mass (g) at start of cycle —>	221

POOL
WEST

	A-1 Be	A-2 Be	A-3 T-147 240	A-4 T-137 215	A-5 T-166 264	A-6 T-121 211	A-7 T-149 240	A-8 Be	A-9 Be	
	B-1 Be	B-2 T-124 198	B-3 T-167 265	B-4* FZC 0051 81	B-5 T-144 241	B-6* FZC 004R 81	B-7 T-168 265	B-8 Sb	B-9 Be	
	C-1 Ir	C-2 T-134 206	C-3 Al	C-4 T-118 174	C-5 T-99 173	C-6 T-9 173	C-7 Al	C-8 T-135 220	C-9 Be	
	D-1 Be	D-2 T-33 148	D-3 T-18 171	D-4* FZC 0053 138	D-5 T-60 148	D-6* FZC 0054 137	D-7 T-85 181	D-8 Be	D-9 Be	
	E-1 Be	E-2 T-169 265	E-3 Al	E-4 T-70 164	E-5 Al	E-6 T-64 150	E-7 MFE-2	E-8 T-170 265	E-9 Be	
	F-1 Be	F-2 T-14 154	F-3 T-55 170	F-4* FZC 004W 48	F-5 T-151 247	F-6* FZC 004Z 47	F-7 T-80 196	F-8 T-74 166	F-9 Be	
	G-1 Be	G-2 Be	G-3 Be	G-4 Be	G-5 Be	G-6 Be	G-7 Be	G-8 Be	G-9 Be	

S N

*Control-rod location.

EAST

FIGURE ORNL-9. Core Loading of the ORR for the Westinghouse Perturbation Experiment (SDMF No. 2).

ORR CORE

Cycle 162-B

Start August 26, 1982

End September 14, 1982

Core location ⟶	A-3
Element identification ⟶	T-365
Initial ^{235}U mass (g) ⟶	285
^{235}U mass (g) at start of cycle ⟶	221

POOL
WEST

A-1 Be	A-2 Al	A-3 T-342 285 236	A-4 T-331 285 250	A-5 T-332 285 250	A-6 T-346 285 252	A-7 T-347 285 235	A-8 Be	A-9 Be
B-1 Be	B-2 Be	B-3 T-356 285 285	B-4* U-015 167 96	B-5 CLE453 284 204	B-6* U-016 167 104	B-7 T-357 285 285	B-8 Be	B-9 Be
C-1 Be	C-2 T-278 265 209	C-3 HFED	C-4 T-95 300 161	C-5 T-174 265 165	C-6 T-194 265 157	C-7 CLE451 282 90	C-8 Al	C-9 Be
D-1 ISO	D-2 T-250 265 195	D-3 T-271 265 196	D-4* U-017 167 158	D-5 T-293X 280 173	D-6* U-018 167 158	D-7 T-257 265 198	D-8 T-234 265 195	D-9 Be
E-1 Be	E-2 T-352 285 263	E-3 Al	E-4 T-233 265 195	E-5 Al	E-6 T-207 265 195	E-7 MFE 4B	E-8 T-355 285 263	E-9 Be
F-1 Be	F-2 T-247 265 184	F-3 T-252 265 201	F-4* U-010 167 36	F-5 T-201 265 201	F-6* U-014 167 65	F-7 T-235 265 195	F-8 T-245 265 195	F-9 TRIGA LEU
G-1 Be	G-2 Be	G-3 Be	G-4 Be	G-5 Be	G-6 Be	G-7 Be	G-8 Be	G-9 Be

S N

*Control rod location.

EAST

FIGURE ORNL-10. Core Loading of the ORR for the B&W Perturbation Experiment (SDMF No. 3).

ORR CORE

Cycle 166-D

Start November 23, 1983

End December 7, 1983

Core location —>	A-3
Element identification —>	T-365
Initial ^{235}U mass (g) —>	285
^{235}U mass (g) at start of cycle —>	221

POOL
WEST

A-1 Be	A-2 Be	A-3 T-361 285 207	A-4 T-418 285 268	A-5 T-430 285 285	A-6 T-431 285 285	A-7 T-382 285 207	A-8 Be	A-9 Be
B-1 Be	B-2** NLE 201 340 237	B-3 T-271 265 155	B-4* U-028 167 89	B-5 T-370 285 207	B-6* U-029 167 88	B-7 T-341 285 194	B-8 Xe	B-9** CLE 202 336 208
C-1 Be	C-2** BSI 201 340 240	C-3 Ir	C-4** NSI 202 340 134	C-5 Ir	C-6** CSI 202 339 134	C-7 Ir	C-8** BSI 202 340 340	C-9 Be
D-1 Be	D-2 T-343 285 211	D-3 T-402 285 211	D-4* U-026 167 160	D-5 T-419 285 269	D-6* U-027 167 160	D-7 T-410 285 247	D-8 T-387 285 211	D-9 Be
E-1 Be	E-2 T-388 285 208	E-3 MFE 4A	E-4 T-404 285 245	E-5 Ir	E-6 T-330 285 212	E-7 MFE 4B	E-8 T-432 285 285	E-9 Be
F-1 Be	F-2 Be	F-3 T-344 285 184	F-4* U-021 167 40	F-5 T-408 285 252	F-6* U-022 167 42	F-7 T-324 285 16	F-8 Be	F-9 Be
G-1 Be	G-2 Be	G-3 Be	G-4 Be	G-5 Be	G-6 Be	G-7 Be	G-8 Be	G-9 Be

S N

*Control rod elements.

**LEU 20 W/o; these elements are low-enriched ^{235}U (20 wt%). All other elements are high-enriched ^{235}U (93 wt%).

EAST

FIGURE ORNL-11. Core Loading of the ORR for the Radiometric and Advanced Sensor Calibration Program (SDMF No. 4, Run No. 1).

ORR CORE

Cycle 166-E

Start December 7, 1983

End December 21, 1983

Core location —>	A-3
Element identification —>	T-365
Initial ^{235}U mass (g) —>	285
^{235}U mass (g) at start of cycle —>	221

POOL
WEST

A-1 Be	A-2 Be	A-3 T-373 285 202	A-4 T-421 285 268	A-5 T-422 285 281	A-6 T-423 285 281	A-7 T-360 285 202	A-8 Be	A-9 Be
B-1 Be	B-2** CLE 202 336 202	B-3** CLE 203 326 122	B-4* U-028 167 81	B-5 T-391 285 202	B-6* U-029 167 81	B-7 T-340 285 195	B-8 Xe	B-9** NLE 201 340 220
C-1 Be	C-2** BSI 202 340 318	C-3 Ir	C-4 T-139 265 156	C-5 Ir	C-6 T-213 265 150	C-7 Ir	C-8** BSI 201 340 318	C-9 Be
D-1 Be	D-2 T-400 285 215	D-3 T-398 285 213	D-4* U-026 167 146	D-5 T-425 285 281	D-6* U-027 167 146	D-7 T-405 285 251	D-8 T-379 285 203	D-9 Be
E-1 Be	E-2 T-362 285 202	E-3 MFE 4A	E-4 T-399 285 239	E-5 Ir	E-6 T-364 285 214	E-7 MFE 4B	E-8 T-424 285 281	E-9 Be
F-1 Be	F-2 Be	F-3 T-351 285 185	F-4* U-021 167 35	F-5 T-411 285 261	F-6* U-022 167 37	F-7 T-307 285 181	F-8 Be	F-9 Be
G-1 Be	G-2 Be	G-3 Be	G-4 Be	G-5 Be	G-6 Be	G-7 Be	G-8 Be	G-9 Be

S N

*Control rod elements.

**LEU 20 w/o; these elements are low-enriched ^{235}U (20 wt%). All other elements are high-enriched ^{235}U (93 wt%).

EAST

FIGURE ORNL-12. Core Loading of the ORR for the Radiometric and Advanced Sensor Calibration Program (SDMF No. 4, Run No. 2).

Results from 3-D neutron source distribution calculations are available on magnetic tape and on mass-storage units at ORNL. These data may be obtained for requests relevant to LWR dosimetry program objectives: however, it is not expected that the 3-D distribution will be used, since transport calculations typically require 2-D input. In particular, 2-D vertical and horizontal neutron source distributions are used as input for two 2-D transport calculations. Results from the horizontal and vertical transport calculations are used in a flux-synthesis technique (Ma84a) to obtain 3-D neutron-flux distributions external to the reactor core. Thus, the 2-D horizontal and vertical source distributions are reported herein. The flux synthesis procedure cited also utilizes a 1-D source distribution which may be obtained by integrating either of the 2-D distributions in the direction transverse to the Z coordinate.

The neutron source distributions (listed in Tables ORNL-11 through ORNL-16) are obtained by integrating the applicable 3-D distribution in the appropriate transverse directions. In particular, the horizontal distribution is defined by

$$S_H(x,z) = \int_o^H dy S(x,y,z) \quad .$$

The vertical distribution is given by

$$S_V(y,z) = \int_o^V dx S(x,y,z) \quad .$$

Note that the coordinate system used for the VENTURE (Vo77) (the diffusion theory computer program used to obtain the 3-D source distributions) calculations designates Y as the vertical axis and Z as the axis perpendicular to the experiment.

Each of the nine numbers listed in each fuel element location of Tables ORNL-11, ORNL-13, and ORNL-15 represents the absolute horizontal plane neutron source (in units of neutrons per square centimeter per second) for one-ninth of the fuel element (when multiplied by 10^{15}) with the ORR at 30 MW. The diffusion theory model for this calculation specifies a three-inch-square pitch for the fuel elements. Thus, each number listed specifies the average source strength [$n/(cm^2 \cdot s)$] over a one-inch-square area.

The nine numbers listed in each square for the vertical distribution, shown in Tables ORNL-14 and 16, have the same units as those for the horizontal plane and represent the same area. The axial profile is broken into one-inch segments and the fuel elements remain on a three-inch-square pitch.

A physical description of each of the SDMF experiments is given in Section 1.7 of NUREG/CR-3321.

TABLE ORNL-11

LISTING OF THE HORIZONTAL PLANE NEUTRON SOURCE DISTRIBUTION FOR THE ORR PSF STARTUP EXPERIMENT

Row \ Col	1	2	3	4	5	6	7	8	9
A	0 0 0	0 0 0	1.299 1.217 1.235	1.139 1.160 1.148	1.317 1.272 1.256	1.014 .9888 .9370	.9694 .9127 .9617	0 0 0	0 0 0
	0 0 0	0 0 0	1.387 1.270 1.279	1.186 1.211 1.192	1.339 1.285 1.271	1.043 1.020 .9636	.9833 .9312 1.037	0 0 0	0 0 0
	0 0 0	0 0 0	1.511 1.407 1.4[illegible]	1.332 1.375 1.351	1.510 1.447 1.428	1.172 1.150 1.079	1.081 1.025 1.178	0 0 0	0 0 0
B	0 0 0	1.588 1.521 1.473	1.77[illegible] 1.668 1.713	.5136 .5403 .5366	1.584 1.512 1.490	.4755 .4653 .4319	1.301 1.217 1.433	0 .1796 0	0 0 0
	0 0 0	1.575 1.492 1.461	1.775 1.738 1.796	.5475 .5796 .5777	1.703 1.624 1.600	.5101 .4980 .4596	1.358 1.271 1.509	0 .3426 0	0 0 0
	0 0 0	1.613 1.514 1.485	1.844 1.821 1.867	.5621 .5972 .6011	1.817 1.745 1.707	.5311 .5130 .4699	1.402 1.335 1.507	0 1.852 0	0 0 0
C	0 0 0	1.748 1.623 1.580	0 0 0	1.386 1.504 1.540	1.515 1.481 1.428	1.356 1.272 1.128	0 0 0	1.308 1.308 1.314	0 0 0
	0 0 0	1.784 1.647 1.596	0 0 0	1.402 1.521 1.569	1.575 1.564 1.486	1.384 1.284 1.133	0 0 0	1.122 1.084 1.138	0 0 0
	0 0 0	1.843 1.706 1.647	0 0 0	1.373 1.457 1.504	1.564 1.552 1.477	1.332 1.232 1.103	0 0 0	1.180 1.171 1.227	0 0 0
D	0 0 0	1.484 1.400 1.374	1.458 1.430 1.375	1.014 1.010 1.047	1.329 1.357 1.258	.9388 .8638 .8141	1.036 1.032 1.058	0 0 0	0 0 0
	0 0 0	1.464 1.383 1.362	1.471 1.439 1.371	.9840 .9685 .9906	1.250 1.277 1.191	.8901 .8252 .7821	.9988 .9817 1.018	0 0 0	0 0 0
	0 0 0	1.368 1.279 1.260	1.341 1.327 1.295	.9717 .9770 .9837	1.152 1.162 1.115	.8835 .8287 .7625	.8119 .7572 .7949	0 0 0	0 0 0
E	0 0 0	1.964 1.786 1.785	0 0 0	1.159 1.214 1.175	0 0 0	1.061 1.007 .8349	0 0 0	1.072 1.199 1.313	0 0 0
	0 0 0	1.807 1.635 1.672	0 0 0	1.184 1.262 1.206	0 0 0	1.087 1.038 .8357	0 0 0	.8862 1.000 1.126	0 0 0
	0 0 0	1.766 1.619 1.669	0 0 0	1.212 1.303 1.235	0 0 0	1.108 1.077 .8825	0 0 0	.8987 .9910 1.098	0 0 0
F	0 0 0	1.154 1.097 1.115	1.189 1.211 1.275	.4797 .5014 .4759	1.615 1.493 1.550	.3881 .3877 .3495	.9627 .8031 .7730	.6848 .6969 .7328	0 0 0
	0 0 0	1.132 1.095 1.118	1.194 1.225 1.311	.4908 .5126 .4838	1.592 1.430 1.509	.3928 .4000 .3701	1.105 .9452 .8946	.7282 .7166 .7333	0 0 0
	0 0 0	1.122 1.115 1.151	1.241 1.281 1.366	.5042 .5240 .4982	1.711 1.556 1.620	.4063 .4126 .3866	1.210 1.057 .9930	.7807 .7503 .7432	0 0 0
G	0 0 0	0 0 0	0 0 0	0 0 0	0 0 0	0 0 0	0 0 0	0 0 0	0 0 0
	0 0 0	0 0 0	0 0 0	0 0 0	0 0 0	0 0 0	0 0 0	0 0 0	0 0 0
	0 0 0	0 0 0	0 0 0	0 0 0	0 0 0	0 0 0	0 0 0	0 0 0	0 0 0

Values listed must be multiplied by 10^{15} to obtain $n/(cm^2 \cdot s)$. These values are obtained by integrating the 3-D volumetric source distribution over the axial (vertical) direction. Note that the "A" row faces the PSF experiment.

TABLE 12

LISTING OF THE VERTICAL PLANE NEUTRON SOURCE DISTRIBUTION FOR THE ORR PSF STARTUP EXPERIMENT

TOP OF REACTOR CORE

G	F	E	D	C	B	A	Row / Depth (in.)
0 0 0	.4812 .4612 .4661	.3602 .3465 .3280	.3278 .3190 .3261	.3821 .3984 .3694	.3514 .3186 .3052	.2788 .2966 .3085	1
0 0 0	.5000 .4828 .4600	.3557 .3420 .3292	.3266 .3222 .3299	.3917 .4058 .3824	.3570 .3269 .3151	.2876 .3018 .3226	2
0 0 0	.5633 .5195 .5085	.3937 .3783 .3652	.3575 .3612 .3685	.4423 .4591 .4348	.4006 .3741 .3621	.3334 .3488 .3703	3
0 0 0	.6433 .5954 .5763	.4454 .4268 .4121	.4012 .4139 .4211	.5084 .5293 .5016	.4565 .4323 .4198	.3903 .4081 .4289	4
0 0 0	.6178 .5758 .5509	.4551 .4360 4.266	.3763 .3997 .4051	.5253 .5469 .5188	.4944 .4721 .4584	.4281 .4477 4.650	5
0 0 0	.6871 .6424 .6129	.5057 .4841 .4745	.4194 .4497 .4564	.5947 .6202 .5884	.5566 .5340 .5191	.4900 .5111 .5270	6
0 0 0	.7500 .7024 .6707	.5536 .5313 .5231	.4632 .4999 .5086	.6678 .6966 .6621	.6225 .5990 .5826	.5570 .5766 5.897	7
0 0 0	.8130 .7637 .7303	.6034 .5826 .5820	.5160 .5643 .5749	.7615 .7881 .7555	.7022 .6787 .6589	.6444 .6509 .6556	8
0 0 0	.8012 .7563 .7224	.6131 .6015 .6497	.5320 .6075 .6141	.8684 .8457 .8607	.8151 .8009 .7681	.8046 .7165 .6996	9
0 0 0	.8517 .8065 .7720	.6554 .6474 .7131	.5847 .6762 .6841	.9734 .9384 .9709	.9107 .8994 .8599	.9232 .7923 .7609	10
0 0 0	.8934 .8476 .8132	.6903 .6822 .7408	.9457 1.054 1.075	1.028 1.006 1.035	1.181 1.165 1.108	.9826 .8521 .8139	11
0 0 0	.9277 .8816 .8475	.7195 .7119 .7697	.9705 1.078 1.105	1.080 1.064 1.092	1.238 1.219 1.161	1.037 .9024 .8588	12
0 0 0	.9769 .9306 .8959	.7339 .7282 .7878	.9912 1.101 1.132	1.114 1.100 1.128	1.285 1.265 1.205	1.078 .9379 .8896	13
0 0 0	.9959 .9500 .9155	.7500 .7455 .8069	1.018 1.133 1.166	1.149 1.135 1.164	1.326 1.305 1.242	1.113 .9666 .9143	14
0 0 0	1.004 .9594 .9254	.7580 .7545 .8173	1.030 1.148 1.182	1.168 1.155 1.186	1.312 1.292 1.229	1.136 .9824 .9270	15
0 0 0	.9976 .9527 .9207	.7550 .7533 .8164	1.030 1.148 1.183	1.168 1.155 1.188	1.316 1.296 1.232	1.139 .9825 .9259	16
0 0 0	1.104 1.053 1.023	.7766 .7787 .8428	1.075 1.196 1.234	1.211 1.197 1.232	1.321 1.300 1.235	1.151 .9896 .9334	17
0 0 0	1.069 1.020 .9936	.7556 .7594 .8221	1.050 1.166 1.203	1.180 1.166 1.201	1.290 1.268 1.203	1.120 .9618 .9071	18
0 0 0	1.026 .9793 .9567	.7279 .7328 .7931	1.014 1.124 1.160	1.137 1.123 1.157	1.237 1.212 1.149	1.075 .9219 .8696	19
0 0 0	.9617 .9169 .9014	.6873 .6941 .7513	.9633 1.061 1.096	1.073 1.059 1.091	1.172 1.144 1.082	1.010 .8651 .8180	20
0 0 0	1.054 .9986 .9859	.6975 .7097 .7664	1.004 1.092 1.131	1.094 1.079 1.113	1.126 1.091 1.030	.9759 .8319 .7927	21
0 0 0	.9558 .9038 .9141	.6422 .6562 .7087	.9341 1.001 1.040	1.003 .9887 1.017	1.038 .9942 .9356	.8828 .7523 .7221	22
0 0 0	.8782 .8354 .8574	.6028 .6173 .6648	.8849 .9333 .9723	.9343 .9205 .9411	.9827 .9280 .8699	.8044 .6879 .6622	23
0 0 0	.8760 .8654 .9050	.6349 .6511 .6889	.9086 .9460 .9866	.9635 .9598 .9637	1.009 .9456 .8856	.8320 .7210 .6702	24
0 0 0	0 0 0	0 0 0	.2762 .2518 .2745	0 0 0	.1600 .1462 .1429	0 0 0	25
0 0 0	0 0 0	0 0 0	.2601 .2312 2.554	0 0 0	.1491 .1340 .1329	0 0 0	26
0 0 0	0 0 0	0 0 0	.2241 .1987 .2200	0 0 0	.1570 .1399 .1397	0 0 0	27
0 0 0	0 0 0	0 0 0	.1901 .1710 .1883	0 0 0	.1661 .1477 .1478	0 0 0	28

BOTTOM OF REACTOR CORE

PSF EXPERIMENT

Values listed must be multiplied by 10^{15} to obtain $n/(cm^2 \cdot s)$. The 3-D neutron volumetric source distribution is integrated over the horizontal transverse direction perpendicular to the axis of the experiment to obtain the values listed. Note that the "A" row faces the PSF experiment.

TABLE ORNL-13

LISTING OF THE HORIZONTAL PLANE NEUTRON SOURCE DISTRIBUTION FOR THE WESTINGHOUSE PERTURBATION EXPERIMENT

PSF EXPERIMENT

Col / Row	1	2	3	4	5	6	7	8	9
A	0 0 0 0 0 0 0 0 0	0 0 0 0 0 0 0 0 0	1.163 1.115 1.150 1.228 1.155 1.186 1.329 1.272 1.311	1.085 1.115 1.124 1.126 1.161 1.166 1.261 1.311 1.317	1.306 1.282 1.282 1.332 1.303 1.309 1.497 1.463 1.470	1.060 1.043 0.997 1.101 1.089 1.040 1.243 1.233 1.173	1.030 0.964 0.954 1.084 0.995 0.979 1.181 1.096 1.024	0 0 0 0 0 0 0 0 0	0 0 0 0 0 0 0 0 0
B	0 0 0 0 0 0 0 0 0	1.179 1.203 1.214 1.104 1.150 1.193 1.044 1.132 1.203	1.476 1.472 1.552 1.513 1.528 1.620 1.577 1.596 1.671	0.510 0.542 0.593 0.541 0.579 0.590 0.555 0.597 0.618	1.586 1.529 1.537 1.683 1.643 1.653 1.805 1.776 1.775	0.530 0.524 0.493 0.569 0.562 0.526 0.597 0.584 0.543	1.413 1.276 1.105 1.490 1.345 1.153 1.552 1.443 1.291	0 0 0 0 0 0 0 0 0	0 0 0 0 0 0 0 0 0
C	0 0 0 0 0 0 0 0 0	0.985 1.146 1.263 0.972 1.153 1.278 1.047 1.223 1.330	0 0 0 0 0 0 0 0 0	1.229 1.370 1.450 1.244 1.390 1.487 1.224 1.338 1.433	1.486 1.687 1.486 1.555 1.564 1.536 1.556 1.582 1.539	1.425 1.362 1.225 1.468 1.389 1.245 1.422 1.342 1.220	0 0 0 0 0 0 0 0 0	1.104 1.020 1.058 1.276 1.237 1.280 1.439 1.462 1.510	0 0 0 0 0 0 0 0 0
D	0 0 0 0 0 0 0 0 0	0.958 1.036 1.091 1.056 1.080 1.113 1.023 1.018 1.043	1.252 1.251 1.230 1.287 1.285 1.249 1.192 1.195 1.181	0.960 0.972 1.043 0.940 0.939 0.996 0.929 0.949 0.998	1.286 1.348 1.274 1.234 1.293 1.225 1.176 1.212 1.174	1.032 0.967 0.933 0.993 0.945 0.938 1.001 0.975 0.984	1.247 1.277 1.340 1.346 1.398 1.466 1.495 1.533 1.557	0 0 0 0 0 0 0 0 0	0 0 0 0 0 0 0 0 0
E	0 0 0 0 0 0 0 0 0	1.618 1.539 1.595 1.536 1.436 1.510 1.541 1.445 1.521	0 0 0 0 0 0 0 0 0	1.140 1.219 1.258 1.184 1.267 1.292 1.201 1.323 1.326	0 0 0 0 0 0 0 0 0	1.165 1.182 1.246 1.199 1.238 1.301 1.238 1.269 1.318	0 0 0 0 0 0 0 0 0	1.830 1.661 1.732 1.625 1.416 1.503 1.568 1.372 1.453	0 0 0 0 0 0 0 0 0
F	0 0 0 0 0 0 0 0 0	1.010 0.978 1.005 1.004 0.986 1.015 1.006 1.013 1.053	1.127 1.157 1.242 1.137 1.180 1.293 1.194 1.247 1.359	0.423 0.450 0.439 0.437 0.464 0.446 0.451 0.475 0.460	1.714 1.608 1.706 1.659 1.515 1.643 1.780 1.648 1.761	0.422 0.440 0.428 0.423 0.442 0.423 0.435 0.450 0.436	1.506 1.374 1.304 1.381 1.278 1.174 1.431 1.283 1.224	1.007 0.960 0.997 0.984 0.958 0.984 1.024 0.989 0.990	0 0 0 0 0 0 0 0 0
G	0 0 0 0 0 0 0 0 0	0 0 0 0 0 0 0 0 0	0 0 0 0 0 0 0 0 0	0 0 0 0 0 0 0 0 0	0 0 0 0 0 0 0 0 0	0 0 0 0 0 0 0 0 0	0 0 0 0 0 0 0 0 0	0 0 0 0 0 0 0 0 0	0 0 0 0 0 0 0 0 0

Values listed must be multiplied by 10^{15} to obtain $n/(cm^2 \cdot s)$. These values are obtained by integrating the 3-D volumetric source distribution over the axial (vertical) direction. Note that the "A" row faces the PSF experiment.

TABLE ORNL-14

LISTING OF THE VERTICAL PLANE NEUTRON SOURCE DISTRIBUTION FOR THE WESTINGHOUSE PERTURBATION EXPERIMENT

TOP OF REACTOR CORE

G			F			E			D			C			B			A			Row / Depth (in.)
0	0	0	0.497	0.477	0.495	0.382	0.367	0.342	0.328	0.300	0.299	0.398	0.376	0.330	0.307	0.274	0.266	0.276	0.288	0.297	1
0	0	0	0.517	0.481	0.494	0.381	0.366	0.348	0.332	0.305	0.298	0.376	0.379	0.335	0.308	0.277	0.271	0.284	0.293	0.311	2
0	0	0	0.584	0.541	0.550	0.425	0.409	0.389	0.367	0.343	0.332	0.434	0.428	0.378	0.345	0.316	0.311	0.330	0.339	0.358	3
0	0	0	0.668	0.622	0.627	0.484	0.464	0.442	0.416	0.395	0.380	0.488	0.495	0.436	0.393	0.366	0.362	0.387	0.398	0.416	4
0	0	0	0.645	0.606	0.607	0.498	0.478	0.460	0.392	0.380	0.364	0.493	0.501	0.440	0.425	0.399	0.394	0.424	0.436	0.451	5
0	0	0	0.719	0.677	0.678	0.556	0.533	0.514	0.439	0.430	0.412	0.561	0.570	0.501	0.480	0.453	0.447	0.487	0.499	0.513	6
0	0	0	0.786	0.743	0.745	0.612	0.588	0.569	0.488	0.480	0.461	0.632	0.643	0.567	0.539	0.510	0.504	0.554	0.565	0.576	7
0	0	0	0.854	0.809	0.814	0.670	0.648	0.637	0.549	0.546	0.525	0.725	0.732	0.653	0.613	0.582	0.574	0.642	0.639	0.642	8
0	0	0	0.847	0.807	0.814	0.683	0.672	0.715	0.571	0.591	0.564	0.821	0.779	0.743	0.722	0.699	0.679	0.782	0.702	0.686	9
0	0	0	0.902	0.863	0.872	0.733	0.727	0.788	0.632	0.663	0.631	0.928	0.869	0.845	0.813	0.792	0.766	0.895	0.778	0.748	10
0	0	0	0.948	0.909	0.922	0.774	0.768	0.821	1.026	1.062	1.035	0.981	0.936	0.904	1.050	1.062	1.019	0.957	0.838	0.812	11
0	0	0	0.986	0.947	0.963	0.809	0.804	0.856	1.057	1.088	1.066	1.033	0.993	0.957	1.114	1.112	1.068	1.012	0.890	0.868	12
0	0	0	1.043	1.005	1.022	0.827	0.824	0.878	1.082	1.114	1.094	1.066	1.076	0.988	1.190	1.156	1.111	1.054	0.929	0.881	13
0	0	0	1.065	1.027	1.046	0.847	0.846	0.902	1.115	1.149	1.130	1.102	1.062	1.022	1.232	1.197	1.149	1.091	0.957	0.907	14
0	0	0	1.076	1.039	1.059	0.857	0.857	0.915	1.131	1.167	1.148	1.123	1.083	1.045	1.222	1.188	1.140	1.115	0.974	0.922	15
0	0	0	1.069	1.032	1.055	0.855	0.857	0.915	1.133	1.169	1.151	1.125	1.085	1.048	1.230	1.195	1.145	1.119	0.976	0.922	16
0	0	0	1.154	1.142	1.168	0.879	0.886	0.945	1.186	1.222	1.201	1.181	1.140	1.104	1.236	1.207	1.152	1.134	0.986	0.933	17
0	0	0	1.148	1.107	1.135	0.855	0.864	0.922	1.158	1.193	1.177	1.152	1.111	1.078	1.209	1.174	1.124	1.106	0.960	0.907	18
0	0	0	1.102	1.063	1.092	0.824	0.834	0.890	1.119	1.151	1.137	1.112	1.072	1.040	1.162	1.126	1.076	1.063	0.921	0.871	19
0	0	0	1.033	0.995	1.027	0.777	0.789	0.842	1.060	1.087	1.075	1.050	1.012	0.981	1.104	1.064	1.015	1.000	0.863	0.820	20
0	0	0	1.130	1.080	1.124	0.784	0.803	0.856	1.106	1.122	1.113	1.095	1.054	1.028	1.147	1.119	0.971	0.970	0.836	0.798	21
0	0	0	1.024	0.976	1.028	0.720	0.739	0.780	1.024	1.029	1.025	1.005	0.966	0.962	0.982	0.930	0.883	0.878	0.757	0.728	22
0	0	0	0.941	0.902	0.962	0.672	0.692	0.737	0.965	0.957	0.960	0.938	0.904	0.878	0.935	0.872	0.826	0.801	0.694	0.670	23
0	0	0	0.939	0.932	1.005	0.703	0.723	0.756	0.980	0.966	0.975	0.972	0.951	0.927	0.959	0.899	0.847	0.836	0.730	0.679	24
0	0	0	0	0	0	0	0	0	0.291	0.266	0.285	0	0	0	0.172	0.156	0.152	0	0	0	25
0	0	0	0	0	0	0	0	0	0.275	0.243	0.266	0	0	0	0.161	0.144	0.141	0	0	0	26
0	0	0	0	0	0	0	0	0	0.236	0.208	0.229	0	0	0	0.145	0.146	0.145	0	0	0	27
0	0	0	0	0	0	0	0	0	0.169	0.179	0.196	0	0	0	0.131	0.151	0.150	0	0	0	28

BOTTOM OF REACTOR CORE

PSF EXPERIMENT

Values listed must be multiplied by 10^{15} to obtain $n/(cm^2 \cdot s)$. The 3-D neutron volumetric source distribution is integrated over the horizontal transverse direction perpendicular to the axis of the experiment to obtain the values listed. Note that the "A" row faces the PSF experiment.

TABLE ORNL-15

LISTING OF THE HORIZONTAL PLANE NEUTRON SOURCE DISTRIBUTION FOR THE B&W PERTURBATION EXPERIMENT

PSF EXPERIMENT

Row \ Col.	1	2	3	4	5	6	7	8	9
A	0 0 0 0 0 0 0 0 0	0 0 0 0 0 0 0 0 0	0.913 0.914 0.959 0.916 0.927 0.983 0.990 1.024 1.092	1.047 1.072 1.112 1.076 1.105 1.145 1.224 1.271 1.315	1.141 1.149 1.194 1.174 1.182 1.175 1.317 1.365 1.336	1.127 1.104 1.080 1.157 1.133 1.109 1.316 1.290 1.254	0.987 0.967 1.018 1.018 1.009 1.099 1.104 1.114 1.222	0 0 0 0 0 0 0 0 0	0 0 0 0 0 0 0 0 0
B	0 0 0 0 0 0 0 0 0	0 0 0 0 0 0 0 0 0	1.337 1.330 1.430 1.466 1.424 1.527 1.555 1.513 1.620	0.521 0.554 0.576 0.564 0.603 0.628 0.599 0.643 0.672	1.317 1.323 1.361 1.433 1.438 1.419 1.543 1.549 1.528	0.621 0.605 0.576 0.674 0.658 0.625 0.724 0.708 0.679	1.444 1.387 1.537 1.548 1.485 1.806 1.781 1.718 1.763	0 0 0 0 0 0 0 0 0	0 0 0 0 0 0 0 0 0
C	0 0 0 0 0 0 0 0 0	1.256 1.268 1.268 1.142 1.185 1.229 1.042 1.149 1.232	0.620 0.629 0.683 0.634 0.849 0.717 0.656 0.681 0.723	1.103 1.211 1.272 1.153 1.261 1.327 1.116 1.200 1.263	1.372 1.377 1.365 1.435 1.440 1.427 1.431 1.432 1.405	1.267 1.257 1.258 1.330 1.317 1.362 1.265 1.254 1.286	0.653 0.654 0.829 0.737 0.728 0.866 0.685 0.691 0.849	0 0 0 0 0 0 0 0 0	0 0 0 0 0 0 0 0 0
D	0 0 0 0 0 0 0 0 0	0.869 1.051 1.177 0.843 1.030 1.160 0.848 0.999 1.112	1.291 1.307 1.312 1.253 1.291 1.277 1.179 1.196 1.193	1.015 1.021 1.084 0.957 0.952 1.004 0.939 0.954 0.996	1.350 1.409 1.343 1.262 1.318 1.256 1.178 1.208 1.174	1.084 1.033 1.031 1.005 0.942 0.903 0.995 0.973 0.987	1.532 1.455 1.391 1.344 1.292 1.350 1.490 1.520 1.460	1.794 1.756 1.357 1.238 1.195 1.747 1.219 1.144 1.191	0 0 0 0 0 0 0 0 0
E	0 0 0 0 0 0 0 0 0	1.152 1.248 1.320 1.219 1.235 1.335 1.280 1.298 1.342	0 0 0 0 0 0 0 0 0	1.185 1.284 1.291 1.204 1.303 1.322 1.757 1.390 1.390	0 0 0 0 0 0 0 0 0	1.294 1.324 1.419 1.314 1.366 1.466 1.353 1.408 1.491	0 0 0 0 0 0 0 0 0	1.576 1.387 1.148 1.511 1.302 1.321 1.469 1.253 1.298	0 0 0 0 0 0 0 0 0
F	0 0 0 0 0 0 0 0 0	0.993 0.980 1.019 0.995 0.983 1.019 1.017 1.025 1.072	1.137 1.174 1.290 1.136 1.188 1.345 1.207 1.273 1.427	0.277 0.296 0.297 0.285 0.306 0.304 0.296 0.316 0.314	1.389 1.309 1.353 1.422 1.312 1.371 1.511 1.411 1.463	0.522 0.535 0.520 0.534 0.547 0.531 0.557 0.566 0.543	1.401 1.306 1.232 1.296 1.179 1.112 1.347 1.228 1.155	1.068 0.958 0.835 1.031 0.933 0.784 1.077 0.974 0.821	0.995 0.855 0.867 0.801 0.623 0.691 0.875 0.692 0.680
G	0 0 0 0 0 0 0 0 0	0 0 0 0 0 0 0 0 0	0 0 0 0 0 0 0 0 0	0 0 0 0 0 0 0 0 0	0 0 0 0 0 0 0 0 0	0 0 0 0 0 0 0 0 0	0 0 0 0 0 0 0 0 0	0 0 0 0 0 0 0 0 0	0 0 0 0 0 0 0 0 0

Values listed must be multiplied by 10^{15} to obtain $n/(cm^2 \cdot s)$. These values are obtained by integrating the 3-D volumetric source distribution over the axial (vertical) direction. Note that the "A" row faces the PSF experiment.

TABLE ORNL-16

LISTING OF THE VERTICAL PLANE NEUTRON SOURCE DISTRIBUTION FOR THE B&W PERTURBATION EXPERIMENT

TOP OF REACTOR CORE

G			F			E			D			C			B			A			Row / Depth (in.)
0	0	0	0.548	0.522	0.561	0.389	0.373	0.332	0.427	0.384	0.385	0.352	0.397	0.349	0.232	0.193	0.184	0.267	0.277	0.287	1
0	0	0	0.558	0.527	0.551	0.380	0.368	0.332	0.427	0.384	0.385	0.358	0.402	0.352	0.216	0.198	0.198	0.273	0.279	0.298	2
0	0	0	0.628	0.579	0.614	0.425	0.408	0.369	0.472	0.431	0.433	0.404	0.461	0.403	0.247	0.228	0.217	0.315	0.321	0.340	3
0	0	0	0.747	0.665	0.697	0.487	0.461	0.418	0.552	0.495	0.494	0.481	0.545	0.474	0.288	0.265	0.252	0.369	0.375	0.394	4
0	0	0	0.685	0.641	0.669	0.497	0.474	0.437	0.513	0.459	0.494	0.460	0.508	0.434	0.320	0.291	0.277	0.399	0.406	0.421	5
0	0	0	0.762	0.714	0.743	0.553	0.526	0.482	0.571	0.550	0.548	0.507	0.582	0.501	0.367	0.332	0.316	0.457	0.464	0.479	6
0	0	0	0.830	0.780	0.815	0.604	0.576	0.530	0.626	0.610	0.602	0.578	0.668	0.573	0.416	0.377	0.358	0.520	0.524	0.537	7
0	0	0	0.899	0.846	0.878	0.657	0.629	0.590	0.695	0.686	0.704	0.674	0.772	0.667	0.482	0.437	0.417	0.603	0.593	0.598	8
0	0	0	0.891	0.843	0.872	0.670	0.652	0.665	0.716	0.740	0.763	0.704	0.757	0.693	0.590	0.539	0.502	0.736	0.665	0.617	9
0	0	0	0.947	0.897	0.928	0.715	0.702	0.737	0.782	0.820	0.850	0.806	0.855	0.796	0.634	0.618	0.572	0.843	0.749	0.694	10
0	0	0	0.992	0.942	0.975	0.756	0.739	0.761	1.177	1.237	1.290	0.854	0.925	0.854	0.679	0.650	0.589	0.897	0.775	0.745	11
0	0	0	1.030	0.980	1.015	0.787	0.773	0.791	1.210	1.260	1.330	0.904	0.986	0.907	1.026	0.540	0.867	0.949	0.824	0.789	12
0	0	0	1.089	1.039	1.074	0.805	0.793	0.812	1.240	1.293	1.370	0.917	1.035	0.972	1.074	0.981	0.905	0.990	0.860	0.820	13
0	0	0	1.110	1.060	1.097	0.824	0.814	0.835	1.277	1.334	1.416	0.953	1.045	0.959	1.117	1.026	0.940	1.028	0.890	0.846	14
0	0	0	1.119	1.071	1.108	0.833	0.827	0.848	1.291	1.352	1.436	0.974	1.068	0.982	1.105	1.010	0.930	1.054	0.909	0.862	15
0	0	0	1.111	1.062	1.101	0.830	0.824	0.848	1.291	1.355	1.439	0.975	1.069	0.984	1.113	1.020	0.939	1.061	0.913	0.865	16
0	0	0	1.044	1.188	1.226	0.805	0.845	0.871	1.343	1.408	1.491	1.113	1.209	1.123	1.716	1.030	0.948	1.082	0.928	0.880	17
0	0	0	1.204	1.148	1.186	0.822	0.824	0.850	1.312	1.375	1.455	1.083	1.175	1.093	1.091	1.009	0.929	1.058	0.907	0.859	18
0	0	0	1.154	1.107	1.142	0.791	0.795	0.822	1.267	1.327	1.403	1.043	1.130	1.052	1.065	0.968	0.891	1.021	0.873	0.828	19
0	0	0	1.080	1.039	1.070	0.766	0.752	0.778	1.199	1.252	1.322	0.975	1.056	0.985	0.986	0.915	0.842	0.963	0.823	0.782	20
0	0	0	1.191	1.124	1.174	0.743	0.755	0.783	1.234	1.274	1.337	1.126	1.200	1.118	0.936	0.878	0.808	0.942	0.804	0.770	21
0	0	0	1.078	1.013	1.069	0.682	0.696	0.721	1.136	1.164	1.219	1.015	1.080	1.027	0.849	0.799	0.736	0.856	0.731	0.706	22
0	0	0	0.991	0.935	0.999	0.639	0.653	0.673	1.070	1.082	1.133	0.940	0.999	0.949	0.800	0.749	0.690	0.785	0.674	0.654	23
0	0	0	0.994	0.981	1.058	0.678	0.693	0.705	1.103	1.108	1.162	0.981	1.052	0.985	0.823	0.765	0.709	0.821	0.716	0.669	24
0	0	0	0	0	0	0	0	0	0.304	0.273	0.298	0	0	0	0.195	0.174	0.169	0	0	0	25
0	0	0	0	0	0	0	0	0	0.287	0.251	0.278	0	0	0	0.181	0.159	0.158	0	0	0	26
0	0	0	0	0	0	0	0	0	0.251	0.218	0.242	0	0	0	0.165	0.141	0.140	0	0	0	27
0	0	0	0	0	0	0	0	0	0.218	0.192	0.217	0	0	0	0.140	0.145	0.141	0	0	0	28

BOTTOM OF REACTOR CORE

PSF EXPERIMENT

Values listed must be multiplied by 10^{15} to obtain n/(cm^2·s). The 3-D neutron volumetric source distribution is integrated over the horizontal transverse direction perpendicular to the axis of the experiment to obtain the values listed. Note that the "A" row faces the PSF experiment.

Future Accomplishments

No additional effort is planned relative to the definition of the irradiation history or neutron source terms of SDMF experiments.

B. ASTM STANDARDS ACTIVITIES

F. W. Stallmann

Objective

The objective of this task is to prepare ASTM Standards which will support recommendations for proposed modifications, data bases, and methodologies related to Codes and Regulatory Guides.

Accomplishments and Status

The three ASTM Standards originating at ORNL E482-82 (E706 IID), E944-83 (E706 IIA), and E1006-84 (E706 II) are now part of the Book of Standards. However, experience gained from recent benchmark tests and power reactors (PCA, PSF, and ANO-I) suggests that updating of the Standards for transport calculation (E482) and adjustment methods (E944) may be desirable. There is an ongoing discussion about such updating in the ASTM E10.05.01 Task Group on Uncertainty Analysis and Computational Procedures which is responsible for these standards. The Task Group met September 27, 1984 in Geesthacht, Germany, and January 15, 1985, in Reno, Nevada. The following topics were discussed for possible inclusion in updated versions of the Standards:

1. Guidance for the determination of uncertainties (variances and covariances) for calculated neutron fluences.

2. Simplification of dosimetry cross-section variances and covariances that are needed for adjustment procedures.

3. Further standardization and simplification of adjustment procedures so that these methods will be more widely used to improve the accuracy of fluence determinations in test and power reactors.

As a basis for further discussions, a paper was circulated among the Task Group members that outlines in more detail some of the essential features and problems of adjustment procedures. It is attached to this report.

ATTACHMENT

DETERMINATION AND SIGNIFICANCE OF COVARIANCES IN NEUTRON SPECTRUM ADJUSTMENT METHODS

Friedemann W. Stallmann

NOTE: This is a revised and expanded version of a paper which was distributed at the Workshop on Adjustment Methods and Uncertainties at the 5th ASTM-EURATOM Symposium on Reactor Dosimetry, September 24-28, 1984, in Geesthacht, Germany. It was redistributed to the members of the E-10.05.01 Task Group on Uncertainty Analysis and Computational Procedures for further consideration and comment.

In earlier workshops on adjustment methods - starting with the first one in Petten in 1975 - our aim has been to put the "unfolding" procedures, as they were called at that time, on a sound mathematical basis. It is generally recognized now that unfolding should be performed with the statistical methods of least squares adjustment. All input data (dosimetry measurements, cross sections, and calculated fluences) are treated as random variables, and uncertainties in the form of variances and covariances must be determined for all these data. This task is far from routine for the fluence and cross section data, particularly in regard to covariances. Many researchers are, therefore, reluctant to use these adjustment methods or try to make improper simplifications. This workshop and the ASTM E10.05.01 Task Group for Uncertainty Analysis appear to be the proper forum to discuss these difficulties and initiate the establishment of guides and standardized procedures to provide the necessary help for the application of these adjustment procedures.

As the first step toward this goal, the following actions are proposed:

1. Variance-covariance information for dosimetry cross sections should be simplified. The current ENDF/B-V and the special dosimetry file use four different formats for this information and require complicated processing codes such as PUFF to convert the ENDF data to a given energy group structure. The following discussion gives some guidance as to what simplifications may be most appropriate.

2. Establishment of guidelines for the determination of calculated fluence variances and covariances. Of particular interest is the question whether "generic" covariances may be used instead of rigorously calculated data.

In the rest of this presentation, a few facts are discussed concerning spectrum adjustment procedures which shed some light on the significance of the covariance information and the required accuracy in determining it. To have something concrete, a logarithmic adjustment is assumed, i.e., only relative variances and covariances are given and adjustments are in the form of positive factors. However, the general rules discussed below apply to all

forms of least squares adjustment. The first items of information are radiometric (foil) dosimetry measurements in the form of reaction rates or reaction probabilities taken at some specified position, p, in the experimental setup with a sensor, s, [e.g., $^{54}Fe(n,p)^{54}Mn$]. The measured value may be called R_E^{ps} (E for experimental). It is also assumed that the corresponding calculated values R_C^{ps} have been determined by folding, in the usual manner, the calculated group fluences, or fluence rates, ϕ_i^p, with the corresponding dosimetry group cross section values, σ_i^s, that is,

$$R_C^{ps} = \sum_{i=1}^{n} \phi_i^p \ \sigma_i^s \quad . \tag{1}$$

Ideally, R_E^{ps} and R_C^{ps} should be equal. Any deviation between calculated and experimental values calls for an adjustment of all values in proportion to their respective uncertainties. The deviation between calculated and experimental values is expressed as the logarithm of the C/E ratios and is called the residual r^{ps} in the context of the least squares adjustment procedure,

$$r^{ps} = \ln(R_C^{ps}/R_E^{ps}) \quad . \tag{2}$$

The adjustment of any quantity x, which is a function of fluence, cross section, and reaction rate values, is determined in the following manner: the residuals as well as the quantity x are subject to random uncertainties and their variances and covariances can be calculated from the variances and covariances of reaction rates, fluences, and cross sections. Let V_{rr} be the covariance matrix of the residuals, V_{xr} the (row) vector of the covariances between x and the residuals, and $\bar{r}$ the (column) vector of the residuals. Adjusted values will be indicated by a tilde (e.g., $\tilde{x}$ for the adjusted value of x). With these definitions,

$$\tilde{x} = x - V_{xr} \ V_{rr}^{-1} \ \bar{r} \tag{3}$$

where V_{rr}^{-1} is the inverse matrix. The variance of the adjusted value $\tilde{x}$ [i.e., the covariance with itself, indicated by the symbol cov(. .)] is

$$cov(\tilde{x} \ \tilde{x}) = cov(x \ x) - V_{xr} \ V_{rr}^{-1} \ V_{rx} \tag{4}$$

where V_{rx} is the transpose to the matrix V_{xr}. Equation (4) indicates a reduction of the variance of the adjusted value relative to the original quantity. Setting a residual, r, for x in Eqs. (3) and (4) indicates that the adjusted residual and its variance is zero, i.e., the adjusted values are consistent

with each other. These and the following equations are obtained through linearization and apply strictly only for small adjustments.

Equations (3) and (4) indicate that the only relevant quantities are the covariances between residuals and between the residuals and the target quantity x. Explicitly, one obtains from Eqs. (1) and (2)

$$\mathrm{cov}(r^{ps}\ r^{p's'}) = \sum_{i=1}^{n}\sum_{j=1}^{n} \frac{\phi_i^p \sigma_i^s}{R_C^{ps}} \frac{\phi_j^{p'} \sigma_j^{s'}}{R_C^{p's'}} [\mathrm{cov}(\phi_i^p \sigma_j^{p'})/\phi_i^p \sigma_j^{p'} + \mathrm{cov}(\sigma_i^s \sigma_j^{s'})/\sigma_i^s \sigma_j^{s'}] +$$

$$\mathrm{cov}(R_E^{ps}\ R_E^{p's'})/R_E^{ps}\ R_E^{p's'} \quad . \tag{5}$$

Note first that

$$\sum_{i=1}^{n} \frac{\phi_i^p \sigma_i^s}{R_C^{ps}} = 1 \tag{6}$$

so that the covariances between r^{ps} and $r^{p's'}$ are weighted averages of the original group fluence or group cross section covariances. The weights are equal to the fraction of the response of the given sensor to neutrons in the particular energy group. They depend primarily on the dosimetry cross section and are only weakly dependent on the neutron spectrum. Thus, one needs not worry about fine details in fluence and cross section covariances, and the covariance values which are determined for one particular neutron spectrum are equally valid for a broad class of similar spectra.

Contributions from cross section and fluence covariances to the matrix V_{rr} obtained through the LSL-M2 adjustment procedure applied to the PSF Metallurgical Experiment are listed in Tables 1 and 2. Present covariance files for cross sections consider only covariances between energy groups of the same sensor resulting in just one value for each sensor in V_{rr} with zero correlation between different sensors. In other words, each sensor has a typical cross section variance which changes only slightly with the spectrum. These variances are listed in the form of relative standard deviations in Table 1.

Table 1. Contributions to V_{rr} from cross-section covariances.

Values are obtained from the LSL-M2 code at various SSC-1 positions in the PSF Metallurgical Experiment. Values at other positions are the same within the three-digit accuracy.

Sensor	Percent standard deviation
$^{63}Cu(n,\alpha)^{60}Co$	5.3
$^{46}Ti(n,p)^{46}Sc$	12.6
$^{54}Fe(n,p)^{54}Mn$	3.6
$^{58}Ni(n,p)^{58}Co$	6.6
$^{238}U(n,f)$	2.0
$^{237}Np(n,f)$	9.4
$^{235}U(n,f)$	4.4
$^{59}Co(n,\gamma)^{60}Co$	19.9
$^{45}Sc(n,\gamma)^{46}Sc$	18.9
$^{58}Fe(n,\gamma)^{59}Fe$	8.1

Fluence contributions to V_{rr} for a number of threshold dosimeters at the same position are given in Table 2 in the form of relative standard deviations and correlations. The values are based on the fluence correlations provided by R. E. Maerker. The correlations are quite high, the higher the more similar the sensor responses are, as expected. The correlations are reduced by a few percent for sensors at different positions. The values for fluence > 1.0 MeV, fluence > 0.1 MeV, and dpa are added to the table. These values are entries to the matrix V_{xr} if x is one of the damage exposure parameters listed above.

The high correlations in the matrix V_{rr} cannot be simply ignored, for instance, by averaging C/E ratios to obtain a common normalization factor. However, simplifications and standardization of the determination of covariances appear feasible, since the covariance matrix V_{rr} is not very sensitive to slight changes in the neutron spectrum. This workshop and the ASTM E10.05.01 Task Group are challenged to provide the necessary recommendations.

Table 2. Contributions to V_{rr} and V_{xr} from fluence covariances.

Values were obtained from the LSL-M2 code for the SSC-2 H-9 position in the PSF Metallurgical Experiment.

	Sensor	Pct. std. dev.	1	2	3	4	5	6	7	8	9
1	$^{63}Cu(n,\alpha)^{60}Co$	17.8	1.000								
2	$^{46}Ti(n,p)^{46}Sc$	17.1	0.987	1.000							
3	$^{54}Fe(n,p)^{54}Mn$	15.8	0.954	0.986	1.000						
4	$^{58}Ni(n,p)^{58}Co$	15.5	0.950	0.982	0.999	1.000					
5	$^{238}U(n,f)$	14.2	0.886	0.921	0.964	0.973	1.000				
6	$^{237}Np(n,f)$	13.2	0.804	0.839	0.891	0.903	0.963	1.000			
7	F>1.0 MeV	13.6	0.848	0.884	0.935	0.945	0.993	0.979	1.000		
8	F>0.1 MeV	12.2	0.776	0.810	0.864	0.877	0.945	0.981	0.968	1.000	
9	dpa	13.0	0.831	0.866	0.914	0.925	0.973	0.995	0.984	0.982	1.000

The following simple example shows how the data in Tables 1 and 2 may be applied to a given adjustment problem. The data were obtained from an HSST metallurgical irradiation experiment performed at the ORR in a modified PSF which is sufficiently similar to the original PSF; the following dosimetry measurements (R_E^{ps}) were made (total reaction probability):

Table 3

$^{46}Ti(n,p)^{46}Sc = 7.156 \times 10^{-8}$
$^{54}Fe(n,p)^{54}Mn = 5.864 \times 10^{-7}$
$^{238}U(n,f)FP = 4.546 \times 10^{-6}$

The calculated values (R_C^{ps}) including damage parameters were

Table 4

$^{46}Ti(n,p)^{46}Sc$	$= 4.502 \times 10^{-8}$
$^{54}Fe(n,p)^{54}Mn$	$= 3.877 \times 10^{-7}$
$^{238}U(n,f)FP$	$= 2.835 \times 10^{-6}$
$F > 1.0$ MeV	$= 1.036 \times 10^{19}$
$F > 0.1$ MeV	$= 6.652 \times 10^{19}$
dpa	$= 2.446 \times 10^{-2}$

One calculates first the C/E ratios R_C^{ps}/R_E^{ps} which are 0.63, 0.66, and 0.62, respectively. The covariance matrix for the logarithm of these ratios can be obtained from Table 2 by first multiplying the correlations with the appropriate variances and then adding the cross-section variances from Table 1 and the measuring variances at the diagonal (5% for non-fission and 8% for the fission monitor). The resulting matrix is

Table 5

	Ti	Fe	U
Ti	4.76	2.66	2.24
Fe	2.66	2.88	2.16
U	2.24	2.16	2.68

(All values to be multiplied by 10^{-2}.)

The calculation did not represent the core leakage correctly, and it is, therefore, assumed that the values are known only up to a normalization factor, which is determined through the measurements. The $^{54}Fe(n,p)^{54}Mn$ reaction is used for normalization, i.e., all calculated values R_C^{ps} are divided by the C/E

ratio R_C^{Fe}/R_E^{Fe} for this reaction. This reduces the number of residuals from three to two; the new residuals are the logarithm of the ratios of the C/E ratios or the differences of the logarithm,

$$r^{sp} = \ln(R_C^{sp}/R_E^{sp}) - \ln(R_C^{Fe}/R_E^{Fe}) \qquad (7)$$

The covariance matrix, Table 5, reduces to

Table 6

	Ti/Fe	U/Fe
Ti/Fe	2.32	0.30
U/Fe	0.30	1.24

(All values to be multiplied by 10^{-2}.)

This is the matrix V_{rr} of the residuals defined in Eq. 7. The inverse V_{rr}^{-1} is

Table 7

	Ti/Fe	U/Fe
Ti/Fe	44.5	-10.8
U/Fe	-10.8	83.2

(These are the actual values.)

The matrix, V_{xr}, for the covariances between damage parameter values and residual values can be calculated in a similar manner starting from Table 2

Table 8

	Ti	Fe	U
F > 1.0 MeV	2.06	2.01	1.92
F > 0.1 MeV	1.69	1.67	1.64
dpa	1.93	1.88	1.80

(All values to be multiplied by 10^{-2}.)

and after normalizing,

Table 9

	Ti/Fe	U/Fe
F > 1.0 MeV/Fe	0.27	0.63
F > 0.1 MeV/Fe	0.24	0.69
dpa/Fe	0.27	0.64

(All values to be multiplied by 10^{-2}.)

The adjustments of the damage parameters are obtained by first multiplying $V_{xr} \cdot V_{rr}^{-1}$ which provides the weights to be applied to the residuals in order to obtain the adjustments in Eq. 3. The result is

Table 10

	W_{Ti}	W_U
F > 1.0 MeV/Fe	0.061	0.493
F > 0.1 MeV/Fe	0.041	0.546
dpa	0.060	0.501

It is interesting to note the small contribution of the $^{46}Ti(n,p)^{46}Sc$ reaction to the adjustment, which is only one-tenth of that for $^{238}U(n,f)$. The main reason is the large cross-section uncertainty for $^{46}Ti(n,p)^{46}Sc$. The $^{238}U(n,f)$ resembles also much more the damage cross sections, although the similarity is much higher for F > 1.0 MeV than for F > 0.1 MeV, which is not reflected in the values in Table 10.

The values of the residuals are

Table 11

$r^{Ti/Fe} = -0.050$

$r^{U/Fe} = -0.058$

(See Eq. 7.)

Thus, the adjustment factors obtained from multiplying the data in Table 10 with the corresponding values in Table 11 (see Eq. 3) become

Table 12. Adjustments of the calculated normalized damage parameter values

$F > 1.0$ MeV/Fe	$= -0.032$
$F > 0.1$ MeV/Fe	$= -0.034$
dpa/Fe	$= -0.032$

Applying these values to Eq. (3) leads to an upward adjustment of roughly 3%. This is in actual numbers,

Table 13

	Calculated	Normalized with Fe	Adjusted
$F > 1.0$ MeV	1.036×10^{19}	1.567×10^{19}	1.618×10^{19}
$F > 0.1$ MeV	6.652×10^{19}	1.006×10^{20}	1.041×10^{20}
dpa	2.446×10^{-2}	3.700×10^{-2}	3.820×10^{-2}

Adjustments are sometimes performed by normalizing calculated damage parameters with several dosimetry measurements and then determining a weighted average with weights which reflect the relative importance of the respective dosimetry sensor to the damage parameter. The weights listed in Table 10 are also the correct weights for this type of adjustment procedure with $W_{Fe} = 1 - W_{Ti} - W_U$. The results will be the same provided the residuals are small enough so that $\ln(1 + x) \simeq x$. The calculation for $F > 1.0$ MeV would be as follows:

Table 14

Normalizing dosimeter	Normalized value	Weight
$^{46}Ti(n,p)^{46}Sc$	1.647×10^{19}	0.061
$^{54}Fe(n,p)^{54}Mn$	1.576×10^{19}	0.446
$^{238}U(n,f)$	1.661×10^{19}	0.493
Weighted average:	1.618×10^{19}	

It may be noted that the weights depend primarily on the calculation, cross section, and measuring variances and covariances. They are not very sensitive to changes in the spectrum and completely independent from the dosimetry measurements. Thus, these weights, once determined for a given set of dosimeters, could be used as a fast and dirty adjustment procedure for a large class of similar spectral environments as long as the accuracy requirements are not too high and the normalized parameters do not differ too much from each other for different dosimeters.

The variances and covariances for the adjusted damage parameters can be obtained from Eq. (4). The original variances of the calculated parameters are given in Table 2. Normalization with $^{54}Fe(n,p)^{54}Mn$ measurements reduces the variances. The variances for the normalized parameters can be obtained in the same manner as the covariances in Table 9. The variances for the adjusted parameters are further reduced with amounts obtained from Eq. (4). The values are given in Table 15; the variances are converted to percent standard deviation in parentheses.

Table 15

	Original	Normalized	Adjusted
F > 1.0 MeV	1.85 (13.6%)	0.71 (8.4%)	0.38 (6.2%)
F > 0.1 MeV	1.49 (12.2%)	1.03 (10.2%)	0.64 (8.0%)
dpa	1.69 (13.0%)	0.81 (9.0%)	0.47 (6.9%)

(All variances are to be multiplied by 10^{-2}.)

These variances (and associated covariances) are also independent from dosimetry measurements and only weakly dependent on the neutron spectrum. The largest contributing factor is the uncertainty of the neutron physics calculations.

Conclusions

Uncertainties in the form of variances and covariances are required as input for the new least squares adjustment procedures. Such data are difficult to obtain and use. Simplifications are needed if adjustments are to be done routinely. Such simplifications are possible since the critical data are spectrum-weighted averages of individual variances and covariances. The foregoing analysis suggests the following lines of action:

1. Cross section variances and covariances

   These values enter the adjustment procedure only as total cross section variances, one for each dosimetry sensor (Table 1). These are independent of any energy group structure and only weakly dependent on the shape of the spectrum. It would be useful to create and distribute cross-section variance tables for some typical neutron spectra to be used as direct input to adjustment procedures. Covariances between different dosimetry materials can be added, if needed. These tables can replace, without significant loss of accuracy, the rather unwieldy original covariance tables in ENDF/B-V.

2. Fluence variances and covariances

   The critical values in Table 2 depend very much on the input variances and covariances (but not much on the shape of the spectrum). Determination of fluence variances and covariances is very difficult. The LEPRICON methodology[1] provides some guidance for determining these variances, but only very few cases have been carried out so far. More experience needs to be accumulated before a decision can be made whether "generic" covariance matrices, similar to Table 2, can be used for neutron transport calculations different from those that were used in determining the covariances.

REFERENCE

1. R. E. Maerker, M. L. Williams, B. L. Broadhead, J. J. Wagschal, and C. V. Fu, Revision and Extension of the Data Base in the LEPRICON Dosimetry Methodology, NP-3841, Electric Power Research Institute, Palo Alto, CA, January 1985.

BIBLIOGRAPHY

BIBLIOGRAPHY

(Al83) A. A. Alberman et al., DOMPAC Dosimetry Experiment Neutron Simulation of the Pressure Vessel of a Pressurized-Water Reactor, Characterization of Irradiation Damage, CEA-R-5217, Centre d'Etudes Nucleaires de Saclay, France, May 1983.

(As79d) ASTM E693, "Standard Practice for Characterizing Neutron Exposures in Ferritic Steels in Terms of Displacements per Atom (dpa)," 1979 Annual Book of ASTM Standards, American Society for Testing and Materials, Philadelphia, PA, current edition.

(As82) ASTM E706-81a, "Master Matrix for LWR Pressure Vessel Surveillance Standards," 1982 Annual Book of ASTM Standards, American Society for Testing and Materials, Philadelphia, PA, Part 45, 1982. (See most recent version of ASTM E706, Annual Book of ASTM Standards, Section 12, Volume 12.02, current edition.)

(As82a) ASTM E482-82, "Standard Guide for Application of Neutron Transport Methods for Reactor Vessel Surveillance," 1982 Annual Book of ASTM Standards, American Society for Testing and Materials, Philadelphia, PA, Part 45, 1982.

(As85b) ASTM E944, "Standard Guide for Application of Neutron Spectrum Adjustment Methods," Annual Book of ASTM Standards, American Society for Testing and Materials, Philadelphia, PA, current edition.

(As85d) ASTM E1006, "Standard Practice for Analysis and Interpretation of Physics-Dosimetry Results for Test Reactors," Annual Book of ASTM Standards, American Society for Testing and Materials, Philadelphia, PA, current edition.

(Ba84) C. A. Baldwin, F. B. K. Kam and F. W. Stallmann, Neutron Spectral Characterization for the Fifth Heavy Section Steel Technology (HSST) Irradiation Series, "Simulator Experiments," NUREG/CR-4031, Vol. 1, ORNL/TM-9423/V1, NRC, Washington, DC, November 1984.

(Br78) S. S. Brenner, R. Wagner and J. A. Spitznagel, "Field-Ion Microscope Detection of Ultra-Fine Defects in Neutron-Irradiated Fe-0.34% Cu Alloy," Metall. Trans. 9A, p. 1971, 1978.

(By80) S. T. Byrne, Omaha Public Power District Fort Calhoun Station Unit No. 1: Post-Irradiation Evaluation of Reactor Vessel Surveillance Capsule W-225, TR-O-MCM-001, Rev. 1, Combustion Engineering Inc., August 1980.

(Cf83) Code of Federal Regulations, 10CFR50, "Domestic Licensing of Production and Utilization Facilities," "General Design Criteria for Nuclear Power Plants," Appendix A; "Fracture Toughness Requirements," Appendix G; "Reactor Vessel Material Surveillance Program Requirements," Appendix H; US Government Printing Office, Washington, DC, current edition.

(Da77) J. A. Davidson, S. L. Anderson and K. V. Scott, Analysis of Capsule V from Northern States Power Company Prairie Island Unit No. 1 Reactor Vessel Radiation Surveillance Program, WCAP-8916, Westinghouse Electric Corp., Pittsburgh, PA, August 1977.

(Da78a) J. A. Davidson, S. L. Anderson and R. P. Shogan, Analysis of Capsule T from the Wisconsin Electric Power Company Point Beach Nuclear Plant Unit No. 2 Reactor Vessel Radiation Surveillance Program, WCAP-9331, Westinghouse Electric Corp., Pittsburgh, PA, August 1978.

(Da79) J. A. Davidson, S. L. Anderson and W. T. Kaiser, Analysis of Capsule T from the Indian Point Unit 3 Reactor Vessel Radiation Surveillance Program, WCAP-9491, Westinghouse Electric Corp., Pittsburgh, PA, April 1979.

(Di82) W. J. Dircks, Pressurized Thermal Shock (PTS), and Enclosure A, "NRC Staff Evaluation of PTS," SECY-82-465, NRC, Washington, DC, November 1982.

(Ei77) N. Von Eickselpasch and R. Seepolt, "Experimentelle Ermittung der Neutronendosis des KRB - Druckgefässes und deren Betriebliche Bedeutung," Atomkernenergie 29, 1977.

(Fa81a) A. Fabry, F. Cops and L. S. Kellogg, "Radiometric Measurements," LWR-PV-SDIP: PCA Experiments and Blind Test, W. N. McElroy, Ed., NUREG/CR-1861, HEDL-TME 80-87, NRC, Washington, DC, p. 2.4-1 - 2.4-31, July 1981.

(Fa81b) A. Fabry, N. Maene, R. Menil, G. Minsart and J. Tissot, "Validation of Gamma-Ray Field Calculations by TLD Measurements," LWR-PV-SDIP: PCA Experiments and Blind Test, NUREG/CR-1861, HEDL-TME 80-87, NRC, Washington, DC, Sec. 5.4, July 1981.

(Fi84) S. B. Fisher, J. E. Harbottle and N. B. Aldridge, "Microstructure Related to Irradiation Hardening in Pressure Vessel Steels, Dimensional Stability and Mechanical Behavior of Irradiated Metals and Alloys," Britsh Nuclear Energy Society, London, 1984.

(Go82b) R. Gold, B. J. Kaiser and J. P. McNeece, "Gamma-Ray Spectrometry in Light Water Reactor Environments," Proc. of the 4th ASTM-EURATOM Symposium on Reactor Dosimetry, Gaithersburg, MD, March 22-26, 1982, NUREG/CP-0029, NRC, Washington, DC, Vol. 1, pp. 267-279, July 1982.

(Go83a) R. Gold, B. J. Kaiser and J. P. McNeece, "Continuous Energy Gamma-Ray Spectrometry," Trans. Am. Nucl. Soc. 45, pp. 228-230, 1983 (invited paper).

(Go84c) R. Gold, J. P. NcNeece and B. J. Kaiser, "Advances in Continuous Gamma-Ray Spectrometry and Applications," HEDL-SA-3125 and Proc. of the 5th International ASTM-EURATOM Symposium on Reactor Dosimetry, Geesthacht, FRG, Germany, September 24-28, 1984.

(Go84d) R. Gold, J. P. McNeece, B. J. Kaiser, T. A. Lewis, P. J. H. Heffer and M. D. Carter, "Janus Probe Perturbation Factors," LWR-PV-SDIP: PCA Experiments, Blind Test, and Physics-Dosimetry Support for the PSF Experiments, NUREG/CR-3318, HEDL-TME 84-1, NRC, Washington, DC, Section 4.4, September 1984.

(Gr84) S. P. Grant and S. L. Earp, "Methods for Extending Life of a PWR Reactor Vessel After Long-Term Exposure to Fast Neutron Radiation, Proc. of the 12th ASTM Symposium on Effects of Radiation on Materials, ASTM STP 870, Williamsburg, VA, June 1984.

(Gu81) G. L. Guthrie, "An Investigation of the Dependence of Charpy Trend-Curve Saturation on Nickel or Copper Concentration," LWR-PV-SDIP Quarterly Progress Report, October - December 1980, NUREG/CR-1241, Vol. 4, HEDL-TME 80-6, NRC, Washington, DC, pp. HEDL-9 - HEDL-17, November 1981.

(Gu82) G. L. Guthrie, W. N. McElroy and S. L. Anderson, "A Preliminary Study of the Use of Fuel Management Techniques for Slowing Pressure Vessel Embrittlement," Proc. of the 4th ASTM-EURATOM Symposium on Reactor Dosimetry, Gaithersburg, MD, March 22-26, 1982, NUREG/CP-0029, NRC, Washington, DC, Vol. 1, pp. 111-120, July 1982.

(Gu82a) G. L. Guthrie, W. N. McElroy and S. L. Anderson, "Investigations of Effects of Reactor Core Loadings on PV Neutron Exposure," LWR-PV-SDIP Quarterly Progress Report, October 1981 - December 1981, NUREG/CR-2345, Vol. 4, HEDL-TME 81-36, NRC, Washington, DC, Section E and Appendix, pp. HEDL-35 - HEDL-36 & HEDL-A1 - HEDL-A46, October 1982.

(Gu83a) G. L. Guthrie, "Pressure Vessel Steel Irradiation Embrittlement Formulas Derived from PWR Surveillance Data," from the ANS Special Session on Correlations and Implications of Neutron Irradiation Embrittlement of Pressure Vessel Steels, Detroit, MI, June 12-16, 1983, Trans. Am. Nucl. Soc. 44, p. 222, June 1983.

(Gu83c) G. L. Guthrie, "Charpy Trend Curve Development Based on PWR Surveillance Data," Proc. of the 11th WRSR Information Meeting, Gaithersburg, MD, October 24-28, 1983, NUREG/CP-0048, NRC, Washington, DC, 1983.

(Gu84) G. L. Guthrie, "Charpy Trend Curves Based on 177 PWR Data Points," LWR-PV-SDIP Quarterly Progress Report, April 1983 - June 1983, NUREG/CR-3391, Vol. 2, HEDL-TME 83-22, NRC, Washington, DC, pp. HEDL-3 - HEDL-15, April 1984.

(Gu84a) G. L. Guthrie, W. N. McElroy and R. L. Simons, "Effect of Thermal Neutrons in Irradiation Embrittlement of PWR Pressure Vessel Plates and Welds," LWR-PV-SDIP Quarterly Progress Report, April 1983 - June 1983, NUREG/CR-3391, Vol. 2, HEDL-TME 83-22, NRC, Washington, DC, HEDL-16 - HEDL-21, April 1984.

(Gu84b) G. L. Guthrie, "HEDL Analysis of the PSF Experiment," Attachment to Minutes of the 14th LWR-PV-SDIP Meeting, HEDL-7511, Hanford Engineering Development Laboratory, Richland, WA, p. A7-1, October 1-5, 1984.

(Gu84d) G. L. Guthrie, E. P. Lippincott and E. D. McGarry, LWR-PV-SDIP: PSF Blind Test Workshop Minutes, HEDL-7467, Hanford Engineering Development Laboratory, Richland, WA, April 9-10, 1984.

(Gu85) G. L. Guthrie, "HEDL Analysis of the Poolside Facility Experiment," LWR-PV-SDIP Semiannual Progress Report, April 1984 - September 1984, NUREG/CR-3746, Vol. 2, HEDL-TME 84-21, NRC, Washington, DC, pp. HEDL-28 - HEDL-52, March 1985.

(Ha84) J. R. Hawthorne, B. H. Menke and A. L. Hiser, LWR-PV-SDIP: Notch Ductility and Fracture Toughness Degradation of A302-B and A533-B Reference Plates from PSF Simulated Surveillance and Through-Wall Irradiation Capsules, NUREG/CR-3295, MEA-2017, Vol. 1, NRC, Washington, DC, April 1984.

(Ha84a) J. R. Hawthorne and B. H. Menke, LWR-PV-SDIP: Postirradiation Notch Ductility and Tensile Strength Determinations for PSF Simulated Surveillance and Through-Wall Specimen Capsules, NUREG/CR-3295, MEA-2017, Vol. 2, NRC, Washington, DC, April 1984.

(Ha85) J. R. Hawthorne, "Radiation Sensitivity and Annealing Parameter Studies," Materials Engineering Research/Pressure Vessel Research, Section 20, Proc. of the NRC 13th WRSR Information Meeting, NBS, Gaithersburg, MD, October 22-25, 1985.

(He84) H. L. Heinisch and F. M. Mann, "Neutron Cross Sections for Defect Production by High Energy Development Cascades in Copper," J. Nucl. Mater. 122 & 123, pp. 1023-1027, 1984.

(He84a) A. S. Heller and A. L. Lowe Jr, Correlations for Predicting the Effects of Neutron Radiation on Linde 80 Submerged-Arc Welds, BAW-1803, Babcock & Wilcox, Owners Group Materials Committee Report, Lynchburg, VA, January 1984.

(Ir70) D. R. Ireland and V. G. Scotti, Examination and Evaluation of Capsule A for the Connecticut Yankee Reactor Pressure Vessel Surveillance Program, Battelle Memorial Institute, Columbus Laboratories, Columbus, OH, October 30, 1970.

(Ka82a) F. B. K. Kam, "Characterization of the Fourth HSST Series of Neutron Spectral Metallurgical Irradiation Capsules," Paper presented at the 4th ASTM-EURATOM Symposium on Reactor Dosimetry, Gaithersburg, MD, March 22-26, 1982, preprints available.

(Ka82b) F. B. K. Kam et al., "Neutron Exposure Parameters for the Fourth HSST Series of Metallurgical Irradiation Capsules," Proc. of the 4th ASTM-EURATOM Symposium on Reactor Dosimetry, Gaithersburg, MD, March 22-26, 1982, NUREG/CP-0029, NRC, Washington, DC, Vol. 2, pp. 1023-1033, July 1982.

(Ka84) F. B. K. Kam, F. W. Stallmann, G. Guthrie, and W. N. McElroy, "LWR Surveillance Dosimetry Improvement Program: PSF Metallurgical Blind Test Results," Trans. of the 12th Water Reactor Safety Research Information Meeting, Gaithersburg, MD, NUREG/CP-0057, NRC, Washington, DC, October 1984.

(Ka84a) B. J. Kaiser, R. Gold and J. P. McNeece, "Si(Li) Gamma-Ray Dosimetry," LWR-PV-SDIP: PCA Experiments, Blind Test, and Physics-Dosimetry Support for the PSF Experiments, NUREG/CR-3318, HEDL-TME 84-1, NRC, Washington, DC, Section 4.3, September 1984.

(Li84b) E. P. Lippincott, F. W. Stallmann and A. F. Thomas, "Derived Exposure Parameters," LWR-PV-SDIP: PCA Experiments, Blind Test, and Physics-Dosimetry Support for the PSF Experiments, NUREG/CR-3318, HEDL-TME 84-1, NRC, Washington, DC, Section 7.2, September 1984.

(Lo75) A. L. Lowe Jr et al., Analysis of Capsule OCI-F from Duke Power Company, Oconee Unit No. 1 Reactor Vessel Materials Surveillance Program, BAW-1421, Babcock & Wilcox, Lynchburg, VA, August 1975.

(Lo77) A. L. Lowe Jr et al., Analysis of Capsule OCI-E from Duke Power Company, Oconee Nuclear Station - Unit 1, BAW-1436, Babcock & Wilcox, Lynchburg, VA, September 1977.

(Lo77a) A. L. Lowe Jr et al., Analysis of Capsule OCII-C from Duke Power Company, Oconee Nuclear Station - Unit 2, BAW-1437, Babcock & Wilcox, Lynchburg, VA, May 1977.

(Lo77b) A. L. Lowe Jr et al., Analysis of Capsule OCII-A from Duke Power Company, Oconee Nuclear Station - Unit 3, BAW-1438, Babcock & Wilcox, Lynchburg, VA, July 1977.

(Lo77c) A. L. Lowe Jr et al., Analysis of Capsule TMI-1E from Metropolitan Edison Company, Three Mile Island Nuclear Station - Unit 1, BAW-1439, Babcock & Wilcox, Lynchburg, VA, January 1977.

(Lo77d) A. L. Lowe Jr et al., Analysis of Capsule ANI-E from Arkansas Power & Light Company, Arkansas Nuclear Station - Unit 1, BAW-1440, Babcock & Wilcox, Lynchburg, VA, April 1977.

(Lo81) A. L. Lowe Jr et al., Analysis of Capsule CR3-B from Florida Power Corporation, Crystal River - Unit 3, BAW-1679, Babcock & Wilcox, Lynchburg, VA, June 1981.

(Lu85) G. E. Lucas, G. R. Odette, P. M. Lombrozo, and J. W. Sheckherd, "Effects of Composition, Microstructure and Temperature on Irradiation Hardening of Pressure Vessel Steels," Proc. of the 12th ASTM Symposium on Effects of Radiation on Materials, Williamsburg, VA, June 1984, ASTM STP 870, American Society for Testing and Materials, Philadelphia, PA, pp. 900-930, 1985.

(Ma73a) T. R. Mager et al., Analysis of Capsule V from the Rochester Gas and Electric Company, R. E. Ginna Unit No. 1 Reactor Vessel Radiation Surveillance Program, FP-RA-1, Westinghouse Electric Corp., Pittsburgh, PA, April 1973.

(Ma83b) T. R. Mager, T. U. Marston and S. E. Yanichko, "Assessing Steady-State Neutron Exposure Effects Through Analyses of Reactor Vessel Surveillance Data," Radiation Embrittlement and Surveillance of Nuclear Reactor Pressure Vessels: An International Study, ASTM STP 819, L. E. Steele, Ed., American Society for Testing and Materials, pp. 155-165, 1983.

(Ma84) T. R. Mager, "Pressured Thermal Shock and Reactor Materials," Trans. Am. Nucl. Soc. 46, pp. 376-381, 1984.

(Ma84a) R. E. Maerker and B. A. Worley, Activity and Fluence Calculations for the Startup and Two-Year Irradiation Experiments Performed at the Poolside Facility, NUREG/CR-3886, ORNL/TM-9265, NRC, Washington, DC, October 1984.

(Ma85a) R. E. Maerker et al., Revision and Expansion of the Data Base in the LEPRICON Dosimetry Methodology, EPRI NP-3841, Electric Power Research Institute, Palo Alto, CA, January 1985.

(Mc69) W. N. McElroy, R. E. Dahl Jr and C. Z. Serpan Jr, "Damage Functions and Data Correlation," Nucl. Appl. Technol. 7, (6), pp. 561-571, December 1969.

(Mc81) W. N. McElroy, Ed., LWR-PV-SDIP: PCA Experiments and Blind Test, NUREG/CR-1861, HEDL-TME 80-87, NRC, Washington, DC, July 1981.

(Mc82c) P. McConnell et al., Irradiated Nuclear Pressure Vessel Steel Data Base, EPRI NP-2428, Electric Power Research Institute, Palo Alto, CA, June 1982.

(Mc84) W. N. McElroy et al., LWR-PV-SDIP 1983 Annual Report, NUREG/CR-3391, Vol. 3, HEDL-TME 83-23, NRC, Washington, DC, January 1984.

(Mc84h) W. N. McElroy et al., "Trend Curve Exposure Parameter Data Development and Testing," HEDL-SA-3126 and Proc. of the 5th ASTM-EURATOM Symposium on Reactor Dosimetry, Geesthacht, FRG, September 24-28, 1984.

(Mc84i) W. N. McElroy, LWR-PV-SDIP: PCA Experiments Blind Test and Physics-Dosimetry Support for the PSF Experiments, NUREG/CR-3318, HEDL-TME 84-1, NRC, Washington, DC, September 1984.

(Mc85) W. N. McElroy et al., LWR-PV-SDIP Semiannual Progress Report, April - September 1984, NUREG/CR-3746, Vol. 2, HEDL-TME 84-21, NRC, Washington, DC, March 1985.

(Mc85a) W. N. McElroy et al., LWR-PV-SDIP 1984 Annual Report, October 1, 1983 - September 30, 1984, NUREG/CR-3746, Vol. 3, HEDL-TME 84-31, NRC, Washington, DC, March 1985.

(Mc85b) W. N. McElroy, Ed., LWR-PV-SDIP: PSF Experiments Summary and Blind Test Results, NUREG/CR-3320, Vol. 1, HEDL-TME 85-4, NRC, Washington, DC, to be published.

(Mc85c) W. N. McElroy, Ed., LWR-PV-SDIP: LWR Power Reactor Surveillance Physcis-Dosimetry Data Base Compendium, NUREG/CR-3319, HEDL-TME 85-3, Hanford Engineering Development Laboratory, Richland, WA, August 1985.

(Mc84k) J. P. McNeece, R. Gold and B. J. Kaiser, "Gamma-Ray Spectrometry," LWR-PV-SDIP: PCA Experiments, Blind Test, and Physics-Dosimetry Support for the PSF Experiments, NUREG/CR-3318, HEDL-TME 84-1, NRC, Washington, DC, Section 4.2, September 1984.

(Me84) Materials Engineering Associates, Structural Integrity of Light Water Reactor Pressure Boundary Integrity: 4-Year Plan, 1984-88, NUREG/CR-3788, MEA-2047, NRC, Washington, DC, September 1984.

(Mi85) L. F. Miller and R. W. Hobbs, Data Acquisition and Control of the HSST Veries V Irradiation Experiment at the ORR, NUREG/CR-3872, Vol. 3, ORNL/TM-9423/V3, NRC, Washington, DC, March 1985.

(No71) E. B. Norris, Analysis of First Surveillance Material Capsule from San Onofre Unit 1, SwRI Project 07-2892, Southwest Research Institute, San Antonio, TX, May 1971.

(No72) E. B. Norris, Analysis of Second Surveillance Material Capsule from San Onofre Unit 1, Final Report, SwRI Project 07-2892, Southwest Research Institute, San Antonio, TX, June 1972.

(No76) E. B. Norris, Reactor Vessel Material Surveillance Program for Turkey Point Unit No. 4 -- Analysis of Capsule T, Final Report, SwRI Project 02-4221, Southwest Research Institute, San Antonio, TX, June 1976.

(No76b) E. B. Norris, Reactor Vessel Material Surveillance Program for H. B. Robinson Unit No. 2 -- Analysis of Capsule V, Final Report, SwRI Project 02-4397, Southwest Research Institute, San Antonio, TX, October 1976.

(No77a) E. B. Norris, Reactor Vessel Material Surveillance Program for Indian Point Unit No. 2 -- Analysis of Capsule T, Final Report, SwRI Project 02-4531, Southwest Research Institute, San Antonio, TX, June 1977.

(No77b) E. B. Norris, Reactor Vessel Material Surveillance Program for Donald C. Cook Unit No. 1 -- Analysis of Capsule T, Final Report, SwRI Project 02-4770, Southwest Research Institute, San Antonio, TX, December 1977.

(No79) E. B. Norris, Reactor Vessel Material Surveillance Program for Capsule S -- Turkey Point Unit No. 3; Capsule S -- Turkey Point Unit No. 4, Final Report, SwRI Projects 02-5131 and 02-5380, Southwest Research Institute, San Antonio, TX, May 1979.

(Od83a) G. R. Odette, "On the Dominant Mechanism of Irradiation Embrittlement of Reactor Pressure Vessel Steels, Scripta Met. 17, pp. 1183-1188, 1983.

(Od84) G. R. Odette and G. E. Lucas, "Irradiation Embrittlement of Reactor Pressure Vessel Steel: Mechanisms, Models and Data Correlations," IAEA Specialist's Symposium on Pressure Vessel Steels, Vienna, Austria, October 1984.

(Od85) G. R. Odette, P. M. Lombrozo and R. A. Wullaert, "The Relationship Between Irradiation-Induced Changes in Strength and Embrittlement of Light Water Reactor Pressure Vessel Steels," Effects of Radiation on Materials, ASTM STP 807, F. A. Garner and J. S. Perrin, Eds., American Society for Testing and Materials, Philadelphia, PA, 1985.

(Pa83) D. Pachur, "Mechanical Properties of Neutron-Irradiated Reactor Pressure Vessel Steel Dependent on Radiation Mechanisms," from the ANS Special Session on Correlations and Implications of Neutron Irradiation Embrittlement of Pressure Vessel Steels, Detroit, MI, June 12-16, 1983, Trans. Am. Nucl. Soc. 44, p. 229, 1983.

(Pe72) J. S. Perrin, J. W. Sheckherd and V. G. Scotti, Examination and Evaluation of Capsule F for the Connecticut Yankee Reactor Pressure Vessel Surveillance Program, NRC, Public Document Room, Washington, DC, March 30, 1972.

(Pe75) J. S. Perrin et al., Surry Unit No. 1 Pressure Vessel Irradiation Capsule Program: Examination and Analysis of Capsule T, Docket 50280-462, NRC, Public Document Room, Washington, DC, June 24, 1975.

(Pe75a) J. S. Perrin et al., Surry Unit No. 2 Pressure Vessel Irradiation Capsule Program: Examination and Analysis of Capsule X, NRC, Public Document Room, Washington, DC, September 2, 1975.

(Pe75b) J. S. Perrin et al., Point Beach Unit No. 2 Pressure Vessel Surveillance Program: Evaluation of Capsule V, NRC, Public Document Room, Washington, DC, June 10, 1975.

(Pe78) J. S. Perrin et al., Zion Nuclear Plant Reactor Pressure Vessel Surveillance Program: Unit No. 1 Capsule T and Unit No. 2 Capsule U, BCL-585-4, Battelle Memorial Institute, Columbus Laboratories, Columbus, OH, March 1978.

(Pe79b) J. S. Perrin et al., Palisades Nuclear Plant Reactor Pressure Vessel Surveillance Program: Capsule A-240, BCL-585-12, Battelle Memorial Institute, Columbus Laboratories, Columbus, OH, March 13, 1979.

(Pe80) J. S. Perrin et al., Maine Yankee Nuclear Plant Reactor Pressure Vessel Surveillance Program: Capsule 263, BCL-585-21, Battelle Memorial Institute, Columbus Laboratories, Columbus, OH, December 21, 1980.

(Pe84) J. S. Perrin, R. A. Wullaert, G. R. Odette and M. P. Lombroso, Physically Based Regression Correlations of Embrittlement Data from Reactor PV Surveillance Programs, EPRI NP-3319, Electric Power Research Institute, Palo Alto, CA, January 1984.

(Ra84) P. N. Randall, "Basis for Revision 2 of US NRC Regulatory Guide 1.99," Proc. 10th MPA Seminar, Stuttgart, FRG, October 10, 1984.

(Re77) Regulatory Guide 1.99, Effects of Residual Elements on Predicted Radiation Damage to Reactor Vessel Materials, Rev. 1, NRC, Washington, DC, April 1977.

(Re85) I. Remec, F. W. Stallmann and F. B. K. Kam, Neutron Spectral Characterization for the Fifth Heavy Section Steel Technology (HSST) Irradiation Series, "Neutronics Exposure Parameters," NUREG/CR-4031, Vol. 3, ORNL/TM-9423/V3, NRC, Washington, DC, March 1985.

(Rh79) W. A. Rhoades, D. B. Simpson, R. L. Childs and W. W. Engle, The DOT-IV Two-Dimensional Discrete Ordinates Transport Code with Space-Dependent Mesh and Quadrature, ORNL/TM-6529, Oak Ridge National Laboratory, Oak Ridge, TN, 1979.

(Ru72) K. C. Russell and L. M. Brown, "A Dispersion Strengthing Model Based on Differing Elastic Module Applied to the Iron-Copper System," Acta Met. 20, July 1972.

(Se71) C. Z. Serpan Jr, "Reliability of Fluence-Embrittlement Projections for Pressure Vessel Surveillance Analysis," Nucl. Technol. 12, pp. 108-118, September 1971.

(Se74) C. Z. Serpan Jr and B. H. Menke, Nuclear Reactor Neutron Energy Spectra, ASTM DS52, American Society for Testing and Materials, Philadelphia, PA, 1974.

(Se82a) S. M. Seltzer and M. J. Berger, "Evaluation of the Collision Stopping Power of Elements and Compounds for Electrons and Positrons," Int. J. Appl. Radia. Isot. 33, pp. 1189-1218, 1982.

(Se85) C. Z. Serpan Jr, "Achievements in Primary Integrity Research-1985," Materials Engineering Research/Pressure Vessel Research, Section 20, Proc. of the NRC 13th WRSR Information Meeting, NBS, Gaithersburg, MD, October 22-25, 1985.

(Si80a) R. L. Simons, "Correlation of Irradiation Effects Data Using Primary Recoil Spectra," DAFS Quarterly Progress Report, July - September 1980, DOE/ER-0046/3, U.S. Department of Energy, Washington DC, pp. 41-75, November 1980.

(Si82a) R. L. Simons et al., "Re-evaluation of the Dosimetry for Reactor Pressure Vessel Surveillance Capsules," Proc. of the 4th ASTM-EURATOM Symposium on Reactor Dosimetry, Gaithersburg, MD, March 22-26, 1982, NUREG/CP-0029, NRC, Washington, DC, Vol. 2, pp. 903-916, July 1982.

(Si82b) R. L. Simons, "Re-evaluation of Dosimetry for Test Reactor Irradiation Used to Obtain ΔNDTT Data for Pressure Vessel Steels," LWR-PV-SDIP Semi-Annual Progress Report, October - December 1982, NUREG/CR-2805, Vol. 4, HEDL-TME 82-21, NRC, Washington, DC, pp. HEDL-14 - HEDL-22, July 1982.

(Si84) R. L. Simons et al., "Re-evaluation of the Physics-Dosimetry from PWR and BWR Pressure Vessel Surveillance Programs," HEDL-SA-3210 and Proc. of the 5th ASTM-EURATOM Symposium on Reactor Dosimetry, Geesthacht, FRG, September 24-28, 1984.

(Sm73) F. A. Smidt and J. A. Sprague, "Property Changes Resulting from Impurity-Defect Interactions in Iron and Pressure Vessel Steel Alloys," Effects of Radiation on the Substructure and Mechanical Properties of Metals and Alloys, ASTM STP 529, American Society for Testing and Materials, Philadelphia, PA, pp. 78-91, 1973.

(St83) F. W. Stallmann, C. A. Baldwin and F. B. K. Kam, Neutron Spectral Characterization of the 4th Nuclear Regulatory Commission Heavy Section Steel Technology 1T-CT Irradiation Experiment: Dosimetry and Uncertainty Analysis, NUREG/CR-3333, ORNL/TM-8789, Oak Ridge National Laboratory, Oak Ridge, TN, July 1983.

(St83a) L. E. Steele, Ed., Status of USA Nuclear Reactor Pressure Vessel Surveillance for Radiation Effects, ASTM STP 784, American Society for Testing and Materials, Philadelphia, PA, January 1983.

(St84a) F. W. Stallmann, "LSL-M1 and LSL-M2: Two Extensions of the LSL Adjustment Procedure for Including Multiple Spectrum Locations," Proc. of the 5th ASTM-EURATOM Symposium on Reactor Dosimetry, Geesthacht, FRG, September 24-28, 1984.

(St84b) F. W. Stallmann, Statistical Evaluation of the Metallurgical Test Data in the ORR-PSF-PVS Irradiation Experiment, NUREG/CR-3815, ORNL/TM-9207, NRC, Washington, DC, August 1984.

(St85) F. W. Stallmann et al., "LWR-PV-SDIP: PSF Metallurgical Blind Test Results," Proc. of the 12th WRSR Information Meeting, October 22-26, 1984, National Bureau of Standards, Gaithersburg, MD, NUREG/CP-0058, Vol. 4, NRC, Washington, DC, January 1985.

(St85a) F. W. Stallmann, Neutron Exposure Parameters for the Fifth Heavy Section Steel Irradiation Series, NUREG/CR-4284, ORNL/TM-9664, NRC, Washington, DC, June, 1985.

(Th84) A. F. Thomas, "Exposure Parameters - RR&A Analysis," LWR-PV-SDIP: PCA Experiments, Blind Test, and Physics-Dosimetry Support for the PSF Experiments, NUREG/CR-3318, HEDL-TME 84-1, NRC, Washington, DC, Section 7.2.3, September 1984.

(Vo77) D. R. Vondy, T. B. Fowler and G. W. Cunningham, VENTURE: A Code Block for Solving Multigroup Neutronics Problems Applying the Finite-Different Diffusion-Theory Approximation to Neutron Transport, Version II, ORNL-5016R2, Oak Ridge National Laboratory, Oak Ridge, TN, 1977.

(Wi82a) T. J. Williams, A. F. Thomas, R. A. Berrisford, M. Austin, R. L. Squires and J. H. Venable, Influence of Neutron Exposure, Chemical Composition and Metallurgical Condition on the Irradiation Shift of Reactor Pressure Vessel Steels, ASTM STP 782, American Society for Testing and Materials, Philadelphia, PA, p. 343, 1982.

(Wi84b) M. L. Williams et al., "Calculation of Neutron Source Distribution in VENUS PWR Mockup Experiment," Proc. of the 5th ASTM-EURATOM Symposium on Reactor Dosimetry, Geesthacht, FRG, September 24-28, 1984.

(Wi85) M. L. Williams, I. Remec and F. B. K. Kam, Neutron Spectral Characterization for the Fifth Heavy Section Steel Technology (HSST) Irradiation Series, "Neutronics Calculations," NUREG/CR-4031, Vol. 2, ORNL/TM-9423/V2, NRC, Washington, DC, March 1985.

(Wu75) R. A. Wullaert and J. W. Shuckherd, Evaluation of the First Maine Yankee Accelerated Surveillance Capsule, CR75-317, Effects Technology, Inc., Goleta Heights, CA, August 15, 1975.

(Ya67) S. E. Yanichko, Connecticut Yankee Reactor Vessel Radiation Surveillance Program, WCAP-7036, Westinghouse Electric Corp., Pittsburgh, PA, April 1967.

(Ya73) S. E. Yanichko et al., Analysis of Capsule S from Carolina Power and Light Company H. B. Robinson Unit 2 Reactor Vessel Radiation Surveillance Program, WCAP-8249, Westinghouse Electric Corp., Pittsburgh, PA, December 18, 1973.

(Ya74) S. E. Yanichko, T. R. Mager and S. Kang, Analysis of Capsule R from the Rochester Gas and Electric Corporation R. E. Ginna Unit 1 Reactor Vessel Radiation Surveillance Program, WCAP-8421, Westinghouse Electric Corp., Pittsburgh, PA, November 1974.

(Ya75) S. E. Yanichko, J. H. Phillips and S. L. Anderson, Analysis of Capsule T from the Florida Power and Light Company Turkey Point Unit 3 Reactor Vessel Radiation Surveillance Program, WCAP-8631, Westinghouse Electric Corp., Pittsburgh, PA, December 1975.

(Ya76) S. E. Yanichko and S. L. Anderson, Analysis of Capsule S from the Wisconsin Electric Power Company and Wisconsin-Michigan Power Company Point Beach Nuclear Plant Unit 1 Reactor Vessel Radiation Surveillance Program, WCAP-8739, Westinghouse Electric Corp., Pittsburgh, PA, 1976.

(Ya77) S. E. Yanichko, S. L. Anderson and K. V. Scott, Analysis of Capsule V from the Wisconsin Public Service Corporation Kewaunee Nuclear Plant Reactor Vessel Radiation Surveillance Program, WCAP-8908, Westinghouse Electric Corp., Pittsburgh, PA, January 1977.

(Ya78) S. E. Yanichko and S. L. Anderson, Analysis of Capsule R from the Wisconsin Electric Power Company Point Beach Nuclear Plant Unit 1 Reactor Vessel Radiation Surveillance Program, WCAP-9357, Westinghouse Electric Corp., Pittsburgh, PA, August 1978.

(Ya79) S. E. Yanichko, S. L. Anderson and W. T. Kaiser, Analysis of Capsule F from the Southern California Edison Company San Onofre Reactor Vessel Radiation Surveillance Program, WCAP-9520, Westinghouse Electric Corp., Pittsburgh, PA, May 1979.

(Ya79a) S. E. Yanichko et al., Analysis of Capsule R from the Wisconsin Electric Power Company Point Beach Nuclear Plant Unit 2 Reactor Vessel Radiation Surveillance Program, WCAP-9635, EPRI RP-1021-3, Westinghouse Electric Corp., Pittsburgh, PA, December 1975.

(Ya80) S. E. Yanichko et al., Analysis of Capsule T from the Salem Unit 1 Reactor Vessel Surveillance Program, WCAP-9678, Westinghouse Electric Corp., Pittsburgh, PA, February 1980.

(Ya81) S. E. Yanichko, S. L. Anderson and W. T. Kaiser, Analysis of Capsule V from Northern States Power Company Prairie Island Unit 2 Reactor Vessel Radiation Surveillance Program, WCAP-9877, Westinghouse Electric Corp., Pittsburgh, PA, March 1981.

(Ya81a) S. E. Yanichko et al., Analysis of Capsule U from the Commonwealth Edison Company Zion Nuclear Plant Unit 1 Reactor Vessel Radiation Surveillance Program, WCAP-9890, EPRI RP-1021-3, Westinghouse Electric Corp., Pittsburgh, PA, March 1981.

(Ya81b) S. E. Yanichko et al., Analysis of the Maine Yankee Reactor Vessel Second Accelerated Surveillance Capsule, WCAP-9875, EPRI RP-1021-3, Westinghouse Electric Corp., Pittsburgh, PA, March 1981.

(Ya81c) S. E. Yanichko et al., Analysis of the Third Capsule from the Commonwealth Edison Company Quad Cities Unit 1 Nuclear Plant Reactor Vessel Radiation Surveillance Program, WCAP-9920, EPRI RP-1021-3, Westinghouse Electric Corporation, Pittsburgh, PA, August 1981.

(Ya82) S. E. Yanichko et al., Analysis of the Fourth Capsule from the Commonwealth Edison Company Dresden Unit 3 Nuclear Plant Reactor Vessel Radiation Surveillance Program, WCAP-10030, EPRI PR-1021-3, Westinghouse Electric Corporation, Pittsburgh, PA, January 1982.

(Ya82a) S. E. Yanichko et al., Analysis of the Third Capsule from the Commonwealth Edison Company Quad Cities Unit 2 Nuclear Plant Reactor Vessel Radiation Surveillance Program, WCAP-10064, EPRI RP-1021-3, Westinghouse Electric Corporation, Pittsburgh, PA, April 1982.

DISTRIBUTION

R5

DOE-HQ/Office of Converter
Reactor Deployment
Nuclear Regulation & Safety Division
NE-12
Washington, DC 20545

JD Griffith, Deputy Director

DOE-HQ/Office of Advanced
Reactor Programs (2)
NE-53
Washington, DC 20545

FX Gavigan
DK Nulton

DOE-HQ/Office of Deputy Asst Secy
For Reactor Deployment
Office of LWR Safety & Technology
NE-42
Washington, DC 20545

DJ McGaff, Manager

DOE-HQ/Office of Technology
Support Programs (4)
Division of Advanced Tech Develop
NE-542
Washington, DC 20545

RJ Neuhold, Director
PB Hemmig
JW Lewellen
A Van Echo

DOE-RL/AMF
Site & Laboratory Management
Division (SMD)
Laboratory Management &
Technology Services Branch
P.O. Box 550
Richland, WA 99352

KR Absher, Chief FED/210-B

Arizona State University (2)
College of Eng & Appl Sciences
Tempe, AZ 85287

JW McKlveen
B. Stewart

Argonne National Laboratory (2)
9700 South Cass Avenue
Argonne, IL 60439

RJ Armani
RR Heinrich, Bldg 316

Babcock & Wilcox Co
Lynchburg Research Center (4)
P.O. Box 1260
Lynchburg, VA 24505

LB Gross RH Lewis
SQ King AA Lowe Jr

Battelle
Pacific Northwest Laboratory
P.O. Box 999
Richland, WA 99352

EP Simonen

Battelle Memorial Institute (2)
505 King Avenue
Columbus, OH 43201

MP Manahan
JS Perrin, ONWI

Bechtel Power Corporation
15740 Shady Grove Road
Gaithersburg, MD 20760

WC Hopkins

Brookhaven National Laboratory (3)
National Neutron Cross-Section Center
Upton, Long Island, NY 11973

JF Carew BA Magurno
S. Pearlstein, Bldg T-197

DISTRIBUTION (Cont'd)

Burns & Roe Inc
633 Industrial Avenue
Paramus, NJ 07672

J. Celnik

Carolina Power & Light Co
P.O. Box 1551
Raleigh, SC 27602

SP Grant

Centre d'Etude de l'Energie Nucléaire
Studiecentrum voor Kernenergie (7)
Boeretang 200
B-2400 Mol, Belgium

J. Debrue
G. DeLeeuw
S. DeLeeuw
P. D'Hondt
A. Fabry
G. Minsart
Ph Van Asbroeck

Combustion Engineering Inc (5)
1000 Prospect Hill Road
Windsor, CT 06095

S. Byrne
G. Cavanaugh
JJ Koziol
RG Shimko
D. Stephen

Comitato Nazional per Energia Nucléare
Centro di Studi Nucleari della Casaccia
Casella Postale 2400
Santa Maria di Galeria
I-00060 Rome, Italy

U. Farinelli

Commissariat a l'Energie Atomique
Centre d'Etudes Nucleaires de Saclay (6)
Boite Postale 2
91190 Gif-sur-Yvette, France

AA Alberman
C. Buchalet (Framatome)
JM Cerles
JP Genthon
P. Mas (Grenoble)
P. Petrequin

Commonwealth Edison
P.O. Box 767
Chicago, IL 60690

E. Steeve

EG&G Idaho Inc (3)
P.O. Box 1625
Idaho Falls, ID 83415

RC Greenwood
Y. Harker
JW Rogers

Electric Power Research Institute (8)
3412 Hillview Avenue
P.O. Box 10412
Palo Alto, CA 94304

T. Griesbach
TU Marston
O. Ozer
T. Passell
AD Rossin
R. Shaw
K. Stahlkopf
JJ Taylor

Energieonderzoek Centrum Nederland
Westerdionweg 3
Postfach 1
NL-1755 ZG, Petten, The Netherlands

WL Zijp

Engineering Services Associates
3320 Bailey
Buffalo, NY 14215

M. Haas

EURATOM
Joint Research Center Ispra (2)
I-21020 Ispra, Varese, Italy

R. Dierckx
H. Rief

DISTRIBUTION (Cont'd)

Florida Power & Light
9250 W. Flager Street
P.O. Box 52100
Miami, FL 33152

JB Sun

Fracture Control Corporation
5951 Encina Road, No. 105
Goleta, CA 93117

P. McConnell

General Electric Co
Vallecitos Nuclear Center
P.O. Box 460
Pleasanton, CA 94566

GC Martin

IKE-Stüttgart (2)
Institüt für Kernenergetik
und Energiesysteme
Pfaffenwaldring 31, Postfach 801140
D-7000, Stüttgart 80 (Vaihingen)
Federal Republic of Germany

G. Hehn
G. Prillinger

International Atomic Energy Agency (2)
Wagramerstrasse 5
Postfach 100
A-1400 Vienna, Austria

A. Sinev
JJ Schmidt

IRT Corporation (3)
P.O. Box 80817
San Diego, CA 92183

NA Lurie WE Selph
C. Preskitt

Italian Atomic Power Authority
National Electric Energy Agency (2)
Viale Regina Margherita 137
Rome, Italy

M. Galliani F. Remondino

Japan Atomic Energy Research Institute (2)
Tokai Research Establishment
Tokai-mura, Naka-gun
Ibaraki-ken, Japan

S. Mizazono
K. Sakurai

Kernforschungsanlage Jülich GmbH (3)
Postfach 1913
D-517 Jülich 1,
Federal Republic of Germany

D. Pachur L. Weise
W. Schneider

Kraftwerk Union Aktiengesellschaft (5)
Postfach 3220
D-8520 Erlangen,
Federal Republic of Germany

A. Gerscha J. Koban
U. Groschel C. Leitz
W. Hofmann

Los Alamos National Laboratory (2)
P.O. Box 1663
Los Alamos, NM 87545

GE Hansen, Group N-2
L. Stewart

Maine Yankee Atomic Power Co
Edison Drive
Augusta, MA 04336

HF Jones Jr

DISTRIBUTION (Cont'd)

Materials Engineering Associates Inc
111 Mel-Mara Drive
Oxen Hill, MD 20021

JR Hawthorne

Max-Planck-Institüt
für Plasma Physik
The NET Team
D-8046 Garching bei München,
Federal Republic of Germany

DR Harries, Technology

National Bureau of Standards
Center of Radiation Research (6)
Gaithersburg, MD 20899

RS Caswell
CM Eisenhauer
DM Gilliam
JA Grundl
G. Lamaze
ED McGarry

Naval Research Laboratory
Engineering Materials Division
Thermostructural Materials Branch
Code 6390
Washington, DC 20375

LE Steele

Nuclear Regulatory Commission (17)
Office of Nuclear Regulatory Research
Division of Engineering Technology
Materials Engineering Branch
5650 Nicholson Road
Washington, DC 20555

Chief
Public Doc Rm (3)
M. Bolotski
M. Dunenseld
R. Gamble
W. Hazelton
KG Hoge
RE Johnson
L. Lois
S. Pawlicki
PN Randall
CZ Serpan
D. Sieno
A. Taboada
M. Vagin

Oak Ridge National Laboratory (9)
P.O. Box X
Oak Ridge, TN 37830

CA Baldwin, Bldg 3001
RG Berggren
GL Guthrie
FBK Kam
AL Lotts
RE Maerker
LS Miller
R. Nanstad
FW Stallm

Radiation Research Associates (2)
3550 Hulen Street
Fort Worth, TX 76107

RM Rubin
MB Wells

Rockwell International
Rocketdyne Division (2)
6633 Canoga Avenue
Canoga Park, CA 91304

H. Farrar IV
BM Oliver

Rolls-Royce & Associates Ltd (5)
P.O. Box 31
Derby DE2 8BJ, UK

M. Austin
P. Burch
R. Squires
AF Thomas
TJ Williams

S.A. Cockerill-Ougree
Recherches et Developments
Division de la Construction Mecanique
B-4100 Seraing, Belgium

J. Widart

DISTRIBUTION (Cont'd)

Science Applications Inc (3)
P.O. Box 2325
La Jolla, CA 92037

W. Hagan
GL Simmons
VV Verbinski

Ship Research Institute
Tokai Branch Office
Tokai-mura, Naka-gun
Ibaraki-ken, Japan

K. Takeuchi

Southwest Research Institute
8500 Calebra Road
P.O. Box 28510
San Antonio, TX 78284

EB Norris

Swiss Federal Institute
for Reactor Research
CH-5303 Würenlingen, Switzerland

F. Hegedus

United Kingdom Atomic Energy Authority
Atomic Energy Research Establishment (2)
Harwell, Oxon OX11 ORA, UK

LM Davies
AJ Fudge

United Kingdom Atomic Energy Authority
Atomic Energy Establishment (3)
Winfrith, Dorchester, Dorset, UK

J. Butler
AK McCracken
A. Packwood

University of Arkansas (2)
Dept of Mechanical Engineering
Fayetteville, AR 72701

CO Cogburn
L. West

University of California
at Santa Barbara (2)
Dept of Chem & Nucl Engineering
Santa Barbara, CA 93106

G. Lucas
GR Odette

Univ of London Reactor Center
Silwood Park, Sunnyhill,
Ascot, Berkshire SL5 7PY, UK

JA Mason

University of Tokyo (2)
Dept of Nuclear Engineering
7-3-1, Hongo
Bunkyo-ku, Tokyo, 113 Japan

M. Nakazawa
J. Sekiguchi

Westinghouse
Nuclear Energy Systems (7)
P.O. Box 355
Pittsburgh, PA 15230

SL Anderson
A. Fero
FL Lau
EP Lippincott
RC Shank
SE Yanichko

Westinghouse
Research and Development Center (2)
1310 Beulah Road
Pittsburgh, PA 15235

FH Ruddy
JA Spitznagel

University of Missouri at Rolla (2)
Dept of Nucl Engineering
Building C
Rolla, MO 65401

DR Edwards
N. Tsoulfanidis

DISTRIBUTION (Cont'd)

HEDL (42)
c/o Supervisor, Documentation
P.O. Box 1970, W/C-123
Richland, WA 99352

HJ Anderson	W/C-28	WN McElroy (2)	W/C-39
RA Bennett	W/D-3	JP McNeece	W/A-56
LD Blackburn	W/A-40	JE Nolan	W/B-65
DG Doran	W/A-57	RE Peterson	W/B-66
EA Evans	W/C-23	CC Preston	W/C-39
FA Garner	W/A-58	JM Ruggles	W/C-33
DS Gelles	W/A-65	RE Schenter	W/A-58
R. Gold	W/C-39	FA Schmittroth	W/A-58
LA James	W/A-40	WF Sheely	W/C-44
LS Kellogg	W/C-39	FR Shober	W/E-3
NE Kenny	W/C-115	RL Simons	W/A-65
RL Knecht	W/A-40	HH Yoshikawa	W/C-44
MK Korenko	W/C-27	Program Files (10)	W/C-39
JJ Laidler	W/B-107	Central Files (2)	W/C-110
WY Matsumoto	W/C-33	Documentation (2)	W/C-123

NRC FORM 335 (2-84) NRCM 1102, 3201, 3202

U.S. NUCLEAR REGULATORY COMMISSION

BIBLIOGRAPHIC DATA SHEET

SEE INSTRUCTIONS ON THE REVERSE

1. REPORT NUMBER (Assigned by TIDC, add Vol. No., if any)
NUREG/CR-4307
HEDL-TME 85-14
Vol. 1

2. TITLE AND SUBTITLE
LWR Pressure Vessel Surveillance Dosimetry Improvement Program: Progress Report -- October 1984-September 1985

3. LEAVE BLANK

4. DATE REPORT COMPLETED
MONTH: September
YEAR: 1985

5. AUTHOR(S)
W.N. McElroy, E.P. Lippincott

6. DATE REPORT ISSUED
MONTH: January
YEAR: 1985

7. PERFORMING ORGANIZATION NAME AND MAILING ADDRESS (Include Zip Code)
Hanford Engineering Development Laboratory
P. O. Box 1970
Richland, WA 99352

8. PROJECT/TASK/WORK UNIT NUMBER

9. FIN OR GRANT NUMBER
B5988

10. SPONSORING ORGANIZATION NAME AND MAILING ADDRESS (Include Zip Code)
Division of Engineering Technology
Office of Nuclear Regulatory Research
U.S. Nuclear Regulatory Commission
Washington, DC 20555

11. TYPE OF REPORT
Technical

b. PERIOD COVERED (Inclusive dates)
October 1984-September 1985

12. SUPPLEMENTARY NOTES
NRC Program Manager is A. Taboada.

13. ABSTRACT (200 words or less)

This report describes progress made in the Light Water Reactor Pressure Vessel Surveillance Dosimetry Improvement Program (LWR-PV-SDIP) during FY84. The primary concern of this program is to improve, test, verify, and standardize the physics-dosimetry-metallurgy and associated reactor and damage analysis procedures and data used for predicting the integrated effects of neutron exposure to LWR-PVs and their support structures. These procedures and data are being recommended in a new and updated set of ASTM standards being prepared, tested, and verified by program participants. These standards, together with parts of the US Code of Federal Regulations and ASME codes, are needed and used for the assessment and control of the condition of LWR-PVs and their support structures during the 30- to 60-year lifetime of a nuclear power plant.

14. DOCUMENT ANALYSIS - a. KEYWORDS/DESCRIPTORS
Light Water Reactor Pressure Vessel Surveillance Dosimetry Improvement Program (LWR-PV-SDIP)

IDENTIFIERS/OPEN-ENDED TERMS

15. AVAILABILITY STATEMENT
Unlimited

16. SECURITY CLASSIFICATION
(This page) Unclassified
(This report) Unclassified

17. NUMBER OF PAGES

18. PRICE

U.S. GOVERNMENT PRINTING OFFICE: 1986-491-620:20446

UNITED STATES
NUCLEAR REGULATORY COMMISSION
WASHINGTON, D.C. 20555